ORP-68804
Revision 0

Corrosion Testing of Inconel and K-3 in LAW Glass, VSL-17R4240-1

Prepared for the U.S. Department of Energy
Assistant Secretary for Environmental Management

P.O. Box 450
Richland, Washington 99352

Approved for Public Release;
Further Dissemination Unlimited

ORP-68804
Revision 0

Corrosion Testing of Inconel and K-3 in LAW Glass, VSL-17R4240-1

H. Gan
Vitreous State Laboratory of The Catholic University of America

I. Joseph
ATKINS

I. L. Pegg
Vitreous State Laboratory of The Catholic University of America

M. Chaudhuri
Vitreous State Laboratory of The Catholic University of America

X. Xie
Vitreous State Laboratory of The Catholic University of America

Z. Feng
Vitreous State Laboratory of The Catholic University of America

Date Published
January 2023

Prepared for the U.S. Department of Energy
Assistant Secretary for Environmental Management

Office of River Protection

P.O. Box 450
Richland, Washington 99352

APPROVED
By Lynn M Ayers at 2:13 pm, Jan 16, 2023

Release Approval Date

Approved for Public Release;
Further Dissemination Unlimited

TRADEMARK DISCLAIMER

Reference herein to any specific commercial product, process, or service by tradename, trademark, manufacturer, or otherwise, does not necessarily constitute or imply its endorsement, recommendation, or favoring by the United States Government or any agency thereof or its contractors or subcontractors.

This report has been reproduced from the best available copy.

Printed in the United States of America

VSL-17R4240-1

Final Report

Corrosion Testing of Inconel and K-3 in LAW Glass

prepared by

Hao Gan, Zhijian Feng, Malabika Chaudhuri, Xiaogang Xie, and Ian L. Pegg

Vitreous State Laboratory
The Catholic University of America
Washington, DC 20064

and

Innocent Joseph
Atkins Energy Federal EPC, Inc.
Calverton, MD 20705

for

Department of Energy
Office of River Protection

December 1, 2017

Rev. 0

Document Title:	Corrosion Testing of Inconel and K-3 in LAW Glass
Document Number and Revision:	VSL-17R4240-1, Rev. 0
Issue Date:	12/1/17
Performing Organization:	Vitreous State Laboratory, The Catholic University of America
Test Plan:	Corrosion Testing of Inconel and K-3 in LAW Glass, VSL-16T4240-1, Rev. 0,

This report describes the results of testing specified by the above Test Plan. The work was performed in compliance with the quality assurance requirements specified in the Test Plan. Results required by the Test Plan are reported. The test results and this report have been reviewed for correctness, technical adequacy, completeness, and accuracy.

I.L. Pegg: _____ **Date:** 12/1/17
VSL Program Director/Principal Investigator

I. Joseph: _____ **Date:** 12/1/17
Atkins Sub-Contract Manager

Table of Contents

List of Tables

List of Figures

List of Abbreviations

ASME	American Society of Mechanical Engineers
ASTM	American Society for Testing and Materials
CUA	Catholic University of America
DOE	Department of Energy
IHLW	Immobilized High Level Waste
ILAW	Immobilized Low Activity Waste
LAW	Low Activity Waste
NIST	National Institute of Standards and Technology
NQA	Nuclear Quality Assurance
ORP	Office of River Protection
QAPP	Quality Assurance Project Plan
SEM-EDS	Scanning Electron Microscopy - Energy Dispersive X-ray Spectroscopy
VSL	Vitreous State Laboratory
WTP	Hanford Tank Waste Treatment and Immobilization Plant
XRD	X-Ray Diffraction
XRF	X-Ray Fluorescence Spectroscopy

SECTION 1.0
INTRODUCTION

About 50 million gallons of high-level mixed waste is currently stored in underground tanks at the United States Department of Energy's (DOE's) Hanford site in the State of Washington. The Hanford Tank Waste Treatment and Immobilization Plant (WTP) will provide DOE's Office of River Protection (ORP) with a means of treating this waste by vitrification for subsequent disposal. The tank waste will be separated into low- and high-activity waste fractions, which will then be vitrified respectively into Immobilized Low Activity Waste (ILAW) and Immobilized High Level Waste (IHLW) products. The ILAW product will be disposed in an engineered facility on the Hanford site while the IHLW product is designed for acceptance into a national deep geological disposal facility for high-level nuclear waste. The ILAW and IHLW products must meet a variety of requirements with respect to protection of the environment before they can be accepted for disposal.

Corrosion of the melter materials of construction by the low activity waste (LAW) glass can significantly affect the life of the WTP LAW melters. The materials that are in contact with molten LAW glass include Inconel 690 alloy and Monofrax™ K-3 refractory. Inconel 690 corrosion has been evaluated in a number of WTP baseline LAW glasses [1-6] but not in the higher waste loading glasses developed in previous work for ORP. K-3 refractory corrosion was evaluated routinely as a part of glass formulation development for both WTP baseline LAW glasses [7-10] and the higher waste loading ORP LAW glasses [11-17]. However, all of these tests were conducted in crucibles that are open to the furnace atmosphere. It is well known that volatile components such as chlorine and sulfur can have significant effects on the corrosion of metallic components. However, when corrosion tests are conducted in experimental setups that are open to the furnace atmosphere, substantial loss of components such as halides and sulfur results. Consequently, the present work focused on conducting corrosion tests in a closed-crucible test configuration where the atmosphere was controlled in order to maintain the concentrations of the volatile components of interest. Similarly, while large amounts of data on K-3 refractory corrosion in LAW glasses have been collected [7-17], because of the loss of volatile components during testing, it was not possible to determine whether components such as chlorine in the glass have an effect on K-3 corrosion. The present work provided data to support such an assessment.

This report presents the results from experiments that were conducted to evaluate the corrosion of Inconel 690 and Monofrax™ K-3 refractory in representative high waste loading LAW glass formulations [15, 16] under conditions where loss of volatile constituents was minimized. The work was conducted according to the corresponding Test Plan [18].

1.1 Quality Assurance

This work was conducted under a quality assurance program compliant with applicable criteria of 10 CFR 830.120; the American Society of Mechanical Engineers (ASME) Nuclear Quality Assurance (NQA)-1-2008 including NQA-1a-2009 addenda; and DOE Order 414.1 D, Quality Assurance. This program is supplemented by a Quality Assurance Project Plan (QAPP) for ORP work that is conducted at the Vitreous State Laboratory (VSL) of the Catholic University of America (CUA) [19]. Test and procedure requirements by which the testing activities are planned and controlled also are defined in this plan. The program is supported by VSL standard operating procedures that were used for this work [20]. Requirements of DOE/RW-0333P are not applicable to this scope of work.

SECTION 2.0
EXPERIMENTAL METHODS

The methods used to conduct corrosion tests on Inconel 690 alloy and Monofrax K-3 refractory under controlled atmosphere conditions are described in this section.

2.1 Experimental Design

The objective of this work was to evaluate corrosion of the melter materials of construction, Inconel 690 and K-3 refractory, in high waste loading LAW glass melts. A main focus was to determine the effect of sulfate and chloride on the corrosion of those materials. Because of their volatility, these species are lost from the melt during typical long-duration corrosion tests. Consequently, alternative test designs are required in order to evaluate the effects of these species. In previous work, Gan et al. [21] developed a closed-crucible method to investigate the solubility of highly volatile sulfur and chlorine species in molten LAW glasses. In that work, it was shown that virtually all of the SO_3 and the majority of the Cl could be retained. Based on those results, the closed-crucible method was adapted for the present work in order to maintain the sulfate and chloride concentrations in representative LAW glass melts that were evaluated with respect to corrosion of Inconel 690 and K-3 test coupons.

Two high waste loading ORP LAW glasses, a high sodium Hanford Envelope A formulation, ORPLA20 [16], and a lower sodium Envelope A formulation, ORPLE12 [15], were selected for corrosion experiments. The compositions of these glasses are given in Table 2.1. ORPLA20 is a high alkali glass with 24 wt% Na_2O that can accommodate 0.70 wt% SO_3 without the formation of secondary sulfate phases. ORPLE12 has a lower Na_2O concentration of 16 wt% and can tolerate a SO_3 concentration of 1.50 wt% without the formation of secondary sulfate phases. These two glass compositions represent, respectively, the high alkali and high sulfate ranges of the ORP-LAW glasses.

The closed crucible tests of Inconel 690 and K-3 refractory were conducted in ORPLA20 and ORPLE12 glass melts with different SO_3 and Cl concentrations. Previous DM10 melter tests with these glass compositions with various SO_3 and Cl concentrations [22, 23] were reviewed to select the SO_3 and Cl concentrations to be used for the closed crucible tests. For ORPLA20, melter tests with 0.86 Cl and 0.7 SO_3 did not show a secondary sulfate phase. Therefore the maximum Cl and SO_3 concentrations for closed crucible tests with ORPLA20 were set at 0.8 Cl and 0.7 SO_3. For ORPLE12, melter tests with 0.42 Cl and 1.1 SO_3 did not show a secondary sulfate phase. Therefore the maximum Cl and S concentrations for closed crucible tests with ORPE12 were set at 0.4 Cl and 1.0 SO_3. In addition, for comparison with previous test results, tests were also conducted with ORPLE12 at 1.25 wt% SO_3 and 0.02 wt% Cl, which are the concentrations used in previous open crucible K-3 refractory corrosion tests with this glass composition.

The test matrices are shown in Table 2.2 for the K-3 corrosion experiments and in Tables 2.3.a and 2.3.b for the Inconel 690 corrosion experiments.

Inconel 690 corrosion tests in OPRLA20 and ORPLE12 glasses were conducted at five conditions, each with different chlorine and sulfate contents, ranging from zero sulfate and chlorine to high sulfate and chlorine. The two LAW formulations were also tested using the standard open crucible metal corrosion procedure so that the data from the present work can be compared to metal corrosion test data collected with the open crucible method over the last two decades.

K-3 refractory corrosion tests in the present work were conducted using only the closed crucible test configuration.

2.2 Glass Preparation

ORPLA20 and ORPLE12 glass samples were prepared from reagent-grade or higher purity chemicals to produce a batch size of approximately 400 grams. Crucible melts were prepared by melting the appropriate combination of well-mixed chemicals at 1200ºC for 75 minutes in a platinum-gold crucible. Mixing of the melt was accomplished mechanically with a platinum stirrer (15 minutes after the start of melting until pouring). The melts were quenched into glass samples by pouring onto a cold graphite plate. Prior to corrosion testing, the compositions of the glasses were confirmed by chemical analysis by X-ray Fluorescence Spectroscopy (XRF) on ground glass samples.

2.3 Inconel 690 Corrosion Tests

Inconel 690 corrosion tests are typically conducted in open crucibles, which results in loss of volatile components such as sulfate and chlorine during the 7-day test. In the present work, two open crucible Inconel 690 corrosion tests were conducted with the high waste loading ORP LAW glasses in order to provide a comparison to previous results with that method. In addition, ten closed crucible tests were conducted with the same base glasses at various chlorine and sulfate concentrations. The closed crucible test system was designed to maintain the concentrations of volatile components such as chlorine and sulfate throughout the duration of the test.

2.3.1 Coupon Preparation

Rectangular coupons of Inconel 690 were machined from the bulk material and their surfaces polished. The dimensions of the coupons were 0.300 by 0.150 inch in cross-section and of sufficient length to be immersed in the molten glass to a depth of 0.7 inch (Figure 2.1). All dimensions of the coupons were measured by micrometer to better than 0.5 mil before the tests. The precision of the parallel surfaces was better than 0.001 inch.

2.3.2 Standard Inconel 690 Corrosion Test

The standard VSL open crucible corrosion tests with molten glass were conducted using a modified American Society for Testing and Materials (ASTM) refractory corrosion procedure [24] using the experimental arrangement shown schematically in Figure 2.2. The experimental setup consists of a 50 ml platinum crucible placed into a quartz crucible holder. On the top of the crucible there is a cover with a 5 mm slot. The coupon is placed through the slot and suspended by a rod that is placed through a hole drilled through one end of the coupon. For each corrosion test, 70 grams of glass is melted at 1150°C (nominal) for 30 minutes; this quantity gives an S/V ratio for these tests of 0.15 cm^{-1} and the crucible is filled to ¾ of its height (29 mm) with glass. The coupon with the lid is preheated at 800°C for about 45 minutes, allowing an oxide layer to form on the coupon, which is then placed into the crucible with the molten glass. The experimental setup is then placed into a furnace that is preheated to 1150°C. After the designated period of time (7 days), the setup is removed from the furnace, the coupon is extracted from the glass, and the glass melt is poured into a graphite mold for further analyses. The coupon with the glass coating is then annealed at 450°C for 2 hours to reduce spalling of the glass coating.

2.3.3 Closed Crucible Inconel 690 Corrosion Test

The closed crucible test was designed to maintain the concentrations of the volatile components such as sulfur and chlorine in the glass melt throughout the duration of the test. In the closed crucible experiment, a 100 ml alumina crucible (99% Al_2O_3) with matched lid is used to contain the standard metal corrosion setup described in Section 2.3.2. A schematic of the closed crucible experimental setup is shown in Figure 2.3. After loading the test crucible with the metal coupon, the assembly is placed inside the alumina crucible with a lid. The lid is sealed completely using a nepheline ceramic paste, which melts to produce a highly viscous sealant at the test temperature. The interior volume within the alumina crucible is further reduced by adding ceramic filler blocks made of Zirmul. The sealed test rig is placed into the test furnace at room temperature and heated to 1150°C at 600°C/hour. The setup is removed from the hot furnace after 7 days of testing and cooled to room temperature in a ventilated cooling chamber. The test temperature and duration for closed crucible Inconel corrosion tests are the same as those used in previous open crucible Inconel corrosion tests. The alumina crucible with lid is then cut open to retrieve the standard test setup. The metal coupon is subsequently removed from the softened glass after reheating to 1000°C briefly in open air. The glass melt is poured and collected for analysis.

2.4 Closed Crucible K-3 Refractory Corrosion Test

Monofrax™ K-3 test coupons are cut from K-3 bricks. Since the material that forms fused-cast K-3 varies from the surface of the brick to its interior (e.g., the interior material tends to contain larger and more numerous pores), the test coupons are cut from material within one inch of the brick surface. All sides of the K-3 coupons are ground parallel with a precision of

better than 2 mil (0.002"). A typical K-3 coupon for closed crucible test measures 0.3 × 0.4 inches in cross-section and is long enough (~ 2.5 inches) to be immersed in the molten glass to a depth of 0.8 inch (Figure 2.4). Similar to the standard VSL open crucible K-3 corrosion test procedure, the closed crucible K-3 corrosion test is modified from ASTM refractory corrosion procedure ASTM C 621 [24]. A schematic of the experimental setup is given in Figure 2.5. For each K-3 refractory corrosion experiment, a test coupon of known dimensions is immersed in 100 grams of molten glass in a 100 ml Pt/Au crucible. The ratio of the exposed surface area of the K-3 test coupons to the volume of molten glass is 0.2 cm^{-1}, which is identical to the VSL standard K-3 corrosion test condition in an open crucible with air bubbling. The method for introduction of the preheated K-3 coupon (800ºC) to molten glass (1150ºC) was identical to the standard VSL procedure. The test device with the K-3 test coupon immersed in 100 grams of molten glass was cooled to room temperature before being sealed with nepheline ceramic paste inside an alumina outer crucible (250 ml) with its matching lid. For K-3 corrosion tests, the double crucible setup was heated from room temperature to 1208°C at 600ºC/hour and kept at 1208°C for 6 days. The test temperature and duration for closed crucible K-3 corrosion tests are the same as those used in previous open crucible K-3 corrosion tests. K-3 corrosion tests are conducted at a temperature 58°C higher than that for the Inconel corrosion tests so that a measurable amount of K-3 corrosion is observed in most samples. The setup was removed from the hot furnace after 6 days of testing and cooled to room temperature in a ventilated cooling chamber. The alumina crucible with lid was then cut open to retrieve the test setup. The K-3 coupon was subsequently removed from the softened glass after reheating to 1150ºC for about 5 minutes in open air. The glass melt was poured and collected for analysis. The K-3 test coupon was sectioned for further characterization. The dimensional losses at the neck and half-down locations were evaluated, as described in Section 2.5.

Modifications were made to the K-3 corrosion test setup in response to the results that were obtained in order to more closely meet the test objectives. These variants are referred to as Stage 1, 2, and 3 tests. The differences between these tests and the issues that led to the changes are described in Section 3.

2.5 Optical Microscopy

After the corrosion tests, the reacted metal coupons were embedded in resin and then sectioned at the mid-point and polished. Similarly, the reacted K-3 refractory coupons were sectioned directly at the mid-point and polished (Figure 2.4). The thickness of the reacted coupon was measured using a measuring microscope, which has a precision of better than 0.05 mil (1.27 μm). Typically, at least 10 transverse lines were measured perpendicular to the length of the coupon. The dimensional loss was calculated as half of the difference of the measured widths between the original and reacted coupons at the neck and half-down locations for both Inconel 690 and K-3 coupons and near the bottom for Inconel 690 coupons (see Figure 2.6). The sectioned metal coupons were further characterized using Scanning Electron Microscopy coupled with Energy Dispersive X-ray Spectroscopy (SEM/EDS) (JEOL JMS 5900LV).

2.6 SEM-EDS

SEM/EDS was used to characterize the microstructure and chemical composition of the corroded Inconel alloy. Particular features of interest include the nature and the degree of scale formation (exterior to metal), grain-boundary damage (interior to metal), and the leaching of key alloy elements (e.g., Cr depletion from interior of the Ni-Cr based alloy). SEM images of the cross-sections of the reacted coupons near the neck, half-down, and bottom regions and point analysis of Cr concentrations perpendicular to the metal-glass interface were acquired for each test coupon.

2.7 Glass Compositional Analysis

The primary method used for glass analysis was XRF on powdered glass samples. A PANalytical AXIOS-max Advanced XRF spectrometer was used for this purpose. Since lithium and boron are not determined by this method, the target values of those two oxides were used in final XRF composition analysis.

The glass samples after corrosion experiments were inspected for the presence of possible salt phases on the surface. Samples were selected to minimize foreign matter, such as metal scale or K-3 particles, before being ground and sieved for XRF analysis. All glass samples from Stage 2 and Stage 3 K-3 corrosion tests were washed with 0.7% HNO_3.

2.8 XRD Analysis of Crystalline Phases in Glass Samples

X-ray Diffraction (XRD) data were gathered using a Thermo-Fisher X-tra theta-theta diffractometer fitted with a Cu X-ray tube. Each sample is ground and sieved to 200 mesh particles. Each powder pattern is scanned from 5 to 80 degrees in 2-theta. JADE9 Software is used to perform the search-match identification of the crystalline phases.

SECTION 3.0
CLOSED CRUCIBLE CORROSION TESTS OF MONOFRAX™ K-3

Monofrax™ K-3 corrosion tests in open crucibles have been routinely performed at VSL in the past twenty years as part of the glass formulation development work. The major issues of concern have been the tendency for increased corrosion with higher alkali melts and formulation changes to mitigate those effects. This is of particular importance in the development of viable high waste loading LAW glasses. However, due to the volatile loss of sulfur and chlorine in such tests, the available data do not allow for an assessment of the effects of those species. Accordingly, an objective of the present work was to develop test methods that would retain these species in order to collect data that would support an assessment of their effects on K-3 corrosion. Section 3.1 describes the difficulties encountered in this work and the modifications that were made to mitigate them. The K-3 corrosion test results obtained with the final test setup are presented in Section 3.2.

3.1 Method Evaluation of Closed Crucible K-3 Corrosion Test

The closed crucible K-3 corrosion test method employed in this work evolved in three stages as a result of experimental difficulties encountered in containing the highly volatile Cl and S species and the contamination caused by reactions of the vapor phase with the AZS-based ceramic cover.

Table 3.1 lists the crucible conditions used for volatile containment and the issues associated with each method. The results from Stage 1 and Stage 2 tests did not yield the desired corrosion data but are, nevertheless, useful to interpret the results from the final tests. A description of each experimental stage and the data collected are provided below.

3.1.1 Stage 1: K-3 Corrosion in Semi-Sealed Crucible

Stage 1 tests employed a quartz crucible with a Zirmul cover and Zirmul for vapor isolation. Eight K-3 corrosion experiments were conducted in Stage 1. All test coupons were measured for their dimension loss and all the glass samples after corrosion experiments were analyzed by XRF for compositional changes. The data are summarized in Table 3.2 and Figures 3.1 and 3.2. The major problem encountered in Stage 1 experiments was insufficient containment of highly volatile Cl and S species. As a result, glass melts after six days at 1208°C had lost the majority of the Cl and SO_3, as shown in the XRF analysis listed in Table 3.2. It is interesting to note that the glass compositions after Stage 1 experiments are similar to the glass analysis of the same formulation tested in open crucibles (Tables 3.3 and 3.5), although it took a longer time for Cl and SO_3 to escape than in the open crucible, presumably due primarily to the lack of air bubbling. Despite the loss of the volatile species, the Stage 1 data provide a useful reference for

the corrosion data ultimately obtained from effectively sealed crucible tests (Stage 3) regarding the impact from Cl and SO_3. These data are particularly useful considering that no open crucible K-3 corrosion data are available for the present test coupon size and crucible volume.

3.1.2 Stage 2: K-3 Corrosion in Sealed Crucible with Zirmul Cover

Stage 2 tests employed a high purity alumina crucible with an alumina cover and Zirmul for vapor isolation. Eight K-3 corrosion experiments were conducted in Stage 2. All test coupons were measured for their dimension loss (Table 3.3, Figures 3.1 and 3.2) and all the glass samples after corrosion experiments were analyzed by XRF for compositional changes (Table 3.4). The high purity alumina crucible and its matching lid prevented the majority of the SO_3 and Cl from escaping in Stage 2 corrosion experiments (Table 3.4). It is interesting to note that the neck dimension losses from all but one experiment in Stage 2 are an order of magnitude less than the results in the corresponding Stage 1 tests (Table 3.3, Figures 3.1 and 3.2). Typical neck dimension loss is only a few thousands of an inch in Stage 2, as compared to several tens of thousands of an inch in Stage 1 tests (and also in previous open crucible tests) (Table 3.3). In agreement with the generally smaller neck dimension loss, Cr_2O_3 concentrations in the reacted glasses barely increased from their starting concentrations (Tables 3.3 and 3.4), which is in sharp contrast to the significant Cr_2O_3 increase in glass samples after Stage 1 experiments (Tables 3.2 and 3.3). A closer examination of the reacted glass compositions suggests that the glass chemistry has changed significantly after Stage 2 corrosion, in particular for Na_2O and SiO_2. Normally, the changes in glass composition are small except for highly volatile elements (such as Cl and S), and key K-3 components Al_2O_3 and Cr_2O_3. It is unusual to observe such extraordinarily large changes in Na_2O and SiO_2 in a test vessel that confined S and Cl well. The selective loss in Na_2O (3-4 wt%) and gain in SiO_2 (3-4 wt%) in Cl-containing ORPLA20 tests and slightly smaller changes in Cl-containing ORPLE12 tests suggested chemical reactions inside the test device, in particular between the Cl-rich vapor and the ceramic cover used for suspending the K-3 test coupon. Inspection of the Zirmul covers used in Stage 2 experiments revealed variable amounts of alteration on the surface of the AZS refractory facing the glass melt, and usually stronger alteration for experiments with Cl-bearing glasses (Figure 3.3). The improved sealing in Stage 2 experiments apparently created a Cl-rich local atmosphere that was corrosive to the AZS refractory cover. Although no direct evidence was acquired to prove this, the consistent pattern of losing Na_2O and gaining SiO_2 for Cl-bearing starting glass samples suggests a strong association between chloride and the observed changes in Na_2O and SiO_2 contents. It is speculated that the volatilization of NaCl from the glass melt, followed by reactions between the Zirmul refractory (a commercial Al_2O_3-ZrO_2-SiO_2 refractory brick) and chloride could have resulted in retention of Na_2O by the AZS accompanied by leaching of SiO_2 from the AZS into the glass melt. Throughout the process, Cl could have been recycled back to the melt allowing for continuous sodium loss and silica leaching due to the significantly higher Cl vapor pressure and low melting point of the chloride. Evidently, the semi-sealed crucible in Stage 1 was unable to maintain a sufficiently Cl-rich atmosphere to initiate such interactions. As a result, relatively minor compositional variations were observed (Table 3.2) and the final glass compositions were similar to those from open crucible experiments (Tables 3.3 and 3.5). It is nevertheless surprising to observe such a drastic drop in K-3 corrosion neck loss with a few percent changes in Na_2O and SiO_2 in the glass melt.

3.1.3 Stage 3: K-3 Corrosion in Sealed Crucible with Pt Cover

In order to prevent the undesirable reactions that complicated the Stage 2 experimental results, in Stage 3 tests a platinum sheet was added to the inner crucible in order to isolate the reactive vapor from direct contact with the Zirmul cover. Thus, Stage 3 tests employed a high purity alumina crucible with an alumina cover and a platinum sheet covering a Zirmul plate for vapor isolation.

Eight K-3 corrosion experiments were conducted in Stage 3. All test coupons were measured for their dimension loss and all the glass samples after corrosion experiments were analyzed by XRF for compositional changes. The data are summarized in Table 3.6 and Figures 3.1 and 3.2. The high purity alumina crucible and its matching lid preserved the majority of the SO_3 and Cl, and more importantly, the Pt sheet worked as intended in isolating the Cl-rich vapor from the Zirmul cover (Tables 3.3 and 3.6). Inspection of the Pt sheet facing the glass surface revealed no significant deposits after the corrosion experiments. The soda loss and silica gain were reduced to levels similar to Stage 1 and open crucible experiments (Table 3.3).

The neck dimension losses of K-3 test coupons from Stage 3 experiments, and in particular those for Cl-free glasses, were closer to those observed in Stage 1 experiments, but were considerably larger than their counterparts from Stage 2 experiments (Table 3.3). The reduction of soda loss and silica gain as well as the increased neck loss in Stage 3 experiments compared to Stage 2 supports the suspected reactions between the Cl-rich vapor phase and the Zirmul cover in Stage 2 tests. As more K-3 was corroded by molten glass in Stage 3, the Cr_2O_3 concentration increased in the reacted glasses (Tables 3.3 and 3.6).

Based on these results, Stage 3 corrosion experiments were used in this work for investigation of the impact of Cl and SO_3 on K-3 corrosion. The results are discussed below in Section 3.2.

3.2 The Effects of Cl and SO_3 on K-3 Corrosion

Stage 3 K-3 corrosion experiments provided the data required to investigate the effects of Cl and SO_3 on K-3 glass contact corrosion. As explained in Section 3.1, the data from Stage 1 tests provide useful reference points for the impact of Cl and SO_3 under the otherwise identical test conditions, except for the gradual loss of volatile Cl and SO_3 that occurred in Stage 1 tests. The experimental results are summarized and analyzed in this section.

The neck dimension loss of a K-3 test coupon provides the most direct indicator of its corrosion resistance to molten glass. The neck loss data for all eight Stage 3 experiments were evaluated against the concentrations of Cl and SO_3 in the two representative LAW formulations (Tables 3.3 and 3.6) in order to identify any patterns or trends.

Table 3.3 lists the dimensional loss and influential glass component changes for each

corrosion experiment in Stage 1 (semi-sealed), Stage 2 (sealed but with Na_2O and SiO_2 contamination), and Stage 3 (sealed, without contamination) as well as two experiments in open crucible conditions from previous work. The neck loss values from those experiments are plotted vs. the concentrations of Cl or SO_3 in the starting glasses in Figures 3.4 – 3.7. Neck loss values from Stage 3 experiments did not show any clear dependence on the starting SO_3 concentration (Figures 3.4, 3.5, and 3.12). However, patterns are evident in Figures 3.6,3.7, and 3.13 showing neck loss vs. starting Cl concentration. For both the ORPLA20 and ORPLE12 base formulations, the neck loss in Cl-free glasses, regardless of their starting sulfate contents, are 0.057 to 0.061 inch for ORPLA20 and 0.033 to 0.037 inch for ORPLE12; these values are similar to those observed in Stage 1 tests (0.048 to 0.062 inch for ORPLA20; 0.030 to 0.034 inch for ORPLE12) where most SO_3 was lost during testing. Evidently, the neck dimension loss is not sensitive to sulfate content in these two Cl-free formulations. In contrast, the neck loss of K-3 test coupons in Cl-containing experiments differed greatly between Stage 1 and Stage 3 tests with the identical starting glass composition. Moreover, the neck dimension loss values in Stage 3 tests *decreased* by several fold from Cl-free to Cl-bearing ORPLA20 or ORPLE12 glasses (Figures 3.6 and 3.7). The correlation or lack thereof in Figures 3.4 – 3.7 suggests that, based on neck loss, for these two formulations the impact of SO_3 is insignificant while Cl significantly suppressed K-3 corrosion.

In view of these results, it is important to distinguish between the effects of dissolved SO_3 and that of a separate molten salt phase. The deleterious effects of a separate molten salt phase on K-3 refractory have been demonstrated in previous work [1, 11, 12, 25]. However, the present work is the first that addresses the effects of dissolved SO_3 (and Cl) without a separate salt phase. The reduced neck loss in Cl-bearing LAW glasses as compared to their Cl-free counterparts is an interesting and somewhat surprising result. Further work is required to understand the reasons for this effect. However, from a practical perspective, both results are encouraging in terms of the potential impacts of high SO_3- and Cl-loading formulations on refractory lifetime, as long as separate salt phases are avoided.

In addition to dimension loss, the extent of K-3 corrosion is also reflected in the change of glass Cr_2O_3 concentrations with respect to their starting values. In view of the low chromium content in the starting glasses, the Cr_2O_3 concentration change due to K-3 dissolution can provide an additional sensitive measure of corrosion. The concentration changes of Cr_2O_3 after K-3 corrosion were therefore often used as a secondary indicator for refractory corrosion under each test condition. The virtually constant Cr_2O_3 concentrations before and after Stage 2 tests are consistent with the observed very small dimension loss (Tables 3.3 and 3.4). Chromium concentrations in Stage 3 glasses showed no clear correlation with the SO_3 content of the starting glasses (Figures 3.8, 3.9, and 3.14); however, chromium concentrations decreased considerably from Cl-free to Cl-bearing ORPLA20 glasses (from around 0.7 wt% to below 0.5 wt%, Figures 3.10 and 3.15). Reduced dissolution of Cr-rich K-3 is correlated with the reduced neck dimension loss observed for the same samples. However, the trend of decreasing Cr_2O_3 with Cl is not followed as well for ORPLE12 (Figure 3.11): one of the Cl-bearing glasses showed a smaller Cr_2O_3 increase with respect to the starting value, whereas the other Cl-bearing glass gave a value similar to that for the Cl-free glass despite its reduced neck loss. Nevertheless, all dimension loss data and the majority of Cr concentration data from Stage 3 tests suggest a negative correlation between K-3 dimension loss and Cl concentration in these LAW glasses.

As noted above, the data from this work are not sufficiently extensive to determine the mechanism for the suppression of K-3 corrosion by dissolved Cl. Nevertheless, the possibility of this being an indirect effect resulting from minor glass composition changes during testing can be addressed. The changes in the concentrations of Cl, SO_3, Na_2O and SiO_2 in the ORPLA20 and ORPLE12 glasses after K-3 corrosion tests can be seen in Figures 3.16 to 3.23. As shown in Figures 3.20 and 3.21, compared to their starting compositions, key glass components Na_2O and SiO_2 changed slightly after the 6-day Stage 3 corrosion tests. In general, K-3 dimension loss tends to be lower in glass melts with lower Na_2O and higher SiO_2. As shown in Figure 3.20 for ORPLA20, the Na_2O concentration decreased from the initial 24 wt% to 22 - 23 wt% in two Cl-free Stage 3 tests. For the same two Cl-free glasses, the Na_2O concentration decreased from 24 wt% to 21.5 wt% in Stage 1 tests. However, for two Cl-bearing variations of ORPLA20, the Na_2O concentration decreased from nearly 23 wt% to around 20 wt% after Stage 3 tests and from 23 wt% to 20 to 20.7 wt% after Stage 1 tests. Thus, it is clear that for Stage 3 tests, approximately 1 wt% more Na_2O was lost from Cl-bearing ORPLA20 melts than from their Cl-free counterparts. However, the sodium concentration changes were similar in Stage 3 and Stage 1 tests for glasses with similar initial chloride contents. Conversely, SiO_2 concentrations increased after the 6-day corrosion tests. As shown in Figure 3.21 and Table 3.3, SiO_2 concentrations increased slightly after Stage 3 tests with two Cl-free glasses, from 43 wt% to around 44 wt%, and slightly more after Stage 1 tests with two Cl-free glasses, to 44 to nearly 45 wt%. In the Cl-containing tests, SiO_2 concentrations in the reacted ORPLA20 glasses are generally higher (44.8 to 45.7 wt%) after Stage 3 tests than after Stage 1 tests (44.9 to 45.3 wt%). Overall, however, the SiO_2 concentrations in the reacted glasses from Stage 3 and Stage 1 tests are very similar. Therefore, the changes in Na_2O and SiO_2 concentrations in the reacted glasses cannot be solely responsible for the observed several fold changes in the neck loss in Stage 1 and Stage 3 tests with identical starting compositions. Similar results were also observed for ORPLE12 Stage 3 and Stage 1 tests (Figures 3.22 and 3.23, Table 3.3). The available data thus strongly suggest that the observed difference in neck loss and Cr_2O_3 concentration are influenced predominantly by the chloride content in the glass melt. It is hypothesized that chloride present in the two LAW formulations reduced the dissolution of K-3 and, consequently, the neck dimension loss, by decreasing the solubility of chromium-rich spinel in the Cl-bearing LAW glass melts. A set of carefully designed experiments is thus recommended to further explore the effects of chloride and sulfate in representative LAW glass melts on the phase stability of key chromium-containing minerals.

Another noteworthy feature associated with the sealed crucible K-3 corrosion experiments is the frequent fracture observed within the K-3 coupons, as shown in the scanned images (Figures 3.1 and 3.2). Often, a major portion of the K-3 test coupons would break off from the main body, resulting in gaps filled by molten glass. Visual inspection did not show signs of alteration along the exposed K-3 fracture surface. Normally, an altered zone would have developed on all exposed K-3 surfaces during the course of six days of K-3 corrosion testing. Therefore, this suggests that the fracture occurred in the very late stage of the tests. It is conceivable that thermal shock produced during the rapid cooling and subsequent rapid heating used to retrieve the test coupon might have contributed to the observed damage.

3.3 Summary and Conclusions from K-3 Corrosion Tests

Overall, the experimental results from K-3 corrosion tests can be summarized as follows:

- Both chloride and sulfate in LAW melts can potentially affect K-3-glass contact corrosion. Both are highly volatile and are difficult to retain in long-duration corrosion tests. It was demonstrated in this work that the majority of the SO_3 and Cl can be retained in a properly sealed double-crucible K-3 corrosion setup. However, the Cl-rich vapor phase was found to be highly reactive to the AZS ceramic cover that was used in Stage 2 tests, resulting in significant soda loss from the glass and silica contamination from the AZS cover. A platinum cover sheet was deployed in Stage 3 tests and worked effectively in isolating the Cl-rich vapor from the AZS ceramic. The closed crucible test method developed in this work has proven effective in containing volatile Cl and S species while inhibiting undesirable contamination. For Cl-free glasses, the method gave comparable results to those obtained from semi-sealed Stage 1 tests as well as those from the standard VSL open crucible tests that have been used in glass formulation development for many years.

- Measured neck dimension losses were evaluated to assess the impacts of chloride and sulfate dissolved in LAW glass melts. The neck loss values for the Cl/S-free base glasses are similar for the various test setups (open, semi-closed, or closed without contamination). The presence of 0.7 wt% SO_3 in Cl-free ORPLA20 (Test LA20K-3) and 1.25 wt% SO_3 in Cl-free ORPLE12 (Test LE12K-3) did not change the neck dimension loss significantly compared to their sulfate/chloride-free counterparts. However, neck loss was reduced several fold in ORPLA20 with 0.8 wt% Cl in SO_3-free ORPLA20 (Test LA20K-2), and similarly in ORPLA20 with 0.7 wt% Cl with 0.7 wt% SO_3 (Test LA20K-4). For ORPLE12, neck loss was reduced considerably also in the two Cl-bearing variations: for Test LE12K-2 with 0.4 wt% Cl and S-free and for Test LE12K-4 with 0.4 wt% Cl and 1 wt% SO_3. Based on these results, K-3 neck dimension loss is not significantly affected by the SO_3 concentration in these LAW glass melts but is strongly affected by the Cl concentration. These trends were also evident in the measured amounts of Cr_2O_3 dissolved from K-3 into the glass melts, with considerably lesser amounts of Cr_2O_3 dissolved in the Cl-containing tests.

- The data from this work are not sufficiently extensive to determine the mechanism for the suppression of K-3 corrosion by dissolved Cl. Nevertheless, the possibility of this being an indirect effect resulting from minor glass composition changes during testing was addressed. That analysis shows that the changes in Na_2O and SiO_2 in the reacted glasses cannot be solely responsible for the observed several fold changes in the neck loss in Stage 1 and Stage 3 tests with identical starting compositions. The available data thus strongly suggest that the observed difference in neck loss and Cr_2O_3 concentration are influenced predominantly by the chloride

content in the glass melt. It is hypothesized that chloride present in the two LAW formulations reduced the dissolution of K-3 and, consequently, the neck dimension loss, by decreasing the solubility of chromium-rich spinel in the Cl-bearing LAW glass melts. A set of carefully designed experiments is thus recommended to further explore the effects of chloride and sulfate in representative LAW glass melts on the phase stability of key chromium-containing minerals.

- Another noteworthy feature associated with the sealed crucible K-3 corrosion experiments is the frequent fracture observed within the K-3 coupons. However, the nature of the fracture surface suggests that the fracture occurred in the very late stage of the tests. It is conceivable that thermal shock from the rapid cooling and subsequent rapid heating used to retrieve the test coupon might have contributed to the observed damage. Further work would be useful to test this explanation.

SECTION 4.0
CLOSED CRUCIBLE CORROSION TESTS OF INCONEL 690

Like Monofrax™ K-3, Inconel 690 Ni-Cr super-alloy has been tested extensively at crucible scale for its suitability as a WTP LAW melter construction material. The relatively high concentrations of SO_3 and Cl in typical LAW glasses have the potential to significantly affect Inconel 690 corrosion. However, due to the volatile loss of sulfur and chlorine in crucible scale corrosion tests, the results from typical open crucible corrosion tests do not allow for an assessment of the effects of those species. Accordingly, an objective of the present work was to develop test methods that would retain these species in order to collect data that would support an assessment of their effects on Inconel corrosion. Recently, two high sulfate HLW glasses were tested in a closed crucible setup for Inconel 690 glass contact corrosion [25]. The results from that work showed that the closed crucible method retained SO_3 well during the 7-day metal corrosion experiments at 1150°C. In addition, other major glass components, such Na_2O and SiO_2, did not show significant change with respect to their starting concentrations. Thus, that work provided the basis for the present study.

A total of 12 Inconel 690 corrosion experiments were conducted in this work, 10 of which were done in a closed crucible setup using a double crucible method; the other two tests were conducted using the standard open crucible method to permit comparisons to previous data (Table 4.1). As discussed in Section 3, it has been observed that Cl-rich vapor trapped within the sealed crucible can lead to large soda loss and silicon contamination from the exposed Zirmul cover. Consequently, the metal corrosion tests with five Cl-bearing formulations were conducted using a platinum cover sheet. The data collected from the 12 tests are discussed in Sections 4.1 and 4.2. The compositions of the base glasses, ORPLA20 and ORPLE12, are given in Table 2.1.

Inconel 690 is used extensively in the WTP melters for electrodes, bubblers, thermowells, level detectors, etc. Inconel 690 is generally quite resistant to attack by molten glass, and to a lesser degree by separate molten salt phases, at the typical melter processing temperature [3]. Under the typical open crucible test condition without a separate molten salt phase, Inconel 690 generally reacts with molten LAW glasses rather slowly. However, highly volatile chlorine is rapidly lost from the melt in such tests. Corrosion by molten chlorides is known to proceed via enhanced inter-granular attack and interior void development due to the high vapor pressure of chloride. Gan et al. identified extensive grain-boundary attack by Cl-bearing LAW glass melts in a deep crucible open to the air [14]. However, the chloride concentration in those tests was not maintained throughout test duration since chloride was still able to evaporate slowly from the open, albeit deep, crucible. Thus the primary objective of the present work was to collect data on Inconel 690 corrosion in melts where the concentrations of Cl and SO_3 are maintained.

Table 4.2 summarizes the corrosion tests performed in this work and the corresponding test conditions. Base formulations, ORPLA20 and ORPLE12 at various Cl and SO_3 concentrations were tested in the closed crucible setup. The test results showed that both chloride and sulfate were well retained within the sealed double crucibles, as discussed below.

Key parameters that are useful for assessing Inconel 690 corrosion damage are:

- The dimensional loss of the test coupons measured at the neck, half-down, and bottom locations;
- Internal structural degradation, as reflected by grain boundary damage via oxidation and void formation;
- Internal compositional alteration, as reflected by dealloying, in particular via the depletion of chromium, which is a critical component in Inconel 690; and
- Oxide scale formation and characteristics.

4.1 Inconel Corrosion in ORPLA20

Glass contact corrosion of Inconel 690 was tested in ORPLA20 formulations with five different SO_3 and Cl concentrations, as listed in Tables 4.1 and 4.2. The open crucible tests and the Cl-free glass closed crucible tests used a Zirmul cover (Tests LA20-1, LA20-4, and LA20-A in Table 4.1). The closed crucible tests with the Cl-bearing glasses used a platinum protection sheet (Tests LA20-2, LA20-3, and LA20-5 in Table 4.1).

As shown in Table 4.1, the five tested ORPLA20 formulations varied in both SO_3 and Cl concentrations. The test conditions and the results of visual inspection of the reacted glass samples are summarized in Table 4.2. Overall, trace to minor spinel crystallization was observed in all five glass samples. A separate yellow salt layer formed on the surface of the reacted glass for all three sulfate-bearing formulations (Tests LA20-3, LA20-4, and LA20-5). Occasionally, the glass contained fragments of dark oxide scale that had spalled off the metal surface. Care was taken to avoid such inclusions when selecting the glass samples for XRF analysis. Although it is not possible to avoid crystalline spinel suspended in glass completely, XRD analysis of the reacted glass from five closed crucible tests and the open crucible test did not show any crystalline phases. The XRF analysis results for glasses before and after Inconel 690 corrosion tests are listed in Table 4.3.

As listed in Tables 4.4 and 4.5, the dimensional changes of the Inconel 690 coupon are in general small after corrosion tests in ORPLA20 melts with zero to medium levels of SO_3. Even at the highest Cl level with zero SO_3 (Test LA20-2), the dimension loss is very small. However, the neck loss increased significantly in Test LA20-4 (0.7 wt% SO_3 and 0 wt% Cl) to 4.5 mil and to 2.5 mil in Test LA20-5 (0.7 wt% SO_3 and 0.67 wt% Cl). At moderate levels of SO_3 and Cl (Test LA20-3), the neck dimension loss is similar to those for the SO_3-free glasses. It is common in the standard open crucible corrosion tests that the reaction between the molten glass and Inconel 690 results in higher chromium content in the glass. Consequently, the increase in glass Cr_2O_3 content is a useful indicator of the extent of metal corrosion. However, the chromium concentration after four of the five closed crucible tests decreased noticeably; the exception is Test 4, which showed a larger neck dimension loss and almost 0.1 wt% increase of Cr_2O_3 in the

final glass. The decrease in chromium content in the reacted glass may be due to spinel crystallization. Ni, Cr, and Fe released from Inconel 690 into the molten glass would favor crystallization of Cr-rich spinel, which could reduce Cr_2O_3 concentration in the glass matrix. In clear contrast to the closed crucible test results, the Inconel test coupon in the open crucible test lost nearly 18 mil at the neck (as compared to 3.5 mil loss in Test 5 with the identical starting glass) and the Cr_2O_3 content in the reacted glass almost doubled. No salt layer was observed after the open crucible test due to the loss of about 100% of the Cl and about 50% of the SO_3 after 7 days at 1150ºC.

Representative SEM images of Inconel 690 coupons after 7-day closed crucible corrosion tests are shown in Figure 4.1. A schematic diagram of a typical metal coupon after corrosion testing is provided in Figure 2.6 in which the neck, half-down, and bottom locations are identified. In order to expose possible edge damage, another section perpendicular to the long axis was made above the half-down location; the SEM images acquired for that location are labeled "edge". The results from assessment of the metal corrosion damage based on SEM images and EDS analysis are summarized in Table 4.5. The internal oxidation and structural damage of Inconel 690 are typically reflected in the grain boundary damage and selective depletion of chromium from the interior of the alloy. Grain boundary damage, as revealed by SEM, is generally evident with numerous pitted pockets near the surface and the development of occlusions of oxide phases up to several hundred microns from the remaining surface of the coupon (Figure 4.1). The depletion of chromium from Inconel 690 was identified from SEM/EDS point analyses that were collected at the neck, half-down, and bottom locations perpendicular to the coupon surface. As shown in Figure 4.2 and summarized in Table 4.5, the Inconel 690 coupon could lose most of its constituent chromium near the alloy surface, with the depleted region being up to 400 microns deep. The Cr concentration in Ni-Cr alloys is a critical parameter for corrosion resistance of the metal under high temperature oxidizing conditions. The metal corrosion rate accelerates significantly once its chromium concentration drops below a critical value (~20 wt%), often leading to catastrophic failure of the metal component.

The depths of the Cr depletion and grain boundary damage from SEM/EDS analysis are presented in Table 4.5 to facilitate association with changes in SO_3 and Cl. Against the baseline Test LA20-1 (SO_3=0 wt% and Cl=0 wt%), an increase in SO_3 alone resulted in deeper Cr depletion and grain boundary damage (Test LA20-4, SO_3=0.7 wt%, Cl=0 wt%) and an increase in Cl alone also resulted in deeper Cr depletion and grain boundary damage (Test LA20-2, SO_3=0 wt%, Cl=0.8 wt%). Moderate increases in both SO_3 and Cl from the baseline resulted in metal damage that was intermediate between those observed in Test LA20-1 and Tests LA20-2 and LA20-4. It is noted that even though a separate salt phase was observed after corrosion Tests LA20-3 and LA20-4, SEM/EDS did not identify a nickel sulfide phase. However, at the high S and high Cl concentrations of Test LA20-5, drop-shaped Ni-sulfide, Sn/Ni-sulfide, and even Sn/Ni alloy were widely present near the metal surface (Figure 4.1e). SEM/EDS indicated much enhanced Cr depletion (up to 450 microns) and deeper grain boundary damage (up to 300 microns). The Cr content near the Test 5 alloy surface was 7%, 17%, and 9% at the neck, half-down, and bottom locations, respectively. In comparison, the Cr content near the Test 1 alloy surface was 21%, 25%, and 25%, respectively (Table 4.4). The Cr contents at these locations for the other three coupons from the closed crucible tests were between 10 to 20 wt%. The results suggest that high sulfate concentration, either alone or in combination with high chloride

concentration, promoted the formation of nickel sulfide, which caused extensive chromium depletion and internal structural damage.

Analysis of metal coupons after Test LA20-2 and Test LA20-5 with high chloride glasses identified interior degradation that was distinct from that observed in Cl-free tests. As shown in images 4 and 11 of Figure 4.1b (Test LA20-2) and images 3, 5, 12, and 14, of Figure 4.1e (Test LA20-5), extensive alteration occurred along the grain boundary area with the reactions creating abundant chromium oxide and rendering the remaining alloy rich in nickel. The alteration progressed to such an extent that the remnant alloy was reshaped into sphere-like nodules. However the Ni alloy would not be molten at the test temperature even without any chromium. Therefore the formation of these spherical alloy nodules must result from gradual depletion and reshaping instead of melting. As shown below in the results from ORPLE12 tests, the enhanced grain boundary damage exemplified by excessive chromium loss, nickel enrichment, and reshaping of the alloy is very likely influenced by high chloride concentrations. Considering the high vapor pressure of many metal chlorides at the test temperature, voids would have formed as metal chlorides volatilized.

In open crucible conditions, Inconel 690 in contact with ORPLA20 resulted in very different damage (Figure 4.1f). A thick and porous zone of chromium oxide grew out from the metal surface with deep grain boundary oxidization up to 700 microns deep. Similarly, chromium depletion is more than 600 microns deep (Table 4.4, Figure 4.2). Moreover, the neck dimension loss is nearly 18 mil, which is five times the neck loss of Test LA20-5 with the identical starting glass composition (Tables 4.4 and 4.5). The Cr_2O_3 content in the glass doubled after 7 days corrosion; however, no nickel sulfide or Ni-enriched nodules were identified in SEM/EDS analysis (Table 4.3). The extensive chromium oxide growth and large increase in glass Cr_2O_3 content suggests that oxidization is probably the main attack mode in the open crucible tests.

4.2 Inconel Corrosion in ORPLE12

Glass contact corrosion of Inconel 690 was tested in ORPLE12 formulations with five different SO_3 and Cl concentrations, as listed in Table 4.1. The open crucible tests and the closed crucible tests with Cl-free glass samples used a Zirmul cover. The closed crucible tests with Cl-bearing glasses used a platinum protection sheet.

The ORPLE12 formulation was developed for high-sulfate Hanford LAW; the glass has intermediate sodium content and includes Li_2O, CaO, and V_2O_5 additives to improve sulfate solubility. As listed in Table 4.1, five glasses with varied SO_3 and Cl in the ORPLE12 base formulation were tested. The test conditions and the results from visual inspection of the reacted glass samples are summarized in Table 4.2. The glass appeared crystal-free after open crucible tests; however, trace spinel crystallization was observed in four of five glass samples after the closed crucible tests. The glass after Test 2 was opaque and the Pt/Au crucible was damaged but glass was retained within the damaged crucible (Figure 4.3). No salt layer formed on the surface of the reacted glass for any of the six tests. Occasionally, glass contained fragments of oxide scale that had spalled off the metal surface. Care was taken to avoid these inclusions when

selecting glass samples for XRF analysis. Although it is impossible to avoid completely the crystalline spinel suspended in glass, XRD analysis of the six glass samples (five from the closed crucible tests, one from the open crucible test) did not detect any crystalline phases. The XRF analyses of glasses before and after metal corrosion experiments are listed in Table 4.3.

As listed in Tables 4.4 and 4.6, the dimensional changes of the Inconel 690 coupons do not show clear trends with sulfate or chloride concentrations. Neck loss values are similar for Tests LE12-1, LE12-2 and LE12-4. As observed in ORPLA20 tests, the Cr_2O_3 content after five closed crucible tests did not correlate with the neck dimension loss value, as is evident by comparing the results for closed crucible Test LE12-4 and the open crucible test, both of which were Cl-free and SO_3-rich. However, the neck loss for the open crucible test is 10 mil while the neck loss for the closed crucible test with the identical starting glass is only 4 mil. The Cr_2O_3 content in both reacted glasses decreased slightly and are virtually identical.

Representative SEM images of Inconel 690 test coupons in the five variations of the ORPLE12 base formulation are shown in Figure 4.4. An assessment of the metal corrosion damage based on SEM images and EDS analysis is summarized in Tables 4.4 and 4.6. The depletion of chromium from Inconel 690 was identified from the SEM/EDS point analyses that were collected at the neck, half-down, and bottom locations perpendicular to the coupon surface. As shown in Figure 4.5 and summarized in Table 4.6, the Inconel 690 coupon often lost most of its constituent chromium near the surface with the depleted region extending up to 400 microns deep (600 microns deep for Test LE12-2). As explained earlier, the Cr concentration in Inconel 690 alloys is one of the critical factors for Ni/Cr alloys to resist corrosion in high temperature oxidizing conditions. The metal corrosion rate accelerates significantly once its chromium concentration drops below a critical value (~20 wt%), often leading to catastrophic failure of the metal component. The depths of the Cr depletion and grain boundary damage from SEM/EDS analysis are shown in Table 4.6 to facilitate association with changes in the starting SO_3 and Cl concentrations.

Against the baseline Test LE12-1 (S=0 wt% and Cl=0 wt%), an increase in SO_3 alone resulted in slightly deeper Cr depletion at the neck region and more extensive grain boundary damage in all three regions (Test LE12-4, SO_3=1.25 wt%, Cl=0 wt%). SEM/EDS identified droplets of Ni-sulfide near the bottom of the metal coupon (Figure 4.4d). An increase in Cl alone resulted in a doubling of the depth of Cr depletion at the half-down region, and multi-fold increases in grain boundary damage at all three locations (Test LE12-2, SO_3=0 wt%, Cl=0.4 wt%). SEM/EDS identified the development of Ni-enriched nodules of various sizes near the surface of the Inconel alloy (Images 3, 7, 9, 10, and 14 of Figure 4.4b). Similar Ni-enriched nodules were observed in the Inconel 690 alloy after two Cl-added corrosion tests with ORPLA20. The nodules are typically Ni-rich, ranging from moderately enriched to nearly pure nickel metal. As discussed in Section 4.1, the Ni-enriched nodule must have originated from the Inconel 690. The nickel metal thus formed, could have reacted with the Pt/Au crucible during the tests and caused the crucible damage observed in Test LE12-2 (Figure 4.3).

A moderate increase in SO_3 and Cl from the baseline Test LE12-1 to Test LE12-3 did not worsen the alloy damage significantly. However, for Test LE12-5 with high-SO_3 and high-Cl, both Cr depletion (400-440 microns) and grain boundary damage (300 microns) increased

considerably. Again, SEM/EDS identified Ni sulfide and Ni-enriched nodules of various sizes along the grain boundaries of the Inconel alloy (Figure 4.4). Common for all four high-Cl glasses (Tests LA20-2 and LA20-5 for OPRLA20, and LE12-2 and LE12-5 for ORPLE12), surface chromium loss was not severe, but grain boundary damage was deep and extensive. The reactions between the Cl-bearing glass melts and the Inconel 690 alloy resulted in characteristic metal nodules of various sizes. The often spherical Ni-enriched alloy nodules appeared similar to the drops of nickel sulfide (images 4, 5, 10, 13, 14, 15, and 16 of Figure 4.4e). However, even with low chromium content, Ni-Fe-Cr alloys would not melt at 1150ºC. A careful examination of the Ni-enriched nodules indicated that the Ni content generally increased and the shape became more rounded as the size of the nodules decreased. Without exception, the presence of these Ni-enriched nodules was accompanied with growth of chromium oxide. The formation of Ni-enriched alloy nodules and chromium oxide carved bay-like areas along the grain boundaries in the alloy. It is not surprising that such interior alteration would have weakened the alloy structure and resulted in deeper Cr depletion.

As stated earlier, the stability of the Inconel 690 alloy depends largely on its chromium content and the alloy becomes significantly more susceptible to corrosion damage as its chromium concentration drops below about 20 wt%. The Cr content at the alloy surface after baseline Test LE12-1 is 19%, 19% and 21% at the neck, half-down, and bottom locations, respectively. However, after Test LE12-4 in the high SO_3 glass, the Cr content at the alloy surface decreased to 4%, 5%, and 20%, respectively (Tables 4.4 and 4.6). The excessive chromium loss is associated with the formation of Ni sulfide (images 8 and 9 of Figure 4.4d). In comparison, the Cr content at the alloy surface in two SO_3-free formulations (Tests 1 and 2) was between 19% and 21 wt%, even though deep and extensive metal damage was observed in Test 2 with the high-Cl formulation. The Cr content at the alloy surface for the two other S-bearing formulations (Tests 3 and 5) was between 14 and 20 wt% (Tables 4.4 and 4.6). The results indicate that high sulfate concentration and, in particular, formation of nickel sulfide (Tests LE12-4 and LE12-5), cause extensive chromium depletion on the surface and deep inside the Ni-Cr alloy as well as significant dimension loss. In contrast, chlorine degraded the structural integrity of the alloy via grain boundary attack, which tended to cause deep and extensive interior chromium loss, instead of massive surface Cr depletion.

In open crucible tests, Inconel 690 in direct contact with ORPLE12 resulted in different damage characteristics (Figure 4.4f) with pronounced grain boundary oxidization up to 200 microns deep. Similarly, chromium depletion was around 360 microns deep (Table 4.4, Figure 4.5). Moreover, as with ORPLA20, neck dimension loss in open crucible tests was more than double that for Test LE12-4 with identical starting glass composition (10 mil vs, 4 mil, Tables 4.4 and 4.6). However, the Cr_2O_3 content in the glass after 7 days of corrosion was similar to that for Test LE12-4 (Table 4.3).

4.3 Inconel 690 Corrosion Mode in Cl and SO_3-Bearing LAW Glasses

Inconel 690 corrosion test data from the closed crucible experiments with two LAW formulations allowed for identification of the characteristic attack modes of sulfate and chloride-rich LAW melts on Inconel 690.

In the standard open crucible corrosion tests that have been conducted previously, oxidization and subsequent dissolution/disintegration of the alloy is the common mode of attack. However, Cl and S are lost in such tests due to their high volatility. The Inconel 690 corrosion test results from the present closed crucible tests thus provide important data to evaluate the Cl and S attack modes for LAW glasses.

Nickel sulfide can form from the reaction between S-rich LAW glass melts and the Inconel 690 alloy. Once formed as a separate phase, molten nickel sulfide can cause serious damage to the alloy. At sufficiently high sulfur concentrations in the molten glass, even within an oxidizing atmosphere, nickel sulfide can nevertheless form due to local reduction as key Inconel components such as Cr are oxidized via interaction with molten glass. Due to the low melting temperature and strong affinity for sulfur, large amounts of nickel can dissolve in nickel sulfide melts (more than 80 wt% Ni at 1150ºC [26]). Therefore, considerable amounts of nickel can be extracted from the Ni-Cr alloy into the sulfide melt, resulting in disintegration of the alloy matrix near the Inconel surface. Nickel sulfide was observed to form in the closed crucible tests with both the ORPLA20 (Test LA20-5) and the ORPLE12 (Tests LE12-4 and LE12-5) formulations at the highest SO_3 concentrations. Typically, nickel sulfide was present as spherical drops of various sizes within the glass adjacent to the metal surface. Formation of nickel sulfide resulted in serious structural damage and chromium depletion near the metal surface. Judged by total chromium loss estimated from the Cr concentration profile near the surface, Test LA20-5 with ORPLA20 showed the greatest chromium loss from the metal (at the neck, half-down, and bottom locations) among the five closed crucible tests with ORPLA20. Both Ni-sulfide and Ni-enriched nodules formed (Table 4.7). Similarly, Test LE12-4 with ORPLE12 showed the greatest chromium loss (at neck and half-down locations), or second greatest loss (bottom location) from Inconel 690 among the five closed crucible tests with ORPLE12. Again, Ni-sulfide formation was observed (Table 4.8). Test LE12-5 with ORPLE12 showed the second most chromium loss (neck, bottom, excluding the open crucible test), or third greatest loss (half down), from the metal among the five closed crucible tests with ORPLE12. Ni-sulfide and Ni-enriched nodules formed in Test LE12-5 (Table 4.8).

The damage to Inconel 690 caused by Cl can be inferred from the association between chloride concentration in the host glass and the characteristic grain boundary attack observed only in reacted metal coupons from tests with Cl-rich glasses. However, no direct evidence was obtained to prove the involvement of chlorine in the corrosion attack on Inconel 690. This is probably due to the highly volatile nature of metal chlorides at the test temperature, such that no chloride was identified within the damaged Inconel alloy. Development of nickel-enriched nodules and the accompanying chromium oxide band within the grain boundaries constitute serious damage to the alloy. At sufficiently high chloride concentrations, Inconel develops interior structural damage typically along grain boundaries with wider and deeper penetration and more extensive Cr depletion [4]. SEM/EDS analysis indicated that the progress of such grain boundary attack would reform the Inconel 690 alloy with progressively higher nickel content in smaller and more rounded nodules. The reaction carved bay-like areas (projected to two dimensions, as shown in SEM images) featuring thick bands of chromium oxide adjacent to Cr-depleted alloy with numerous Ni-enriched nodules further away from the recessed alloy along the grain boundary. Contact of these Ni-enriched alloy nodules with the Pt/Au crucible likely caused the crucible damage observed in Test LE12-2 with the ORPLE12 formulation. Reaction

along the Inconel 690 grain boundaries inevitably damaged the metal structure and promoted chromium loss through the enlarged grain boundaries.

Judged by total chromium loss from the Cr concentration profile, the Inconel 690 coupon from Test LA20-2 with ORPLA20 (high Cl alone) lost more chromium from the metal (at the neck, half-down and bottom locations) than the baseline Test LA20-1 with the S and Cl-free base glass (Table 4.7). The Inconel coupon from Test LE12-2 with ORPLE12 has the highest chromium loss at the half-down and bottom locations of all the test coupons for the ORPLE12 formulation (Table 4.8, Figure 4.5). The nearly flat Cr concentration profile up to 400 microns in the half-down region is distinctly different from the typical diffusion-controlled loss profile [27], suggesting a different transport mode for chromium and oxygen through the alloy (Figure 4.5). The results from SEM/EDS analysis indicated a different attack mode by Cl-rich glasses in all four closed crucible tests (Tests LA20-2 and LA20-5 for ORPLA20, and LE12-2 and LE12-5 for ORPLE12). Although the enhanced metal damage along the grain boundaries did not result in as much surface chromium loss as that for S-rich glasses via formation of nickel sulfide, the deep-reaching Cr depletion caused by Cl-rich LAW glass melts results in a significantly degraded alloy structure.

4.4 Summary and Conclusions from Inconel 690 Corrosion Tests

Inconel corrosion in LAW glass was investigated at five different Cl and SO_3 concentrations for two representative LAW glasses at the typical melter processing temperature. The closed crucible test setup was able to retain highly volatile sulfur and chlorine species over the duration of the Inconel 690 corrosion tests.

The test results indicate that the test conditions using the closed crucible method differed somewhat from those for the open crucible method beyond the compositional change caused by Cl/SO_3 volatilization. In particular, the test results indicate that the conditions are much more oxidizing in the open crucible tests and much more reducing in the closed crucible tests; obviously, the Inconel 690 coupon itself provides the source of reductants. Therefore the Inconel 690 corrosion rates from the two test conditions may not be directly comparable and comparisons of glass composition effects should be made only within a given test type. Generally, Inconel 690 exhibited greater dimensional loss and internal structural damage in the open crucible tests. However, retention of the volatile Cl and SO_3 necessitated tests in the closed crucible setup.

The dimension loss of Inconel 690 coupons and the change in Cr_2O_3 content of the reacted glasses, although commonly useful for evaluation of metal corrosion, did not fully capture the characteristic attack by sulfur and chlorine that was observed, and thus were not used as the main indicators for metal damage in S/Cl-rich LAW melts. No consistent trend in these parameters was evident, probably due to complications from spinel crystallization and the presence of sulfate/chloride salt (persistent or transient) and metal sulfides. Therefore, the Cr concentration in the alloy, and associated depletion profiles, provided a better defined and likely more reliable indicator of metal damage. Among the five S and Cl concentrations examined, the

S and Cl-free base formulation (Tests LA20-1 and LE12-1) consistently showed the least damage.

Molten nickel sulfide can form when sulfur is present in the glass, and is extremely detrimental since it can extract Ni from Inconel, disrupting the alloy matrix and depleting Cr greatly, both on the alloy surface and to substantial depths inside. Test LA20-5 with ORPLA20 and Test LE12-4 with ORPLE12, both showed Ni sulfide drops and ranked worst for damage among their corresponding group of five S/Cl variations. In Cl-rich glasses, development of Ni-enriched nodules within the grain boundaries was also found to result in significant degradation of Inconel 690, with the enlarged grain boundaries facilitating material transport and deeper alteration. This is particularly evident from Test LE12-2 with ORPLE12 at the half-down and bottom locations (Figure 4.5). The overall damage ranked by Cr depletion is second only to that for the S-rich test with ORPLE12 and is worse in the bottom area for ORPLE12. Therefore, the addition of either S or Cl or both can significantly affect the type and extent of corrosion damage to Inconel 690. It should be noted, however, that these effects are likely also sensitive to the prevailing redox conditions. Consequently, additional studies to examine the effects of S and Cl under the more oxidizing conditions that are typical of the WTP melter systems would be useful. This presents challenges for the experimental design since in the closed test systems required to retain the volatile S and Cl species, the metal alloy drives the redox towards reducing conditions.

SECTION 5.0
REFERENCES

[1] "Corrosion of K-3 Refractory and Metal Alloys in RPP-WTP LAW Glasses," H. Gan, X.D. Lu, I. Vidensky, C. Paul, and I.L. Pegg, Final Report, VSL-01R3540-1, Vitreous State Laboratory, The Catholic University of America, Washington, DC, March 2001.

[2] Electrical Corrosion of Inconel 690 Electrode Materials for Radioactive Waste Glass Melters," H. Gan, L. Fu, F. Perez-Cardenas, A.C. Buechele, R.K. Mohr, I.L. Pegg, and P.B. Macedo, Corrosion of Materials by Molten Glass, Eds. G. Pecoraro, J. Marra, and J. Wenzel, *Ceramic Transactions*, vol. 78, p. 327, (1996).

[3] "LAW High Temperature Materials Assessment," I. Vidensky, M. Chaudhuri, H. Gan, G. Diener, L. Andre, R. K. Mohr, and I. L. Pegg, Final Report, VSL-04R4950-1, Rev. 0, Vitreous State Laboratory, The Catholic University of America, Washington, DC, January 15, 2005.

[4] "Corrosion of Inconel-690 Electrodes in Waste Glass Melts," H. Gan, A.C. Buechele, C.-W. Kim, X. Huang, R.K. Mohr and I.L. Pegg, Mat. Res. Soc. Symp. Proc. **556** (1998).

[5] "RPP Pilot Melter Bubbler Life Extension Test Results Report," TRR-PLT-061 Rev. 0, Duratek, Inc., December 19, 2003.

[6] "Corrosion Testing of Bubbler Materials for LAW Vitrification," I. Vidensky, H. Gan, R.K. Mohr, and I.L. Pegg, Final Report, VSL-04R4430-1, Rev. 0, Vitreous State Laboratory, The Catholic University of America, Washington DC, July 20, 2004.

[7] "Glass Formulation and Testing with TWRS LAW Simulants," Final Report to Duratek Inc. and BNFL Inc., I.S. Muller and I.L. Pegg, Vitreous State Laboratory, The Catholic University of America, Washington, DC, January 16, 1998.

[8] "Glass Formulation And Testing With RPP-WTP LAW Simulants," I.S. Muller, A.C. Buechele, and I.L. Pegg, Final Report, VSL-01R3560-2, Vitreous State Laboratory, The Catholic University of America, Washington, DC, February 23, 2001.

[9] "Baseline LAW Glass Formulation Testing," I.S. Muller and I.L. Pegg, Final Report, VSL-03R3460-1, Rev. 0, Vitreous State Laboratory, The Catholic University of America, Washington, DC, August 8, 2003.

[10] "Glass Formulations to Support Melter Testing", I.S. Muller and I.L. Pegg, Final Report, VSL-03R3460-2, Rev. 0, Vitreous State Laboratory, The Catholic University of America, Washington, DC, February 6, 2004.

[11] "Glass Formulation Testing to Increase Sulfate Incorporation," K. S. Matlack, M. Chaudhuri, H. Gan, I.S. Muller, W. Gong, and I.L. Pegg, Final Report, VSL-04R4960-1, Rev. 0, Vitreous State Laboratory, The Catholic University of America, Washington, DC, February 28, 2005.

[12] "Glass Formulation Testing to Increase Sulfate Volatilization from Melter," K.S. Matlack, W. Gong, and I.L. Pegg, Final Report, VSL-04R4970-1, Rev. 0, Vitreous State Laboratory, The Catholic University of America, Washington, DC, February, 24 2005.

[13] "LAW Envelope C Glass Formulation Testing to Increase Waste Loading," K.S. Matlack, W. Gong, I.S. Muller, I. Joseph, and I.L. Pegg, Final Report, VSL-05R5900-1, Rev. 0, Vitreous State Laboratory, The Catholic University of America, Washington, DC, January 27, 2006.

[14] "LAW Envelope A and B Glass Formulation Testing to Increase Waste Loading," K.S. Matlack, H. Gan, I.S. Muller, I. Joseph, and I.L. Pegg, Final Report, VSL-06R6900-1, Rev. 0, Vitreous State Laboratory, The Catholic University of America, Washington, DC, March 23, 2006.

[15] "Enhanced LAW Glass Formulation Testing," K.S. Matlack, I. Joseph, W. Gong, I.S. Muller, and I.L. Pegg, Final Report, VSL-07R1130-1, Rev. 0, Vitreous State Laboratory, The Catholic University of America, Washington, DC, October 5, 2007.

[16] "Glass Formulation Development and DM10 Melter Testing with ORP LAW Glasses," K.S. Matlack, I. Joseph, W. Gong, I.S. Muller, and I.L. Pegg, Final Report, VSL-09R1510-2, Rev. 0, Vitreous State Laboratory, The Catholic University of America, Washington, DC, June 12, 2009.

[17] "Waste Loading Enhancements for Hanford LAW Glasses," I.S. Muller, K.S. Matlack, H. Gan, I. Joseph, and I.L. Pegg, Final Report, VSL-10R1790-1, Rev. 0, Vitreous State Laboratory, The Catholic University of America, Washington, DC, December 1, 2010.

[18] "Corrosion Testing of Inconel and K-3 in LAW Glass," H. Gan and I. L. Pegg, VSL-16T4240-1, Rev. 0, Vitreous State Laboratory, The Catholic University of America, Washington, DC, July 28, 2016.

[19] "Quality Assurance Project Plan for ORP/ RPP-WTP Support Activities Conducted by VSL," Vitreous State Laboratory, QAPP-ORP, Rev. 6, Vitreous State Laboratory, The Catholic University of America, Washington, DC, September 14, 2016.

[20] "Master List of Controlled VSL Manuals and Standard Operating Procedures in Use," QA-MLCP, Rev. 155, Vitreous State Laboratory, The Catholic University of America, Washington, DC, June 19, 2017.

[21] "Effect of Minor Components on Salt Formation," H. Gan, Z. Feng, A.E. Papathanassiu and I.L. Pegg, Final Report, VSL-15R3550-1, Rev. 0, Vitreous State Laboratory, The Catholic University of America, Washington, DC, December 22, 2015.

[22] "Melter Tests to Define LAW Halide, Chromium and Phosphate Concentrations," K.S. Matlack, I.S. Muller, I. Joseph, and I.L. Pegg, Final Report, VSL-14R3070-1, Rev. 0, Vitreous State Laboratory, The Catholic University of America, Washington, DC, February 21, 2014.

[23] "Melter Tests to Define LAW Halide Concentrations, Phase 2," K.S. Matlack, H. Gan, Z. Feng, I.S. Muller, I. Joseph, and I.L. Pegg, Final Report, VSL-14R3280-1, Rev. 0, Vitreous State Laboratory, The Catholic University of America, Washington, DC, December 30, 2014.

[24] "Standard Test Method for Isothermal Corrosion Resistance of Refractories to Molten Glass," ASTM C 621-09, American Society for Testing and Materials, West Conshohocken, PA, 2009.

[25] "Management of High Sulfur HLW," K.S. Matlack, W. Kot, H. Gan, Z. Feng, I.L. Pegg and I. Joseph, Final Report, VSL-13R2920-1, Rev. 0, Vitreous State Laboratory, The Catholic University of America, Washington, DC, October 31, 2013.

[26] "Phase Diagrams for Ceramists," Volume II (Figure 3951), the American Ceramic Society, Inc. (1969).

[27] "Inconel 690 Corrosion in WTP HLW Glass Melts Rich in Aluminum, Bismuth, Chromium or Aluminum/Sodium," Z. Feng, H. Gan and I.L. Pegg, Final Report VSL-08R1370-1, Rev. 0, Vitreous State Laboratory, The Catholic University of America, Washington, DC, September 23, 2008.

Table 2.1. ORPLA20 and ORPLE12 Glass Compositions Used in Melter Tests (wt%).

Component	ORPLA20 [16]	ORPLE12 [15]
Al_2O_3	6.65	7.58
B_2O_3	8.74	9.82
CaO	3.32	10.02
Cr_2O_3	0.50	0.50
Cs_2O[(a)]	-	0.15
Fe_2O_3	0.19	0.24
K_2O	0.53	0.55
Li_2O	-	2.49
MgO	0.92	1.04
Na_2O	24.00	16.00
SiO_2	42.33	41.27
SnO_2	2.74	-
TiO_2	-	0.01
V_2O_5	-	1.74
ZnO	2.74	3.21
ZrO_2	5.96	3.53
Cl	0.67	0.02
F	0.00	0.20
P_2O_5	0.00	0.12
SO_3	0.70	1.50
SUM	100.0	100.0

– Empty data field
(a) Cs_2O that was added as a spike in melter tests was removed for the present tests.

Table 2.2. Test Matrix for Closed Crucible K-3 Refractory Corrosion Tests.

Test Number	Material	Glass ID	Temperature	Test Duration	SO_3 (wt%)*	Cl (wt%)*
LA20K-1	K-3 Refractory	ORPLA20	1208°C	6 days	0.00	0.00
LA20K-2	K-3 Refractory	ORPLA20	1208°C	6 days	0.00	0.80
LA20K-3	K-3 Refractory	ORPLA20	1208°C	6 days	0.70	0.00
LA20K-4	K-3 Refractory	ORPLA20	1208°C	6 days	0.70	0.67
LE12K-1	K-3 Refractory	ORPLE12	1208°C	6 days	0.00	0.00
LE12K-2	K-3 Refractory	ORPLE12	1208°C	6 days	0.00	0.40
LE12K-3	K-3 Refractory	ORPLE12	1208°C	6 days	1.25	0.02
LE12K-4	K-3 Refractory	ORPLE12	1208°C	6 days	1.00	0.40

* Target concentration.

Table 2.3a. Test Matrix for Open Crucible Inconel 690 Corrosion Tests.

Test Number	Material	Glass ID	Temperature	Test Duration	SO_3 (wt%)*	Cl (wt%)*
LA20-A	Inconel 690	ORPLA20	1150°C	7 days	0.70	0.67
LE12-A	Inconel 690	ORPLE12	1150°C	7 days	1.25	0.02

* Target concentration.

Table 2.3b. Test Matrix for Closed Crucible Inconel 690 Corrosion Tests.

Test Number	Material	Glass ID	Temperature	Test Duration	SO_3 (wt%)*	Cl (wt%)*
LA20-1	Inconel 690	ORPLA20	1150°C	7 days	0.00	0.00
LA20-2	Inconel 690	ORPLA20	1150°C	7 days	0.00	0.80
LA20-3	Inconel 690	ORPLA20	1150°C	7 days	0.35	0.40
LA20-4	Inconel 690	ORPLA20	1150°C	7 days	0.70	0.00
LA20-5	Inconel 690	ORPLA20	1150°C	7 days	0.70	0.67
LE12-1	Inconel 690	ORPLE12	1150°C	7 days	0.00	0.00
LE12-2	Inconel 690	ORPLE12	1150°C	7 days	0.00	0.40
LE12-3	Inconel 690	ORPLE12	1150°C	7 days	0.50	0.20
LE12-4	Inconel 690	ORPLE12	1150°C	7 days	1.25	0.02
LE12-5	Inconel 690	ORPLE12	1150°C	7 days	1.00	0.40

* Target concentration.

Table 3.1. Method Evaluation of Closed Crucible K-3 Corrosion Tests.

Stage	Containment Method	Vapor Isolation	Experimental Problem	Indicators	Failure Caused By	Solution	Impact to K-3 Corrosion
Stage One	Quartz crucible with Zirmul cover	Zirmul	Loss of Cl and SO_3	Loss of majority of Cl and SO_3	Difficulty in sealing irregular-shaped quartz crucible	Replace quartz crucible by alumina crucible	Similar to open crucible corrosion
Stage Two	High purity alumina crucible with alumina cover	Zirmul	Na_2O loss and SiO_2 gain	Significant loss in Na_2O and gain in SiO_2	Reaction between Cl-rich vapor and Zirmul cover	Add Pt sheet for isolation of Cl-rich vapor from Zirmul cover	Suppression of K-3 corrosion
Stage Three	High purity alumina crucible with alumina cover	Pt Sheet	Acceptable	NA	NA	NA	Acceptable

Table 3.2a. XRF Analysis (wt%) of ORPLA20 Glasses from Stage 1 K-3 Corrosion Tests.

Test Date	10/28/16-11/03/16			10/28/16-11/03/16			11/22/16-11/28/16			4/12/17-4/18/17				10/28/16-11/03/16			8/10/16-8/16/16		
Test ID	LA20-1s			LA20-2s1			LA20-2s2			LA20-2s3				LA20-3s			LA20-4s		
Test Condition	Semi-sealed in fused silica crucible			Semi-sealed in fused silica crucible			Semi-sealed in fused silica crucible			Semi-sealed in alumina crucible with Pt sheet				Semi-sealed in fused silica crucible			Semi-sealed in fused silica crucible		
Sample ID	A20-Cl0S0		A20-CLP0S0-K3G	A20-ClP8S0		A20-CLP8S0-K3G	A20-ClP8S0		A20-CLP8S0-K3GR	A20-CLP8S0R		A20-CLP8S0R-K3G	A20-CLP8S0R-K3G-W	A20-Cl0Sp7		A20-CL0SP7-K3G	ORPLA20		ORPLA20-K3GR
Data Type	Target	XRF		Target	XRF		Target	XRF		Target	XRF			Target	XRF		Target	XRF	
Sample History	Before		After	Before		After	Before		After	Before		After		Before		After	Before		After
Al_2O_3	6.65	6.50	8.25	6.65	6.81	8.29	6.65	6.81	8.37	6.65	7.14	8.47	8.68	6.65	6.83	8.44	6.69	6.07	8.55
B_2O_3#	8.74	8.74	8.74	8.74	8.74	8.74	8.74	8.74	8.74	8.74	8.74	8.74	8.74	8.74	8.74	8.74	8.73	8.73	8.73
CaO	3.32	3.39	3.35	3.32	3.55	3.54	3.32	3.55	3.60	3.32	3.43	3.50	3.54	3.32	3.42	3.49	3.32	3.55	3.38
Cr_2O_3	0.50	0.47	0.66	0.50	0.54	0.69	0.50	0.54	0.57	0.50	0.47	0.67	0.67	0.50	0.46	0.76	0.50	0.66	0.62
Fe_2O_3	0.19	0.23	0.39	0.19	0.23	0.33	0.19	0.23	0.40	0.19	0.23	0.38	0.40	0.19	0.23	0.38	0.19	0.28	0.44
K_2O	0.53	0.54	0.45	0.53	0.54	0.45	0.53	0.54	0.42	0.53	0.51	0.54	0.54	0.53	0.52	0.44	0.54	0.53	0.47
Li_2O#	0.00	0.00	0.00	0.00	0.00	0.00	0.00	0.00	0.00	0.00	0.00	0.00	0.00	0.00	0.00	0.00	0.00	0.00	0.00
MgO	0.92	0.91	0.96	0.92	0.81	0.96	0.92	0.81	0.95	0.92	0.94	0.99	0.96	0.92	0.89	0.99	0.92	0.94	0.92
Na_2O	24.00	23.94	21.44	24.00	22.78	20.05	24.00	22.78	19.83	24.00	23.20	21.25	21.32	24.00	24.19	21.64	24.00	23.23	20.58
P_2O_5	0.00	0.01	0.02	0.00	0.01	0.03	0.00	0.01	0.03	0.00	0.02	0.02	0.02	0.00	0.02	0.02	0.00	0.01	0.02
SiO_2	43.71	43.36	44.85	42.91	43.25	45.68	42.91	43.25	45.33	42.91	44.24	44.80	44.22	43.01	42.90	44.14	42.30	43.10	44.74
SnO_2	2.74	2.71	2.42	2.74	2.66	2.68	2.74	2.66	2.72	2.74	2.15	2.31	2.39	2.74	2.38	2.41	2.74	2.76	2.63
TiO_2	0.00	0.04	0.05	0.00	0.05	0.05	0.00	0.05	0.06	0.00	0.05	0.06	0.05	0.00	0.03	0.04	0.00	0.00	0.03
V_2O_5	0.00	0.00	0.00	0.00	0.00	0.00	0.00	0.00	0.00	0.00	0.00	0.00	0.00	0.00	0.00	0.00	0.00	0.00	0.00
ZnO	2.74	2.81	2.52	2.74	2.86	2.51	2.74	2.86	2.63	2.74	2.59	2.43	2.47	2.74	2.64	2.38	2.74	2.86	2.49
ZrO_2	5.96	6.17	5.78	5.96	6.27	5.86	5.96	6.27	6.15	5.96	5.55	5.63	5.79	5.96	5.79	5.64	5.95	5.94	5.75
Cl	0.00	0.01	0.00	0.80	0.73	0.01	0.80	0.73	0.01	0.80	0.58	0.04	0.04	0.00	0.00	0.00	0.68	0.63	0.01
SO_3	0.00	0.03	0.02	0.00	0.03	0.02	0.00	0.03	0.02	0.00	0.03	0.02	0.03	0.70	0.77	0.33	0.70	0.39	0.30
SUM	100.00	99.85	99.87	100.00	99.84	99.87	100.00	99.84	99.82	100.00	99.87	99.85	99.85	100.00	99.81	99.82	100.00	99.68	99.66
K-3 Coupon ID	A20-CLP0S0-K3B**			A20-CLP8S0-K3B**			A20-CLP8S0-K3BR**			A20-CLP8S0R-K3B**				A20-CL0SP7-K3B**			ORPLA20-K3BR*		
Neck Loss	0.048"			0.017"			0.024"			0.027"				0.062"			0.034"		
Half Down Loss	0.0"			EXPANDED			0.002"			EXPANDED				0.002"			0		
Alteration Zone	0.024"			0.016"			0.021"			0.022"				0.023"			0.021"		

*measured under microscope; **measured on scanned image; # Target concentration

Table 3.2b. XRF Analysis (wt%) of ORPLE12 Glasses from Stage One K-3 Corrosion Tests.

Test Date	11/22/16-11/28/16			7/5/17-7/11/17			8/10/16-8/16/16			11/22/16-11/28/16		
Test ID	LE12-1s			LE12-2s			LE12-3s			LE12-4s		
Test Condition	Semi-sealed in fused silica crucible			Semi-sealed in alumina crucible with Pt Cover			Semi-sealed in fused silica crucible			Semi-sealed in fused silica crucible		
Sample ID	E12-CL0S0		E12-CL0SO-K3G	E12-CLP4S0		E12-CLP4S0-NSP-K3G	ORPLE12		ORPLE12-K3GR	E12-CLP4S1		E12-CLP4S1-K3G
Data Type	Target	XRF		Target	XRF		Target	XRF		Target	XRF	
Sample History	Before		After	Before		After	Before		After	Before		After
Al_2O_3	7.58	7.63	9.19	7.58	7.53	9.13	7.58	7.35	9.33	7.58	7.47	9.24
B_2O_3[#]	9.82	9.82	9.82	9.82	9.82	9.82	9.82	9.82	9.82	9.82	9.82	9.82
CaO	10.02	10.58	10.51	10.02	10.83	10.13	10.02	10.95	10.46	10.02	10.47	10.94
Cr_2O_3	0.50	0.55	0.71	0.50	0.60	0.54	0.50	0.68	0.65	0.50	0.56	0.76
Cs_2O	0.15	0.19	0.00	0.15	0.21	0.00	0.15	0.00	0.00	0.15	0.19	0.00
Fe_2O_3	0.24	0.27	0.45	0.24	0.27	0.36	0.24	0.28	0.46	0.24	0.27	0.44
K_2O	0.55	0.54	0.45	0.55	0.54	0.59	0.55	0.58	0.44	0.55	0.53	0.47
Li_2O[#]	2.49	2.49	2.49	2.49	2.49	2.49	2.49	2.49	2.49	2.49	2.49	2.49
MgO	1.04	1.00	1.01	1.04	0.99	1.17	1.04	1.09	1.07	1.04	1.00	1.11
Na_2O	16.00	15.42	13.68	16.00	14.35	13.00	16.00	16.69	14.03	16.00	16.38	14.16
P_2O_5	0.12	0.08	0.11	0.12	0.14	0.14	0.12	0.14	0.14	0.12	0.13	0.12
SiO_2	42.79	42.69	42.89	42.39	42.94	44.44	41.27	41.50	42.39	41.39	40.52	41.47
SnO_2	0.00	0.00	0.00	0.00	0.00	0.01	0.00	0.00	0.00	0.00	0.00	0.00
TiO_2	0.01	0.06	0.07	0.01	0.07	0.06	0.01	0.03	0.04	0.01	0.06	0.08
V_2O_5	1.74	1.84	1.86	1.74	1.84	1.76	1.74	0.00	1.89	1.74	1.83	1.86
ZnO	3.21	3.21	3.05	3.21	3.29	2.72	3.21	3.36	2.90	3.21	3.20	3.12
ZrO_2	3.53	3.51	3.61	3.53	3.63	3.36	3.53	3.48	3.57	3.53	3.62	3.64
Cl	0.00	0.02	0.00	0.40	0.36	0.19	0.02	0.03	0.01	0.40	0.32	0.00
SO_3	0.00	0.03	0.02	0.00	0.03	0.03	1.50	1.24	0.23	1.00	1.05	0.18
SUM	99.79	99.93	99.91	99.79	99.92	99.92	99.79	99.74	99.91	100.00	99.91	99.89
K-3 Coupon ID	E12-CL0S0-K3B**			E12-CLP4S0-NSP-K3B*			ORPLE12-K3BR*			E12-CLP4S1-K3B**		
Neck Loss	0.036"			0.010"			0.030"			0.051"		
Half Down Loss	0.011"			EXPANDED			0.002"			0.005"		
Alteration Zone	0.020"			0.023"			0.023"			0.024"		

*measured under microscope; **measured on scanned image; [#] Target concentration

Table 3.3. Summary of Results of K-3 Refractory Dimension Loss and Composition Change of Glass. Oxide contents are in wt%; ΔCl % and ΔSO_3 % are percentage of loss.

Base Glass	Test ID	Test Number	Agitation method	Seal Condition	Stage	Sample washed (Y/N)	Neck Loss (inch)	Half Down Loss (inch)	Alteration Depth (inch)	Starting Cr_2O_3
ORPLA20	LA20-1s	LA20K-1	Static	Semi-Closed	1	N	0.048	0.000	0.024	0.47
	LA20-1c	LA20K-1	Static	Closed	2	Y	0.000	0.000	0.026	0.47
	LA20-1p	LA20K-1	Static	Closed+Pt	3	Y	0.061	0.000	0.026	0.47
	LA20-2s1	LA20K-2	Static	Semi-Closed	1	N	0.017	0.000	0.016	0.54
	LA20-2s2	LA20K-2	Static	Semi-Closed	1	N	0.024	0.002	0.021	0.54
	LA20-2s3	LA20K-2	Static	Semi-Closed (Pt)	1	N	0.027	0.000	0.022	0.47
	LA20-2c1	LA20K-2	Static	Closed	2	Y	0.005	0.003	0.016	0.54
	LA20-2c2	LA20K-2	Static	Closed (repeat)	2	N	0.016	0.000	0.020	0.47
	LA20-2p	LA20K-2	Static	Closed+Pt	3	Y	0.010	0.001	0.024	0.47
	ORPLA20	NA	Air Bubbled	**Open***	0	N	0.039	0.003	0.026	0.48
	LA20-3s	LA20K-3	Static	Semi-Closed	1	N	0.062	0.002	0.023	0.46
	LA20-3c	LA20K-3	Static	Closed	2	Y	0.033	0.003	0.028	0.46
	LA20-3p	LA20K-3	Static	Closed+Pt	3	Y	0.057	0.002	0.027	0.46
	LA20-4s	LA20K-4	Static	Semi-Closed	1	N	0.034	0.000	0.021	0.66
	LA20-4c	LA20K-4	Static	Closed	2	Y	0.002	0.001	0.020	0.49
	LA20-4p	LA20K-4	Static	Closed+Pt	3	Y	0.006	0.001	0.026	0.49
	LA20-4cb	LA20K-4	***Static, Blank***	Closed	2	Y	NA	NA	NA	0.49
ORPLE12	LE12-1s	LE12K-1	Static	Semi-Closed	1	N	0.036	0.011	0.020	0.55
	LE12-1c	LE12K-1	Static	Closed	2	Y	0.000	0.000	0.029	0.55
	LE12-1p	LE12K-1	Static	Closed+Pt	3	Y	0.037	0.003	0.027	0.55
	LE12-2s	LE12K-2	Static	Semi-Close+Pt	1	N	0.010	0.000	0.023	0.60
	LE12-2c	LE12K-2	Static	Closed	2	Y	0.004	0.001	0.020	0.60
	LE12-2p	LE12K-2	Static	Closed+Pt	3	Y	0.005	0.000	0.026	0.60
	ORPLE12	NA	Air Bubbled	**Open***	0	N	0.031	0.000	0.031	0.63
	LE12-3s	LE12K-3	Static	Semi-Closed	1	N	0.030	0.002	0.023	0.63
	LE12-3c	LE12K-3	Static	Closed	2	Y	0.000	0.000	0.025	0.53
	LE12-3p	LE12K-3	Static	Closed+Pt	3	Y	0.033	0.004	0.027	0.53
	LE12-4s	LE12K-4	Static	Semi-Closed	1	N	0.051	0.005	0.024	0.56
	LE12-4c	LE12K-4	Static	Closed	2	Y	0.002	0.002	0.021	0.56
	LE12-4p	LE12K-4	Static	Closed+Pt	3	Y	0.015	0.000	0.017	0.56

*: Standard open-to-air K-3 corrosion. Data reported previously [15, 16].

Table 3.3. Summary of Results of K-3 Refractory Dimension Loss and Composition Change of Glass. Oxide contents are in wt%; ΔCl % and ΔSO_3 % are percentage of loss (continued).

Base Glass	Test ID	Ending Cr_2O_3	ΔCr_2O_3	Starting Cl	Ending Cl	Δ Cl (%)	Starting SO_3	Ending SO_3	ΔSO_3 (%)	Starting Na_2O	Ending Na_2O
ORPLA20	LA20-1s	0.66	0.19	0.01	0.00		0.03	0.02		23.94	21.44
	LA20-1c	0.43	-0.04	0.01	0.01		0.03	0.04		23.94	22.29
	LA20-1p	0.75	0.29	0.01	0.09		0.03	0.03		23.94	22.09
	LA20-2s1	0.69	0.15	0.73	0.01	-98.37	0.03	0.02		22.78	20.05
	LA20-2s2	0.57	0.04	0.73	0.01	-98.91	0.03	0.02		22.78	19.83
	LA20-2s3	0.67	0.21	0.58	0.04	-93.30	0.03	0.03		23.20	21.32
	LA20-2c1	0.38	-0.16	0.73	0.56	-23.98	0.03	0.04		22.78	17.34
	LA20-2c2	0.50	0.03	0.58	0.52	-10.48	0.03	0.03		23.20	19.62
	LA20-2p	0.48	0.01	0.58	0.62	0.00	0.03	0.03		23.20	19.53
	ORPLA20	0.88	0.40	0.00	0.00		0.59	0.19	-67.97	24.29	23.34
	LA20-3s	0.76	0.29	0.00	0.00		0.77	0.33	-57.22	24.19	21.64
	LA20-3c	0.48	0.01	0.00	0.00		0.77	0.66	-14.56	24.19	22.39
	LA20-3p	0.70	0.23	0.00	0.00		0.77	0.72	-5.98	24.19	22.91
	LA20-4s	0.62	-0.04	0.63	0.01	-98.10	0.39	0.30	-23.92	23.23	20.58
	LA20-4c	0.36	-0.13	0.59	0.42	-28.89	0.72	0.40	-43.99	22.92	17.11
	LA20-4p	0.43	-0.06	0.59	0.47	-19.66	0.72	0.49	-31.28	22.92	20.11
	LA20-4cb	0.38	-0.11	0.59	0.39	-32.99	0.72	0.44	-38.41	22.92	18.13
ORPLE12	LE12-1s	0.71	0.16	0.02	0.00		0.03	0.02		15.42	13.68
	LE12-1c	0.51	-0.05	0.02	0.02		0.03	0.05		15.42	15.24
	LE12-1p	0.67	0.11	0.02	0.01		0.03	0.03		15.42	15.73
	LE12-2s	0.54	-0.06	0.36	0.19	-48.03	0.03	0.03		14.35	13.00
	LE12-2c	0.47	-0.13	0.36	0.28	-21.35	0.03	0.03		14.35	11.64
	LE12-2p	0.47	-0.12	0.36	0.32	-10.11	0.03	0.03		14.35	12.89
	ORPLE12	1.10	0.47	0.03	0.00		1.05	0.04	-96.19	15.74	14.51
	LE12-3s	0.66	0.03	0.03	0.01		1.05	0.23	-78.19	15.74	14.14
	LE12-3c	0.52	-0.01	0.02	0.03		1.30	1.34	0.00	16.47	15.11
	LE12-3p	0.68	0.16	0.02	0.01		1.30	1.07	-17.95	16.47	15.33
	LE12-4s	0.76	0.20	0.32	0.00	-100.00	1.05	0.18	-83.22	16.38	14.15
	LE12-4c	0.42	-0.14	0.32	0.25	-19.68	1.05	1.12	0.00	16.38	12.09
	LE12-4p	0.71	0.15	0.32	0.26	-17.78	1.05	1.09	0.00	16.38	13.65

*: Standard open-to-air K-3 corrosion. Data reported previously [15, 16].

Table 3.3. Summary of Results of K-3 Refractory Dimension Loss and Composition Change of Glass. Oxide contents are in wt%; ΔCl % and ΔSO$_3$ % are percentage of loss (continued).

Base Glass	Test ID	ΔNa$_2$O	Starting SiO$_2$	Ending SiO$_2$	Δ SiO$_2$
ORPLA20	LA20-1s	-2.50	43.36	44.85	1.49
	LA20-1c	-1.64	43.36	45.08	1.72
	LA20-1p	-1.85	43.36	43.96	0.60
	LA20-2s1	-2.73	43.25	45.68	2.42
	LA20-2s2	-2.95	43.25	45.33	2.08
	LA20-2s3	-1.89	44.24	44.22	-0.02
	LA20-2c1	-5.44	43.25	47.53	4.28
	LA20-2c2	-3.59	44.24	46.29	2.05
	LA20-2p	-3.67	44.24	45.72	1.48
	ORPLA20	-0.95	42.34	42.34	0.00
	LA20-3s	-2.55	42.90	44.14	1.24
	LA20-3c	-1.80	42.90	43.79	0.89
	LA20-3p	-1.28	42.90	43.73	0.84
	LA20-4s	-2.65	43.10	44.74	1.64
	LA20-4c	-5.81	42.99	47.72	4.73
	LA20-4p	-2.81	42.99	44.80	1.81
	LA20-4cb	-4.78	42.99	47.65	4.65
ORPLE12	LE12-1s	-1.74	42.69	42.89	0.20
	LE12-1c	-0.18	42.69	43.46	0.76
	LE12-1p	0.31	42.69	42.42	-0.28
	LE12-2s	-1.36	42.94	44.44	1.49
	LE12-2c	-2.71	42.94	45.33	2.39
	LE12-2p	-1.46	42.94	43.64	0.70
	ORPLE12	-1.23	41.41	40.74	-0.67
	LE12-3s	-1.60	41.41	42.55	1.14
	LE12-3c	-1.36	41.54	41.85	0.32
	LE12-3p	-1.14	41.54	40.99	-0.54
	LE12-4s	-2.22	40.52	41.46	0.94
	LE12-4c	-4.29	40.52	43.65	3.13
	LE12-4p	-2.73	40.52	41.57	1.05

*: Standard open-to-air K-3 corrosion. Data reported previously [15, 16].

Table 3.4a. XRF Analysis (wt%) of ORPLA20 Glasses from Stage Two K-3 Corrosion Tests.

Test Date	2/07/17-2/13/17				1/24/17-1/30/17				7/5/17-7/11/17			1/24/17-1/30/17			
Test ID	LA20-1c				LA20-2c1				LA20-2c2			LA20-3c			
Test Condition	Sealed in alumina crucible with Zirmul cover				Sealed in alumina crucible with Zirmul cover				Sealed in alumina crucible with Zirmul cover			Sealed in alumina crucible with Zirmul cover			
Sample ID	A20-Cl0S0		A20-CLP0S0-K3GR2	A20-CLP0S0-K3GR2-W	A20-Clp8S0		A20-CLP8S0-K3GR2	A20-CLP8S0-K3GR2-W	A20-CLP8S0R		A20-CLP8S0R-S-K3G	A20-CL0SP7		A20-CL0SP7-K3GR	A20-CL0SP7-K3GR-W
Data Type	Target		XRF		Target		XRF		Target		XRF	Target		XRF	
Sample History	Before		After	After Salt Wash	Before		After	After Salt Wash		Before	After	Before		After	After Salt Wash
Al_2O_3	6.65	6.50	8.19	8.02	6.65	6.81	8.68	8.69	6.65	7.14	8.48	6.65	6.83	8.46	8.53
B_2O_3[#]	8.74	8.74	8.74	8.74	8.74	8.74	8.74	8.74	8.74	8.74	8.74	8.74	8.74	8.74	8.74
CaO	3.32	3.39	3.13	3.24	3.32	3.55	3.66	3.68	3.32	3.43	3.39	3.32	3.42	3.26	3.34
Cr_2O_3	0.50	0.47	0.42	0.43	0.50	0.54	0.39	0.38	0.50	0.47	0.50	0.50	0.46	0.47	0.48
Fe_2O_3	0.19	0.23	0.35	0.32	0.19	0.23	0.37	0.36	0.19	0.23	0.34	0.19	0.23	0.41	0.44
K_2O	0.53	0.54	0.40	0.44	0.53	0.54	0.60	0.57	0.53	0.51	0.73	0.53	0.52	0.45	0.42
Li_2O[#]	0.00	0.00	0.00	0.00	0.00	0.00	0.00	0.00	0.00	0.00	0.00	0.00	0.00	0.00	0.00
MgO	0.92	0.91	0.96	0.93	0.92	0.81	0.97	1.00	0.92	0.94	1.01	0.92	0.89	0.97	0.97
Na_2O	24.00	23.94	23.14	22.29	24.00	22.78	17.69	17.34	24.00	23.20	19.62	24.00	24.19	22.26	22.39
P_2O_5	0.00	0.01	0.02	0.02	0.00	0.01	0.03	0.02	0.00	0.02	0.02	0.00	0.02	0.02	0.01
SiO_2	43.71	43.36	44.62	45.08	42.91	43.25	47.09	47.53	42.91	44.24	46.29	43.01	42.90	44.03	43.79
SnO_2	2.74	2.71	2.36	2.49	2.74	2.66	2.68	2.71	2.74	2.15	2.33	2.74	2.38	2.51	2.48
TiO_2	0.00	0.04	0.04	0.04	0.00	0.05	0.06	0.06	0.00	0.05	0.06	0.00	0.03	0.04	0.05
V_2O_5	0.00	0.00	0.00	0.00	0.00	0.00	0.00	0.00	0.00	0.00	0.00	0.00	0.00	0.00	0.00
ZnO	2.74	2.81	2.23	2.29	2.74	2.86	2.37	2.33	2.74	2.59	2.33	2.74	2.64	2.19	2.17
ZrO_2	5.96	6.17	5.22	5.49	5.96	6.27	5.93	5.85	5.96	5.55	5.49	5.96	5.79	5.37	5.39
Cl	0.00	0.01	0.03	0.01	0.80	0.73	0.57	0.56	0.80	0.58	0.52	0.00	0.00	0.03	0.02
SO_3	0.00	0.03	0.04	0.04	0.00	0.03	0.04	0.04	0.00	0.03	0.03	0.70	0.77	0.67	0.66
Al_2O_3	100.00	99.85	99.87	99.87	100.00	99.84	99.85	99.85	100.00	99.87	99.88	100.00	99.81	99.87	99.86
K-3 Coupon ID	A20-CLP0S0-K3BR2*				A20-CLP8S0-K3BR2*				A20-CLP8S0R-S-K3B*			A20-CL0SP7-K3BR*			
Neck Loss	0.0"				0.005"				0.016"			0.033"			
Half Down Loss	0.0"				0.003"				EXPANDED			0.003"			
Alteration Zone	0.026"				0.016"				0.020"			0.028"			

*Measured under microscope

[#] Target concentration

Table 3.4a. XRF Analysis (wt%) of ORPLA20 Glasses from Stage Two K-3 Corrosion Tests (continued).

Test Date	1/6/17-1/12/17				2/21/17-2/27/17			
Test ID	LA20-4c				LA20-4cb			
Test Condition	Sealed in alumina crucible with Zirmul cover				Sealed in alumina crucible with Zirmul cover			
Sample ID	A20-CLP7SP7		A20-CLP7SP7-K3G	A20-CLP7SP7-K3G-W	A20-CLP7SP7		A20-CLP7SP7-K3G2	A20-CLP7SP7-K3G2-W
Data Type	Target		XRF		Target		XRF	
Sample History	Before		After	After Salt Wash	Before		After	After Salt Wash
Al_2O_3	6.65	6.61	8.32	8.88	6.65	6.61	7.68	7.52
B_2O_3#	8.74	8.74	8.74	8.74	8.74	8.74	8.74	8.74
CaO	3.32	3.60	3.46	3.57	3.32	3.60	3.61	3.59
Cr_2O_3	0.50	0.49	0.37	0.36	0.50	0.49	0.40	0.38
Fe_2O_3	0.19	0.22	0.34	0.37	0.19	0.22	0.25	0.24
K_2O	0.53	0.53	0.52	0.45	0.53	0.53	0.68	0.66
Li_2O#	0.00	0.00	0.00	0.00	0.00	0.00	0.00	0.00
MgO	0.92	0.92	0.94	1.09	0.92	0.92	0.95	0.93
Na_2O	24.00	22.92	18.33	17.11	24.00	22.92	19.17	18.13
P_2O_5	0.00	0.02	0.02	0.02	0.00	0.02	0.09	0.03
SiO_2	42.33	42.99	45.24	47.72	42.33	42.99	46.20	47.65
SnO_2	2.74	2.71	2.48	2.54	2.74	2.71	2.45	2.34
TiO_2	0.00	0.04	0.06	0.05	0.00	0.04	0.04	0.05
V_2O_5	0.00	0.00	0.00	0.00	0.00	0.00	0.00	0.00
ZnO	2.74	2.76	2.20	2.33	2.74	2.76	2.75	2.76
ZrO_2	5.96	6.03	5.62	5.84	5.96	6.03	5.90	6.00
Cl	0.67	0.59	0.70	0.42	0.67	0.59	0.44	0.39
SO_3	0.70	0.72	2.52	0.40	0.70	0.72	0.50	0.44
Al_2O_3	100.00	99.88	99.85	99.87	100.00	99.88	99.83	99.84
K-3 Coupon ID	A20-CLP7SP7-K3B*				No K-3 Coupon Used			
Neck Loss	0.002"							
Half Down Loss	0.001"							
Alteration Zone	0.020"							

*Measured under microscope

Target concentration

Table 3.4b. XRF Analysis (wt%) of ORPLE12 Glasses from Stage Two K-3 Corrosion Tests.

Test Date	2/7/17-2/13/17				2/24/17-3/2/17				2/7/17-2/13/17				1/6/17-1/12/17			
Test ID	LE12-1c				LE12-2c				LE12-3c				LE12-4c			
Test Condition	Sealed in alumina crucible with Zirmul cover				Sealed in alumina crucible with Zirmul cover				Sealed in alumina crucible with Zirmul cover				Sealed in alumina crucible with Zirmul cover			
Sample ID	E12-CL0S0		E12-CL0SO-K3GR	E12-CL0SO-K3GR-W	E12-CLP4S0		E12-ClP4S0-K3G	E12-ClP4S0-K3G-W	E12-5		E12-5-K3G	E12-5-K3G-W	E12-CLP4S1		E12-CLP4S1-K3G	E12-CLP4S1-K3G-W
Data Type	Target	XRF			Target	XRF			Target	XRF			Target	Before	After	After Salt Wash
Sample History	Before		After	After Salt Wash	Before		After	After Salt Wash	Before		After	After Salt Wash		XRF	XRF	XRF
Al_2O_3	7.58	7.63	9.13	9.13	7.58	7.53	9.12	9.28	7.58	7.62	9.65	9.63	7.58	7.47	9.82	9.82
B_2O_3[#]	9.82	9.82	9.82	9.82	9.82	9.82	9.82	9.82	9.82	9.82	9.82	9.82	9.82	9.82	9.82	9.82
CaO	10.02	10.58	9.96	9.71	10.02	10.83	10.63	10.52	10.02	9.91	9.86	9.64	10.02	10.47	10.47	10.31
Cr_2O_3	0.50	0.55	0.46	0.51	0.50	0.60	0.47	0.47	0.50	0.53	0.44	0.52	0.50	0.56	0.48	0.42
Cs_2O	0.15	0.19	0.00	0.00	0.15	0.21	0.00	0.00	0.02	0.00	0.00	0.00	0.15	0.19	0.00	0.00
Fe_2O_3	0.24	0.27	0.37	0.34	0.24	0.27	0.24	0.40	0.24	0.25	0.45	0.46	0.24	0.27	0.44	0.42
K_2O	0.55	0.54	0.44	0.43	0.55	0.54	0.55	0.54	0.55	0.56	0.47	0.42	0.55	0.53	0.41	0.42
Li_2O[#]	2.49	2.49	2.49	2.49	2.49	2.49	2.49	2.49	2.49	2.49	2.49	2.49	2.49	2.49	2.49	2.49
MgO	1.04	1.00	1.03	1.09	1.04	0.99	1.12	1.12	1.04	0.96	1.13	1.12	1.04	1.00	1.12	1.20
Na_2O	16.00	15.42	14.39	15.24	16.00	14.35	11.64	11.49	16.00	16.47	14.87	15.11	16.00	16.38	12.40	12.09
P_2O_5	0.12	0.08	0.09	0.08	0.12	0.14	0.16	0.15	0.12	0.12	0.14	0.13	0.12	0.13	0.14	0.15
SiO_2	42.79	42.69	43.84	43.46	42.39	42.94	45.07	45.33	41.27	41.54	41.68	41.85	41.39	40.52	42.93	43.65
SnO_2	0.00	0.00	0.00	0.00	0.00	0.00	0.00	0.00	0.00	0.00	0.00	0.00	0.00	0.00	0.00	0.00
TiO_2	0.01	0.06	0.06	0.07	0.01	0.07	0.06	0.06	0.01	0.05	0.06	0.06	0.00	0.06	0.06	0.08
V_2O_5	1.74	1.84	1.72	1.68	1.74	1.84	1.83	1.83	1.74	1.74	1.69	1.66	1.74	1.83	1.81	1.77
ZnO	3.21	3.21	2.69	2.63	3.21	3.29	2.81	2.69	3.21	2.98	2.52	2.46	3.21	3.20	2.67	2.55
ZrO_2	3.53	3.51	3.35	3.18	3.53	3.63	3.47	3.42	3.53	3.34	3.26	3.19	3.53	3.62	3.49	3.38
Cl	0.00	0.02	0.03	0.02	0.40	0.36	0.30	0.28	0.02	0.02	0.03	0.03	0.40	0.32	0.27	0.25
SO_3	0.00	0.03	0.04	0.05	0.00	0.03	0.03	0.03	1.50	1.30	1.33	1.34	1.00	1.05	1.11	1.12
SUM	99.79	99.93	99.90	99.92	99.80	99.92	99.79	99.92	99.66	99.70	99.89	99.93	100.00	99.91	99.91	99.93
K-3 Coupon ID	E12-CL0S0-K3BR*				E12-CLP4S0-K3B*				E12-5-K3B*				E12-CLP4S1-K3BR*			
NK LOSS	0.0"				0.004"				0.0"				0.002"			
HD LOSS	EXPANDED				0.001"				EXPANDED				0.002"			

*Measured under microscope; [#] Target concentration

Table 3.5. XRF Analysis (wt%) of Glass ORPLA20 and ORPLE12 Before and After Open Crucible Corrosion Tests.

Test Date	10/30/14-11/5/14			12/12/06-12/18/06		
Test Condition	Open with air bubbling			Open with air bubbling		
Formulation ID	ORPLA20 [16]			ORPLE12 [15]		
Sample ID	ORPLA20R1		ORPLA20R1-K3G	ORPLE12		ORPLE12-K3G
Data Type	Target	XRF		Target	XRF	
Sample History	Before		After	Before		After
Al_2O_3	6.65	6.52	8.52	7.60	8.05	10.45
B_2O_3[#]	8.74	8.74	8.74	9.85	9.85	9.85
CaO	3.32	3.43	3.39	10.05	10.21	10.16
Cr_2O_3	0.50	0.48	0.88	0.50	0.63	1.10
Cs_2O	0.00	0.00	0.00	0.15	0.16	0.02
Fe_2O_3	0.19	0.23	0.44	0.24	0.29	0.59
K_2O	0.53	0.54	0.35	0.55	0.61	0.41
Li_2O[#]	0.00	0.00	0.00	2.50	2.50	2.50
MgO	0.93	0.88	0.98	1.05	0.86	1.16
Na_2O	24.00	24.29	23.34	16.00	15.74	14.51
P_2O_5	0.00	0.00	0.00	0.12	0.19	0.17
SiO_2	42.33	42.34	42.34	41.41	41.41	40.74
SnO_2	2.74	2.66	2.58	0.00	0.00	0.00
V_2O_5	0.00	0.00	0.00	1.75	1.84	1.87
ZnO	2.74	2.70	2.39	3.22	3.20	2.87
ZrO_2	5.96	5.97	5.64	3.54	3.23	3.40
Cl	0.67	0.00	0.01	0.00	0.03	0.00
SO_3	0.70	0.59	0.19	1.25	1.05	0.04
SUM	100.00	99.82	99.78	98.53	98.76	99.80
Coupon Name	ORPLA20R1-K3B			ORPLE12-K3		
Neck Loss (inch)	0.039			0.031		
HD Loss (inch)	0.003			0		
Alter Zone (inch)	0.026			0.031		

[#] Target concentration

Table 3.6a. XRF Analysis (wt%) of ORPLA20 Glasses from Stage Three K-3 Corrosion Tests.

Test Date	4/21/17-4/27/17				4/28/17-5/4/17			
Test ID	LA20-1p				LA20-2p			
Test Condition	Alumina Crucible with Pt Cover				Alumina Crucible with Pt Cover			
Sample ID	A20-Cl0S0		A20-CLP0S0-K3GR3	A20-CLP0S0-K3GR3-W	A20-CLP8S0R		A20-CLP8S0R-K3GR	A20-CLP8S0R-K3GR-W
Data Type	Target	XRF	XRF		Target	XRF		
Sample History	Before		After	After Salt Wash	Before		After	After Salt Wash
Al_2O_3	6.65	6.50	8.19	8.20	6.65	7.14	8.34	8.58
B_2O_3[#]	8.74	8.74	8.74	8.74	8.74	8.74	8.74	8.74
CaO	3.32	3.39	3.37	3.22	3.32	3.43	3.48	3.56
Cr_2O_3	0.50	0.47	0.76	0.75	0.50	0.47	0.49	0.48
Fe_2O_3	0.19	0.23	0.41	0.37	0.19	0.23	0.35	0.37
K_2O	0.53	0.54	0.45	0.42	0.53	0.51	0.83	0.85
Li_2O[#]	0.00	0.00	0.00	0.00	0.00	0.00	0.00	0.00
MgO	0.92	0.91	0.94	0.98	0.92	0.94	1.05	0.98
Na_2O	24.00	23.94	22.43	23.09	24.00	23.20	20.01	19.53
P_2O_5	0.00	0.01	0.02	0.01	0.00	0.02	0.01	0.01
SiO_2	43.71	43.36	43.72	43.96	42.91	44.24	45.13	45.72
SnO_2	2.74	2.71	2.41	2.39	2.74	2.15	2.54	2.38
TiO_2	0.00	0.04	0.00	0.00	0.00	0.05	0.05	0.05
V_2O_5	0.00	0.00	0.00	0.00	0.00	0.00	0.00	0.00
ZnO	2.74	2.81	2.50	2.33	2.74	2.59	2.36	2.28
ZrO_2	5.96	6.17	5.80	5.35	5.96	5.55	5.89	5.70
Cl	0.00	0.01	0.01	0.00	0.80	0.58	0.57	0.62
SO_3	0.00	0.03	0.03	0.03	0.00	0.03	0.04	0.03
SUM	100.00	99.85	99.77	99.85	100.00	99.87	99.87	99.88
K-3 Coupon ID	A20-CLP0S0-K3BR3*				A20-CLP8S0R-K3BR*			
Neck Loss	0.061"				0.010"			
Half Down Loss	0.001"				0.001"			
Alteration Zone	0.026"				0.024"			

*Measured under microscope

[#] Target concentration

Table 3.6a. XRF Analysis (wt%) of ORPLA20 Glasses from Stage Three K-3 Corrosion Tests (continued).

Test Date	4/5/17-4/11/17				4/5/17-4/11/17			
Test ID	LA20-3p				LA20-4p			
Test Condition	Alumina Crucible with Pt Cover				Alumina Crucible with Pt Cover			
Sample ID	A20-CLOSP7		A20-CL0SP7-K3GR2	A20-CL0SP7-K3GR2-W	A20-CLP7SP7		A20-CLP7SP7-K3G3	A20-CLP7SP7-K3G3-W
Data Type	Target	XRF	XRF		Target	XRF	XRF	
Sample History	Before		After	After Salt Wash	Before		After	After Salt Wash
Al_2O_3	6.65	6.83	8.57	8.32	6.65	6.61	8.54	8.53
B_2O_3	8.74	8.74	8.74	8.74	8.74	8.74	8.74	8.74
CaO	3.32	3.42	3.34	3.29	3.32	3.60	3.42	3.67
Cr_2O_3	0.50	0.46	0.74	0.70	0.50	0.49	0.42	0.43
Fe_2O_3	0.19	0.23	0.41	0.40	0.19	0.22	0.38	0.37
K_2O	0.53	0.52	0.42	0.41	0.53	0.53	0.53	0.56
Li_2O	0.00	0.00	0.00	0.00	0.00	0.00	0.00	0.00
MgO	0.92	0.89	0.97	0.95	0.92	0.92	0.96	0.96
Na_2O	24.00	24.19	22.67	22.91	24.00	22.92	20.29	20.11
P_2O_5	0.00	0.02	0.01	0.01	0.00	0.02	0.02	0.02
SiO_2	43.01	42.90	43.19	43.73	42.33	42.99	44.96	44.80
SnO_2	2.74	2.38	2.23	2.10	2.74	2.71	2.55	2.30
TiO_2	0.00	0.03	0.05	0.06	0.00	0.04	0.05	0.06
V_2O_5	0.00	0.00	0.00	0.00	0.00	0.00	0.00	0.00
ZnO	2.74	2.64	2.32	2.27	2.74	2.76	2.33	2.43
ZrO_2	5.96	5.79	5.45	5.27	5.96	6.03	5.65	5.92
Cl	0.00	0.00	0.01	0.00	0.67	0.59	0.49	0.47
SO_3	0.70	0.77	0.73	0.72	0.70	0.72	0.54	0.49
SUM	100.00	99.81	99.85	99.87	100.00	99.88	99.87	99.85
K-3 Coupon ID	A20-CL0SP7-K3BR2*				A20-CLP7SP7-K3B3*			
Neck Loss	0.057"				0.006"			
Half Down Loss	0.002"				0.001"			
Alteration Zone	0.027"				0.026			

*Measured under microscope

Table 3.6b. XRF Analysis (wt%) of ORPLE12 Glasses from Stage Three K-3 Corrosion Tests.

Test Date	4/12/17-4/18/17				4/5/17-4/11/17			
Test ID	LE12-1p				LE12-2p			
Test Condition	Sealed Alumina Crucible with Pt Cover				Sealed Alumina Crucible with Pt Cover			
Samlple ID	E12-CL0S0		E12-CL0SO-K3GR2	E12-CL0SO-K3GR2-W	E12-CLP4S0		E12-ClP4S0-K3G2	E12-ClP4S0-K3G2-W
Data Type	Target	XRF	XRF		Target	XRF	XRF	
Sample History	Before		After	After Salt Wash	Before		After	After Salt Wash
Al_2O_3	7.58	7.63	9.11	9.17	7.58	7.53	9.19	9.05
B_2O_3	9.82	9.82	9.82	9.82	9.82	9.82	9.82	9.82
CaO	10.02	10.58	10.08	9.89	10.02	10.83	10.33	10.50
Cr_2O_3	0.50	0.55	0.66	0.67	0.50	0.60	0.50	0.47
Cs_2O	0.15	0.19	0.00	0.00	0.15	0.21	0.00	0.12
Fe_2O_3	0.24	0.27	0.39	0.40	0.24	0.27	0.40	0.43
K_2O	0.55	0.54	0.47	0.47	0.55	0.54	0.72	0.66
Li_2O	2.49	2.49	2.49	2.49	2.50	2.49	2.49	2.49
MgO	1.04	1.00	1.12	1.06	1.04	0.99	1.06	1.08
Na_2O	16.00	15.42	15.32	15.73	16.00	14.35	13.14	12.89
P_2O_5	0.12	0.08	0.08	0.08	0.12	0.14	0.13	0.14
SiO_2	42.79	42.69	42.36	42.42	42.39	42.94	43.98	43.64
SnO_2	0.00	0.00	0.00	0.00	0.00	0.00	0.00	0.00
TiO_2	0.01	0.06	0.07	0.06	0.01	0.07	0.05	0.07
V_2O_5	1.74	1.84	1.72	1.69	1.74	1.84	1.77	1.87
ZnO	3.21	3.21	2.84	2.74	3.21	3.29	2.62	2.74
ZrO_2	3.53	3.51	3.38	3.23	3.53	3.63	3.38	3.60
Cl	0.00	0.02	0.01	0.00	0.40	0.36	0.34	0.32
SO_3	0.00	0.03	0.03	0.03	0.00	0.03	0.03	0.03
SUM	99.79	99.93	99.93	99.93	99.80	99.92	99.93	99.92
K-3 Coupon ID	E12-CL0S0-K3BR2**				E12-CLP4S0-K3B2*			
NLOSS	0.037"				0.005"			
HDLOSS	0.003"				0.0"			
AZONE	0.027"				0.026"			

*Measured under microscope

**Measured on scanned image

Table 3.6b. XRF Analysis (wt%) of ORPLE12 Glasses from Stage Three K-3 Corrosion Tests (continued).

Test Date	4/12/17-4/18/17				4/5/17-4/11/17			
Test ID	LE12-3p				LE12-4p			
Test Condition	Sealed Alumina Crucible with Pt Cover				Sealed Alumina Crucible with Pt Cover			
Samlple ID	E12-5		E12-5-K3GR	E12-5-K3GR-W	E12-CLP4S1		E12-CLP4S1-K3G2	E12-CLP4S1-K3G2-W
Data Type	Target	XRF	XRF		Target	XRF	XRF	
Sample History	Before		After	After Salt Wash	Before		After	After Salt Wash
Al_2O_3	7.58	7.62	9.40	9.18	7.58	7.47	9.64	9.35
B_2O_3	9.82	9.82	9.82	9.82	9.82	9.82	9.82	9.82
CaO	10.02	9.91	10.04	10.29	10.02	10.47	10.24	10.64
Cr_2O_3	0.50	0.53	0.68	0.68	0.50	0.56	0.72	0.71
Cs_2O	0.15	0.22	0.00	0.00	0.15	0.19	0.00	0.00
Fe_2O_3	0.24	0.25	0.44	0.41	0.24	0.27	0.42	0.45
K_2O	0.55	0.56	0.51	0.48	0.55	0.53	0.54	0.54
Li_2O	2.49	2.49	2.49	2.49	2.49	2.49	2.49	2.49
MgO	1.04	0.96	1.10	1.06	1.04	1.00	1.06	1.02
Na_2O	16.00	16.47	15.07	15.33	16.00	16.38	13.98	13.65
P_2O_5	0.12	0.12	0.13	0.13	0.12	0.13	0.13	0.13
SiO_2	41.27	41.54	41.22	40.99	41.39	40.52	41.68	41.57
SnO_2	0.00	0.00	0.00	0.00	0.00	0.00	0.00	0.00
TiO_2	0.01	0.05	0.06	0.07	0.01	0.06	0.07	0.07
V_2O_5	1.74	1.74	1.74	1.75	1.74	1.83	1.78	1.85
ZnO	3.21	2.98	2.78	2.76	3.21	3.20	2.63	2.74
ZrO_2	3.53	3.34	3.40	3.39	3.53	3.62	3.39	3.55
Cl	0.02	0.02	0.01	0.01	0.40	0.32	0.26	0.26
SO_3	1.50	1.30	1.02	1.07	1.00	1.05	1.07	1.09
SUM	99.79	99.92	99.91	99.92	100.00	99.91	99.92	99.91
K-3 Coupon ID	E12-5-K3BR*				E12-CLP4S1-K3B2**			
NLOSS	0.033"				0.015"			
HDLOSS	0.0035"				0			
AZONE	0.027"				0.017"			

*Measured under microscope

**Measured on scanned image

Table 4.1. Test Matrix for Closed/Open Crucible Inconel 690 Corrosion Tests.

Test Number	Material for Testing	Glass	Temperature	Test Duration	Test Condition	SO_3 (wt%)*	Cl (wt%)*
LA20-1	Inconel 690	ORPLA20	1150°C	7 days	Closed	0.00	0.00
LA20-2	Inconel 690	ORPLA20	1150°C	7 days	Closed	0.00	0.80
LA20-3	Inconel 690	ORPLA20	1150°C	7 days	Closed	0.35	0.40
LA20-4	Inconel 690	ORPLA20	1150°C	7 days	Closed	0.70	0.00
LA20-5	Inconel 690	ORPLA20	1150°C	7 days	Closed	0.70	0.67
LA20-A	Inconel 690	ORPLA20	1150°C	7 days	*Open*	0.70	0.67
LE12-1	Inconel 690	ORPLE12	1150°C	7 days	Closed	0.00	0.00
LE12-2	Inconel 690	ORPLE12	1150°C	7 days	Closed	0.00	0.40
LE12-3	Inconel 690	ORPLE12	1150°C	7 days	Closed	0.50	0.20
LE12-4	Inconel 690	ORPLE12	1150°C	7 days	Closed	1.25	0.02
LE12-5	Inconel 690	ORPLE12	1150°C	7 days	Closed	1.00	0.40
LE12-A	Inconel 690	ORPLE12	1150°C	7 days	*Open*	1.25	0.02

* Target concentration.

Table 4.2a. Visual Inspection of ORPLA20 Glasses After Inconel 690 Corrosion Tests.

Condition (wt%)	SO_3=0	SO_3=0.35	SO_3=0.7
Cl=0	LA20-1 in closed crucible: Zirmul Cover Minor crystallization	-	LA20-4 in closed crucible: Zirmul Cover Trace crystallization Sulfate Separation
Cl=0.4	-	LA20-3 in closed crucible: Pt Cover Crystallization Sulfate Separation	-
Cl=0.8 (0.67 for LA20-5/LA20-A)	LA20-2 in closed crucible: Pt Cover Minor crystallization	-	LA20-5 in closed crucible: Pt Cover Crystallization Sulfate Separation LA20-A *in Open Crucible:* *Opaque Glass*

- Empty data field

Table 4.2b. Visual Inspection of ORPLE12 Glasses After Inconel 690 Corrosion Tests.

Condition (wt%)	SO_3=0	SO_3=0.50	SO_3=1.25 (1.0 for LE12-5)
Cl=0	LE12-1 in closed crucible: Zirmul Cover Trace crystallization	-	LE12-4 in closed crucible: Zirmul Cover Trace crystallization. LE12-A *in Open Crucible: Crystal-free*
Cl=0.2	-	LE12-3 in closed crucible: Pt Cover Trace crystallization	-
Cl=0.4	LE12-2 in closed crucible: Zirmul Cover Pt Crucible Damaged Opaque glass	-	LE12-5in closed crucible: Pt Cover Trace crystallization

-
- Empty data field

Table 4.3. XRF Analysis (wt%) of Glasses Before and After Inconel 690 Corrosion Tests.

Parent Glass	ORPLA20		ORPLE12	
Test Number	LA20-A		LE12-A	
Test Condition	Open		Open	
Data Type	Starting Glass	Ending Glass	Starting Glass	Ending Glass
GLASS ID	**ORPLA20-2**	**ORPLA20-INC690-A**	**ORPLE12-2**	**ORPLE12-INC690-A-R**
Al_2O_3	6.09	6.789	7.24	7.936
B_2O_3	8.73	8.73	9.82	9.82
Bi_2O_3	-	-	-	-
CaO	3.51	3.565	10.67	10.486
Cr_2O_3	0.64	1.091	0.666	0.625
Cs_2O	-	-	0.149	-
Fe_2O_3	0.224	0.397	0.273	0.289
HfO_2	0.137	0.116	0.078	0.075
I	0.118	-	-	-
K_2O	0.52	0.39	0.567	0.478
Li_2O	-	-	2.49	2.49
MgO	0.982	0.859	1.08	1.029
Na_2O	23.6	21.575	16.57	14.351
NiO	-	0.609	-	0.088
P_2O_5	0.016	0.02	0.139	0.126
SO_3	0.585	0.331	1.2	0.223
SiO_2	43.18	43.321	40.59	43.512
SnO_2	2.56	2.818	0.005	-
TiO_2	0.007	0.04	0.03	0.036
V_2O_5	-	-	1.78	1.794
Y_2O_3	0.017	0.013	0.009	0.01
ZnO	2.78	2.913	3.26	3.135
ZrO_2	5.65	6.384	3.35	3.485
Cl	0.644	-	0.027	0.011
SUM	99.99	99.96	99.99	100.00

- Empty data field

Table 4.3. XRF Analysis (wt%) of Glasses Before and After Inconel 690 Corrosion Tests (continued).

Parent Glass	ORPLA20		ORPLA20	
Test Number	LA20-1		LA20-2	
Test Condition	Closed		Closed/Pt Cover	
Data Type	Starting Glass	Ending Glass	Starting Glass	Ending Glass
GLASS ID	**A20-Clp0S0**	**ORPLA20-INC690-1-R**	**A20-Clp8S0R**	**ORPLA20-INC690-2R2**
Al_2O_3	6.501	7.002	6.799	7.664
B_2O_3	8.74	8.74	8.74	8.74
Bi_2O_3	0.009	0.003		0.015
CaO	3.392	3.293	3.178	3.304
Cr_2O_3	0.468	0.403	0.414	0.307
Cs_2O	-	-	-	-
Fe_2O_3	0.229	0.202	0.214	0.219
HfO_2	0.117	0.113	0.101	0.105
I	-	-	-	-
K_2O	0.543	0.517	0.471	0.696
Li_2O	-	-	-	-
MgO	0.907	0.863	0.891	0.914
Na_2O	23.938	23.252	24.652	21.372
NiO	-	-	-	0.006
P_2O_5	0.012	0.019	0.013	0.027
SO_3	0.028	0.022	0.031	0.025
SiO_2	43.358	45.488	43.593	46.165
SnO_2	2.707	1.971	2.427	1.851
TiO_2	0.044	0.049	0.028	0.051
V_2O_5	-	-	-	-
Y_2O_3	0.017	0.015	0.013	0.014
ZnO	2.808	2.594	2.487	2.537
ZrO_2	6.165	5.446	5.287	5.383
Cl	0.014	0.01	0.626	0.604
SUM	100.00	100.00	99.97	100.00

- Empty data field

Table 4.3. XRF Analysis (wt%) of Glasses Before and After Inconel 690 Corrosion Tests (continued).

Parent Glass	ORPLA20		ORPLA20	
TestNumber	LA20-3		LA20-4	
Test Condition	Closed/Pt Cover		Closed	
Data Type	Starting Glass	Ending Glass	Starting Glass	Ending Glass
GLASS ID	**A20-Clp4SP35**	**ORPLA20-INC690-3R2-R**	**A20-CL0Sp7**	**ORPLA20-INC690-4-R**
Al_2O_3	6.731	7.109	6.831	7
B_2O_3	8.74	8.74	8.74	8.74
Bi_2O_3	-	0.006	-	-
CaO	3.391	3.349	3.423	3.408
Cr_2O_3	0.486	0.329	0.463	0.548
Cs_2O	-	-	-	-
Fe_2O_3	0.22	0.212	0.231	0.233
HfO_2	0.104	0.114	0.103	0.111
I	-	-	-	-
K_2O	0.489	0.681	0.517	0.424
Li_2O	-	-	-	-
MgO	0.921	0.913	0.892	0.884
Na_2O	24.615	22.26	24.189	22.681
NiO	-	-	-	0.086
P_2O_5	0.022	0.015	0.02	0.014
SO_3	0.51	0.556	0.769	0.793
SiO_2	42.473	45.027	42.895	44.414
SnO_2	2.514	2.057	2.376	2.452
TiO_2	0.037	0.047	0.031	0.033
V_2O_5	-	-	-	-
Y_2O_3	0.014	0.017	0.016	0.017
ZnO	2.629	2.597	2.635	2.57
ZrO_2	5.732	5.622	5.794	5.582
Cl	0.361	0.344	-	0.01
SUM	99.99	100.00	99.93	100.00

- Empty data field

Table 4.3. XRF Analysis (wt%) of Glasses Before and After Inconel 690 Corrosion Tests (continued).

Parent Glass	ORPLA20		ORPLE12	
Test Number	LA20-5		LE12-1	
Test Condition	Closed/Pt Cover		Closed	
Data Type	Starting Glass	Ending Glass	Starting Glass	Ending Glass
GLASS ID	**A20-CLP7SP7**	**ORPLA20-INC690-5R2**	**E12-Cl0S0**	**ORPLE12-INC690-1R-R**
Al_2O_3	6.612	7.42	7.625	7.845
B_2O_3	8.74	8.74	9.82	9.82
Bi_2O_3	-	-	-	-
CaO	3.603	3.281	10.584	10.31
Cr_2O_3	0.487	0.345	0.553	0.638
Cs_2O	-	-	0.191	0.11
Fe_2O_3	0.215	0.208	0.272	0.275
HfO_2	0.105	0.116	0.054	0.063
I	-	-	-	-
K_2O	0.534	0.613	0.539	0.532
Li_2O	-	-	2.49	2.49
MgO	0.916	0.896	1.001	0.976
Na_2O	22.917	22.098	15.415	14.642
NiO	-	0.016	-	0.062
P_2O_5	0.015	0.023	0.081	0.068
SO_3	**0.716**	0.6	0.025	0.025
SiO_2	42.994	45.292	42.693	43.438
SnO_2	2.708	2.022	-	0.121
TiO_2	0.043	0.054	0.06	0.065
V_2O_5	-	-	1.839	1.838
Y_2O_3	0.018	0.014	0.011	-
ZnO	**2.761**	2.491	3.214	3.19
ZrO_2	**6.032**	5.297	3.511	3.465
Cl	**0.585**	0.473	0.015	0.022
SUM	100.00	100.00	100.00	100.00

- Empty data field

Table 4.3. XRF Analysis (wt%) of Glasses Before and After Inconel 690 Corrosion Tests (continued).

Parent Glass	ORPLE12		ORPLE12	
Test Number	LE12-2		LE12-3	
Test Condition	Closed/Crucible Damage		Closed/Pt Cover	
Data Type	Starting Glass	Ending Glass	Starting Glass	Ending Glass
GLASS ID	**E12-Clp4S0**	**ORPLE12-INC690-2**	**E12-Clp2Sp5**	**ORPLE12-INC690-3R**
Al_2O_3	7.526	8.232	7.516	8.012
B_2O_3	9.82	9.82	9.82	9.82
Bi_2O_3	-	0.015	-	-
CaO	10.829	10.838	10.571	10.229
Cr_2O_3	0.596	1.083	0.577	0.649
Cs_2O	0.214	0.113	0.193	-
Fe_2O_3	0.265	0.321	0.272	0.259
HfO_2	0.074	0.076	0.08	0.058
I	-	-	-	-
K_2O	0.543	0.699	0.568	0.491
Li_2O	2.49	2.49	2.49	2.49
MgO	0.994	0.975	0.972	0.991
Na_2O	14.353	12.835	14.863	13.967
NiO	-	0.167	-	0.026
P_2O_5	0.14	0.167	0.126	0.135
SO_3	0.029	0.017	0.532	0.566
SiO_2	42.942	43.537	42.435	43.985
SnO_2	-	-	-	0.107
TiO_2	0.069	0.076	0.033	0.057
V_2O_5	1.837	1.82	1.87	1.759
Y_2O_3	0.01	0.011	0.012	0.008
ZnO	3.286	2.822	3.268	3.038
ZrO_2	3.627	3.541	3.615	3.181
Cl	0.356	0.336	0.173	0.171
SUM	100.00	99.99	99.99	100.00

- Empty data field

Table 4.3. XRF Analysis (wt%) of Glasses Before and After Inconel 690 Corrosion Tests (continued).

Parent Glass	ORPLE12		ORPLE12	
Test Number	LE12-4		LE12-5	
Test Condition	Closed		Closed/Pt Cover	
Data Type	Starting Glass	Ending Glass	Starting Glass	Ending Glass
GLASS ID	**ORPLE12-2**	**ORPLE12-INC690-B-R2**	**ORPLE12***	**ORPLE12-INC690-5R**
Al_2O_3	7.24	7.884	7.468	8.111
B_2O_3	9.82	9.82	9.820	9.82
Bi_2O_3	-	0.008	-	-
CaO	10.67	9.98	10.480	10.403
Cr_2O_3	0.666	0.639	0.560	0.738
Cs_2O	0.149		0.193	0.074
Fe_2O_3	0.273	0.252	0.274	0.272
HfO_2	0.078	0.057	0.073	0.065
I	-	-	-	-
K_2O	0.567	0.447	0.532	0.569
Li_2O	2.49	2.49	2.490	2.49
MgO	1.08	0.966	1.005	1.039
Na_2O	16.57	15.864	16.337	14.39
NiO	-	0.057	-	0.008
P_2O_5	0.139	0.12	0.133	0.126
SO_3	1.2	0.904	1.031	1.122
SiO_2	40.59	42.641	40.570	42
SnO_2	0.005	-	0.000	-
TiO_2	0.03	0.033	0.060	0.072
V_2O_5	1.78	1.742	1.826	1.858
Y_2O_3	0.009	0.008	0.012	0.01
ZnO	3.26	2.912	3.207	3.19
ZrO_2	3.35	3.166	3.616	3.386
Cl	0.027	0.012	0.310	0.252
SUM	99.99	100.00	100.00	100.00

* More than one crucible melt glass samples was used. Target calculated from mixing ratio.
\- Empty data field

Table 4.4. Summary of Key Parameters of Inconel 690 Coupon Damage After Corrosion Tests.

Test Condition					Initial wt%	
Glass	Test Number	Test Condition	Reacted coupon ID	Reacted glass ID	SO_3	Cl
ORPLA20	LA20-1	Closed	INC690-ORPLA20-1	ORPLA20-INC690-1	0	0
ORPLA20	LA20-2	Closed	INC690-ORPLA20-2R2	ORPLA20-INC690-2R2	0	0.8
ORPLA20	LA20-3	Closed	INC690-ORPLA20-3R2	ORPLA20-INC690-3R2	0.35	0.4
ORPLA20	LA20-4	Closed	INC690-ORPLA20-4	ORPLA20-INC690-4	0.7	0
ORPLA20	LA20-5	Closed	INC690-ORPLA20-5R2	ORPLA20-INC690-5R2	0.7	0.67
ORPLA20	LA20-A	Open	INC690-ORPLA20-A	ORPLA20-INC690-A	0.7	0.67
ORPLE12	LE12-1	Closed	INC690-ORPLE12-1R	ORPLE12-INC690-1R	0	0
ORPLE12	LE12-2	Closed	INC690-ORPLE12-2	ORPLE12-INC690-2	0	0.4
ORPLE12	LE12-4	Closed	INC690-ORPLE12-3R	ORPLE12-INC690-3R	0.5	0.2
ORPLE12	LE12-4	Closed	INC690-ORPLE12-B	ORPLE12-INC690-B	1.25	0.02
ORPLE12	LE12-A	Open	INC690-ORPLE12-A	ORPLE12-INC690-A	1.25	0.02
ORPLE12	LE12-5	Closed	INC690-ORPLE12-5R	ORPLE12-INC690-5R	1	0.4

Table 4.4. Summary of Key Parameters of Inconel 690 Coupon Damage After Corrosion Tests (continued).

Glass	Test Number	Dimension Loss (mil inch)			Scale Thickness (μm)		
		Neck	Half down	Bottom	Neck	Half down	Bottom
ORPLA20	LA20-1	0	0.5	1	50	15	30
ORPLA20	LA20-2	1.5	~0	0.5	20	25	30
ORPLA20	LA20-3	1.5	2	1.5	20	30	40
ORPLA20	LA20-4	4.5	0.5	0.5	60	20	30
ORPLA20	LA20-5	2.5	2	2	3	5	5
ORPLA20	LA20-A	17.5	2.5	4	250	200	250
ORPLE12	LE12-1	5	0	0	40	30	30
ORPLE12	LE12-2	4.5	3.5	4	40	50	70
ORPLE12	LE12-4	~0	~0	2	30	30	30
ORPLE12	LE12-4	4	1.5	0	30	20	30
ORPLE12	LE12-A	10	0	1	30	30	40
ORPLE12	LE12-5	2	2	3	50	3	50

Table 4.4. Summary of Key Parameters of Inconel 690 Coupon Damage After Corrosion Tests (continued).

Glass	Test Number	Grain Boundary Damage (μm)			Cr Depletion Depth (μm)		
		Neck	Half down	Bottom	Neck	Half down	Bottom
ORPLA20	LA20-1	50	50	80	250	190	200
ORPLA20	LA20-2	100	150	150	320	280	340
ORPLA20	LA20-3	120	120	120	210	370	400
ORPLA20	LA20-4	250	80	100	370	280	260
ORPLA20	LA20-5	300	250	250	450	320	350
ORPLA20	LA20-A	700	700	450	630	640	610
ORPLE12	LE12-1	100	100	80	320	260	290
ORPLE12	LE12-2	500	500	600	260	600	630
ORPLE12	LE12-4	100	100	100	310	310	300
ORPLE12	LE12-4	300	150	150	400	250	200
ORPLE12	LE12-A	200	200	100	250	360	320
ORPLE12	LE12-5	300	300	300	430	430	400

Table 4.4. Summary of Key Parameters of Inconel 690 Coupon Damage After Corrosion Tests (continued).

Glass	Test Number	Cr wt% on Alloy Surface		
		Neck	Half down	Bottom
ORPLA20	LA20-1	21	25	25
ORPLA20	LA20-2	12	17	14
ORPLA20	LA20-3	22	19	20
ORPLA20	LA20-4	15	22	22
ORPLA20	LA20-5	7	17	9
ORPLA20	LA20-A	3	9	5
ORPLE12	LE12-1	19	19	21
ORPLE12	LE12-2	20	21	21
ORPLE12	LE12-4	14	18	17
ORPLE12	LE12-4	4	5	20
ORPLE12	LE12-A	7	22	22
ORPLE12	LE12-5	16	20	20

Table 4.5. Inconel 690 Damage After ORPLA20 Corrosion Tests.

Condition (wt%)	SO_3=0	SO_3=0.35	SO_3=0.7
Cl=0	LA20-1 in closed crucible: Neck Loss=~0 mil Cr Depletion Depth: 250/190/200 microns Grain Boundary Damage: 50/50/80 microns Continuous oxide scale No secondary Cl/S phase	-	LA20-4 in closed crucible: Neck Loss=4.5 mil Cr Depletion Depth: 370/280/260 microns Grain Boundary Damage: 250/80/100 microns Moderately preserved oxide scale No secondary Cl/S phase
Cl=0.4	-	LA20-3 in closed crucible: Neck Loss=1.5 mil Cr Depletion Depth: 210/370/400 microns Grain Boundary Damage: 120/120/120 microns Detached oxide scale No secondary Cl/S phase	-
Cl=0.8 (or 0.67)	LA20-2 in closed crucible: Neck Loss=1.5 mil Cr Depletion Depth: 320/280/340 microns Grain Boundary Damage: 100/150/150 microns Detached oxide scale No Secondary Cl/S phase Ni-enriched Inconel nodules	-	LA20-5 in closed crucible: Neck Loss=2.5 mil Cr Depletion Depth: 450/320/350 microns Grain Boundary Damage: 300/250/250 microns Detached oxide scale Ni-sulfide, Sn/Ni-sulfide, Sn-Ni alloy, Ni-enriched Inconel nodules LA20-A *in Open Crucible:* *Neck Loss=17.5 mil* *Cr depletion Depth:* *630/640/610* microns Grain Boundary Damage: 700/700/450 microns Thick and loose oxide scale

- Empty data field

Table 4.6. Inconel 690 Damage After ORPLE12 Corrosion Tests.

Condition (wt%)	SO_3=0	SO_3=0.50	SO_3=1.25 (1.0)
Cl=0	LE12-1 in closed crucible: Neck Loss=5 mil Cr Depletion Depth: 320/260/290 microns Grain Boundary Damage: 100/100/80 microns Mostly continuous oxide scale No secondary Cl/S phase	-	LE12-4 in closed crucible: Neck Loss=4 mil Cr Depletion Depth: 400/250/200 microns Grain Boundary Damage: 300/150/150 microns Moderately preserved oxide scale Ni-Sulfide near bottom *LE12-A in Open Crucible:* N*eck Loss=10 mil* *Cr Depletion Depth:* *250/360/320* microns *Grain Boundary Damage:* *200/200/100* microns *Moderately preserved loose oxide scale*
Cl=0.2	-	LE12-3 in closed crucible: Neck Loss=0mil Cr Depletion Depth: 310/310/300 microns Grain Boundary Damage: 100/100/100 microns Discontinuous oxide scale No secondary Cl/S phase	-
Cl=0.4	LE12-2 in closed crucible: Neck Loss=4.5mil Cr Depletion Depth: 260/600/630 microns Grain Boundary Damage: 500/500/600 microns Loose oxide scale with extensive metal break off Ni-enriched nodules near alloy surface	-	LE12-5 in closed crucible: Neck Loss=2 mil Cr Depletion Depth: 430/440/400 microns Grain Boundary Damage: 300/300/300 microns Detached oxide scale Ni-sulfide Ni-enriched nodules near alloy surface

- Empty data field

Table 4.7. Ranking of Inconel 690 Damage for ORPLA20 Corrosion Tests.

Attributes	Neck Cr Depletion Ranking for ORPLA20					
	1st	2nd	3rd	4th	5th	5th
Test Number	LA20-A	LA20-5	LA20-4	LA20-2	LA20-3	LA20-1
Cl wt% glass	Lost	High	0	High	Mid	0
SO_3 wt% glass	Lost	High	High	0	Mid	0
Ni Sulfide	-	NiS	NiS	-	-	-
Ni Nodule	-	Ni Nodule	-	Ni Nodule	-	-
Inconel Surface Cr wt%	3	7	15	12	22	21

Attributes	Half-Down Cr Depletion Ranking for ORPLA20					
	1st	2nd	3rd	4th	5th	6th
Test Number	LA20-A	LA20-5	LA20-3	LA20-2	LA20-4	LA20-1
Cl wt% glass	Lost	High	Mid	High	0	0
SO_3 wt% glass	Lost	High	Mid	0	High	0,
Ni Sulfide	-	NiS	-	-	NiS	-
Ni Nodule	-	Ni Nodule	-	Ni Nodule	-	-
Inconel Surface Cr wt%	9	17	19	17	22	25

Attributes	Bottom Cr Depletion Ranking for ORPLA20					
	1st	2nd	3rd	4th	5th	6th
Test Number	LA20-A	LA20-5	LA20-2	LA20-3	LA20-4	LA20-1
Cl wt% glass	Lost	High	High	Mid	0	0
SO_3 wt% glass	Lost	High	0	Mid	High	0,
Ni Sulfide	-	NiS	-	-	NiS	-
Ni Nodule	-	Ni Nodule	Ni Nodule	-	-	-
Inconel Surface Cr wt%	5	9	14	20	22	25

- Empty data field

Table 4.8. Ranking of Inconel 690 Damage for ORPLE12 Corrosion Tests.

Attributes	Cr Depletion Ranking for ORPLE12					
	1st	2nd	3rd	4th	5th	5th
Test Number	LE12-4	LE12-A	LE12-5	LE12-3	LE12-2	LE12-1
Cl wt%	0	Lost	High	Mid	High	0
SO_3 wt%	High	Lost	High	Mid	0	0
Ni Sulfide	NiS	-	NiS	-	-	-
Ni Nodule	-	-	Ni Nodule	-	Ni Nodule	-
Inconel Surface Cr wt%	4	7	16	14	20	19
Attributes	Half Down Cr Depletion Ranking for ORPLE12					
	1st	2nd	3rd	4th	5th	6th
Test Number	LE12-4	LE12-2	LE12-5	LE12-3	LE12-1	LE12-A
Cl wt%	0	High	High	Mid	0	Lost
SO_3 wt%	High	0	High	Mid	0	Lost
Ni Sulfide	NiS	-	NiS	-	-	-
Ni Nodule	-	Ni Nodule	Ni Nodule	-	-	-
Inconel Surface Cr wt%	5	21	20	18	19	22
Attributes	Bottom Cr Depletion Ranking for ORPLE12					
	1st	2nd	3rd	4th	5th	5th
Test Number	LE12-2	LE12-5	LE12-3	LE12-A	LE12-1	LE12-4
Cl wt%	High	High	Mid	Lost	0	0
SO_3 wt%	0	High	Mid	Lost	0	High
Ni Sulfide	-	NiS	-	-	-	NiS
Ni Nodule	Ni Nodule	Ni Nodule	-	-	-	-
Inconel Surface Cr wt%	21	20	17	22	21	20

- Empty data field

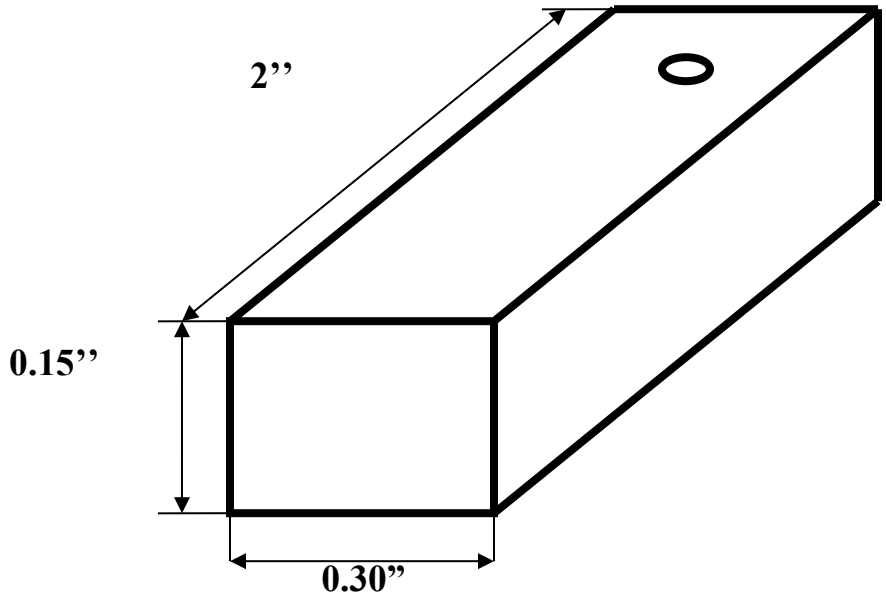

Figure 2.1. Schematic diagram of an Inconel 690 coupon showing typical dimensions.

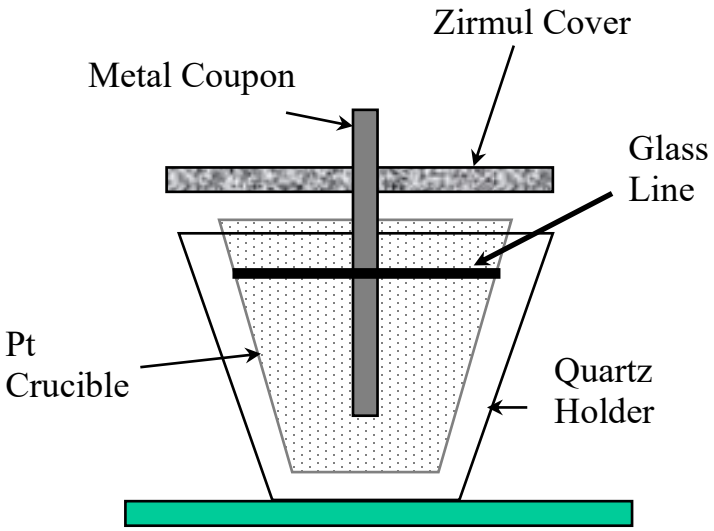

Figure 2.2. Experimental setup for open crucible Inconel 690 corrosion tests.

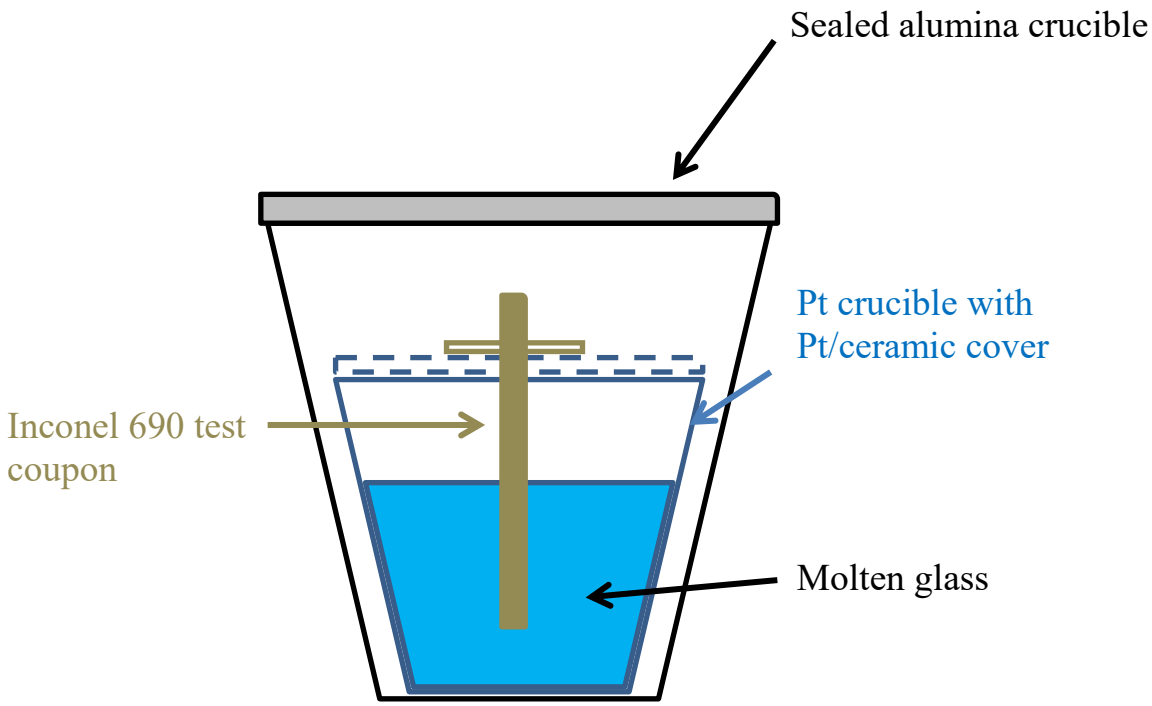

Figure 2.3. Experimental setup for closed crucible Inconel 690 corrosion tests.

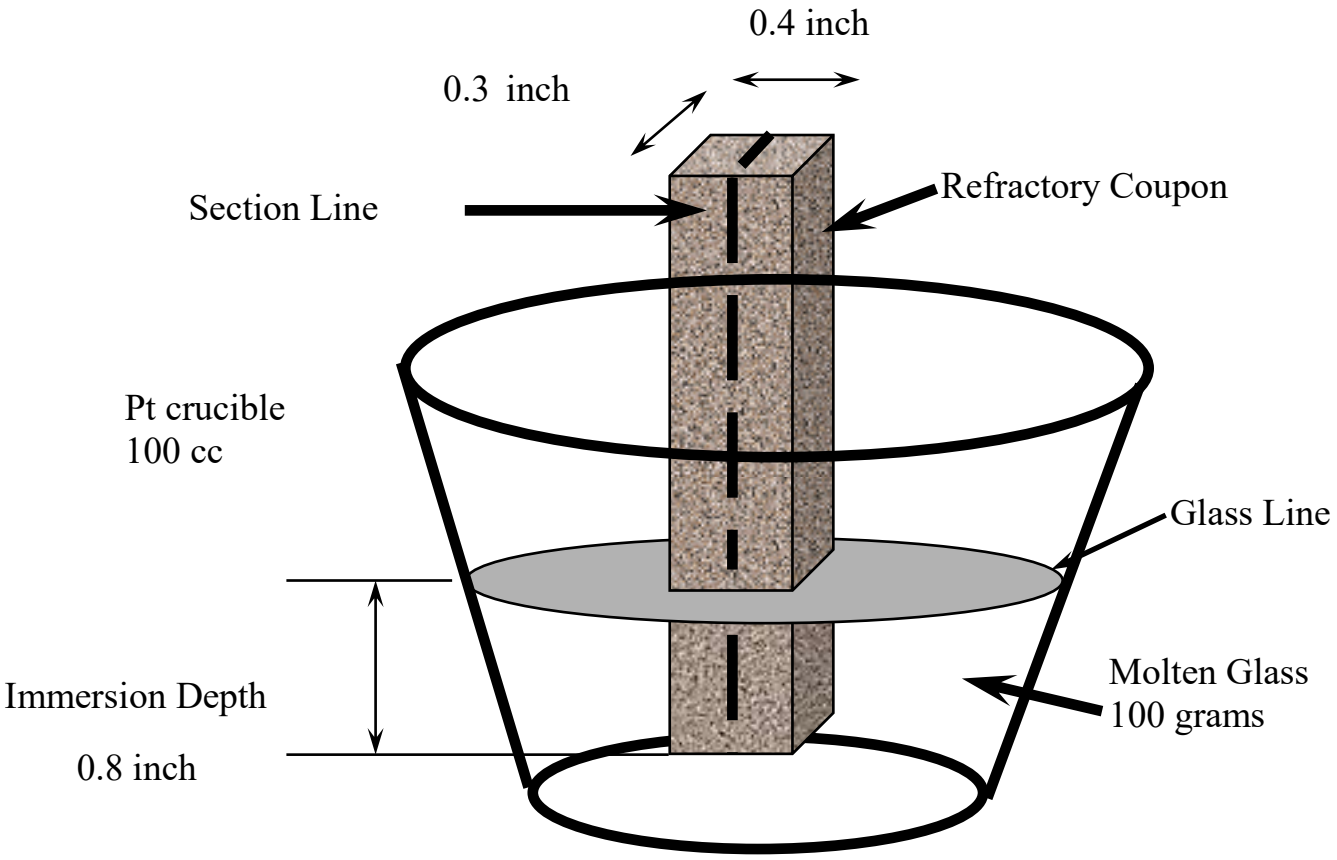

Figure 2.4. Dimensions of K-3 refractory coupon and crucible for closed crucible corrosion tests.

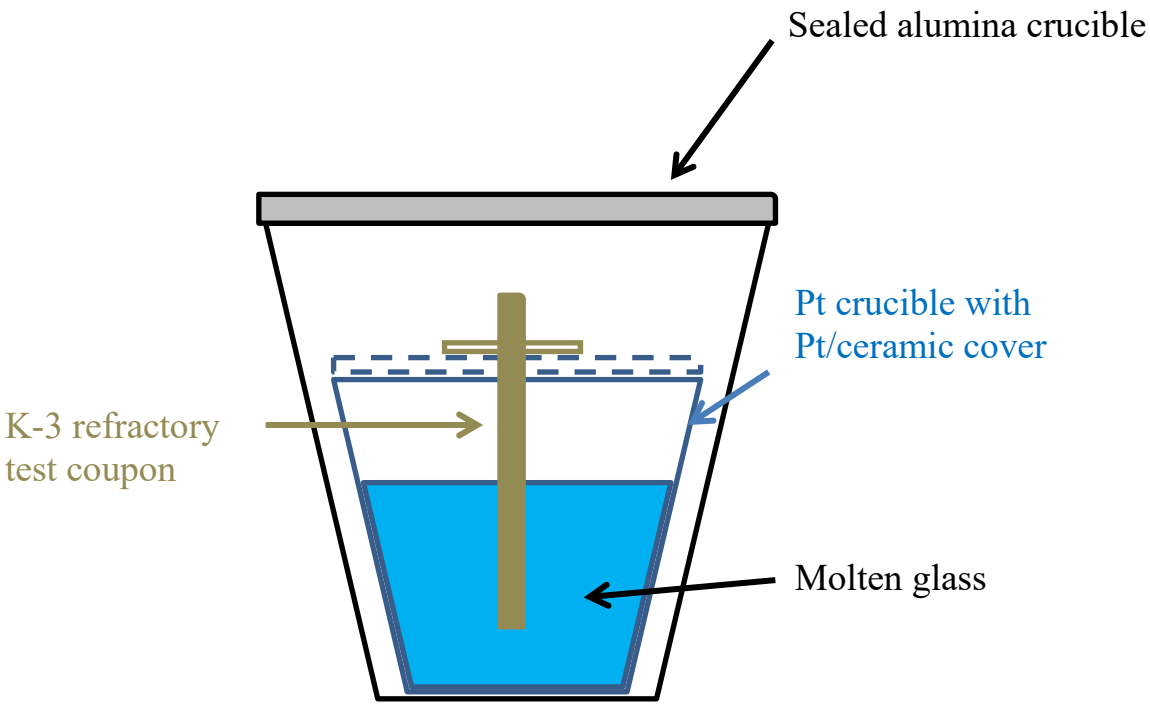

Figure 2.5. Experimental setup for closed crucible K-3 refractory corrosion tests.

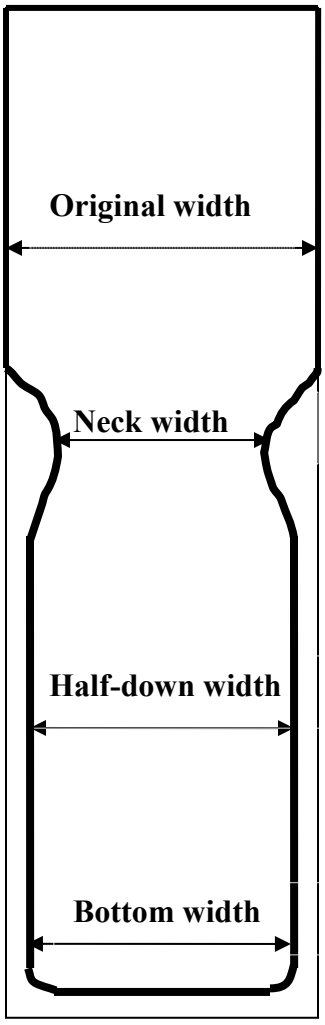

Figure 2.6. Schematic diagram of the cross section of a reacted test coupon (Inconel or K-3) after a typical glass contact corrosion test.

Stage 1 Reacted K-3 Coupons (Semi Sealed)

Test ID	LA20-1s	LA20-2s1	LA20-2s2	LA20-2s3	LA20-3s	LA20-4s
Reacted K3 coupon cross section images			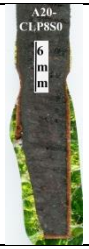			
K3 coupon ID	A20-CLP0S0-K3B	A20-CLP8S0-K3B	A20-CLP8S0-K3BR	A20-CLP8S0R-K3B	A20-CL0SP7-K3B	ORPLA20-K3BR
NECK LOSS	0.048”	0.017”	0.024”	0.027”	0.062”	0.034”
HALF DOWN LOSS	0”	EXPANDED	0.002”	EXPANDED	0.002”	0”
ALTERED ZONE	0.024”	0.016”	0.021”	0.022”	0.023”	0.021”

Stage 2 Reacted K3 Coupons (Sealed)

Test ID	LA20-1c	LA20-2c1	LA20-2c2	LA20-3c	LA20-4c
Reacted K3 coupon cross section images					
K3 coupon ID	A20-CLP0S0-K3BR2	A20-CLP8S0-K3BR2	A20-CLP8S0R-S-K3B	A20-CL0SP7-K3BR	A20-CLP7SP7-K3B
NECK LOSS	0”	0.005”	0.016”	0.033”	0.002”
HALF DOWN LOSS	0”	0.003”	EXPANDED	0.003”	0.001”
ALTERED ZONE	0.026”	0.016”	0.020	0.028”	0.020”

Stage 3 Reacted K3 Coupons (Sealed with Pt Sheet)

Test ID	LA20-1p	LA20-2p	LA20-3p	LA20-4p
Reacted K3 coupon cross section images				
K3 coupon ID	A20-CLP0S0-K3BR3	A20-CLP8S0R-K3BR	A20-CL0SP7-K3BR2	A20-CLP7SP7-K3B3
NECK LOSS	0.061”	0.001”	0.057”	0.006”
HALF DOWN LOSS	0.001”	0.001”	0.002”	0.001”
ALTERED ZONE	0.026”	0.024”	0.027”	0.026”

Figure 3.1. Cross sectional images of K-3 test coupons after corrosion experiments in ORPLA20. All dimension changes of K-3 coupons in Stage 2 and Stage 3 and LA20-4s in Stage 1 were by microscope, the rest were from scanned images.

Stage 1 Reacted K-3 Coupons (Semi-Sealed)

Test ID	LE12-1s	LE12-2s	LE12-3s	LE12-4s
Reacted K-3 coupon cross section images				
K-3 coupon ID	E12-CL0S0-K-3B**	E12-CLP4S0-NSP-K-3B*	ORPLE12-K-3BR*	E12-CLP4S1-K-3B**
NECK LOSS	0.036”	0.010”	0.030”	0.051”
HALF DOWN LOSS	0.011”	EXPANDED	0.002”	0.005”
ALTERED ZONE	0.020”	0.023”	0.023”	0.024”

Stage 2 Reacted K-3 Coupons (Sealed)

Test ID	LE12-1c	LE12-2c	LE12-3c	LE12-4c
Reacted K-3 coupon cross section images				
K-3 coupon ID	E12-CL0S0-K-3BR*	E12-CLP4S0-K-3B*	E12-5-K-3B*	E12-CLP4S1-K-3BR*
NECK LOSS	0”	0.004”	0”	0.002”
HALF DOWN LOSS	EXPANDED	0.001”	EXPANDED	0.002”
ALTERED ZONE	0.029”	0.020”	0.025”	0.021”

Stage 3 Reacted K-3 Coupons (Sealed with Pt Sheet)

Test ID	LE12-1p	LE12-2p	LE12-3p	4p
Reacted K-3 coupon cross section images				
K-3 coupon ID	E12-CL0S0-K-3BR2**	E12-CLP4S0-K-3B2*	E12-5-K-3BR*	E12-CLP4S1-K-3B2**
NECK LOSS	0.037”	0.005”	0.033”	0.015”
HALF DOWN LOSS	0.003”	0”	0.004”	0”
ALTERED ZONE	0.027”	0.026”	0.027”	0.017”

Figure 3.2. Cross sectional images of K-3 test coupons after corrosion experiments in ORPLE12 (* Measured by Microscope. ** Measured from Scanned image).

a)

b)

Figure 3.3. Photographs of interior side of Zirmul cover a) after Stage Two K-3 corrosion experiment (Test LA20-2c2), and b) clean Zirmul cover before corrosion experiment.

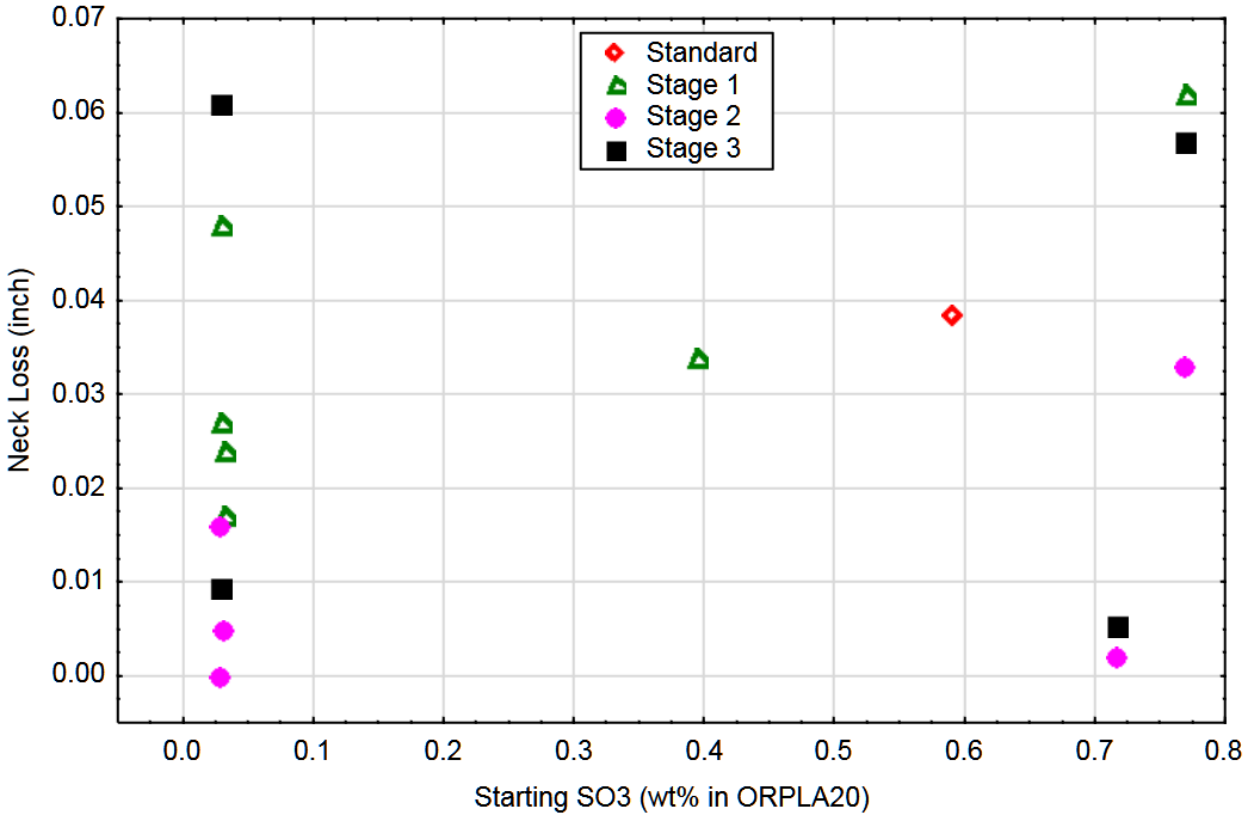

Figure 3.4. Neck dimension loss of K-3 test coupons vs. starting SO_3 wt% in ORPLA20 glasses. Symbols indicate test condition: open-to-air (standard), semi-sealed (Stage 1), sealed with Zirmul cover (Stage 2), and sealed with Pt cover (Stage 3).

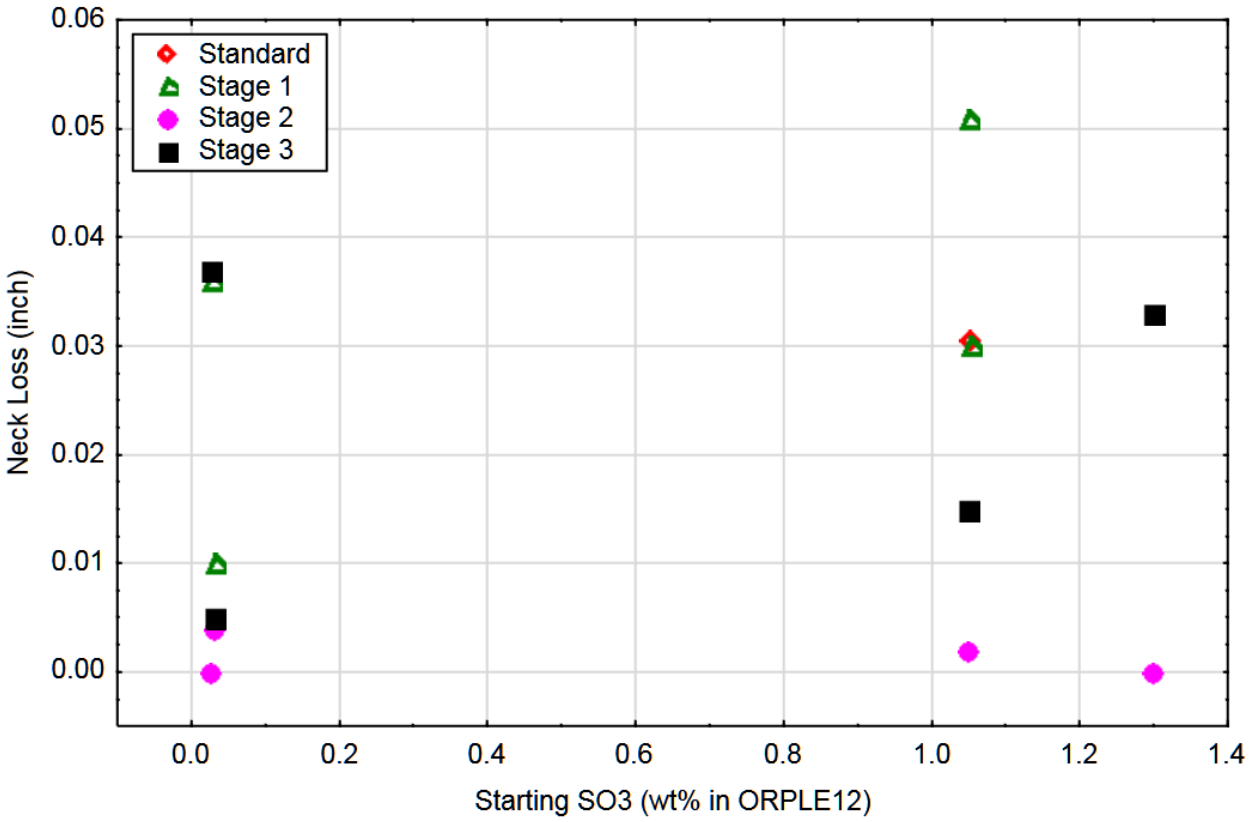

Figure 3.5. Neck dimension loss of K-3 test coupons vs. starting SO_3 wt% in ORPLE12 glasses. Symbols indicate test condition: open-to-air (standard), semi-sealed (Stage 1), sealed with Zirmul cover (Stage 2), and sealed with Pt cover (Stage 3).

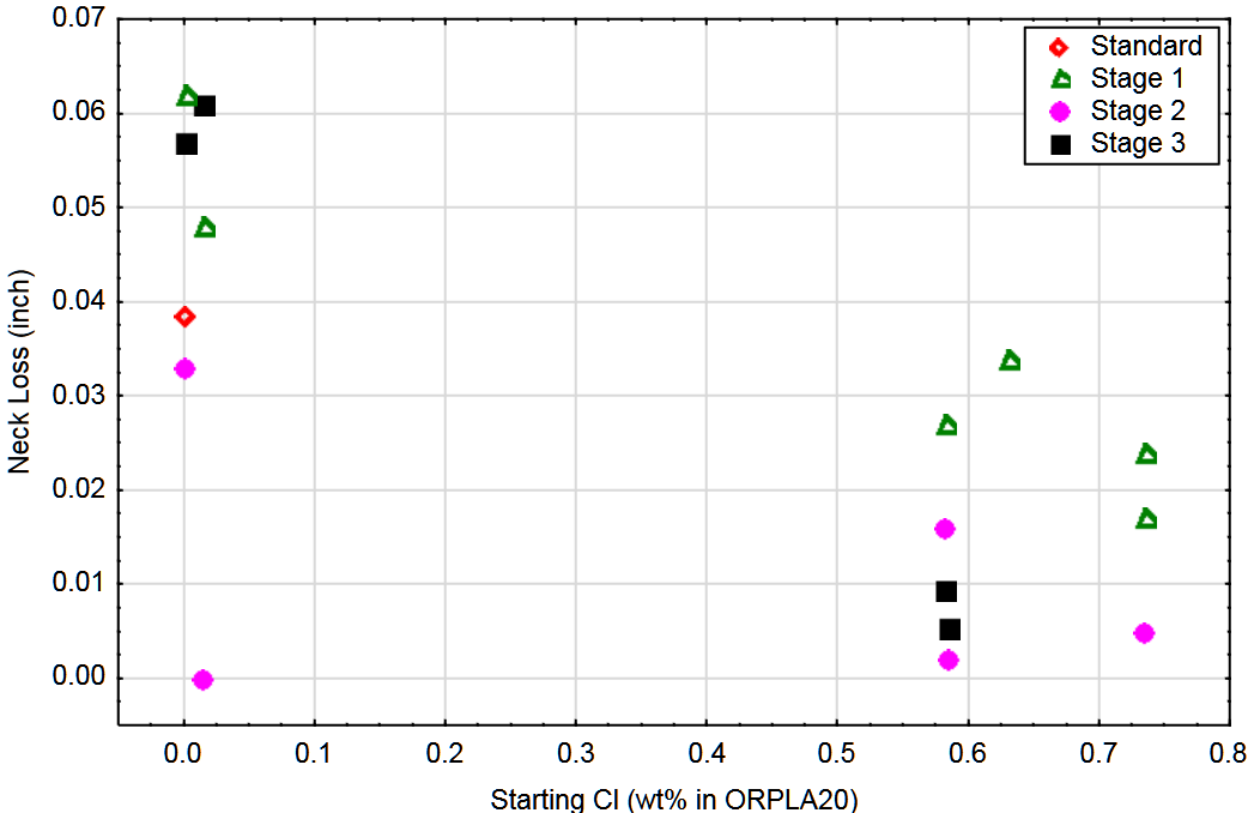

Figure 3.6. Neck dimension loss of K-3 test coupons vs. starting Cl wt% in ORPLA20 glasses. Symbols indicate test condition: open-to-air (standard), semi-sealed (Stage 1), sealed with Zirmul cover (Stage 2), and sealed with Pt cover (Stage 3).

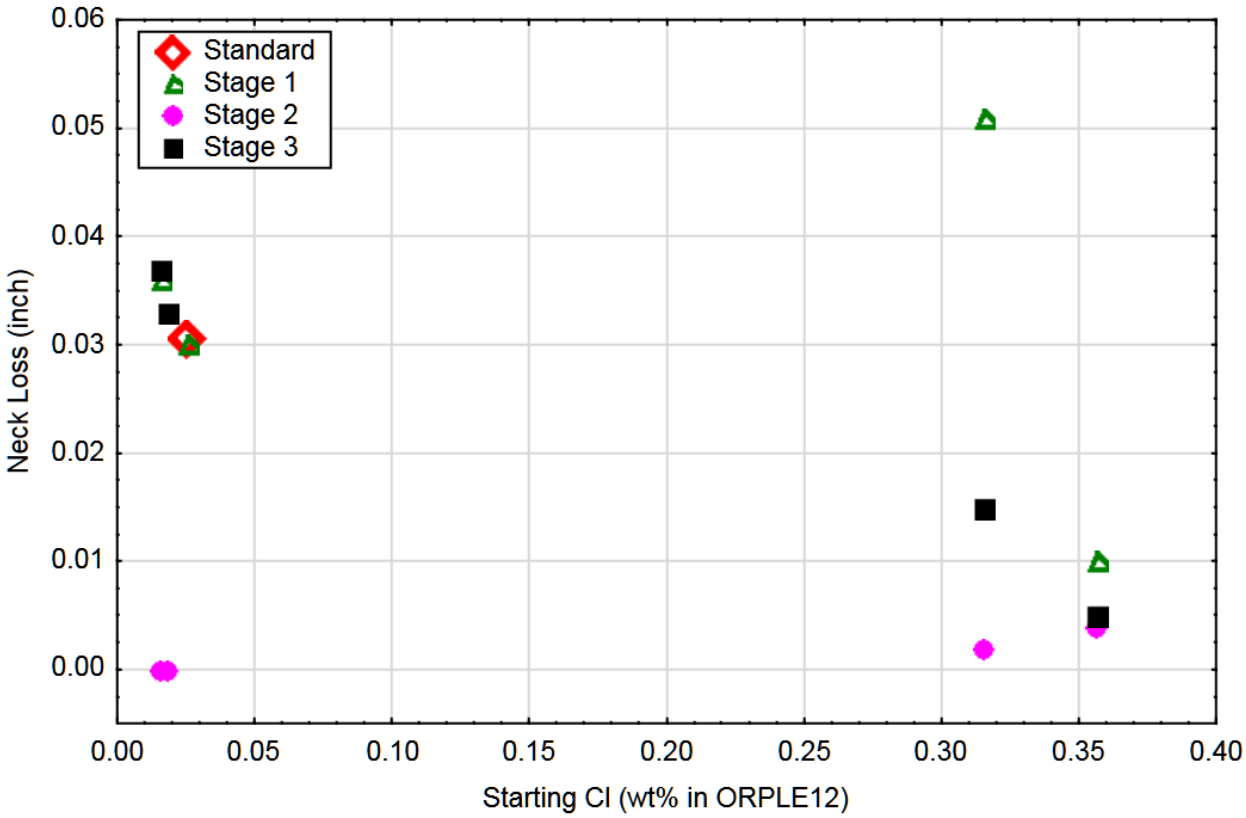

Figure 3.7. Neck dimension loss of K-3 test coupons vs. starting Cl wt% in ORPLE12 glasses. Symbols indicate test condition: open-to-air (standard), semi-sealed (Stage 1), sealed with Zirmul cover (Stage 2), and sealed with Pt cover (Stage 3).

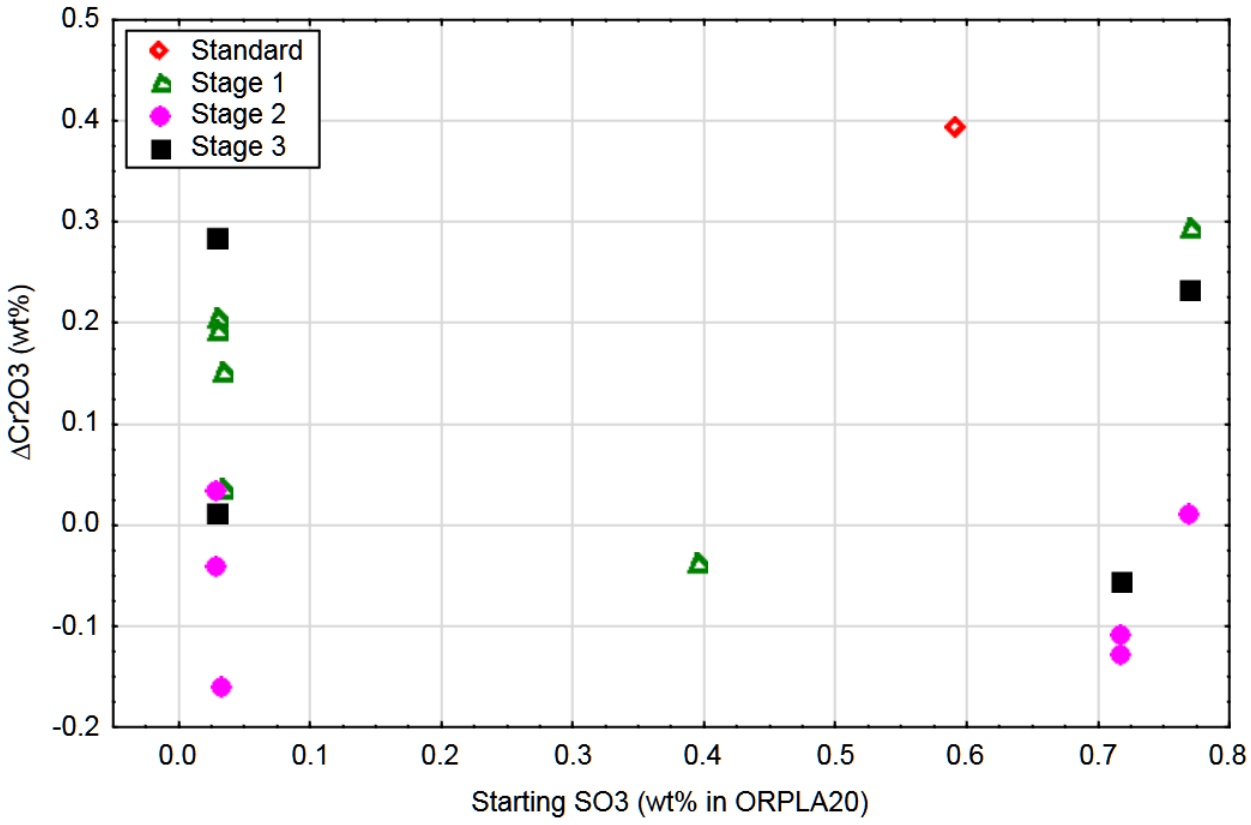

Figure 3.8. Change of Cr_2O_3 wt% in ORPLA20 glasses (after vs. before) vs. starting SO_3 wt% in glasses. Symbols indicate test condition: open-to-air (standard), semi-sealed (Stage 1), sealed with Zirmul cover (Stage 2), and sealed with Pt cover (Stage 3).

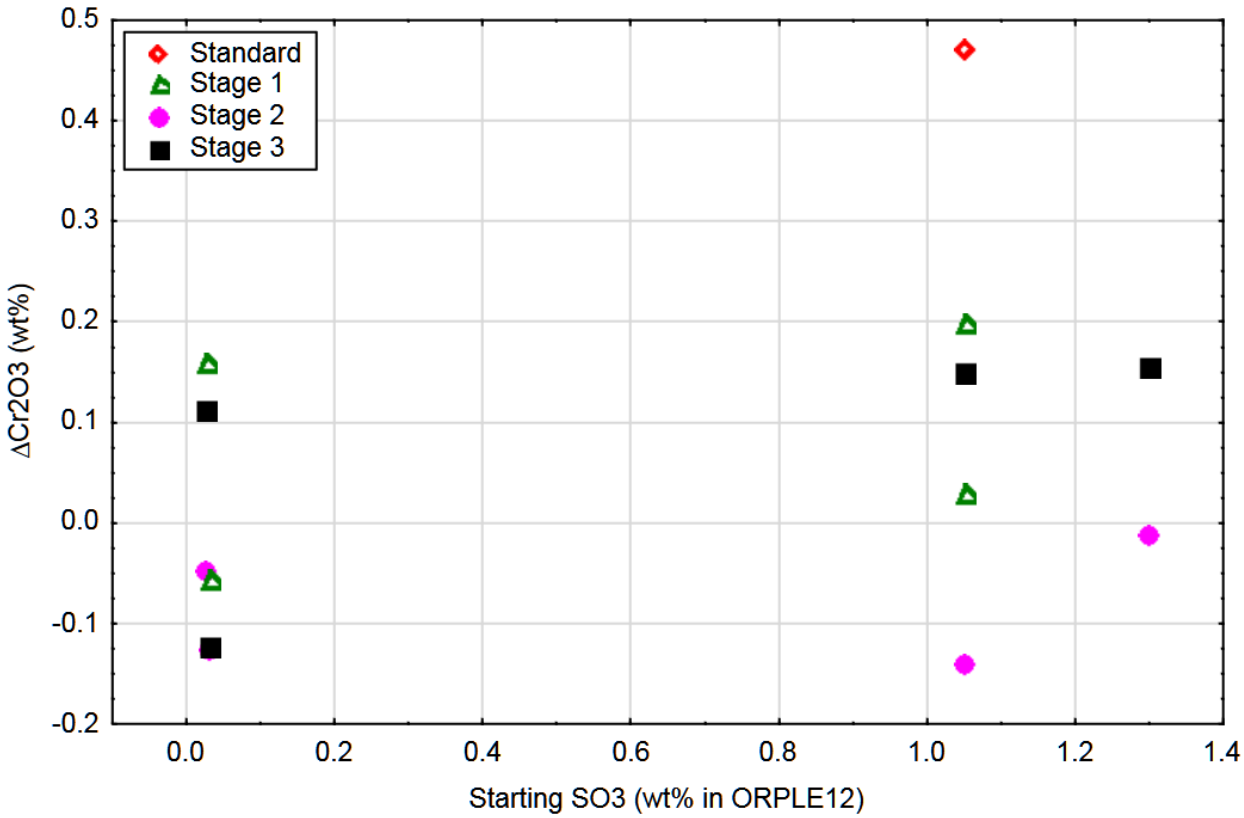

Figure 3.9. Change of Cr_2O_3 wt% in ORPLE12 glasses (after vs. before) vs. starting SO_3 wt% in glasses. Symbols indicate test condition: open-to-air (standard), semi-sealed (Stage 1), sealed with Zirmul cover (Stage 2), and sealed with Pt cover (Stage 3).

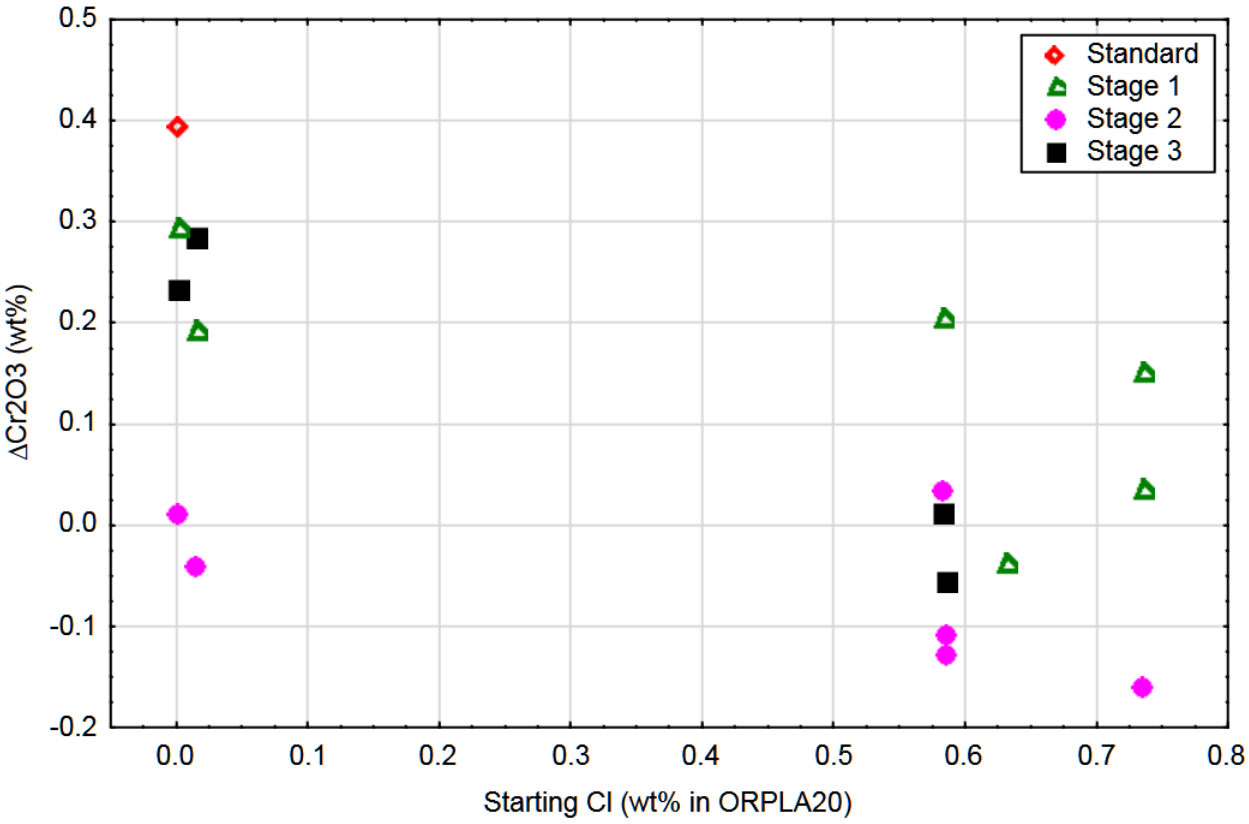

Figure 3.10. Change of Cr_2O_3 wt% in ORPLA20 glasses (after vs. before) vs. starting Cl wt% in glasses. Symbols indicate test condition: open-to-air (standard), semi-sealed (Stage 1), sealed with Zirmul cover (Stage 2), and sealed with Pt cover (Stage 3).

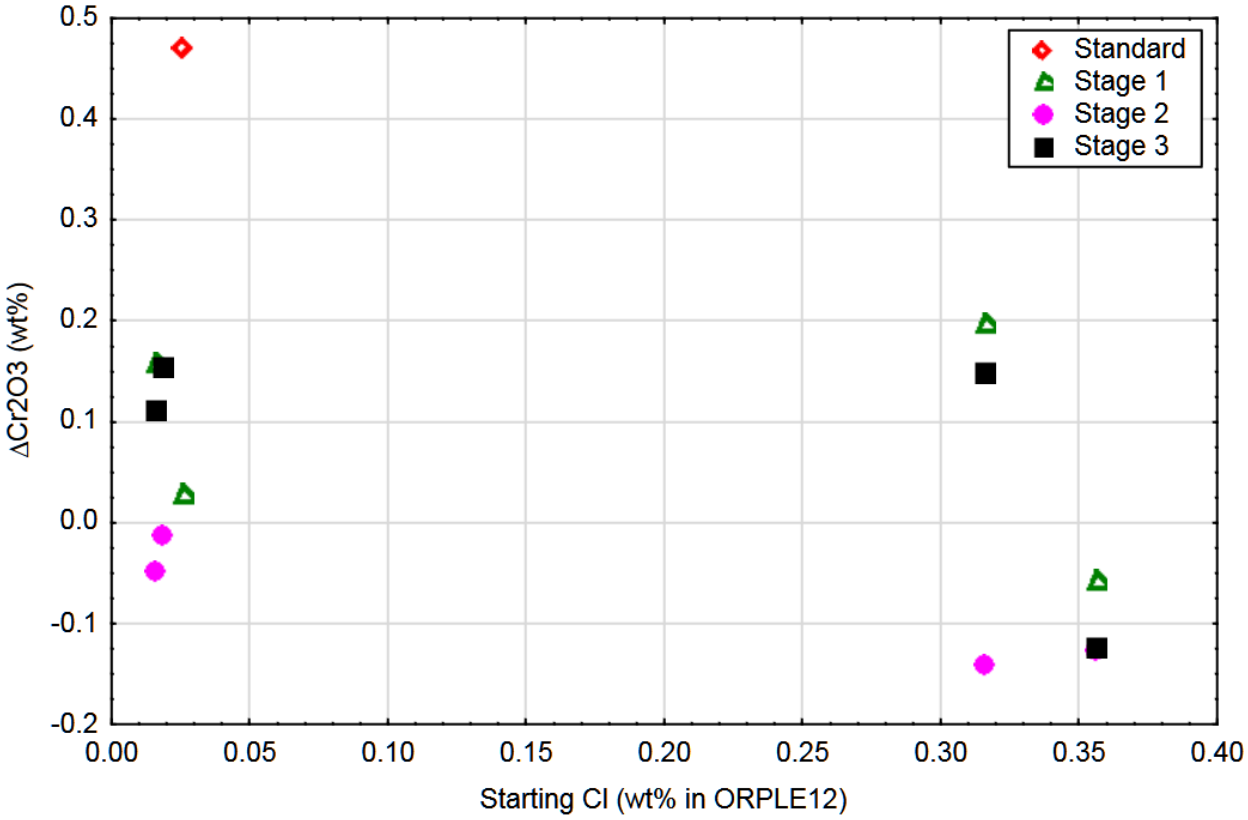

Figure 3.11. Change of Cr_2O_3 wt% in ORPLE12 glasses (after vs. before) vs. starting Cl wt% in glasses. Symbols indicate test condition: open-to-air (standard), semi-sealed (Stage 1), sealed with Zirmul cover (Stage 2), and sealed with Pt cover (Stage 3).

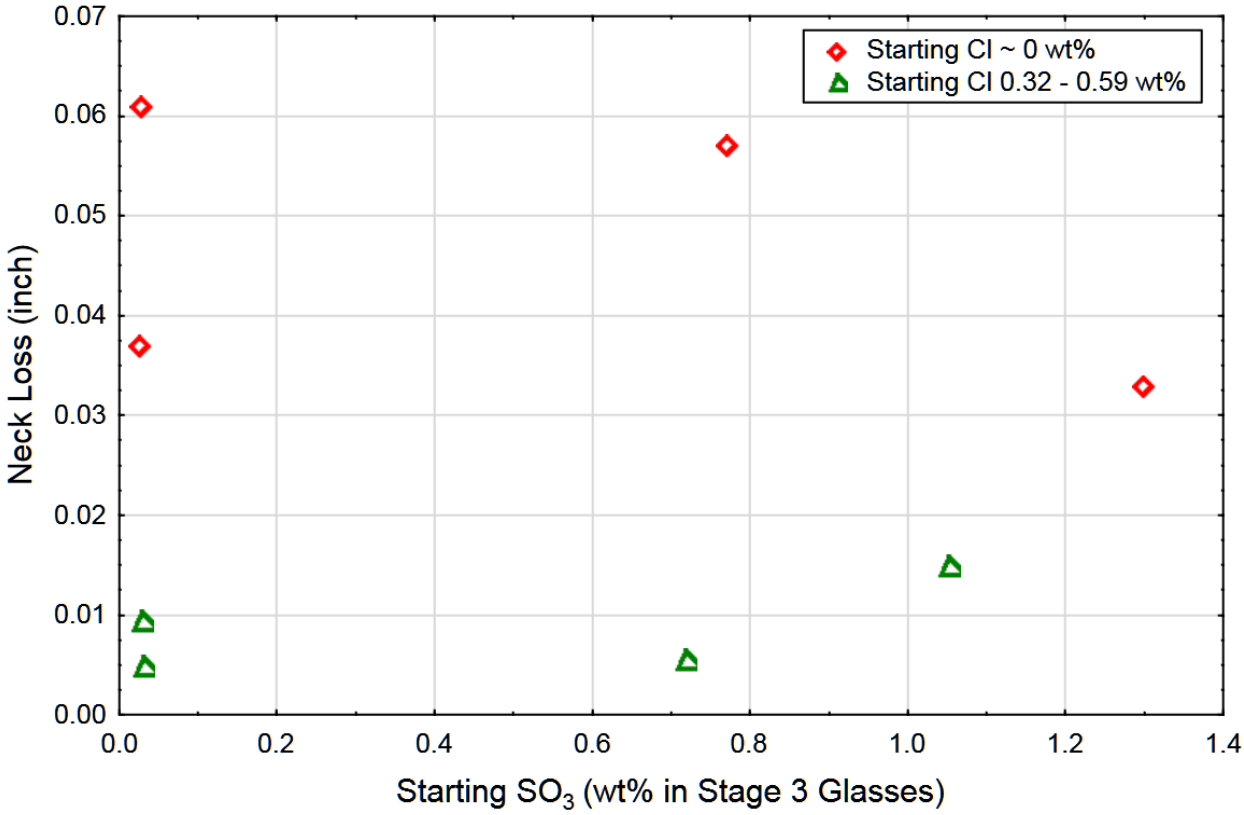

Figure 3.12. Neck dimension loss of K-3 test coupons vs. starting SO_3 wt% in Stage 3 glasses. Symbols indicate starting Cl wt% in the glasses.

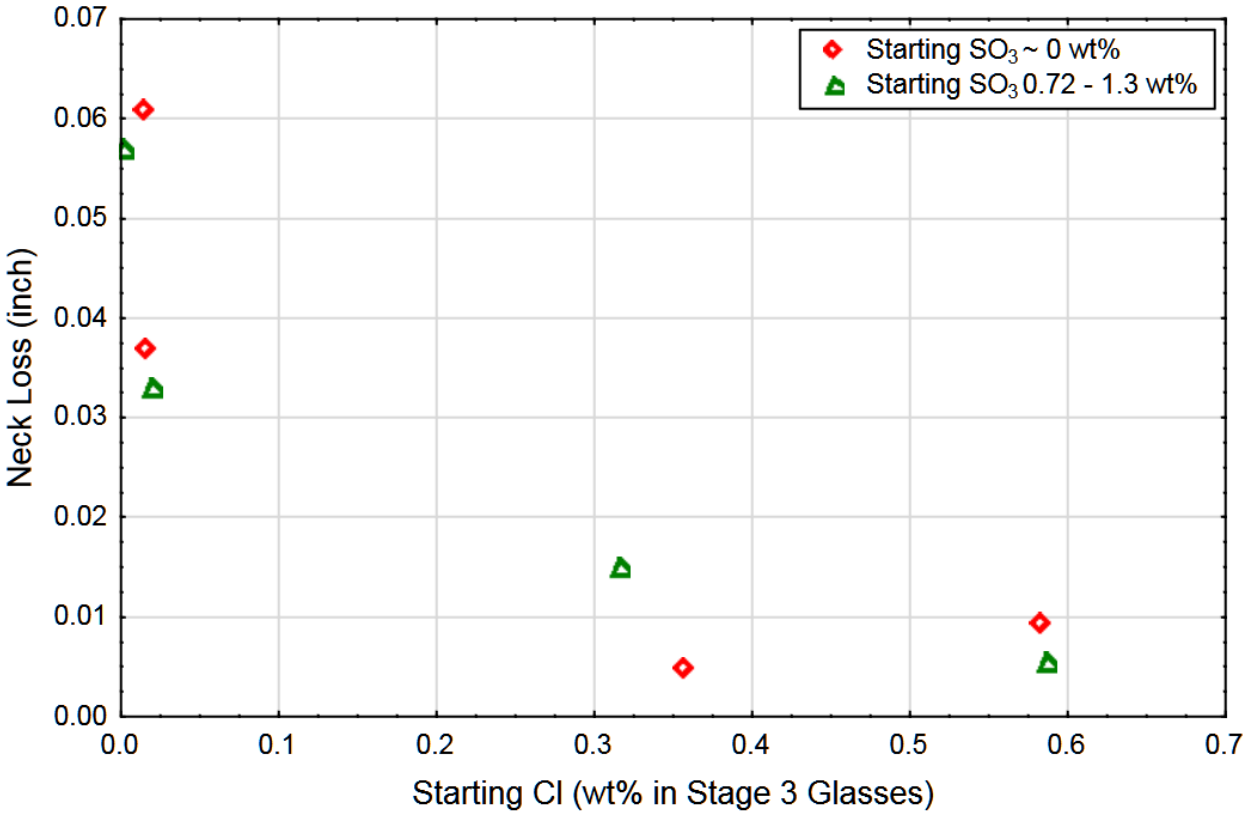

Figure 3.13. Neck dimension loss of K-3 test coupons vs. starting Cl wt% in Stage 3 glasses. Symbols indicate starting SO_3 wt% in the glasses.

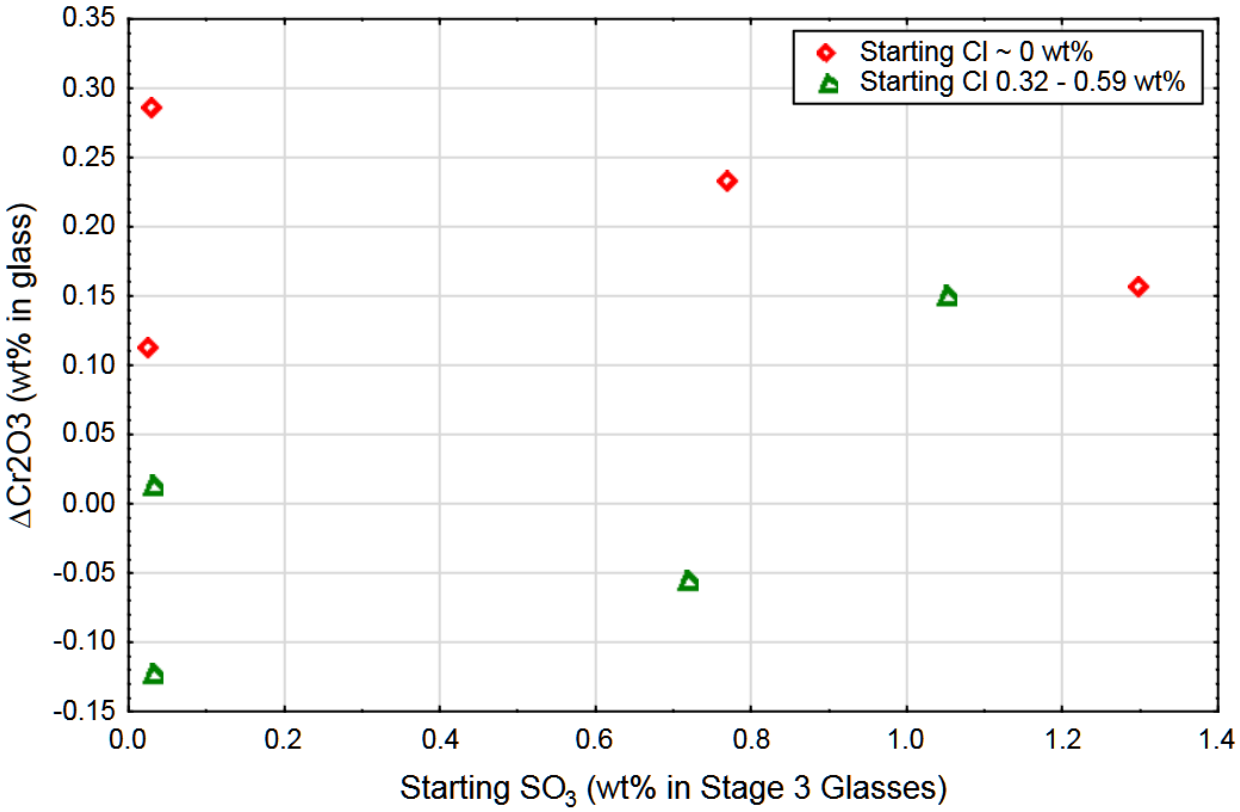

Figure 3.14 Change of Cr_2O_3 wt% in glasses (after vs. before) vs. starting SO_3 wt% in Stage 3 glasses. Symbols indicate starting Cl wt% in the glasses.

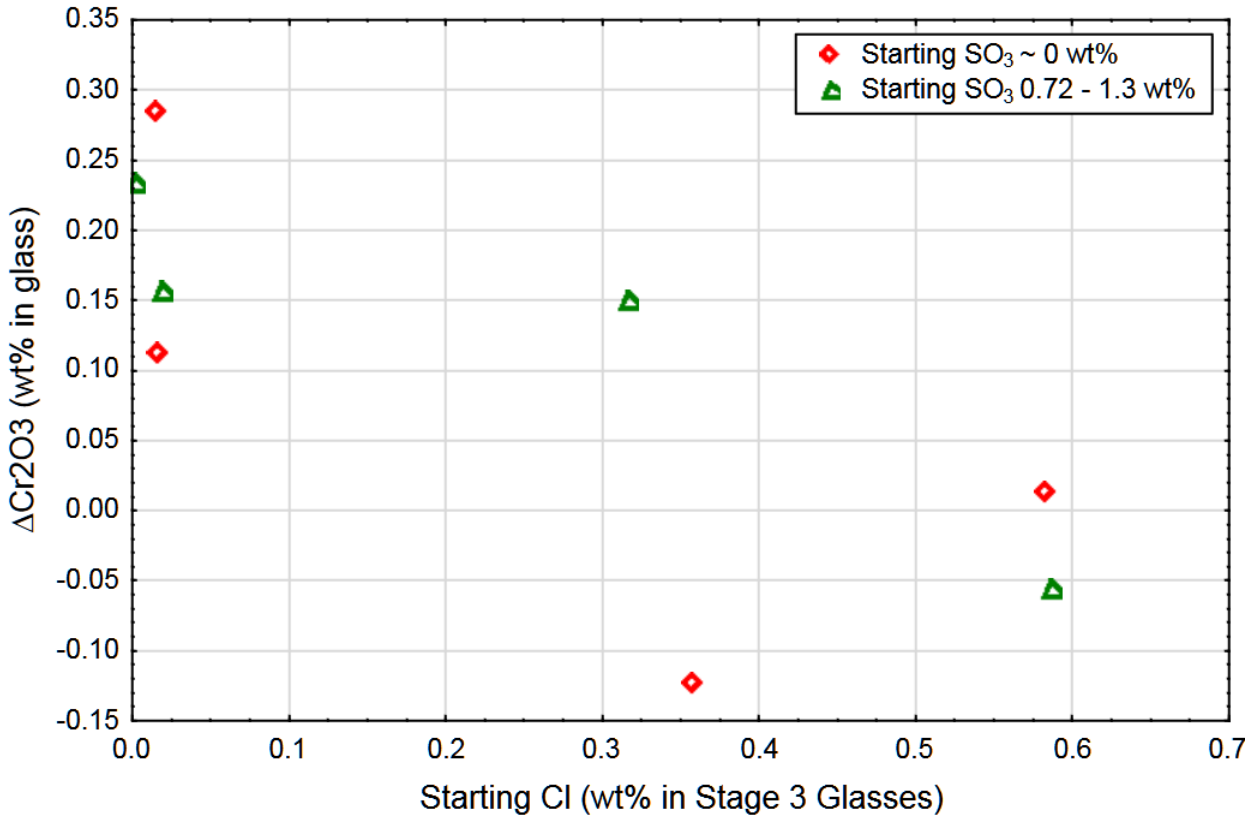

Figure 3.15. Change of Cr_2O_3 wt% in glasses (after vs. before) vs. starting Cl wt% in Stage 3 glasses. Symbols indicate SO_3 wt% in starting glasses.

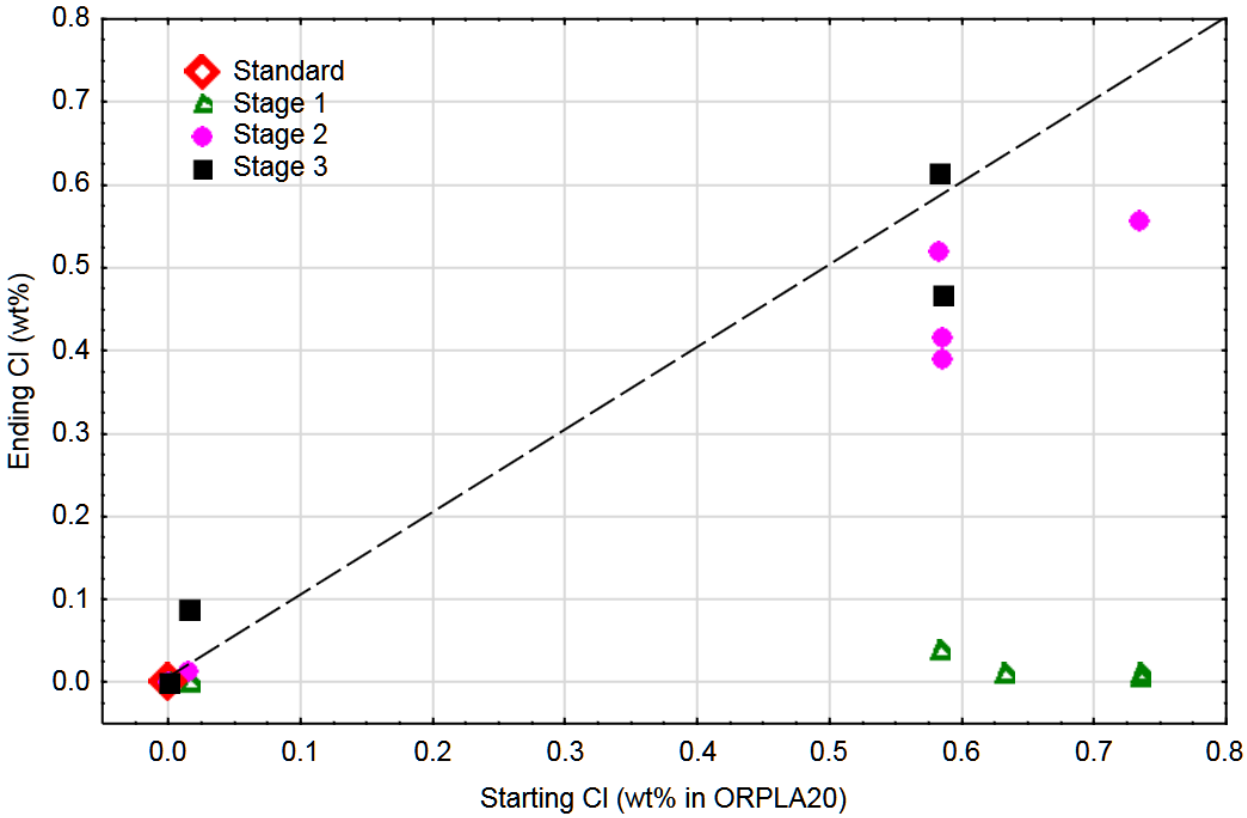

Figure 3.16. Retention of Cl in ORPLA20 glasses (ending Cl wt% vs. starting Cl wt%). Symbols indicate test condition: open-to-air (standard), semi-sealed (Stage 1), sealed with Zirmul cover (Stage 2), and sealed with Pt cover (Stage 3).

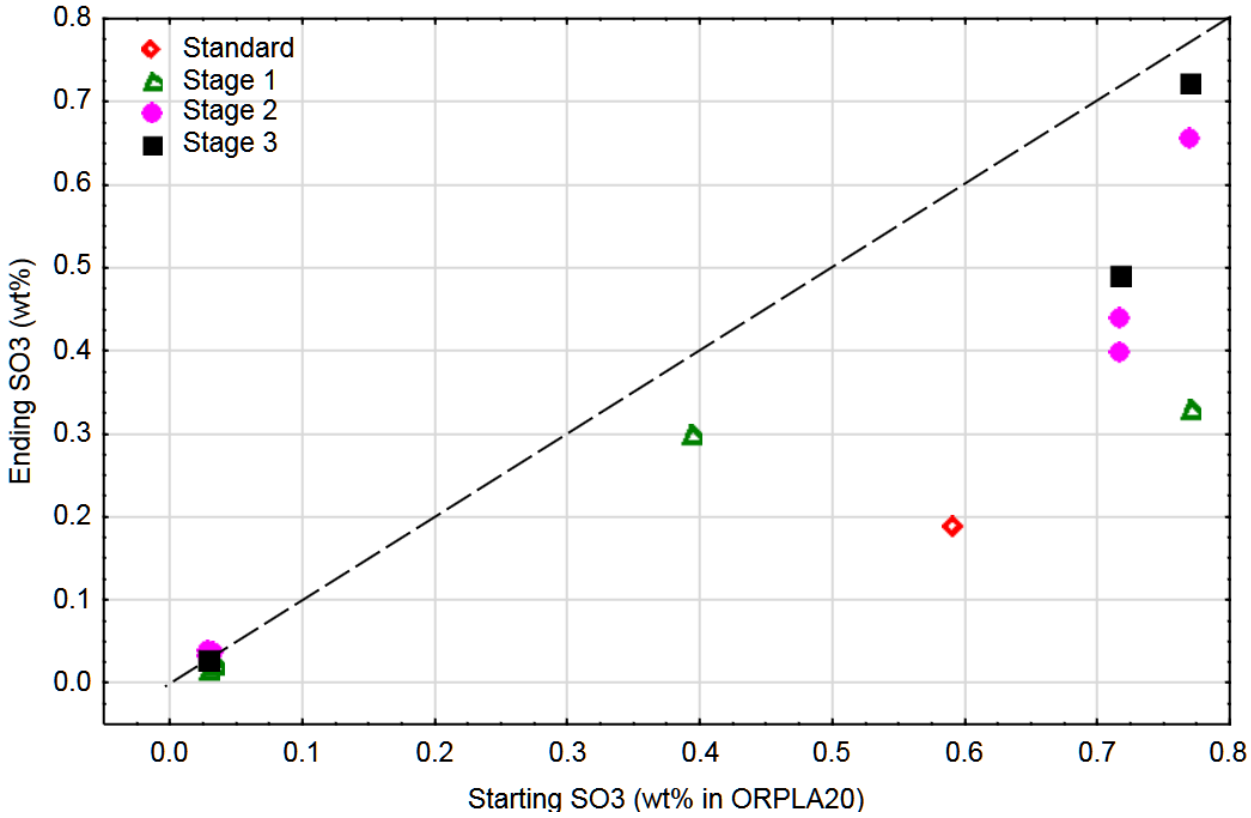

Figure 3.17. Retention of SO_3 in ORPLA20 glasses (ending SO_3 wt% vs. starting SO_3 wt%). Symbols indicate test condition: open-to-air (standard), semi-sealed (Stage 1), sealed with Zirmul cover (Stage 2), and sealed with Pt cover (Stage 3).

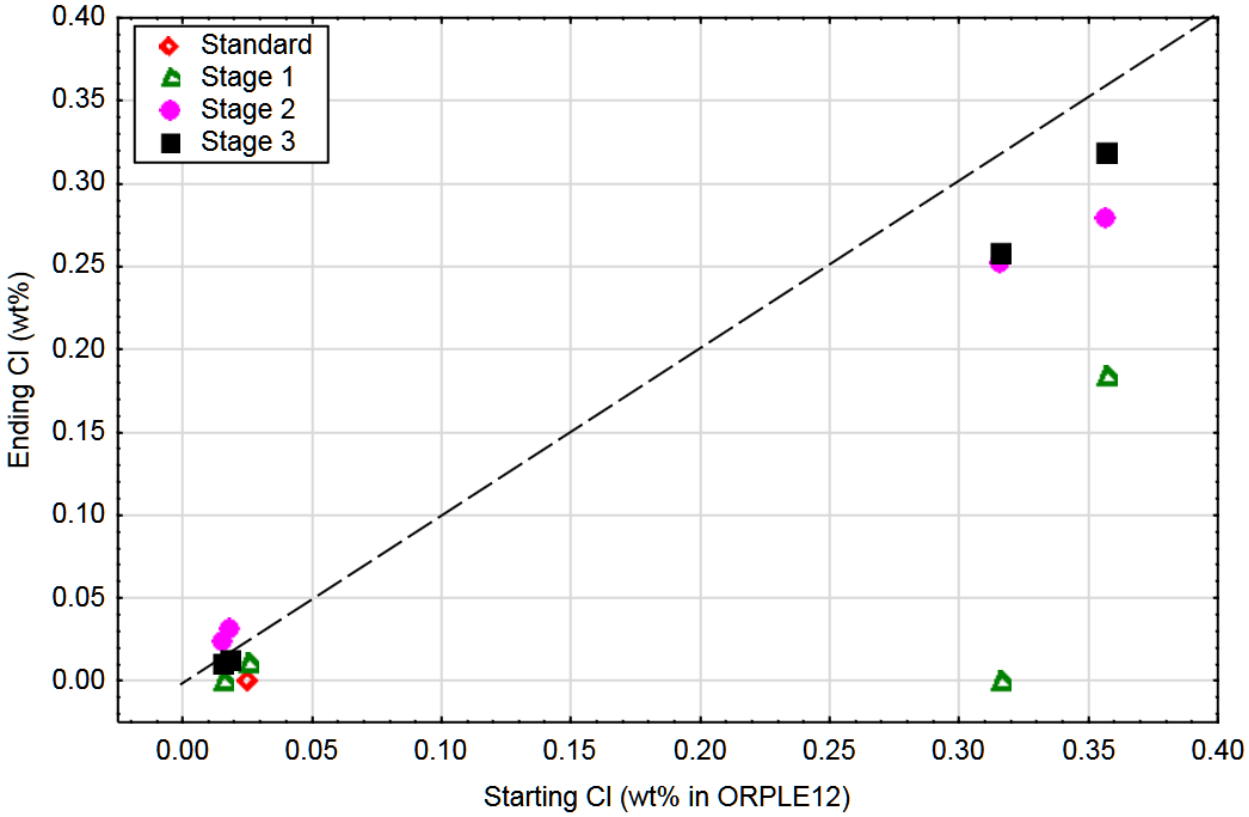

Figure 3.18. Retention of Cl in ORPLE12 glasses (ending Cl wt% vs. starting Cl wt%). Symbols indicate test condition: open-to-air (standard), semi-sealed (Stage 1), sealed with Zirmul cover (Stage 2), and sealed with Pt cover (Stage 3).

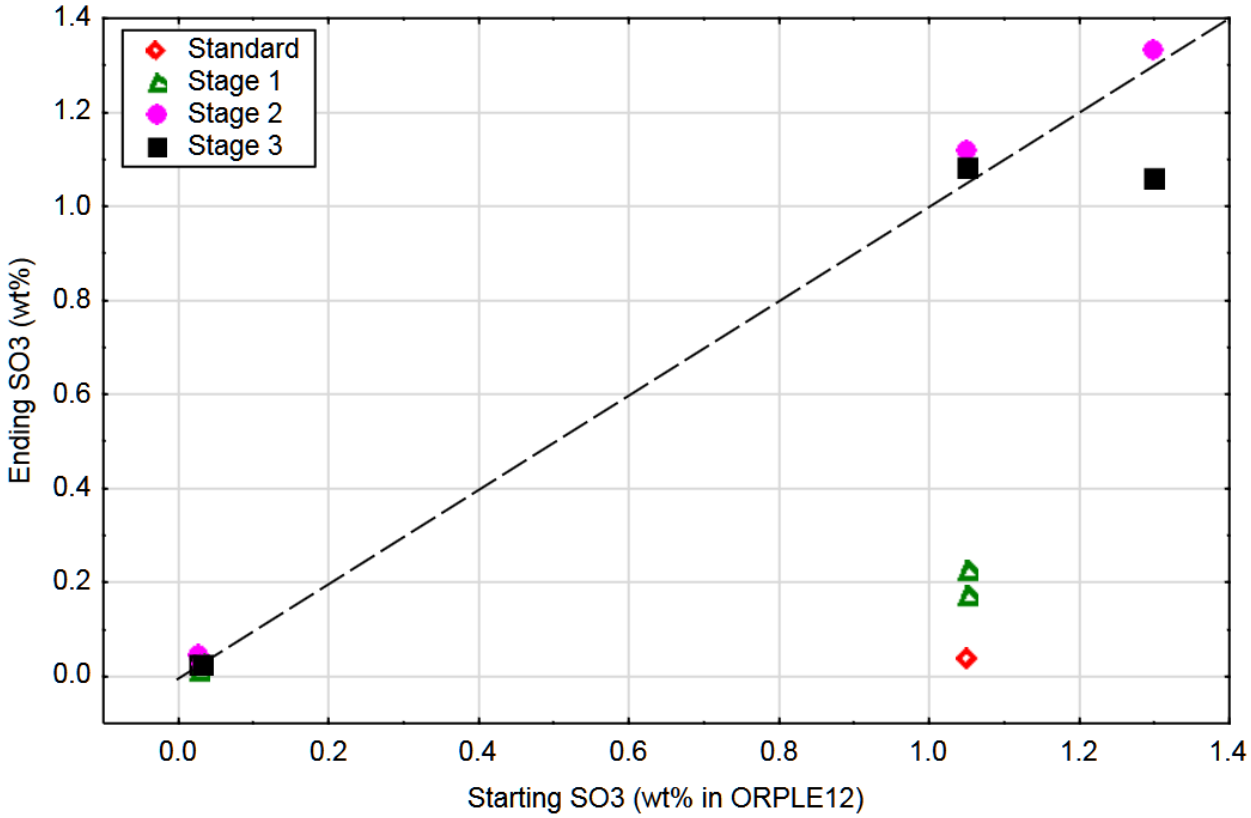

Figure 3.19. Retention of SO_3 in ORPLE12 glasses (ending SO_3 wt% vs. starting SO_3 wt%). Symbols indicate test condition: open-to-air (standard), semi-sealed (Stage 1), sealed with Zirmul cover (Stage 2), and sealed with Pt cover (Stage 3).

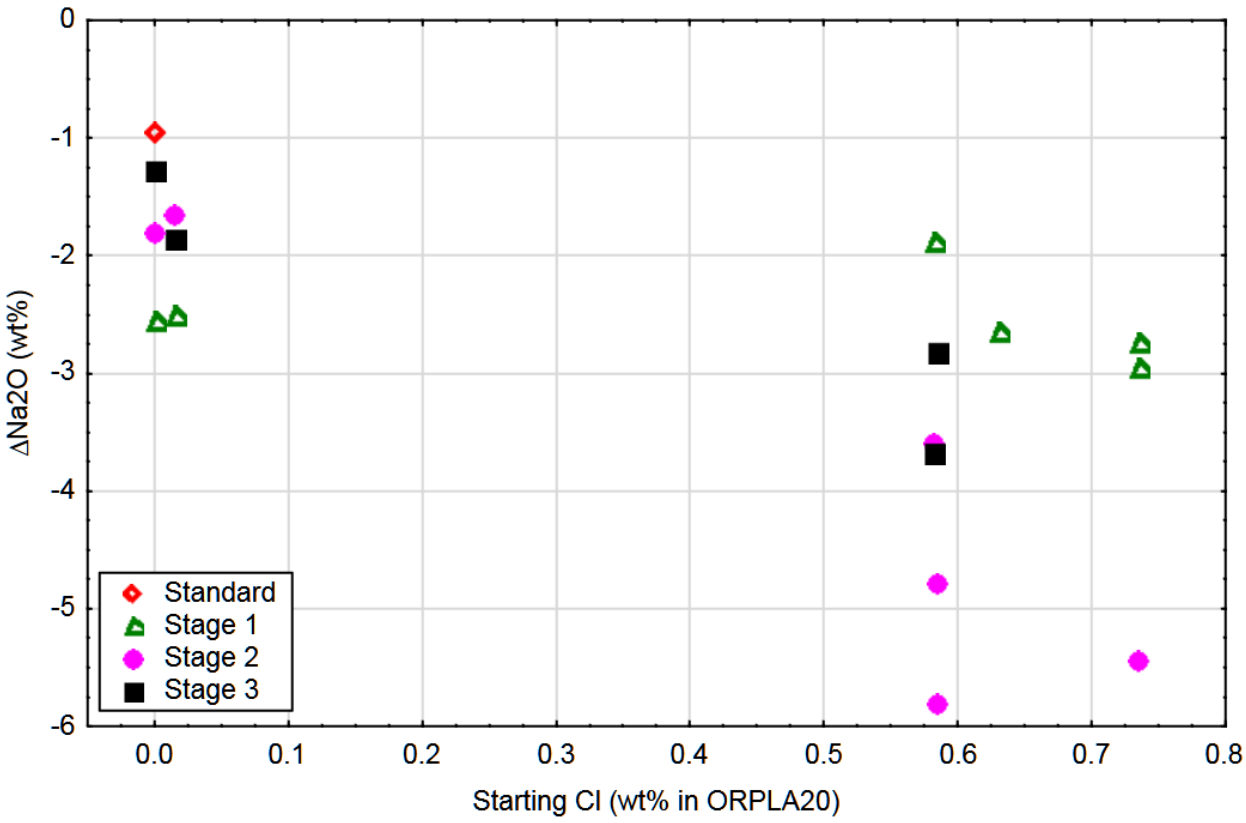

Figure 3.20. Change of Na_2O wt% in ORPLA20 glasses (after vs. before) vs. starting Cl wt% in glasses. Symbols indicate test condition: open-to-air (standard), semi-sealed (Stage 1), sealed with Zirmul cover (Stage 2), and sealed with Pt cover (Stage 3).

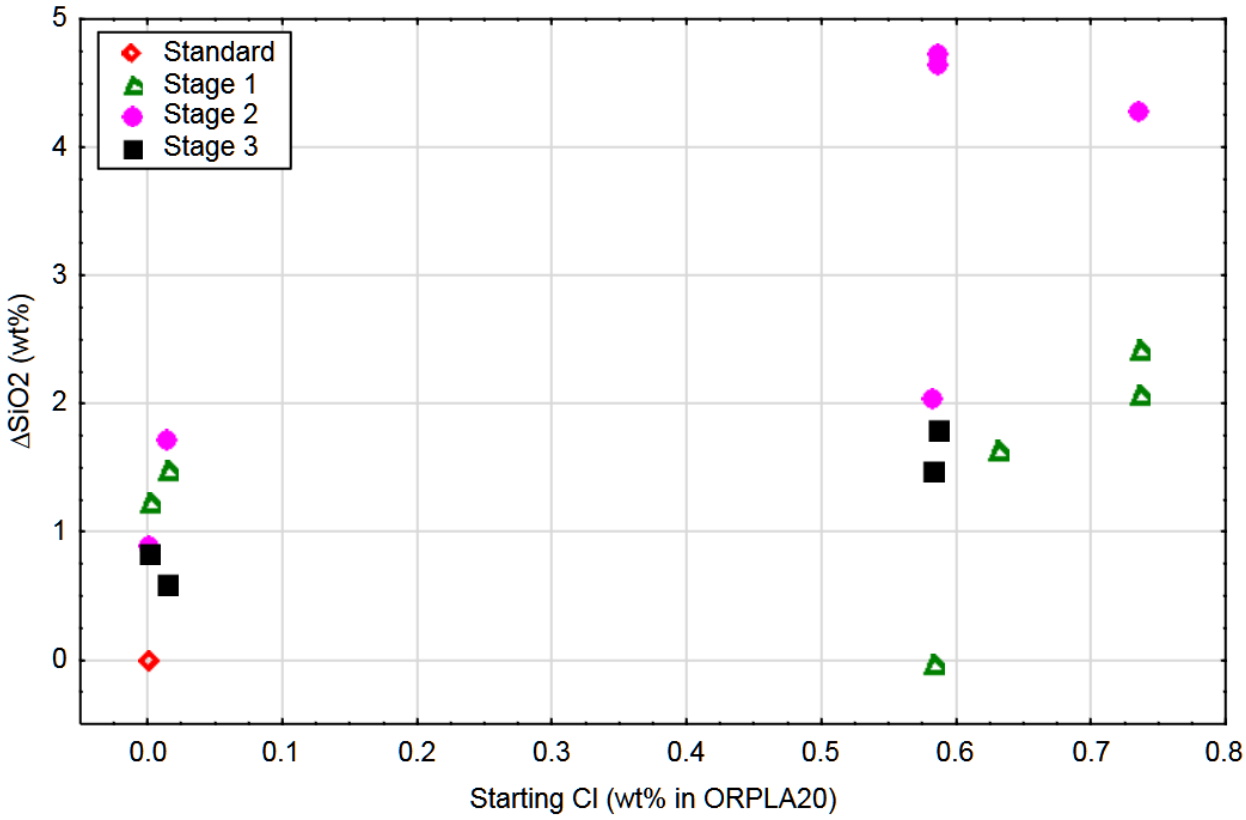

Figure 3.21. Change of SiO_2 wt% in ORPLA20 glasses (after vs. before) vs. starting Cl wt% in glasses. Symbols indicate test condition: open-to-air (standard), semi-sealed (Stage 1), sealed with Zirmul cover (Stage 2), and sealed with Pt cover (Stage 3).

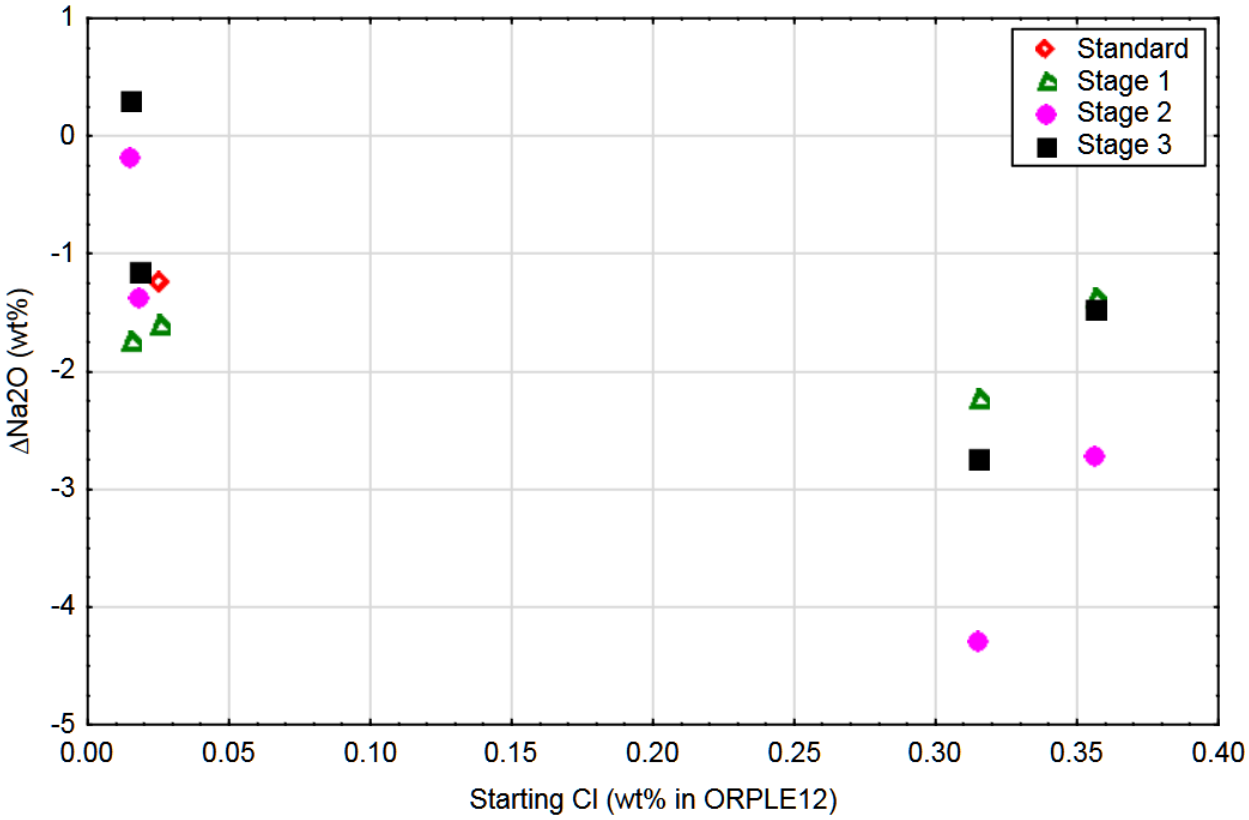

Figure 3.22. Change of Na_2O wt% in ORPLE12 glasses (after vs. before) vs. starting Cl wt% in glasses. Symbols indicate test condition: open-to-air (standard), semi-sealed (Stage 1), sealed with Zirmul cover (Stage 2), and sealed with Pt cover (Stage 3).

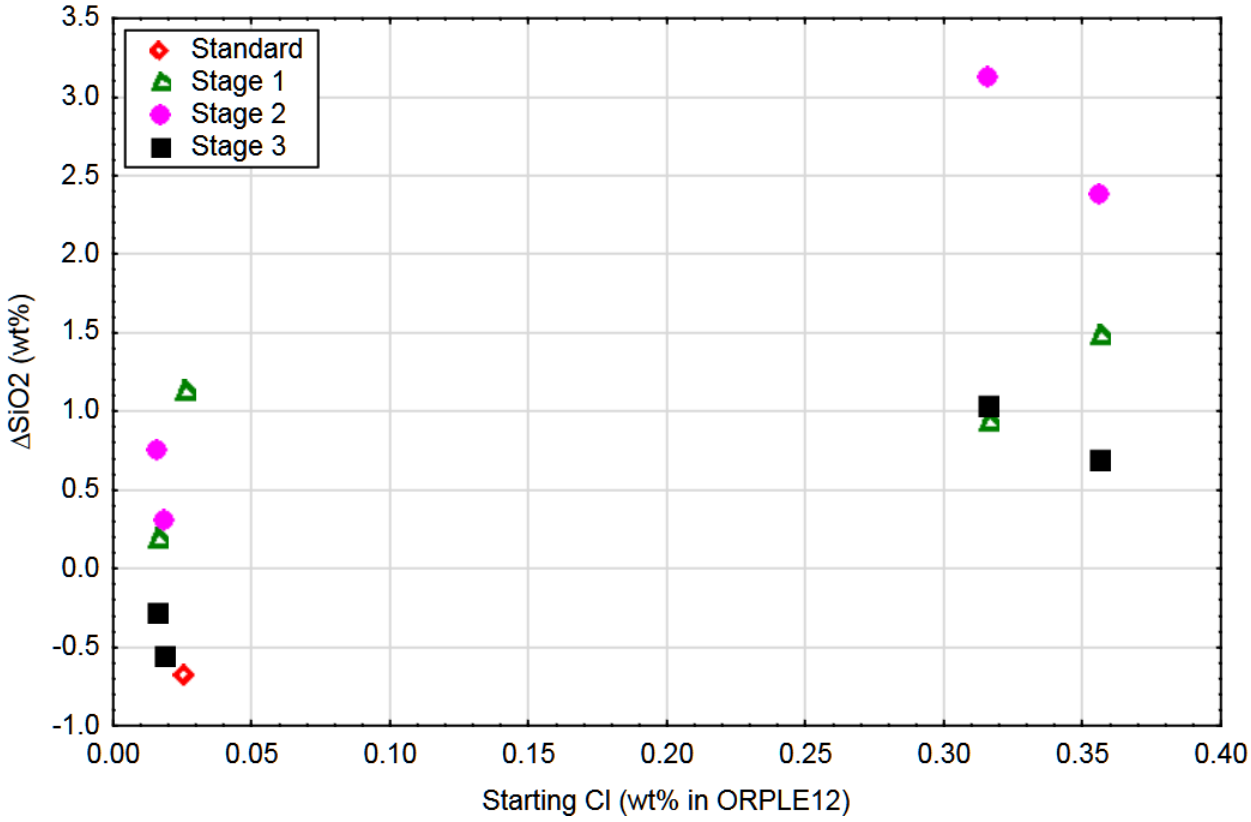

Figure 3.23. Change of SiO_2 wt% in ORPLE12 glasses (after vs. before) vs. starting Cl wt% in glasses. Symbols indicate test condition: open-to-air (standard), semi-sealed (Stage 1), sealed with Zirmul cover (Stage 2), and sealed with Pt cover (Stage 3).

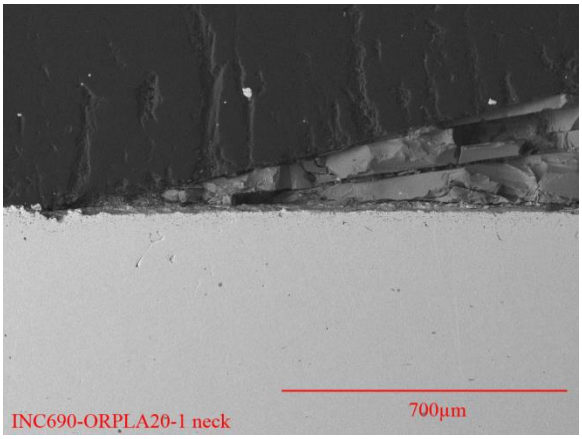

(1) Inconel 690 (light grey, lower half) at Neck region with glass (darker grey adjacent to alloy surface).

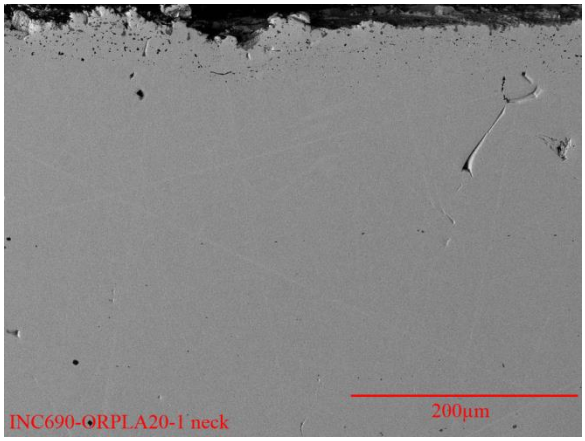

(2) Inconel 690 (light grey) at Neck region.

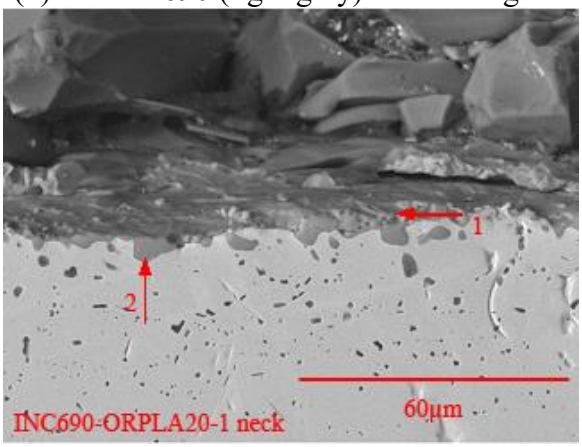

(3) Inconel 690 (light grey, lower half) at Neck region with darker grey oxide pockets within and on surface of alloy (#1, #2 for Cr_2O_3).

Figure 4.1a. SEM images of Inconel 690 after LA20-1 test (closed crucible corrosion) in ORPLA20.

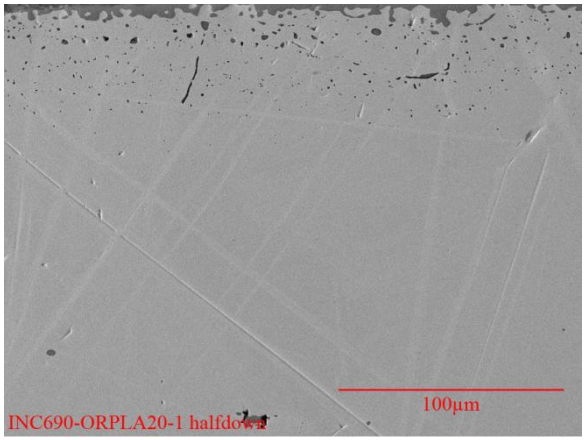

(4) Inconel 690 (light grey) at Half-down region.

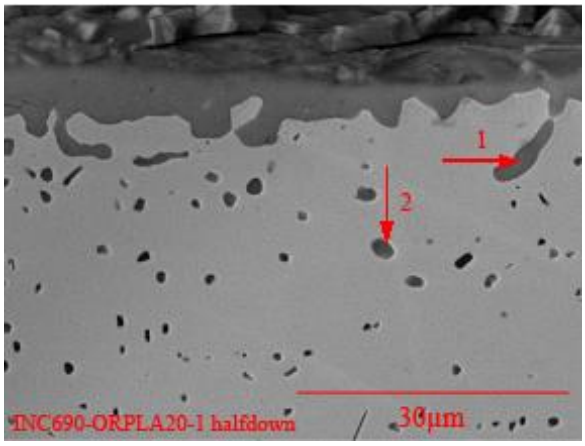

(5) Inconel 690 (light grey) at Half-down region with darker grey oxides pockets within and on surface of alloy (#1, #2 for Cr-rich oxide)

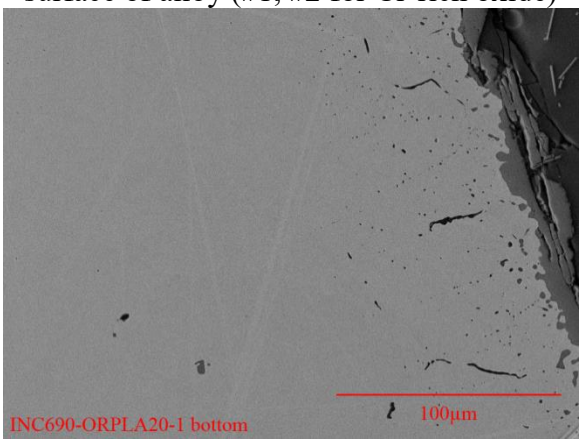

(6) Inconel 690 (light grey) at Bottom

Figure 4.1a. SEM images of Inconel 690 after LA20-1 test (closed crucible corrosion) in ORPLA20 (continued).

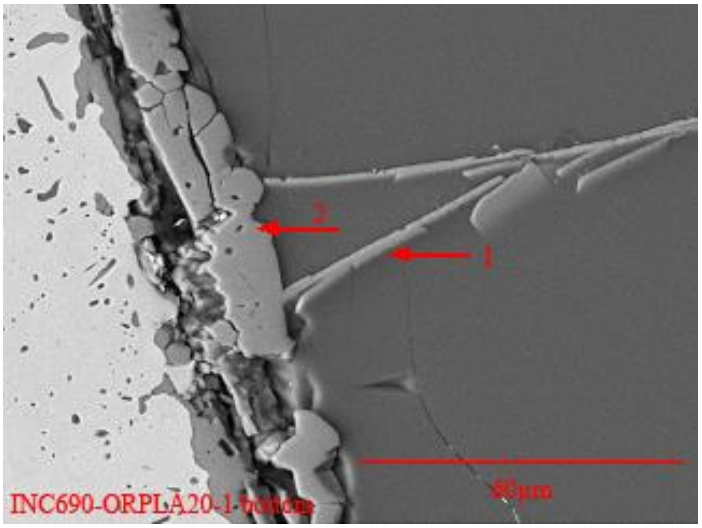

(7) Inconel 690 (light grey) at Bottom region (#1, #2 for Cr oxide)

Figure 4.1a. SEM images of Inconel 690 after LA20-1 test (closed crucible corrosion) in ORPLA20 (continued).

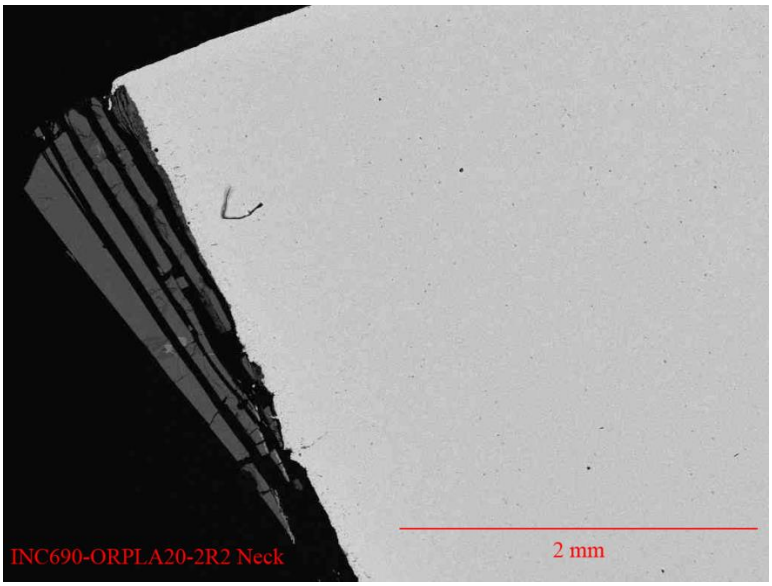

(1) Inconel 690 (light grey) at Neck region.

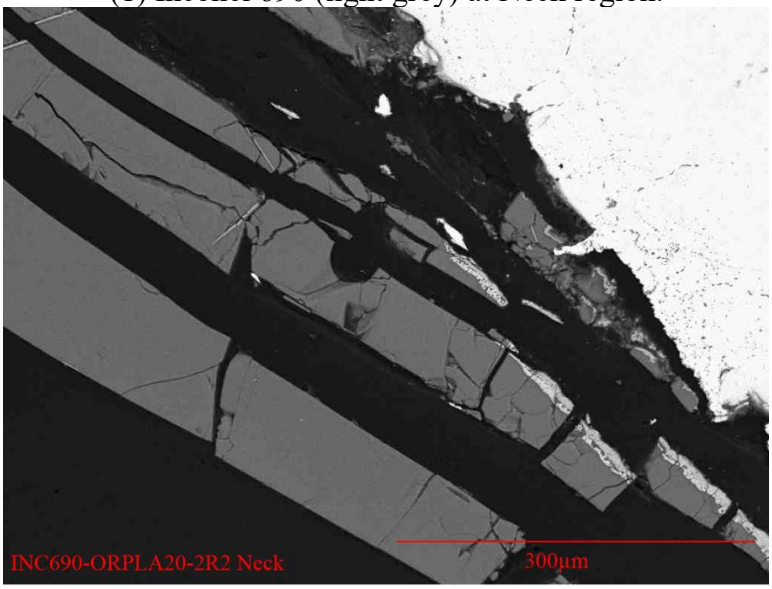

(2) Inconel 690 (bright upper right) at Neck region. Detached scale is visible between alloy and glass (darker grey).

Figure 4.1b. SEM images of Inconel 690 after LA20-2 test (closed crucible corrosion) in ORPLA20.

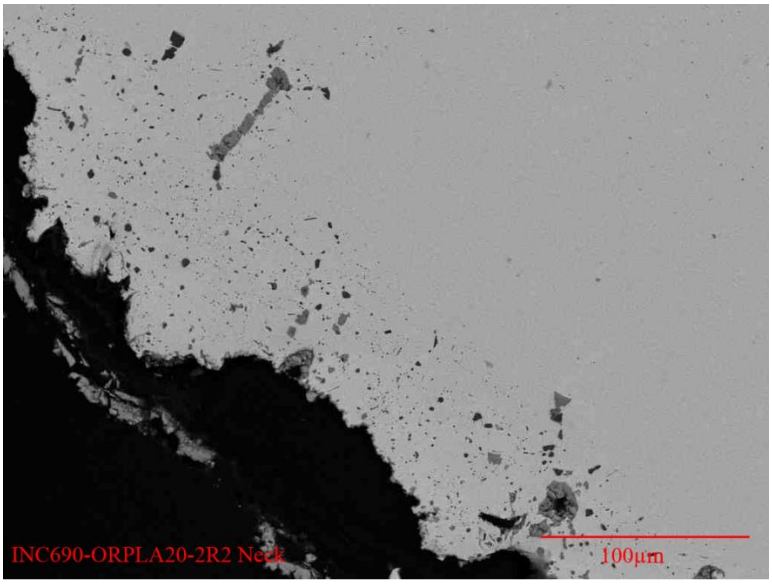

(3) Inconel 690 (light grey) at Neck region.

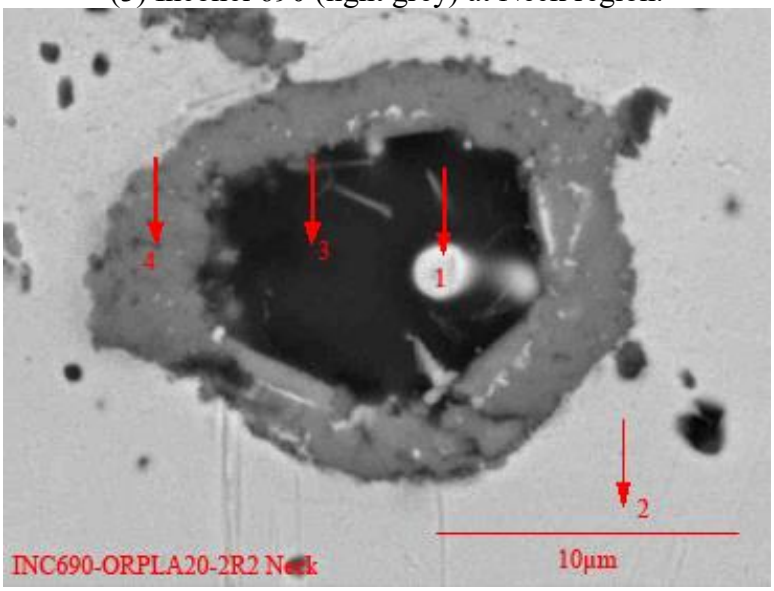

(4) Alteration within Inconel 690 at Neck region. (#1, #2: Ni-enriched alloy; #3: Cl-bearing glass; #4: Cr oxide)

Figure 4.1b. SEM images of Inconel 690 after LA20-2 test (closed crucible corrosion) in ORPLA20 (continued).

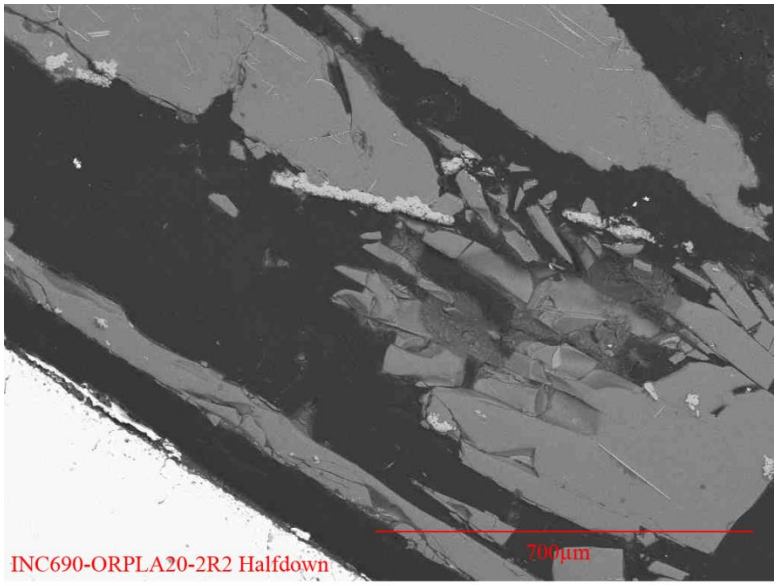

(5) Inconel 690 (light grey, lower left) at Half-down region

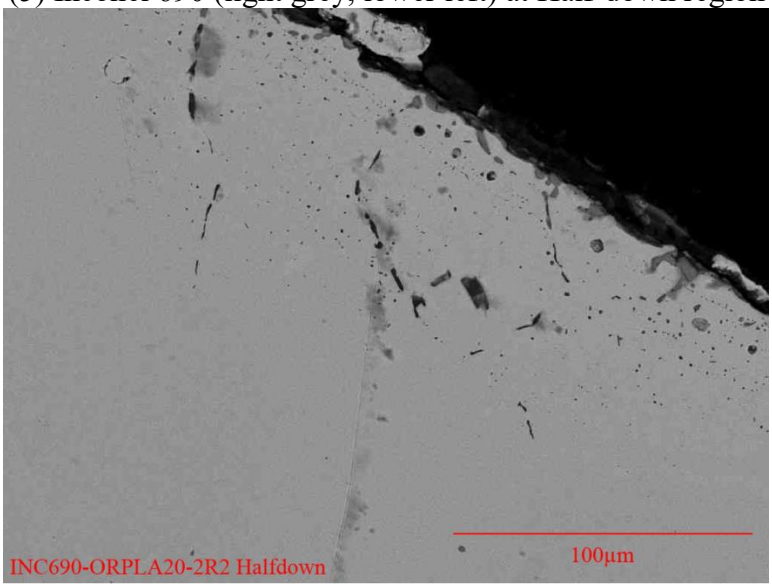

(6) Inconel 690 (light grey) at Half-down region

Figure 4.1b. SEM images of Inconel 690 after LA20-2 test (closed crucible corrosion) in ORPLA20 (continued).

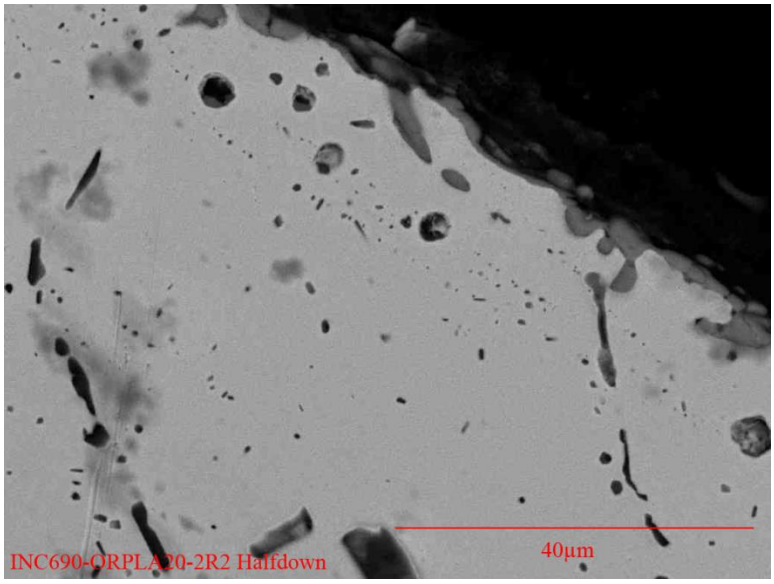

(7) Inconel 690 (light grey) at Half-down region.

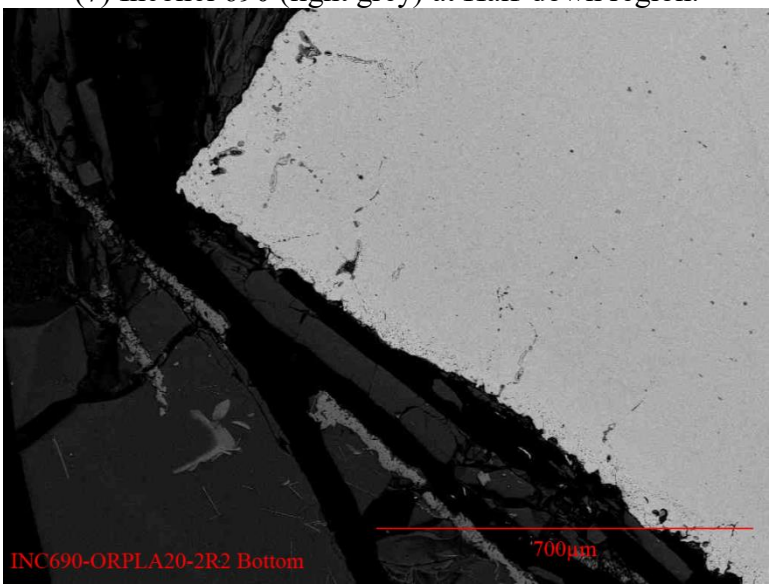

(8) Inconel 690 (light grey) at Bottom region.

Figure 4.1b. SEM images of Inconel 690 after LA20-2 test (closed crucible corrosion) in ORPLA20 (continued).

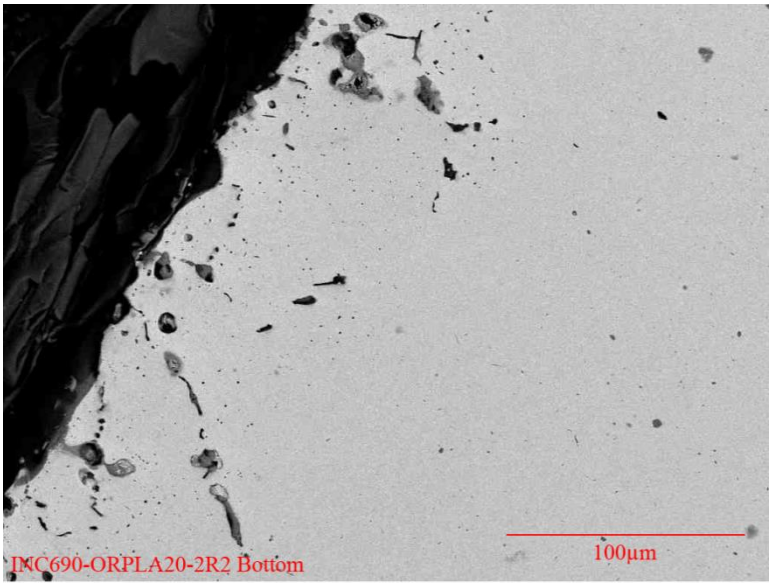

(9) Inconel 690 (light grey) at Bottom region.

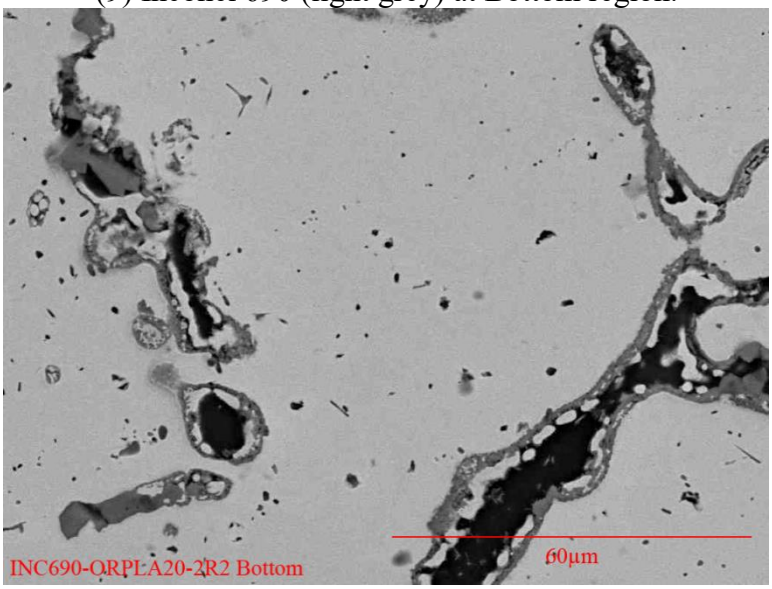

(10) Details of grain boundary damage within Inconel 690 at Bottom region.

Figure 4.1b. SEM images of Inconel 690 after LA20-2 test (closed crucible corrosion) in ORPLA20 (continued).

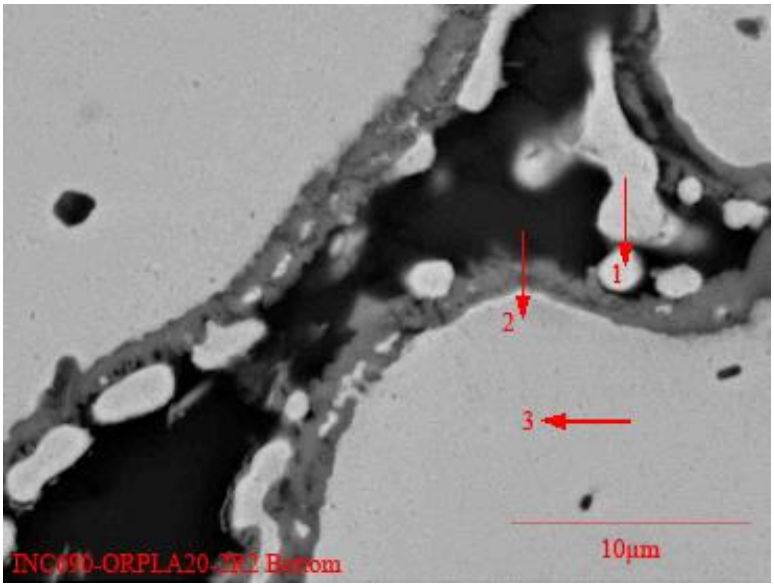

(11), Details of grain boundary damage at Bottom region (Cr oxide: grey band; Ni-enriched alloy, #1: 91 wt% Ni; #2, #3: 74wt% Ni)

Figure 4.1b. SEM images of Inconel 690 after LA20-2 test (closed crucible corrosion) in ORPLA20 (continued).

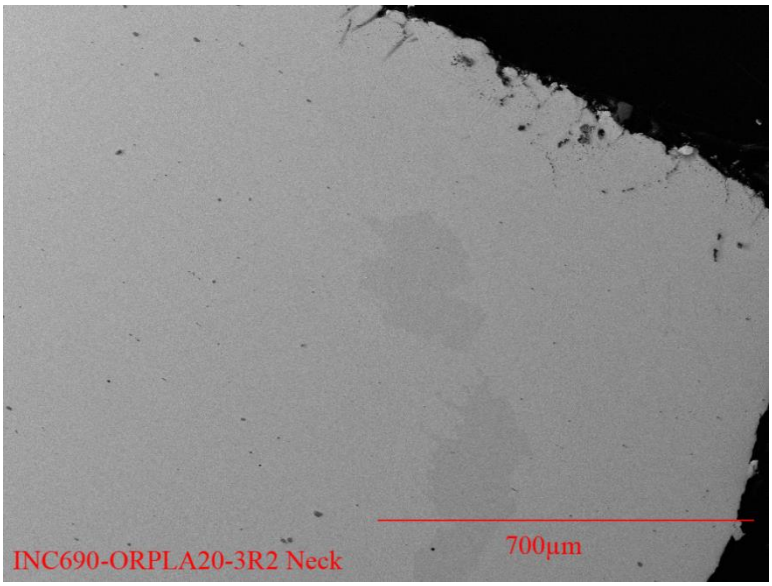

(1) Inconel 690 (light grey) at Neck region.

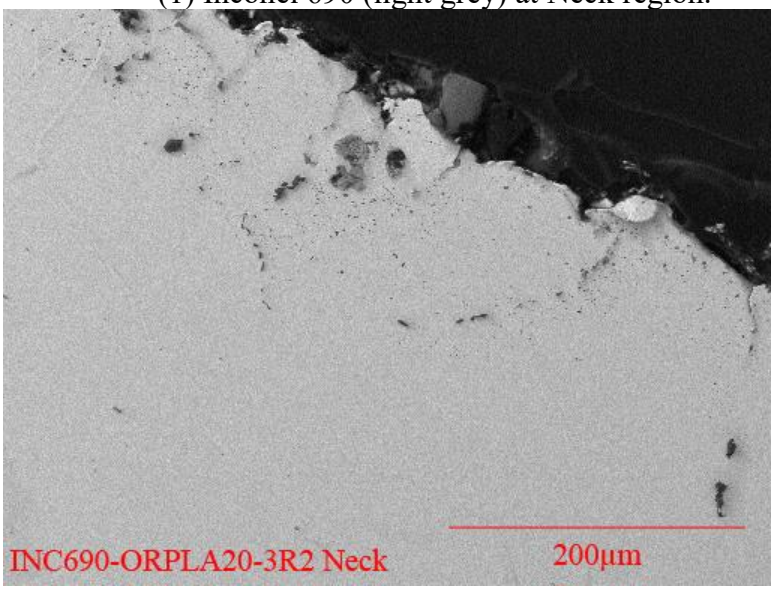

(2) Inconel 690 (light grey) at Neck region.

Figure 4.1c. SEM images of Inconel 690 after LA20-3 test (closed crucible corrosion) in ORPLA20.

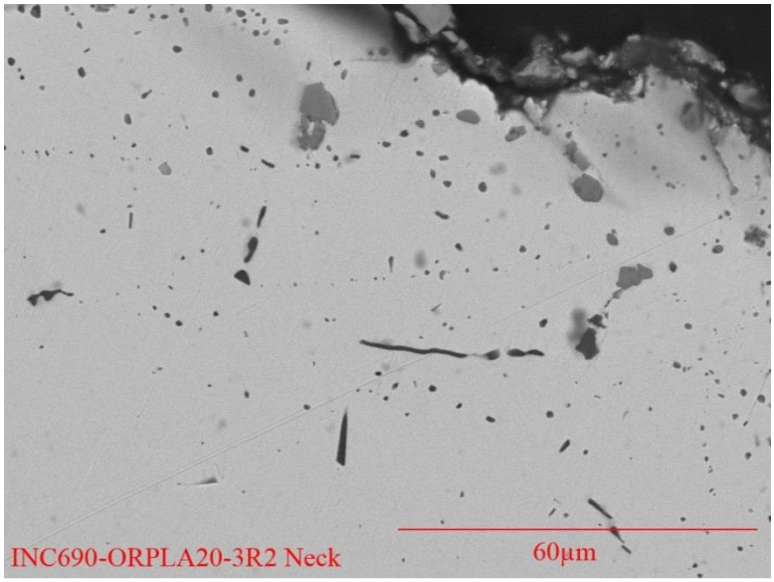

(3) Inconel 690 (light grey) at Neck region.

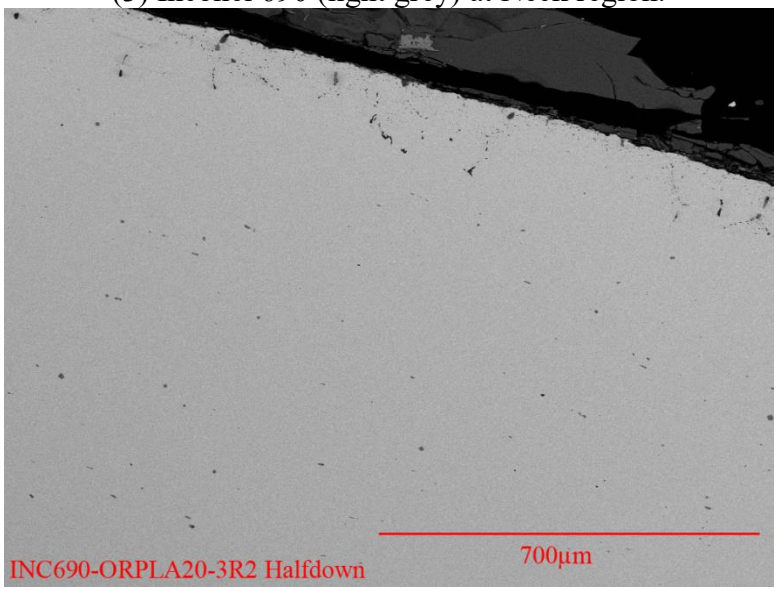

(4) Inconel 690 (light grey) at Half-down region.

Figure 4.1c. SEM images of Inconel 690 after LA20-3 test (closed crucible corrosion) in ORPLA20 (continued).

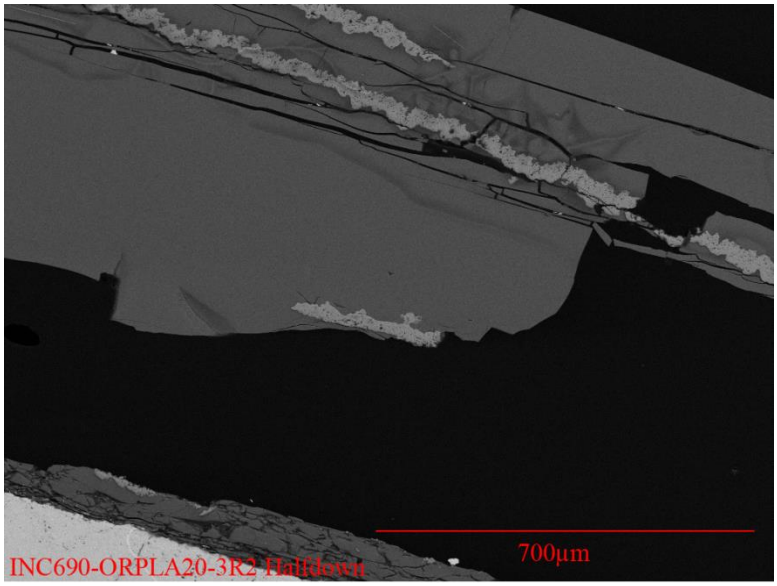

(5) Inconel 690 (light grey, lower left) at Half-down region. Detached scale is visible in approximately parallel alignment within nearby glass.

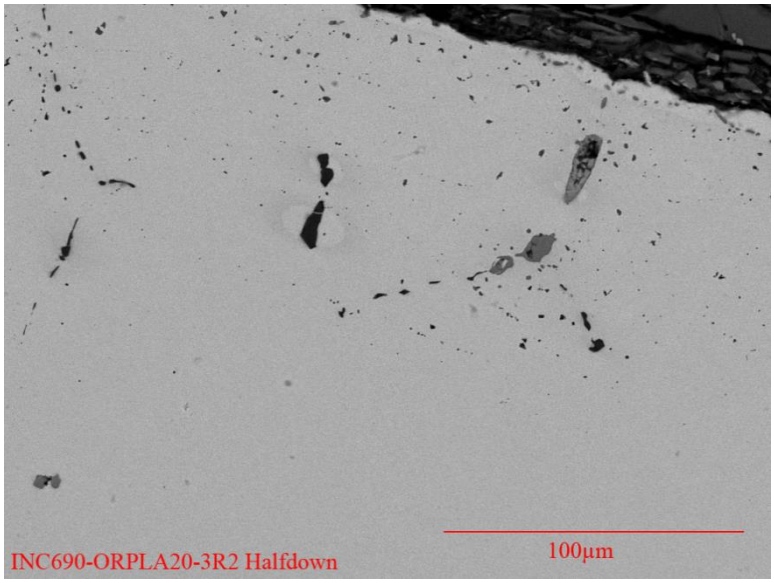

(6) Inconel 690 (light grey) at Half-down region

Figure 4.1c. SEM images of Inconel 690 after LA20-3 test (closed crucible corrosion) in ORPLA20 (continued).

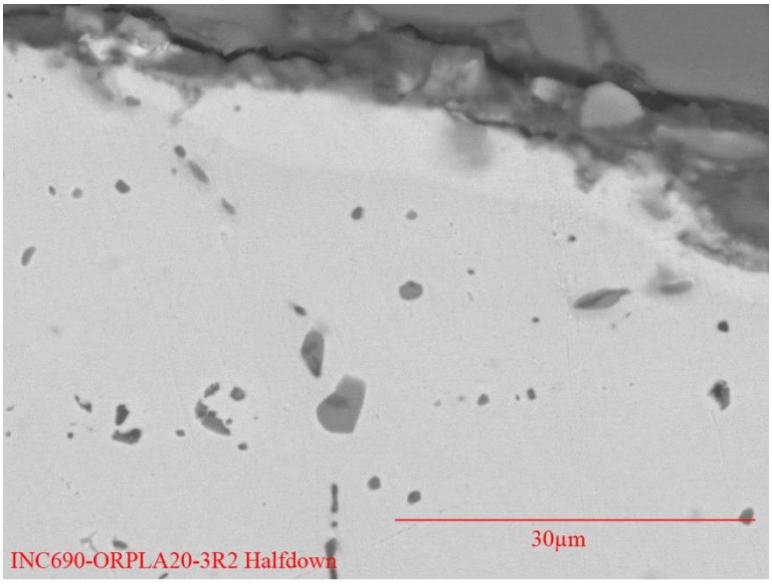

(7) Inconel 690 (light grey) at Half-down region

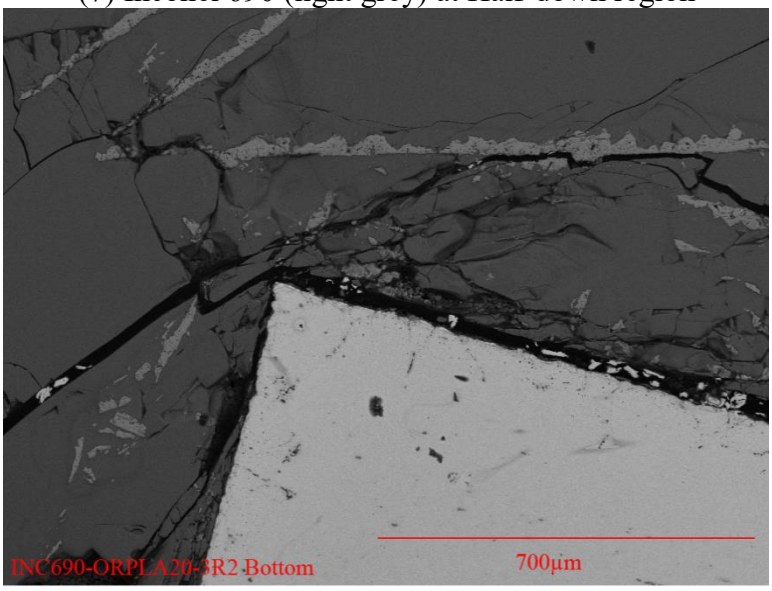

(8) Inconel 690 (light grey) at Bottom region. Detached oxide scale is visible within nearby glass.

Figure 4.1c. SEM images of Inconel 690 after LA20-3 test (closed crucible corrosion) in ORPLA20 (continued).

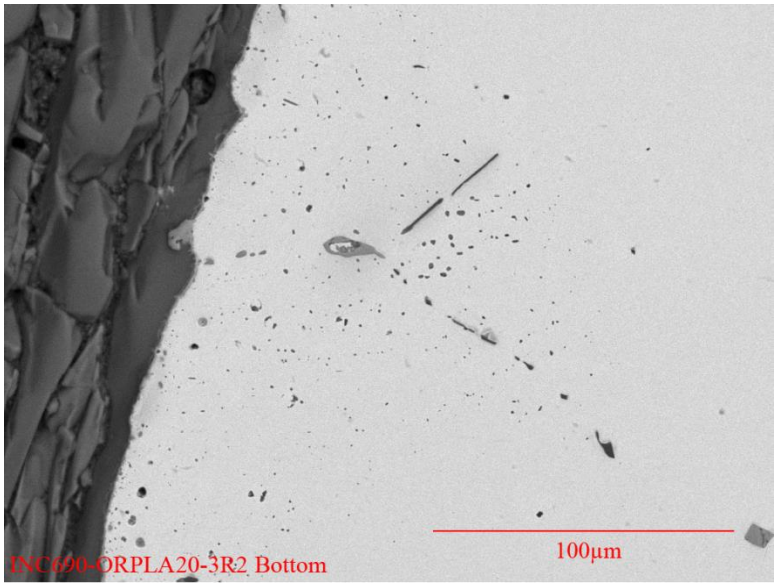

(9) Inconel 690 (light grey) at Bottom region.

Figure 4.1c. SEM images of Inconel 690 after LA20-3 test (closed crucible corrosion) in ORPLA20 (continued).

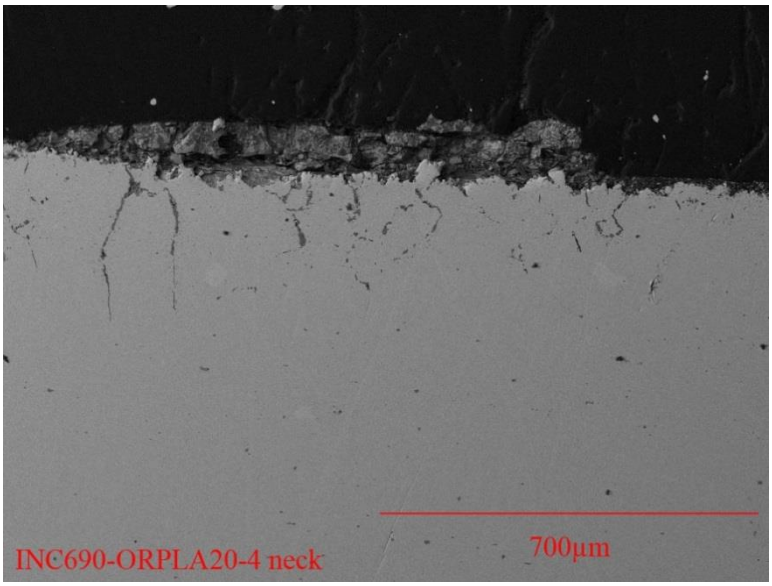

(1) Inconel 690 (light grey) at Neck region.

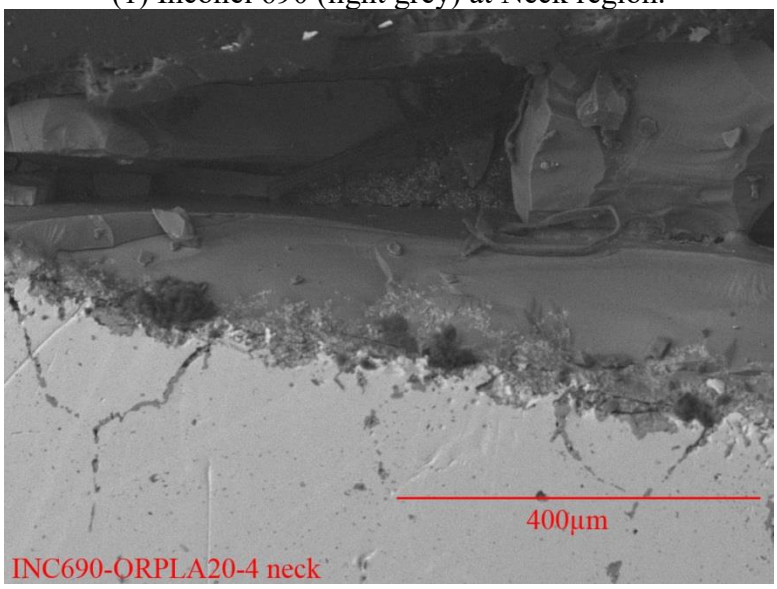

(2) Inconel 690 (light grey) at Neck region

Figure 4.1d. SEM images of Inconel 690 after LA20-4 test (closed crucible corrosion) in ORPLA20.

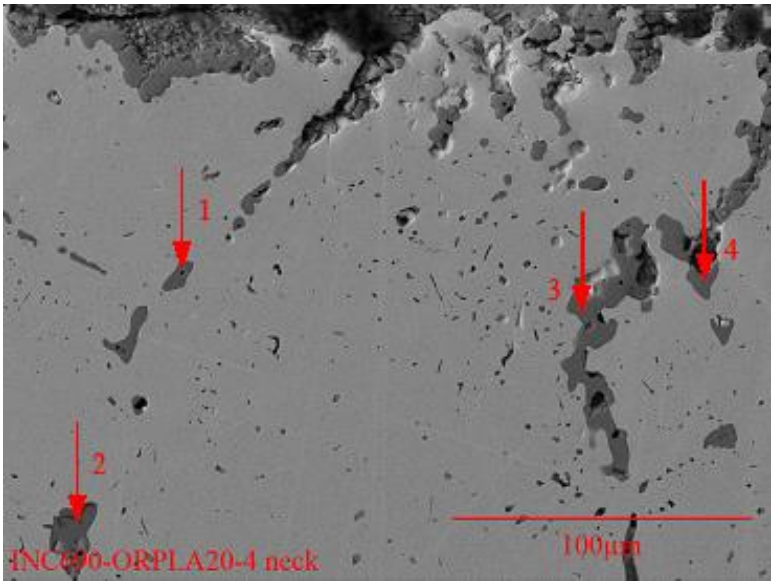

(3) Inconel 690 (light grey) at Neck region with details of Cr oxide (#1-#4).

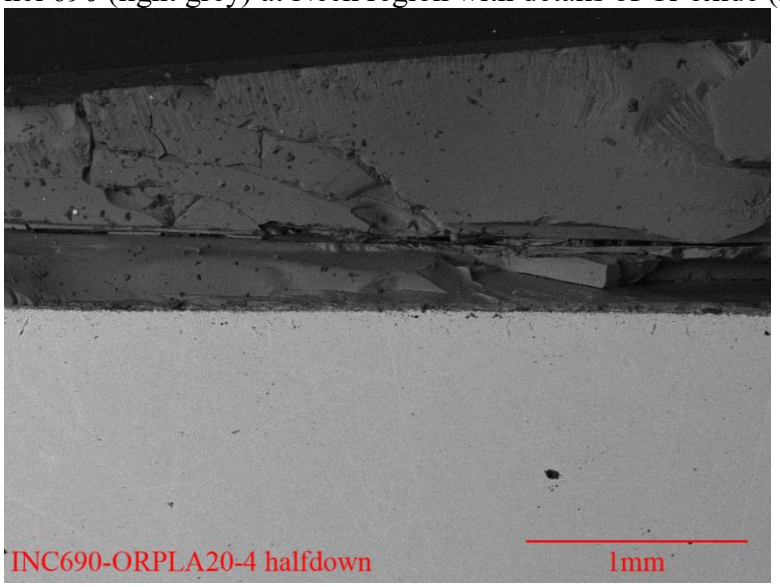

(4) Inconel 690 (light grey) at Half-down region.

Figure 4.1d. SEM images of Inconel 690 after LA20-4 test (closed crucible corrosion) in ORPLA20 (continued).

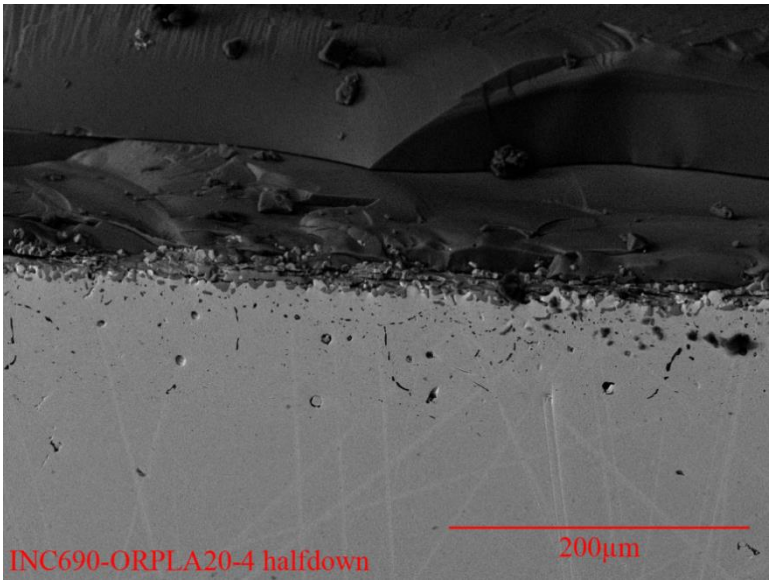

(5) Inconel 690 (light grey) at Half-down region.

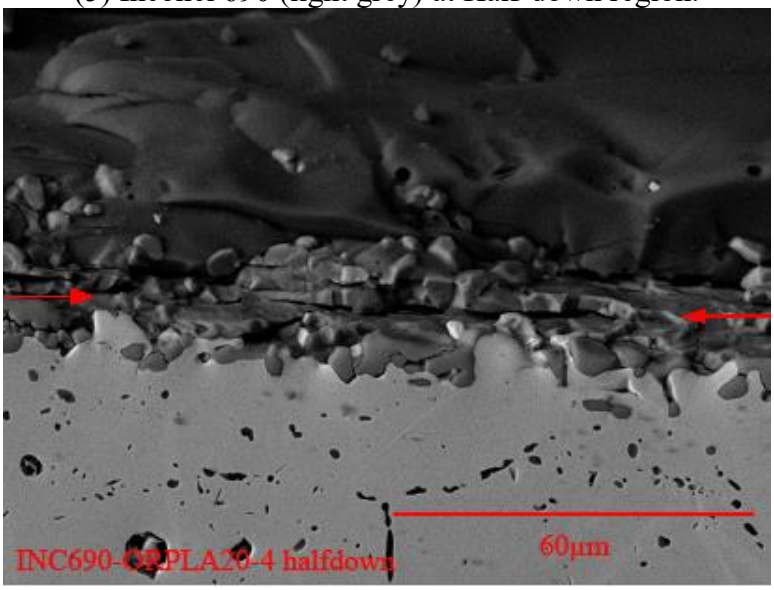

(6) Inconel 690 (light grey) at Half-down region (arrows indicate Cr oxide).

Figure 4.1d. SEM images of Inconel 690 after LA20-4 test (closed crucible corrosion) in ORPLA20 (continued).

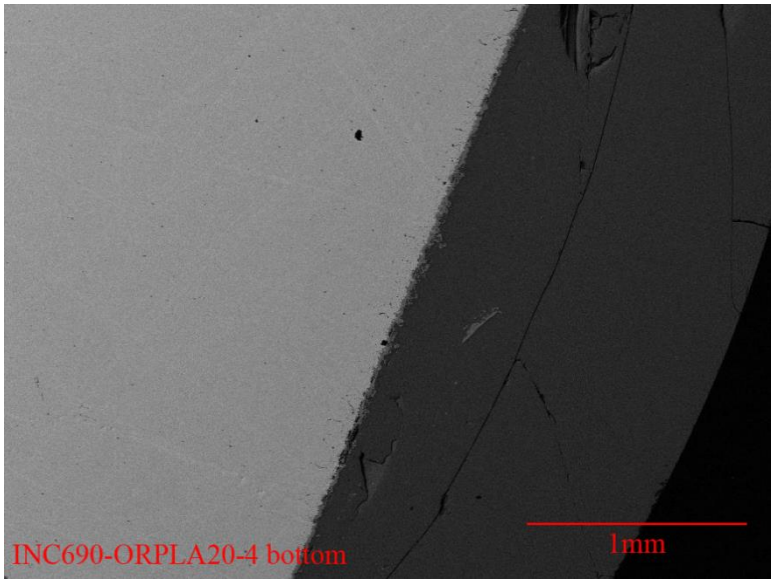

(7) Inconel 690 (light grey) at Bottom region.

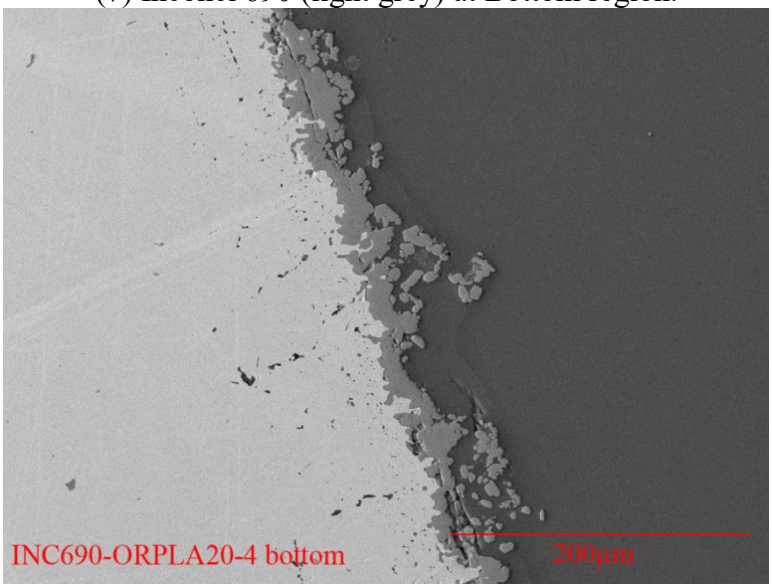

(8) Inconel 690 (light grey) at Bottom region with oxide scale (mid grey)

Figure 4.1d. SEM images of Inconel 690 after LA20-4 test (closed crucible corrosion) in ORPLA20 (continued).

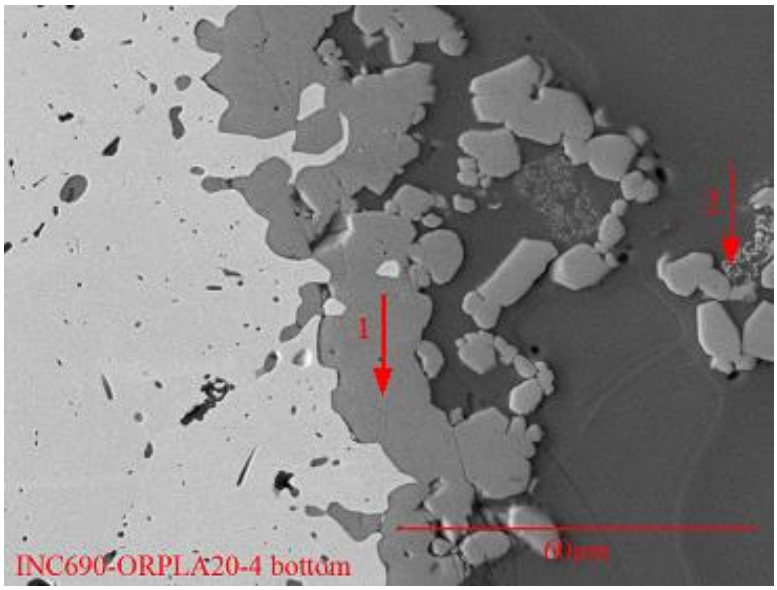

(9) Inconel 690 (light grey) at Bottom region with Cr oxide (#1, #2)

Figure 4.1d. SEM images of Inconel 690 after LA20-4 test (closed crucible corrosion) in ORPLA20 (continued).

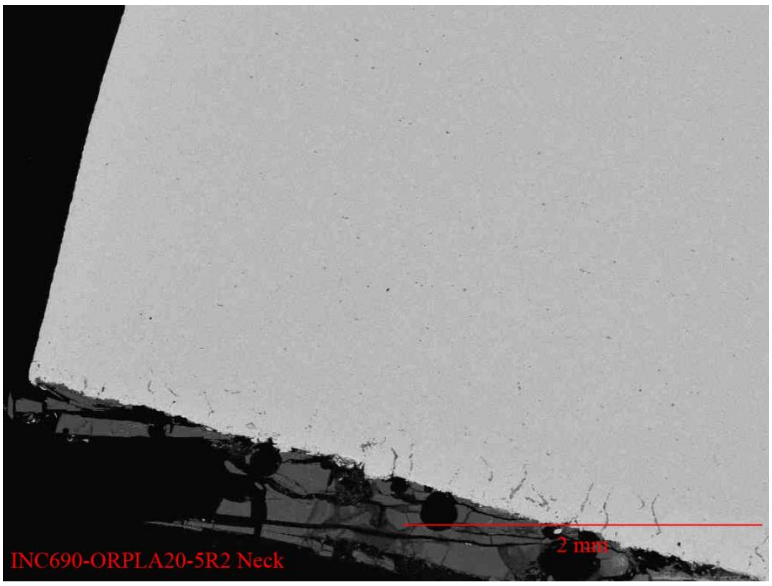

(1) Inconel 690 (light grey) at Neck region

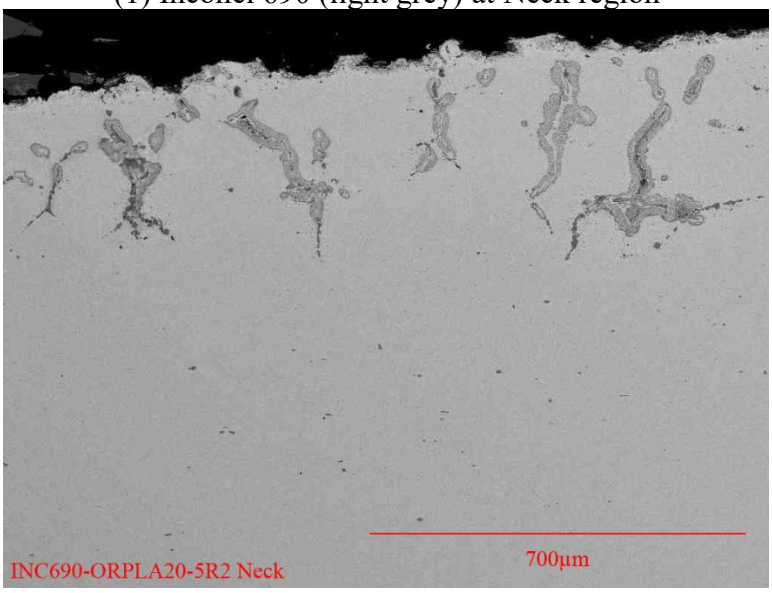

(2) Inconel 690 (light grey) at Neck region with characteristic grain boundary damage associated with Cl-bearing molten glass

Figure 4.1e. SEM images of Inconel 690 after LA20-5 test (closed crucible corrosion) in ORPLA20.

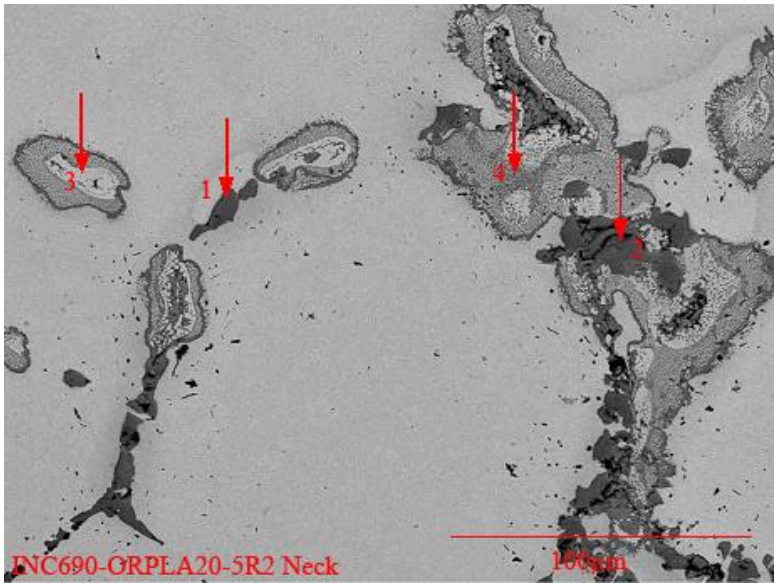

(3) Inconel 690 (light grey) at Neck region. Details of grain boundary damage: #1, #2: Cr oxide; #3: Ni-enriched nodule, 87 wt% Ni; #4: mixture of Cr oxide and Ni-based alloy.

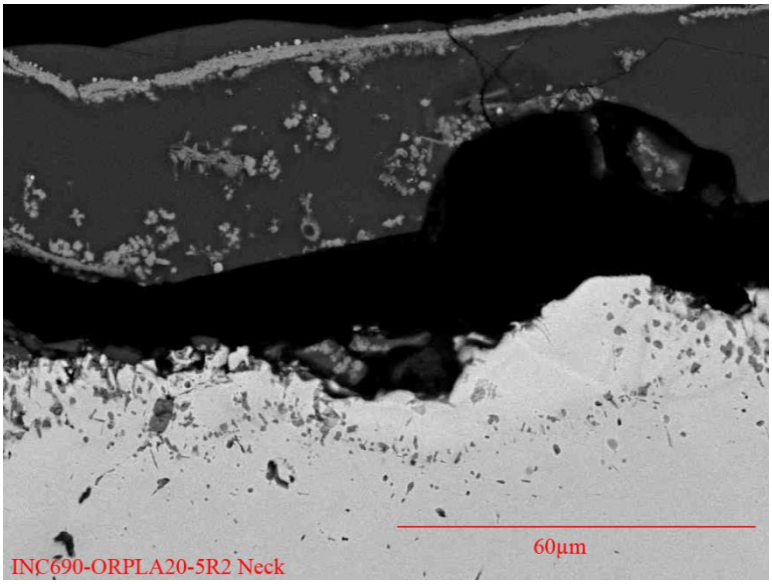

(4) Inconel 690 (light grey, low half) at Neck region. Oxide scale was spalled off from alloy surface.

Figure 4.1e. SEM images of Inconel 690 after LA20-5 test (closed crucible corrosion) in ORPLA20 (continued).

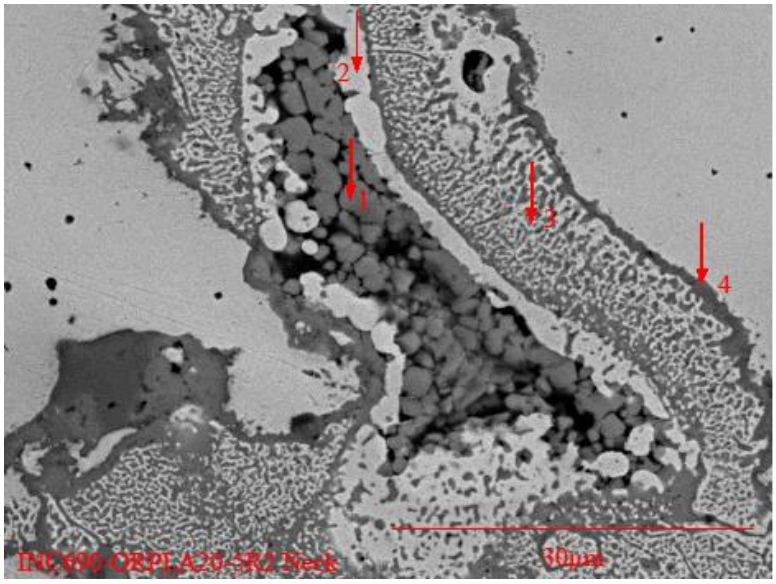

(5) Details of grain boundary damage at Neck: #2: 93 wt% Ni alloy; #4: Cr oxide; #1: mixture of predominantly Cr oxide and Ni-based alloy; #3: mixture of Cr oxide and Ni-based alloy.

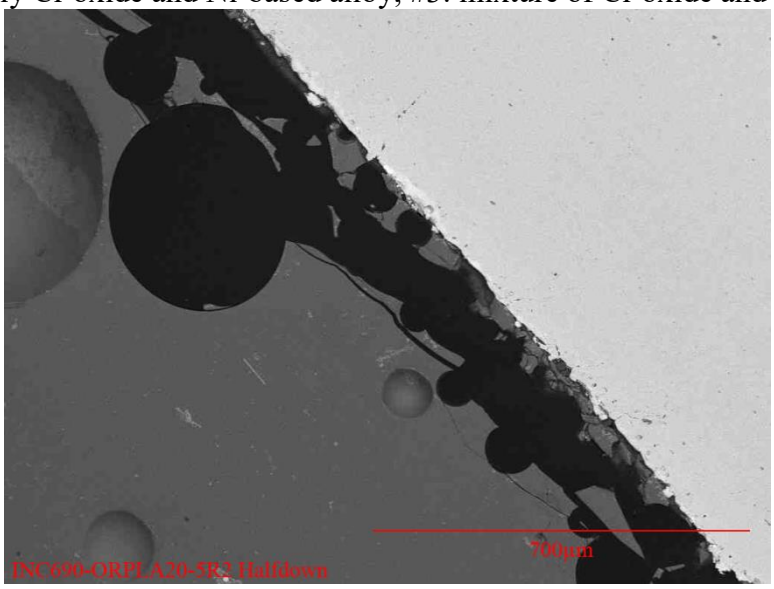

(6) Inconel 690 (light grey) at Half-down region.

Figure 4.1e. SEM images of Inconel 690 after LA20-5 test (closed crucible corrosion) in ORPLA20 (continued).

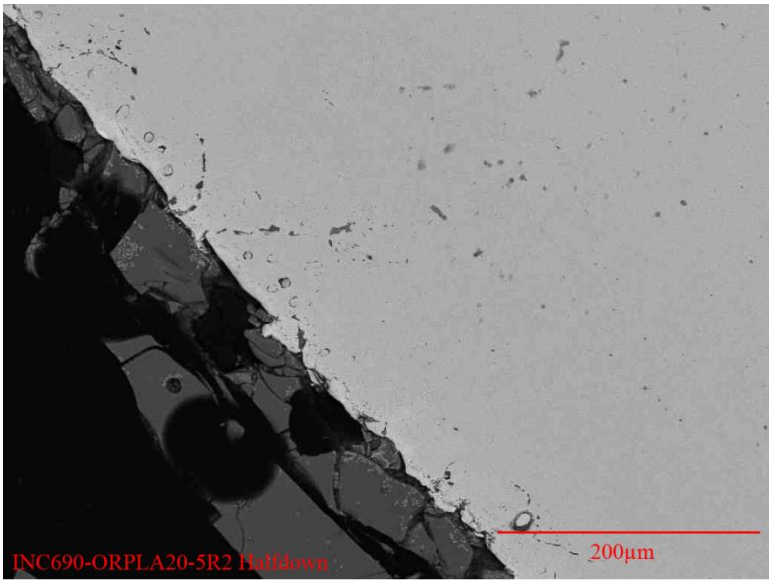

(7) Inconel 690 (light grey) at Half-down region.

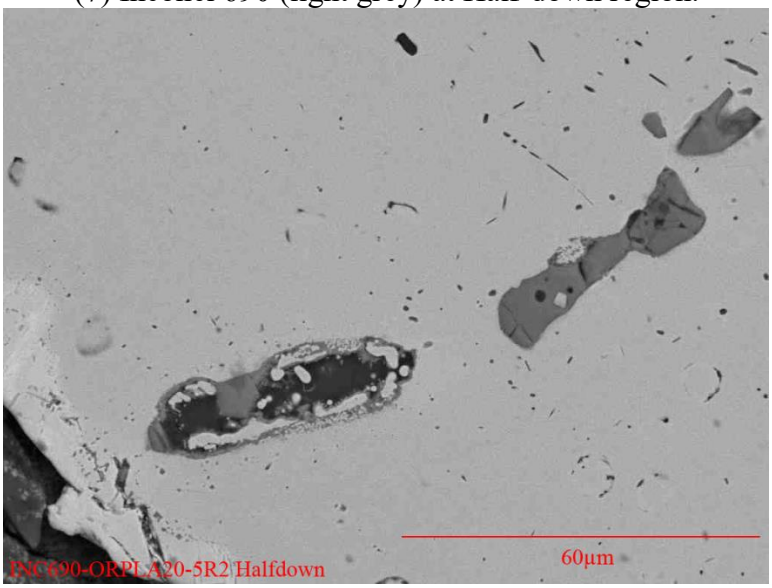

(8) Inconel 690 (light grey) Half-down region with details of grain boundary damage.

Figure 4.1e. SEM images of Inconel 690 after LA20-5 test (closed crucible corrosion) in ORPLA20 (continued).

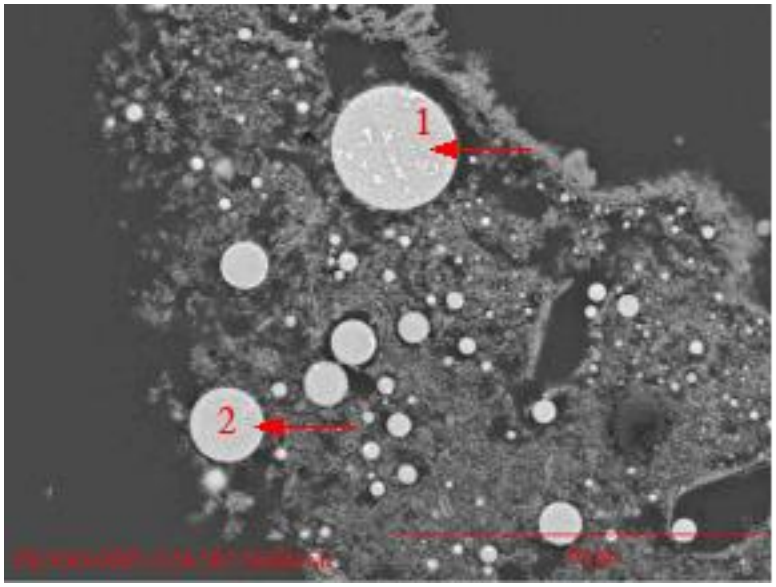

(9) Ni-sulfide with minor amount of Sn (#1, #2) at Half-down region. Inconel alloy is not included in image.

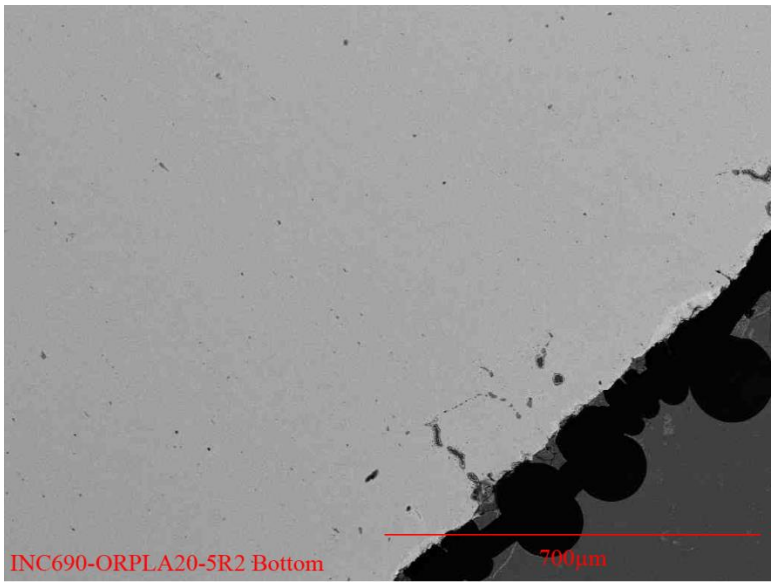

(10) Inconel 690 (light grey) at Bottom region.

Figure 4.1e. SEM images of Inconel 690 after LA20-5 test (closed crucible corrosion) in ORPLA20 (continued).

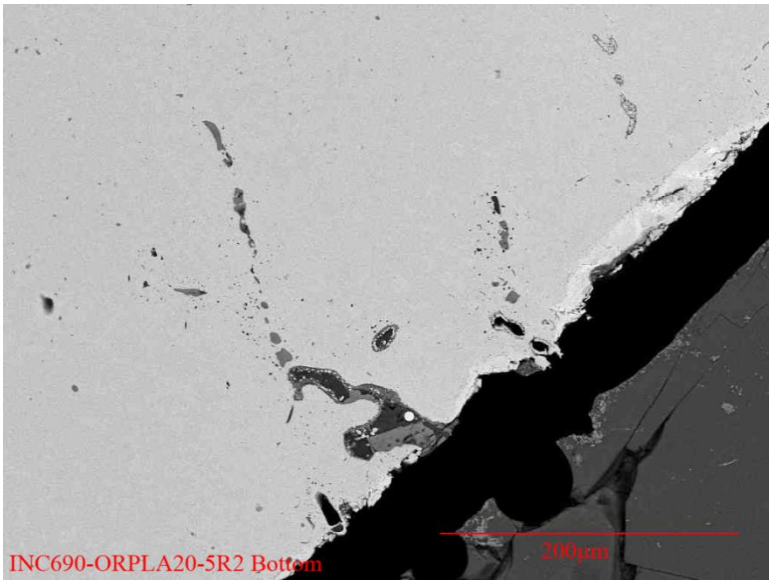

(11) Inconel 690 (light grey) at Bottom region.

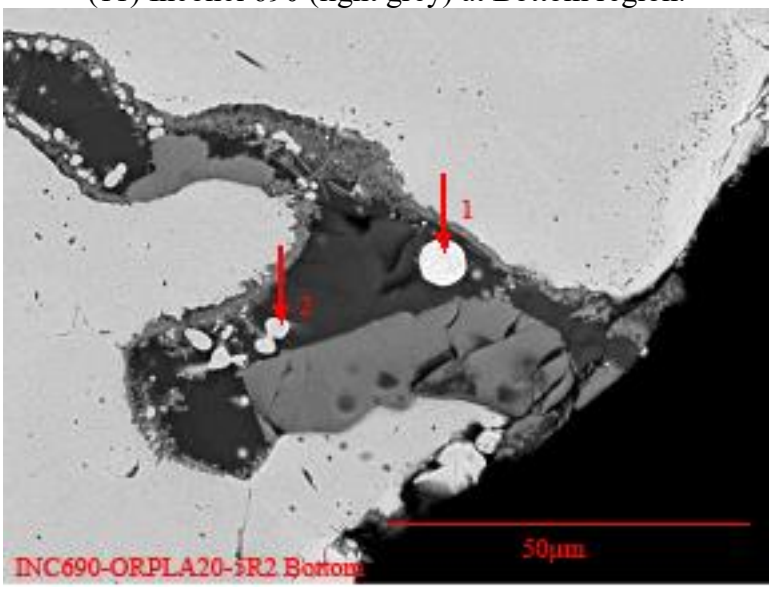

(12) Detail of grain boundary damage at Bottom region (#1: 78 wt% Ni, 19 wt% Sn; #2: 85 wt% Ni, 3 wt% Sn)

Figure 4.1e. SEM images of Inconel 690 after LA20-5 test (closed crucible corrosion) in ORPLA20 (continued).

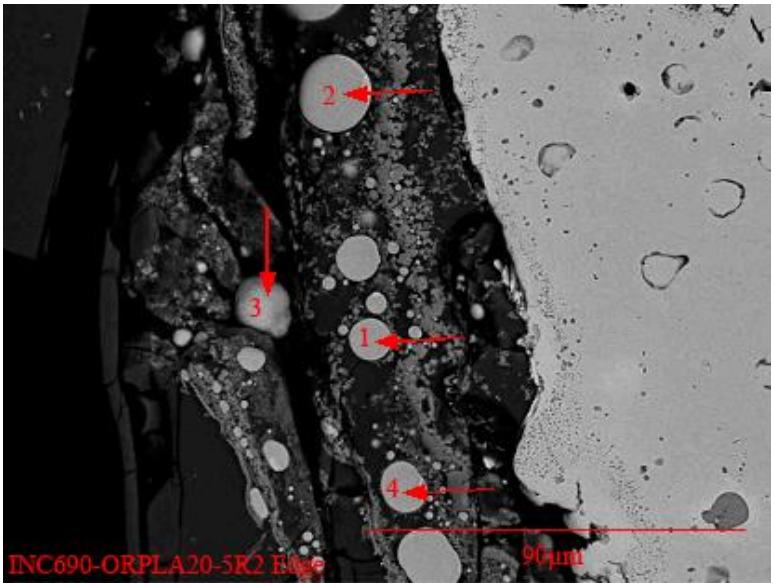

(13) Ni-sulfide near Inconel alloy at Edge (#1-#4:)

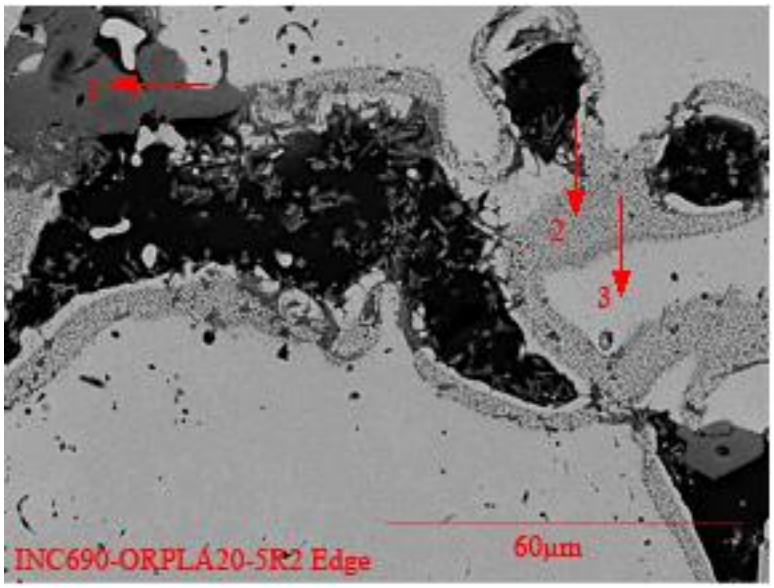

(14) Grain boundary damage details at Edge (#1: Cr oxide; #2: mixture of Cr oxide and Ni-based alloy; #3: 80 wt% Ni alloy)

Figure 4.1e. SEM images of Inconel 690 after LA20-5 test (closed crucible corrosion) in ORPLA20 (continued).

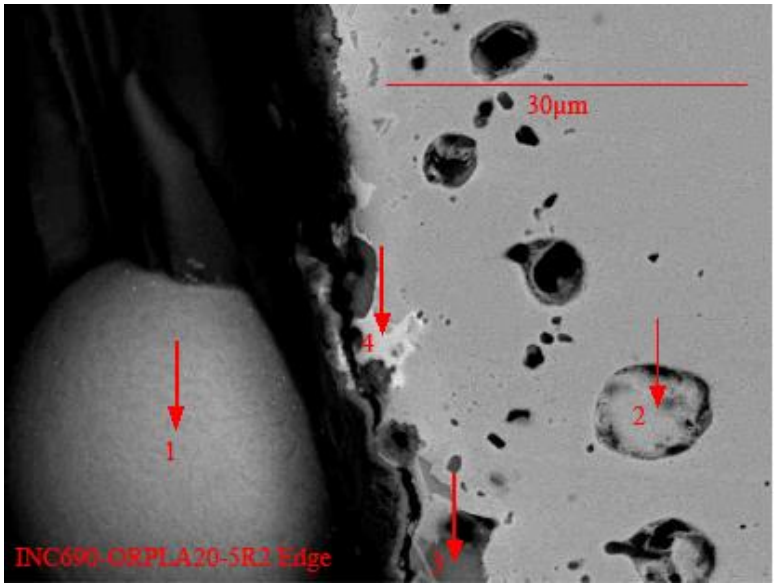

(15) Details of altered alloy at Edge (#1: Ni sulfide; #2: Ni-enriched alloy; #3: Ni-Cr sulfide; #4:

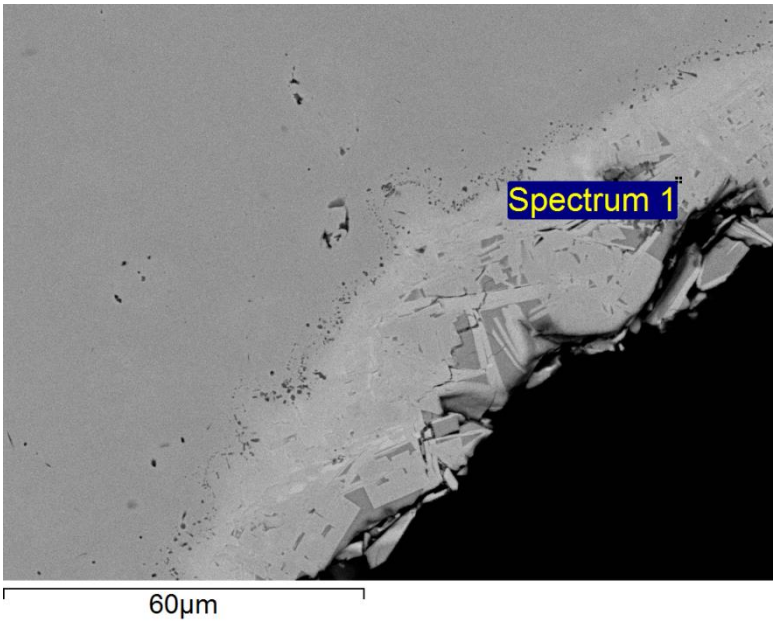

Sn/Ni alloy)

(16) Ni Crystal near alloy's surface as indicated by "Spectrum 1".

Figure 4.1e. SEM images of Inconel 690 after LA20-5 test (closed crucible corrosion) in ORPLA20 (continued).

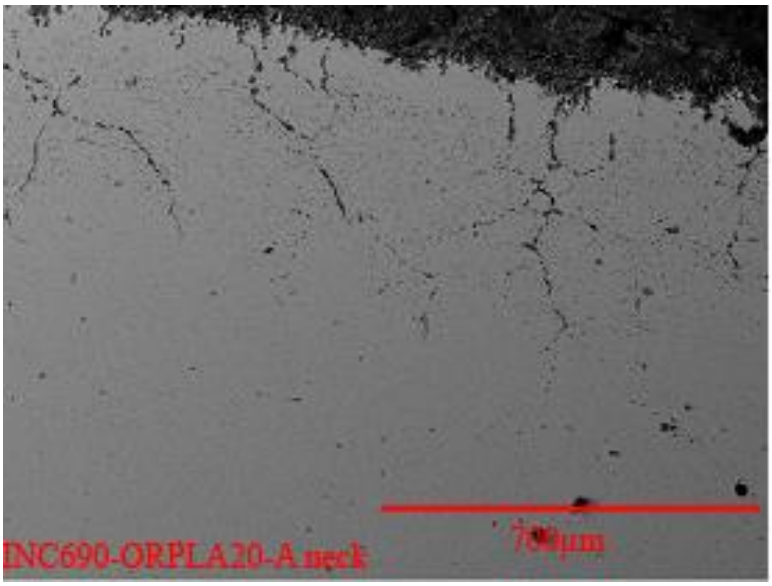

(1) Inconel 690 at Neck region.

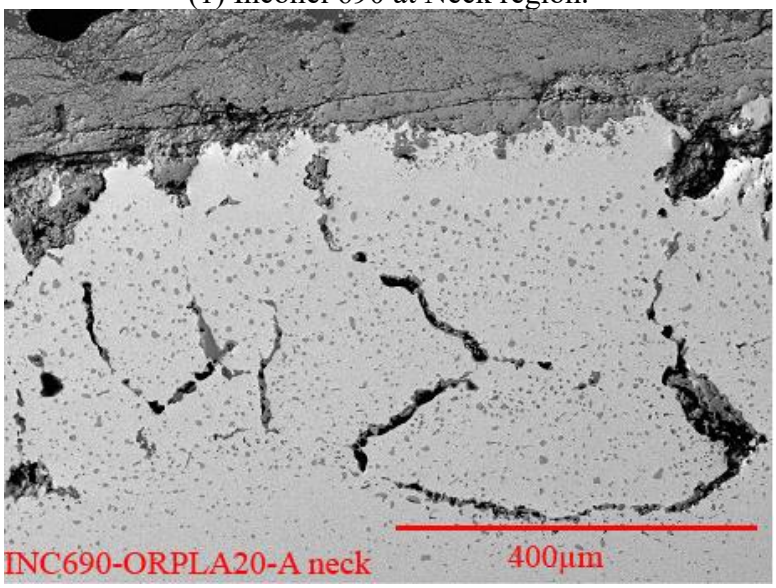

(2) Inconel 690 at Neck region with thick Cr oxide scale.

Figure 4.1f. SEM images of Inconel 690 after LA20-A test (open to air) in ORPLA20.

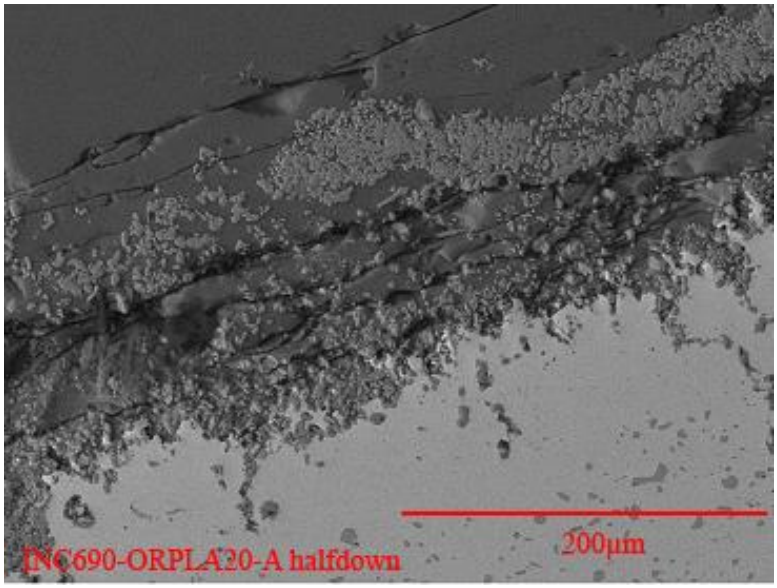

(3) Inconel 690 at Half-down region with thick Cr oxide scale.

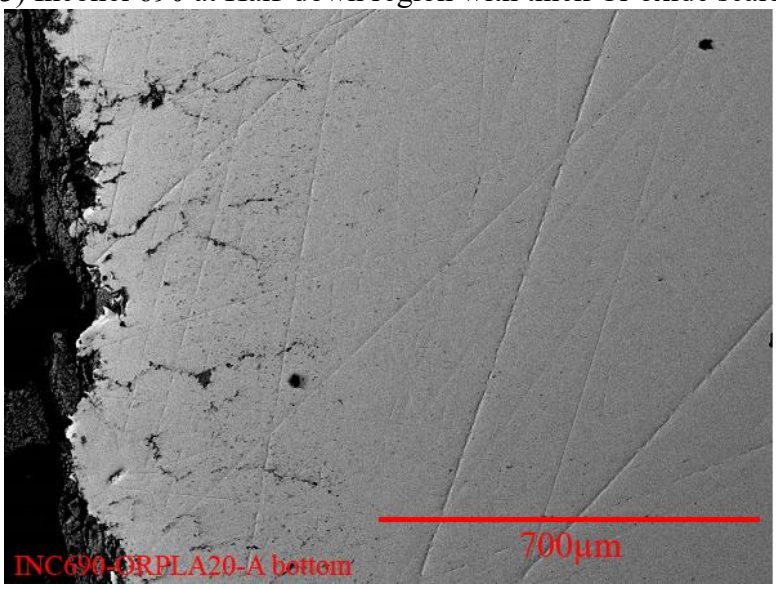

(4) Inconel 690 (light grey) at Bottom region.

Figure 4.1f. SEM images of Inconel 690 after LA20-A test (open to air) in ORPLA20 (continued).

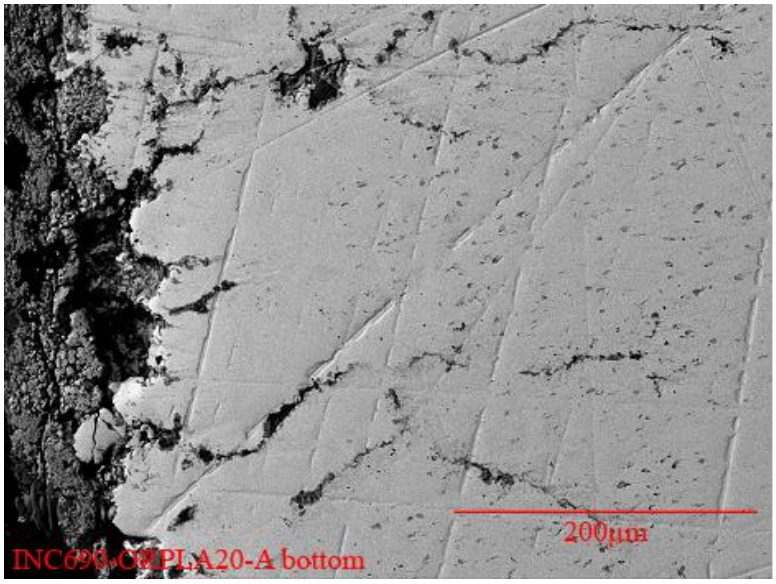

(5) Inconel 690 (light grey) at Bottom region with deep interior oxidization along grain boundary.

Figure 4.1f. SEM images of Inconel 690 after LA20-A test (open to air) in ORPLA20 (continued).

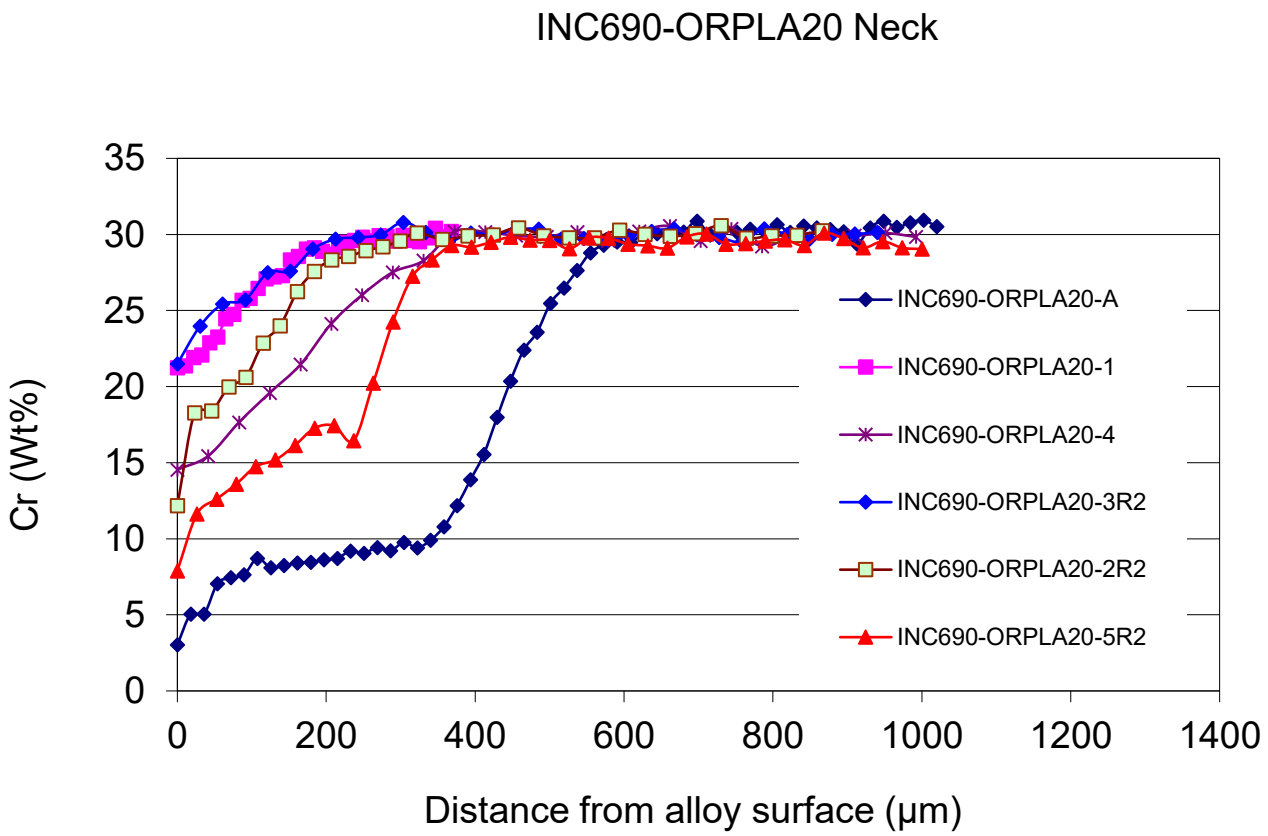

Figure 4.2a. Chromium concentration (Cr wt% in alloy) vs. distance from alloy surface at neck location for ORPLA20 glasses for tests LA20-1 (INC690-ORPLA20-1), LA20-2 (INC690-ORPLA20-2R2), LA20-3 (INC690-ORPLA20-3R2), LA20-4 (INC690-ORPLA20-4), LA20-5 (INC690-ORPLA20-5R2), and LA20-A (INC690-ORPLA20-A).

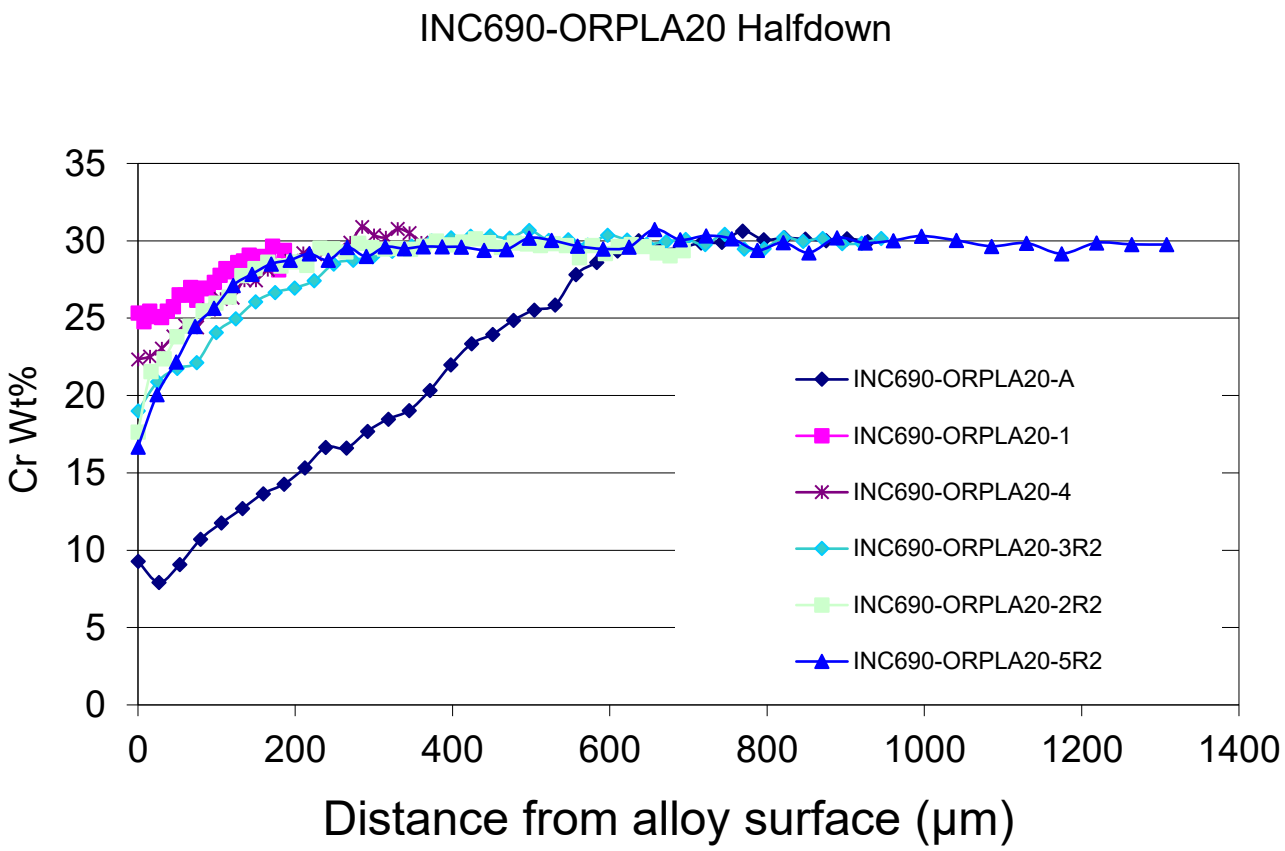

Figure 4.2b. Chromium concentration (Cr wt% in alloy) vs. distance from alloy surface at half-down location for ORPLA20 glasses for tests LA20-1 (INC690-ORPLA20-1), LA20-2 (INC690-ORPLA20-2R2), LA20-3 (INC690-ORPLA20-3R2), LA20-4 (INC690-ORPLA20-4), LA20-5 (INC690-ORPLA20-5R2), and LA20-A (INC690-ORPLA20-A).

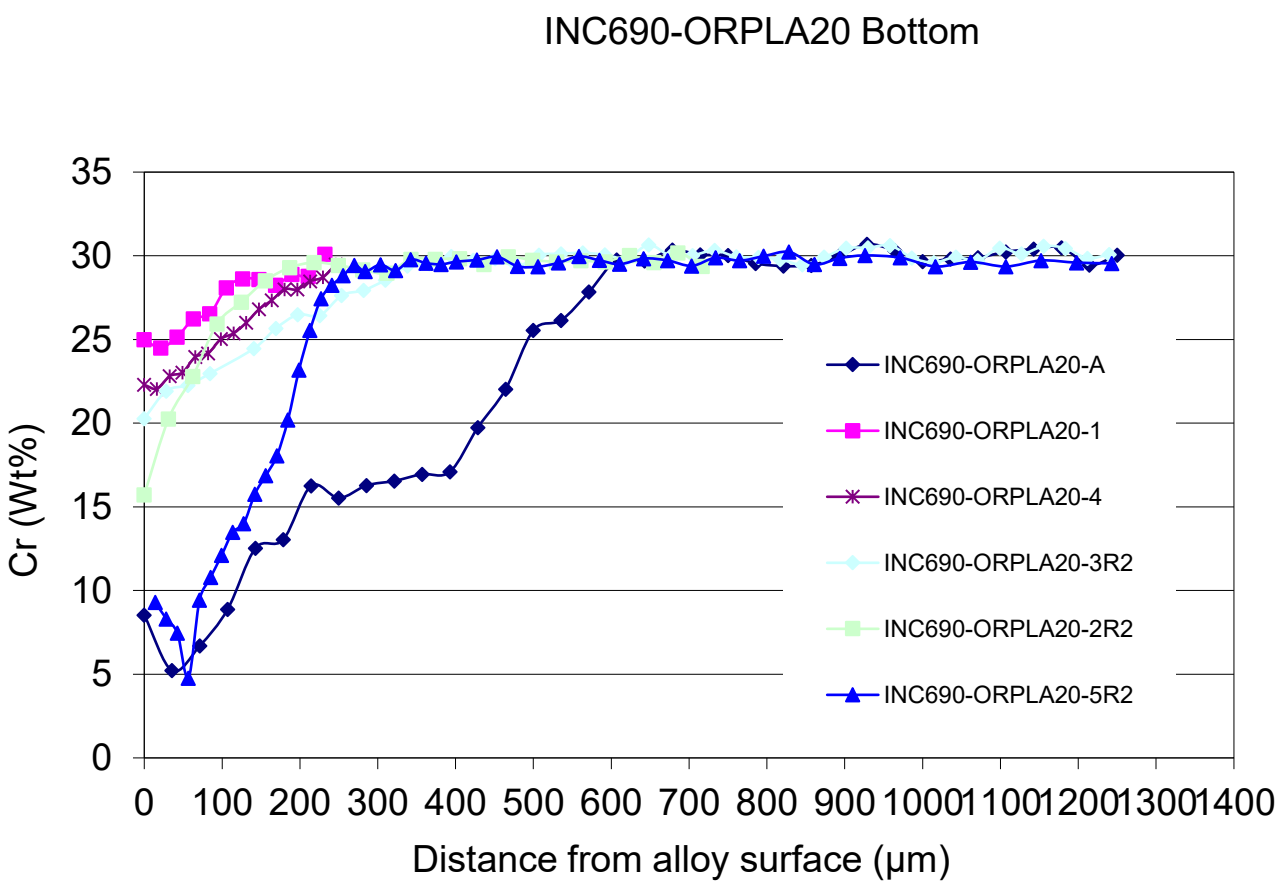

Figure 4.2c. Chromium concentration (Cr wt% in alloy) vs. distance from alloy surface at bottom location for ORPLA20 glasses for tests LA20-1 (INC690-ORPLA20-1), LA20-2 (INC690-ORPLA20-2R2), LA20-3 (INC690-ORPLA20-3R2), LA20-4 (INC690-ORPLA20-4), LA20-5 (INC690-ORPLA20-5R2), and LA20-A (INC690-ORPLA20-A).

Figure 4.3. Damaged Pt/Au crucible after LE12-2 test in ORPLE12 .

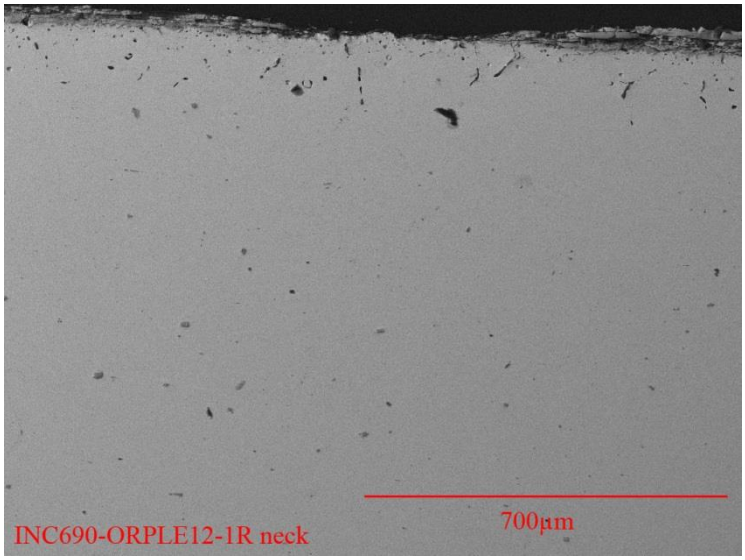

(1) Inconel 690 alloy (light grey) at Neck region.

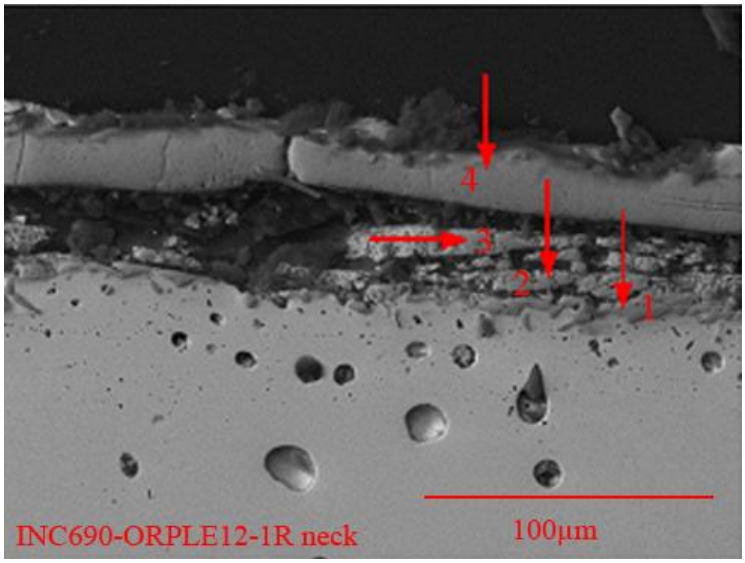

(2) Inconel 690 alloy (light grey) at Neck (#1-#4: Cr oxide)

Figure 4.4a. SEM images of Inconel 690 coupon after LE12-1 test (closed crucible corrosion) in ORPLE12.

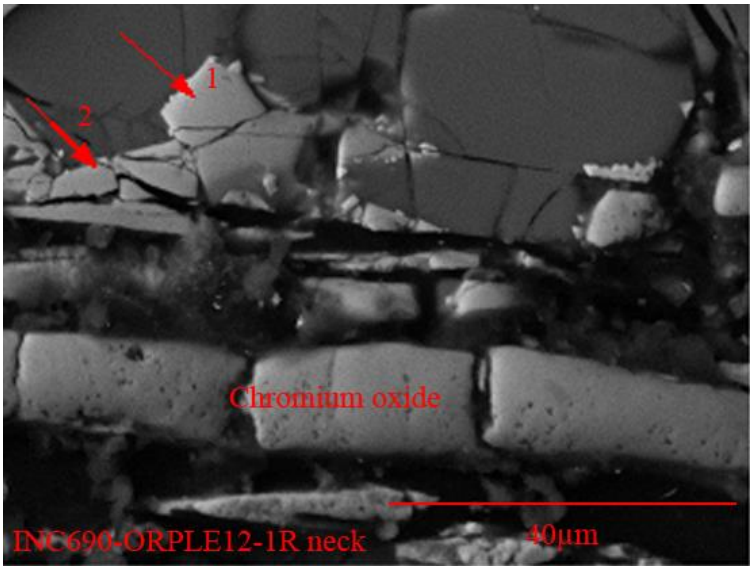

(3) Inconel 690 alloy (light grey) at Neck (#1, #2: Ni-Zn-Cr spinel)

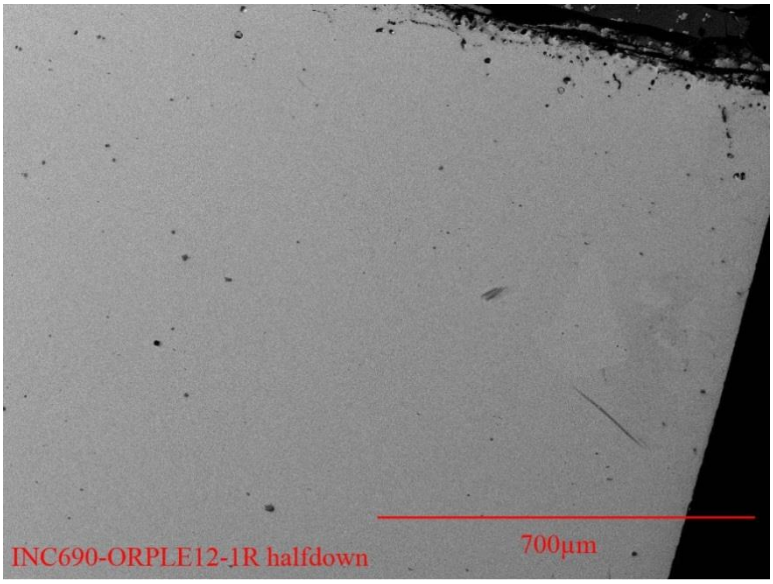

(4) Inconel 690 alloy (light grey) at Half-down region

Figure 4.4a. SEM images of Inconel 690 coupon after LE12-1 test (closed crucible corrosion) in ORPLE12 (continued).

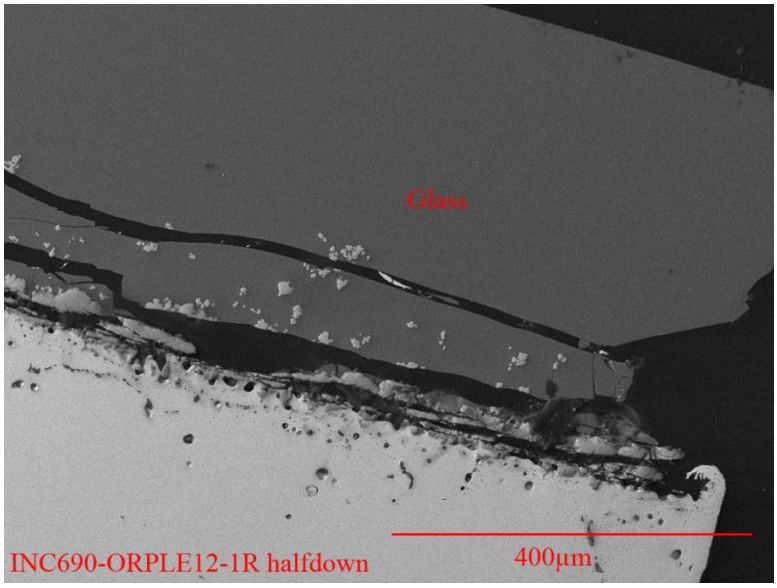

(5) Inconel 690 alloy (light grey) at Half-down region

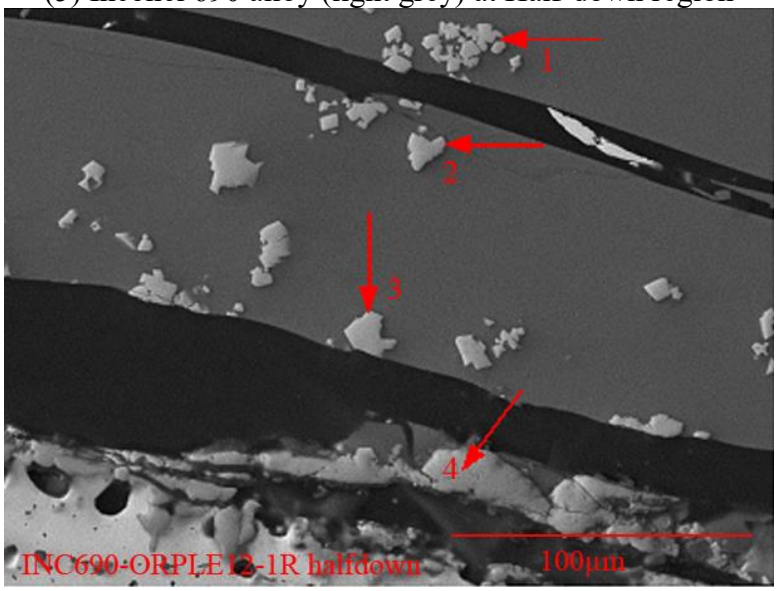

(6) Inconel 690 alloy (light grey) at Half-down region (#1-#3: Zn-Cr spinel; #4: Cr oxide)

Figure 4.4a. SEM images of Inconel 690 coupon after LE12-1 test (closed crucible corrosion) in ORPLE12 (continued).

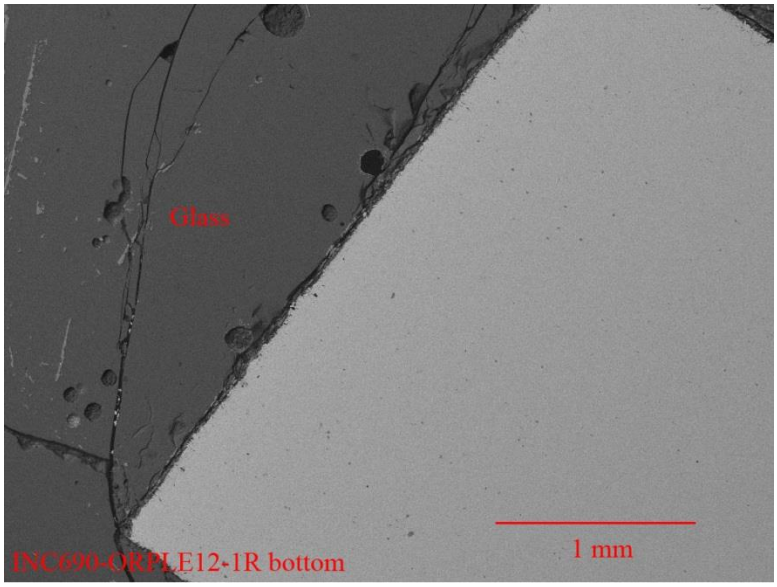

(7) Inconel 690 alloy (light grey) at Bottom region

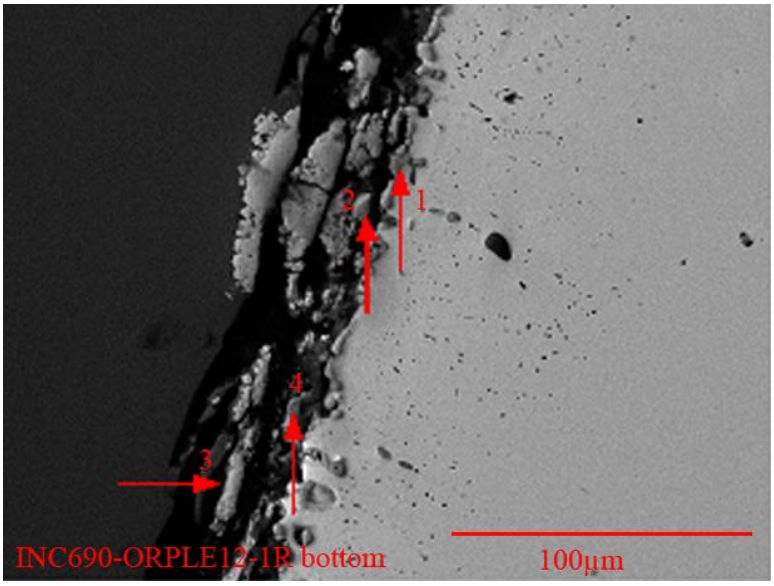

(8) Inconel 690 alloy (light grey) at Bottom region (#1-#4: Cr oxide)

Figure 4.4a. SEM images of Inconel 690 coupon after LE12-1 test (closed crucible corrosion) in ORPLE12 (continued).

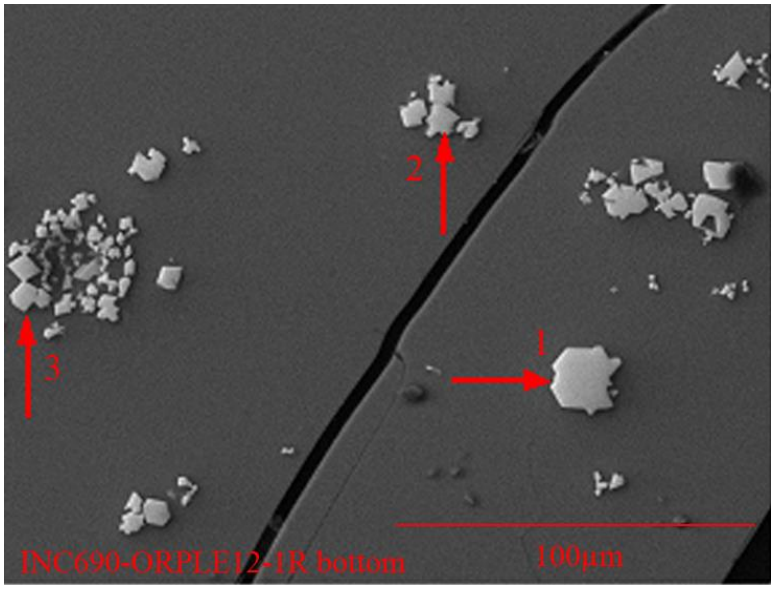

(9) #1-#3: Zn-Cr spinel near alloy at Bottom region

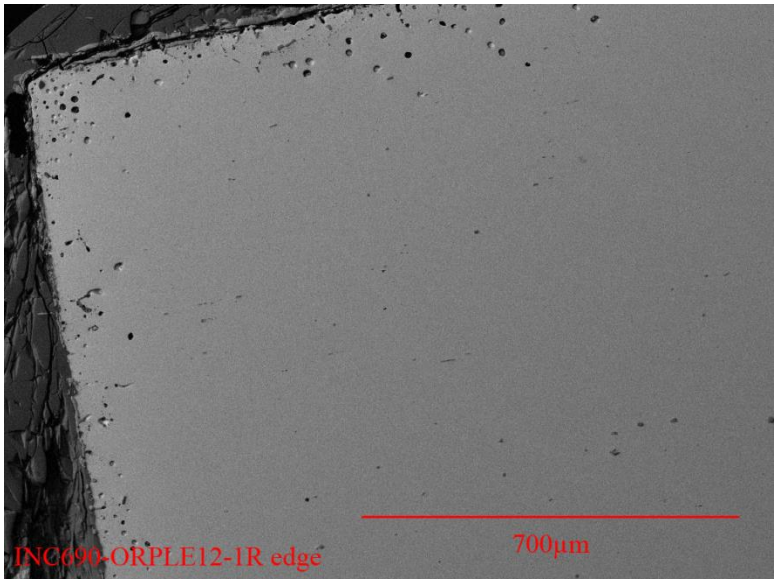

(10) Inconel 690 alloy (light grey) at edge

Figure 4.4a. SEM images of Inconel 690 coupon after LE12-1 test (closed crucible corrosion) in ORPLE12 (continued).

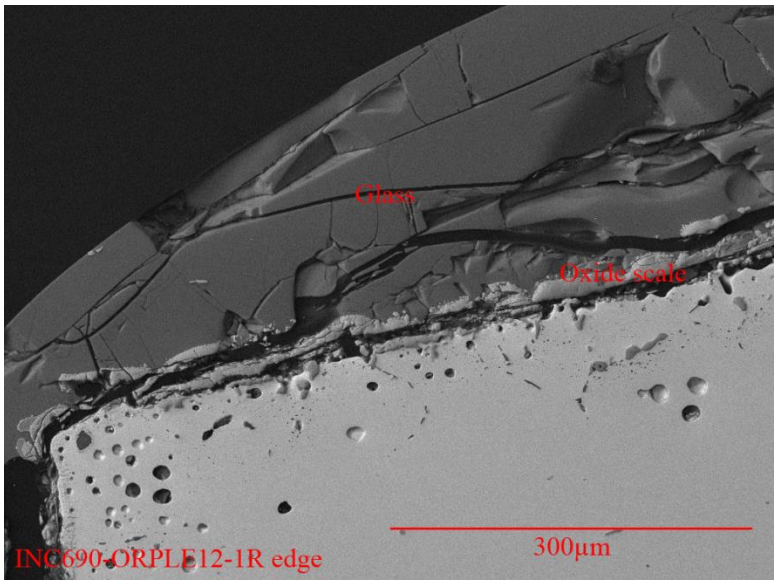

(11) Inconel 690 alloy (light grey) at edge.

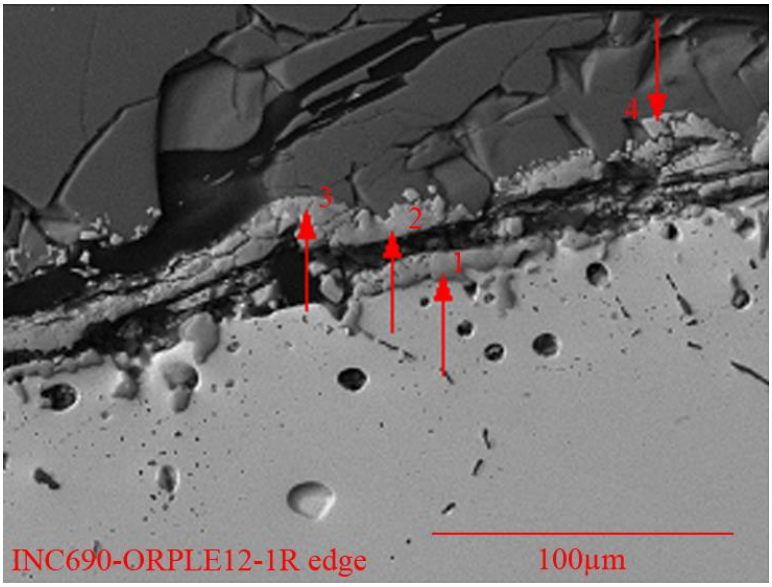

(12) Inconel 690 alloy (light grey) at edge (#1, #3: Cr_2O_3; #2, #4: Zn-Cr spinel)

Figure 4.4a. SEM images of Inconel 690 coupon after LE12-1 test (closed crucible corrosion) in ORPLE12 (continued).

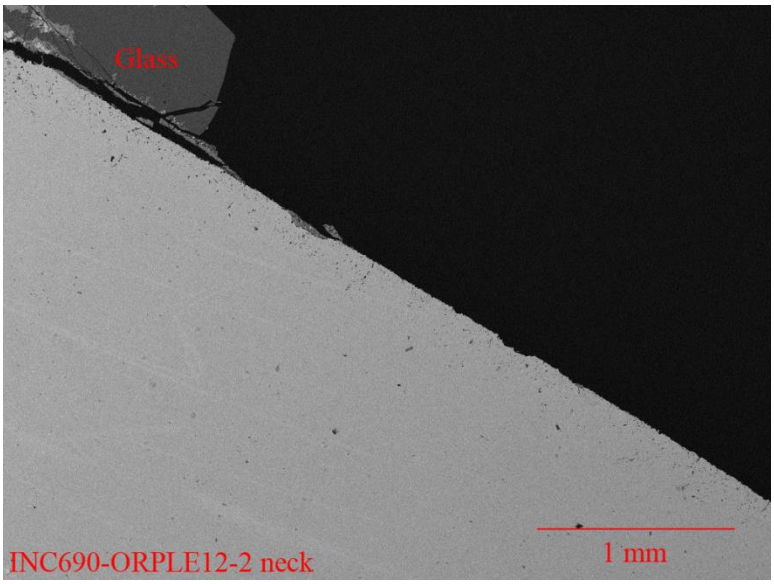

(1) Inconel 690 alloy (light grey) at Neck region.

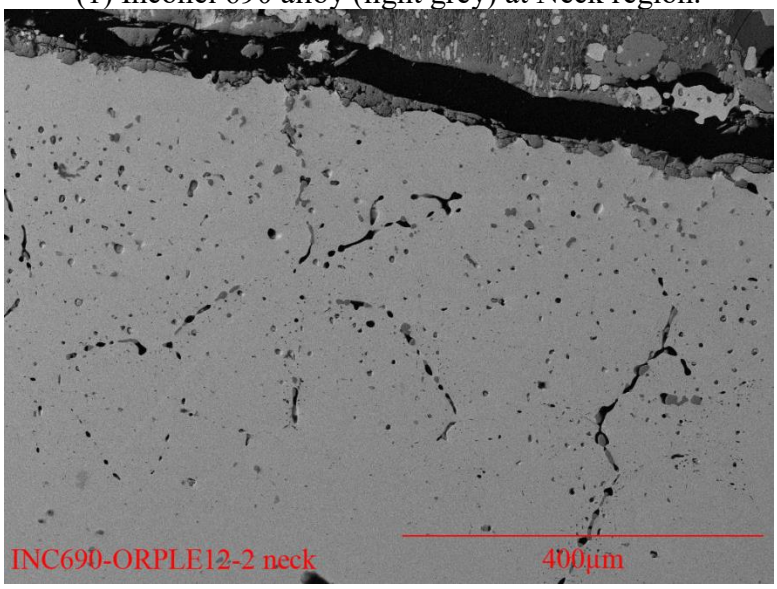

(2) Inconel 690 alloy (light grey) at Neck region with deep grain boundary attack.

Figure 4.4b. SEM images of Inconel 690 coupon after LE12-2 test (closed crucible corrosion) in ORPLE12.

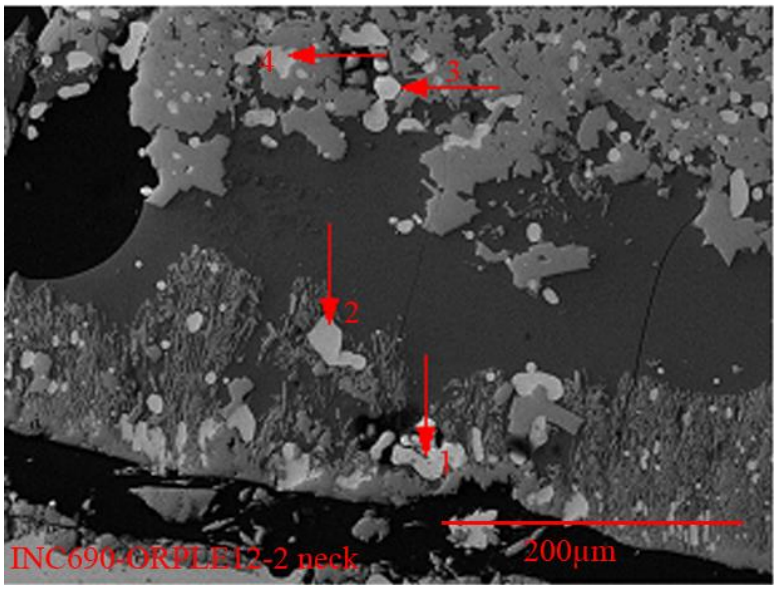

(3) Massive alloy break down with wide spread of Ni nodules (~99 wt% Ni for #1-#4) at Neck region

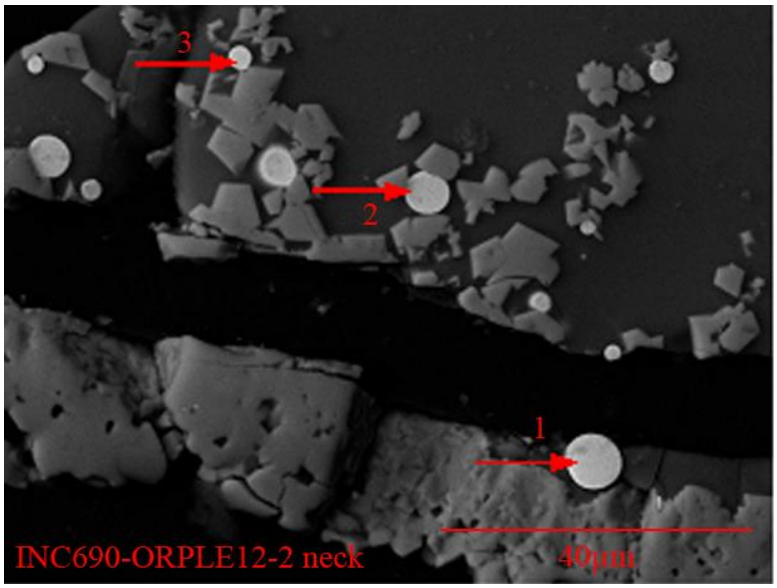

(4) Ni-sulfide with Bi at neck region (#1, #2, #3, source of contamination unknown)

Figure 4.4b. SEM images of Inconel 690 coupon after LE12-2 test (closed crucible corrosion) in ORPLE12 (continued).

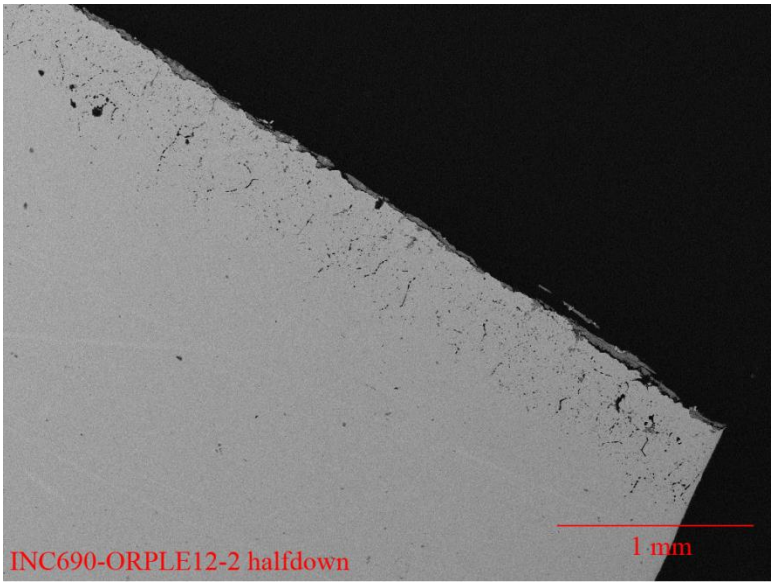

(5) Inconel 690 alloy (light grey) at Half-down region

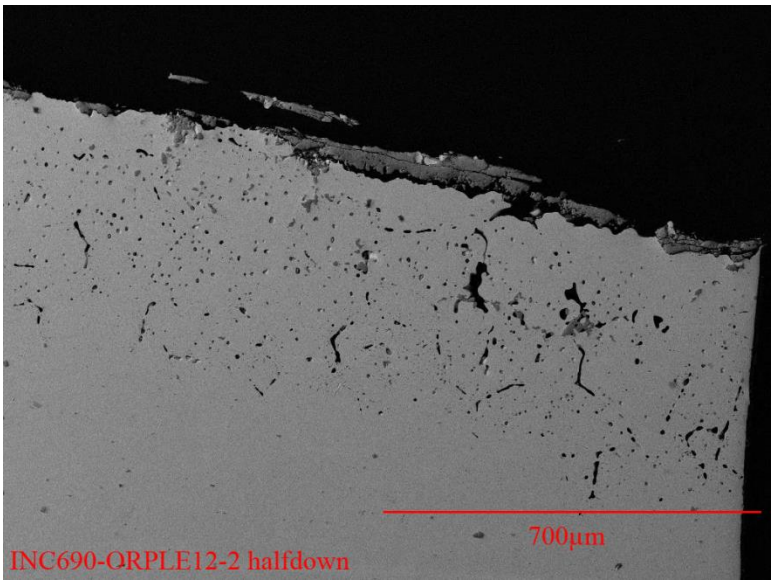

(6) Inconel 690 alloy (light grey) at Half-down region with deep internal damage

Figure 4.4b. SEM images of Inconel 690 coupon after LE12-2 test (closed crucible corrosion) in ORPLE12 (continued).

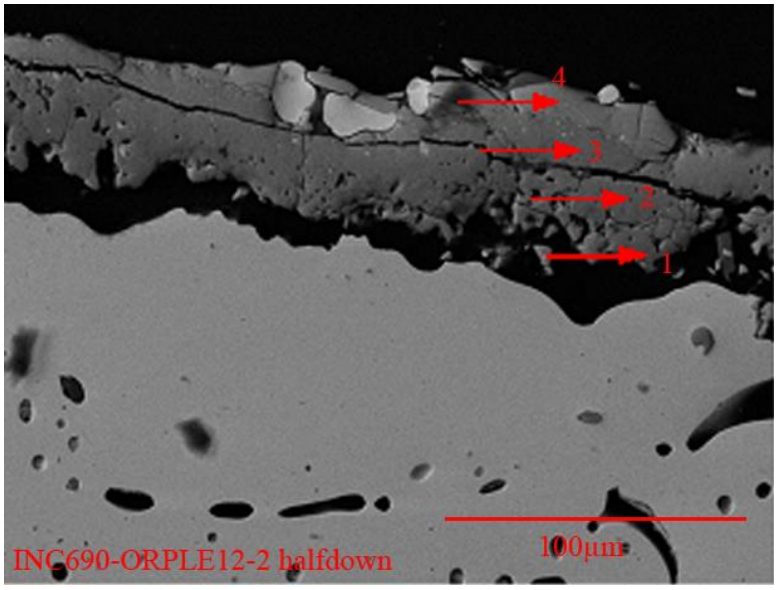

(7) Inconel 690 alloy (light grey) at Half-down region (#1-#3: Cr oxide; #4: Zn-Cr spinel; Bright Ni nodules near top)

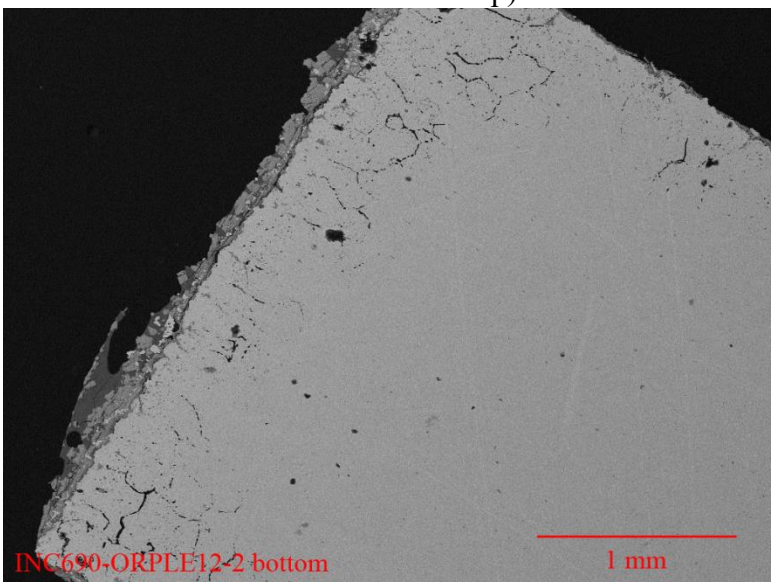

(8) Inconel 690 alloy (light grey) at Bottom region

Figure 4.4b. SEM images of Inconel 690 coupon after LE12-2 test (closed crucible corrosion) in ORPLE12 (continued).

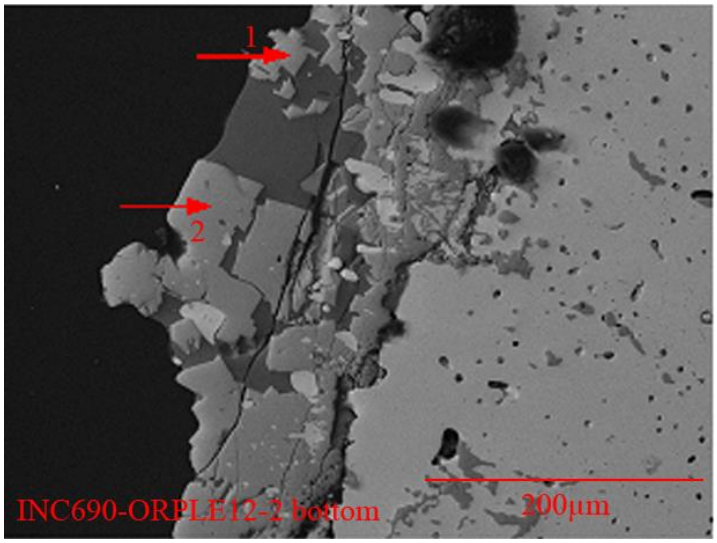

(9) Inconel 690 alloy (light grey) at Bottom region (#1, #2: Zn-Cr spinel, Bright Ni nodule imbedded with grey Cr oxide between spinel and Inconel alloy)

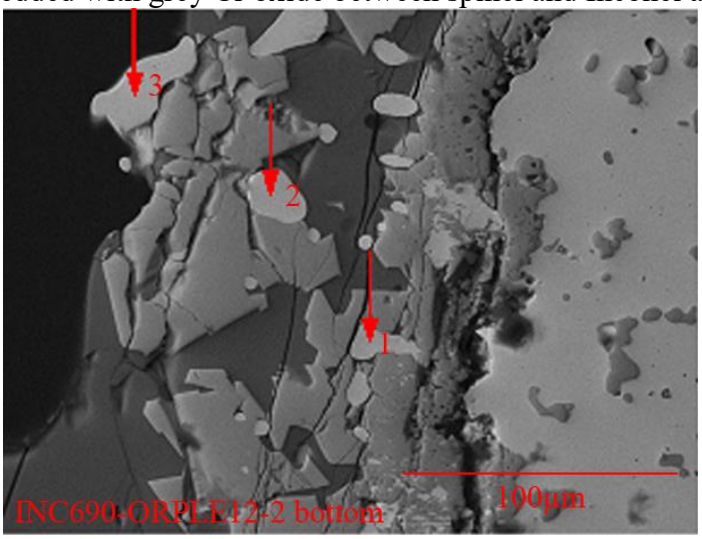

(10) Ni nodule (#1-#3) at Bottom region near Inconel 690 alloy (light grey, right side)

Figure 4.4b. SEM images of Inconel 690 coupon after LE12-2 test (closed crucible corrosion) in ORPLE12 (continued).

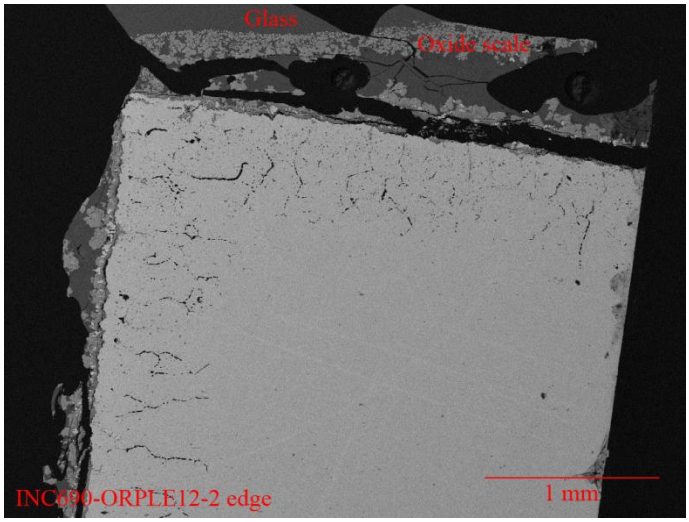

(11) Inconel 690 alloy (light grey) at edge

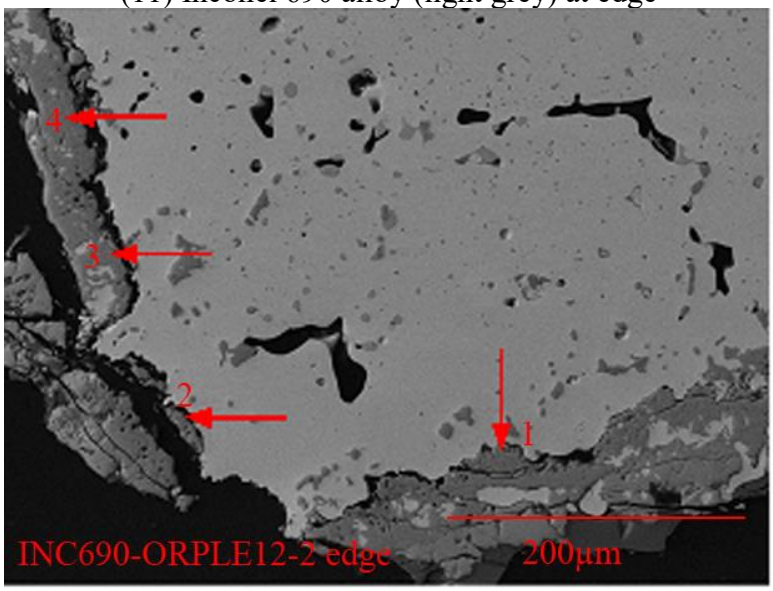

(12) Inconel 690 alloy (light grey) at edge (#1-#4: Cr oxide)

Figure 4.4b. SEM images of Inconel 690 coupon after LE12-2 test (closed crucible corrosion) in ORPLE12 (continued).

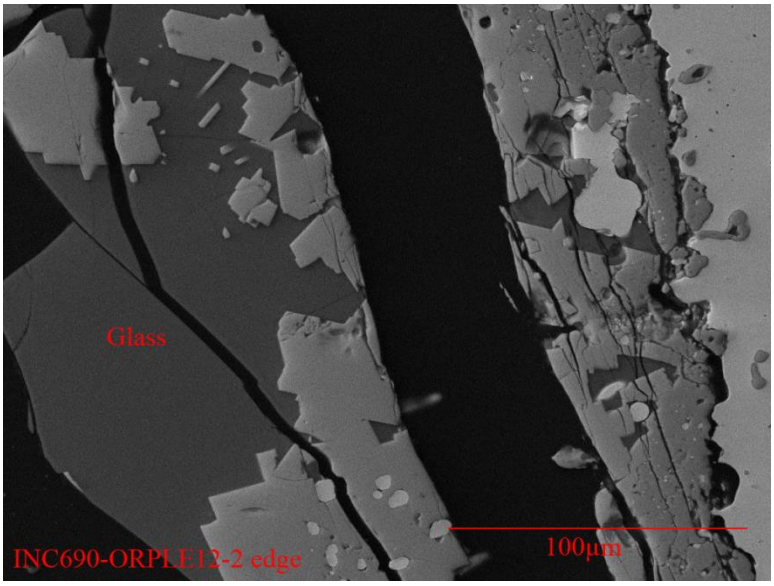

(13) Inconel 690 alloy (light grey, right side) at edge. Zn-Cr spinel is present within glass on left. Cr oxide scale is between spinel and alloy in the middle embed with Ni-enriched nodule.

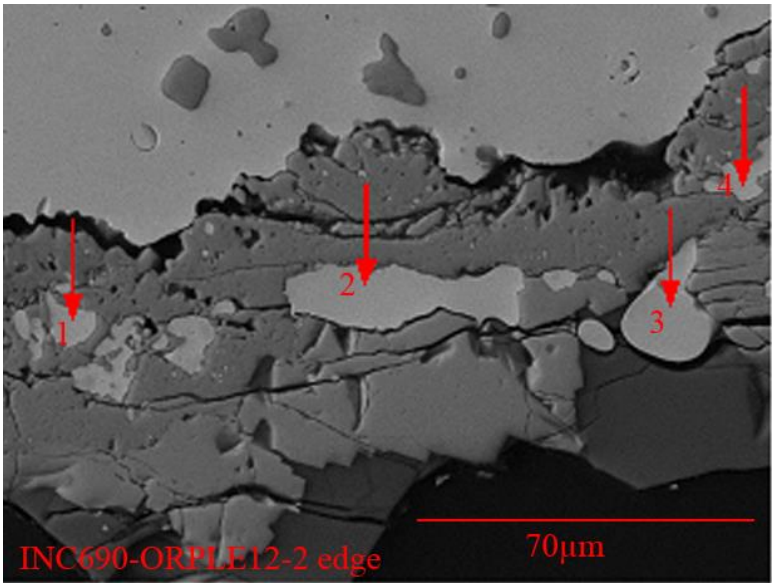

(14) Inconel 690 alloy (light grey, top) at edge with numerous Ni-enriched nodules of different Ni wt% (#1: 74 wt%; #4: 88 wt%; #2: 97 wt%; #3: 98 wt%)

Figure 4.4b. SEM images of Inconel 690 coupon after LE12-2 test (closed crucible corrosion) in ORPLE12 (continued).

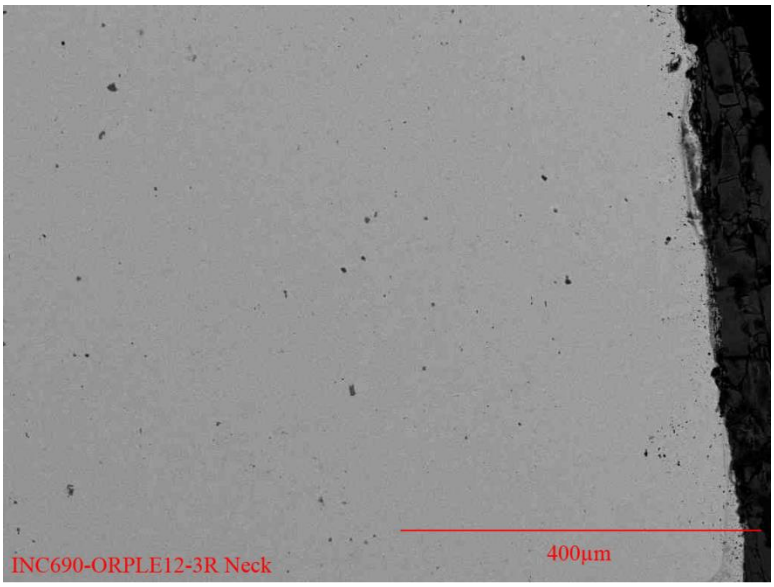

(1) Inconel 690 alloy (light grey) at Neck region.

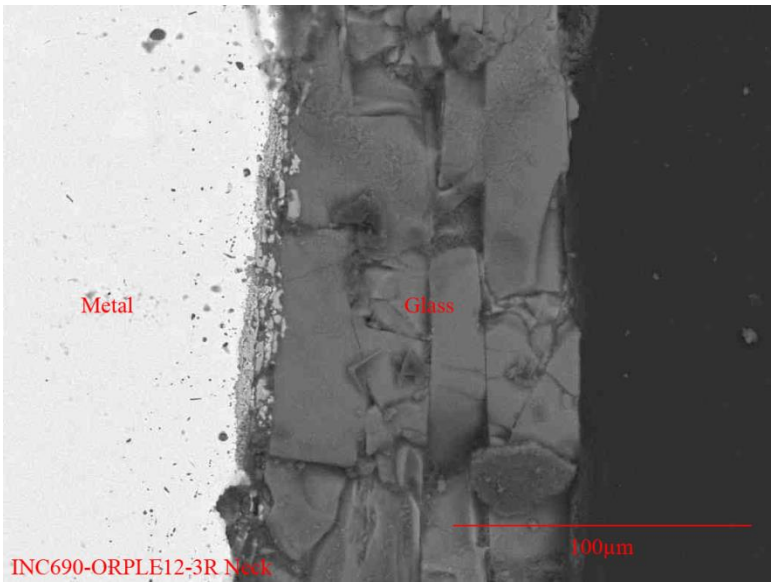

(2) Inconel 690 alloy (light grey, left side) at Neck region.

Figure 4.4c. SEM images of Inconel 690 coupon after LE12-3 test (closed crucible corrosion) in ORPLE12.

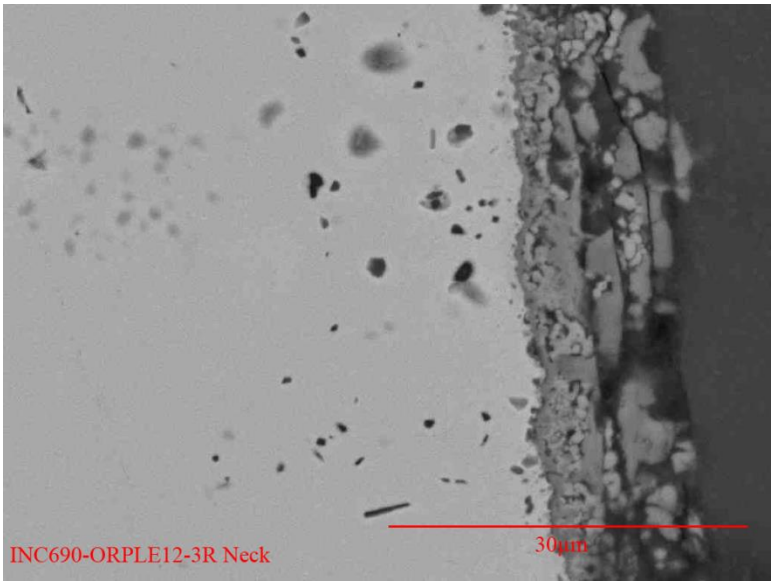

(3) Inconel 690 alloy (light grey) at Neck region

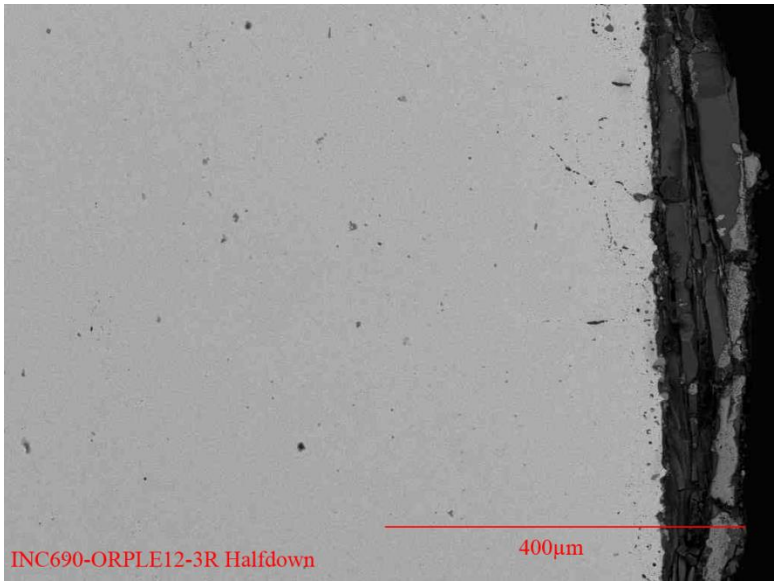

(4) Inconel 690 alloy (light grey) at Half-down region with detached scale to its right side

Figure 4.4.c. SEM images of Inconel 690 coupon after LE12-3 test (closed crucible corrosion) in ORPLE12 (continued).

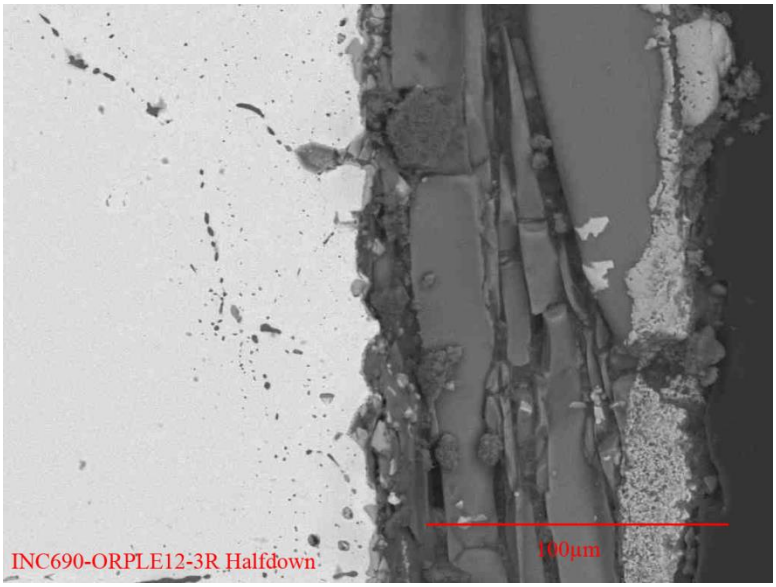

(5) Details of detached scale at Half-down region.

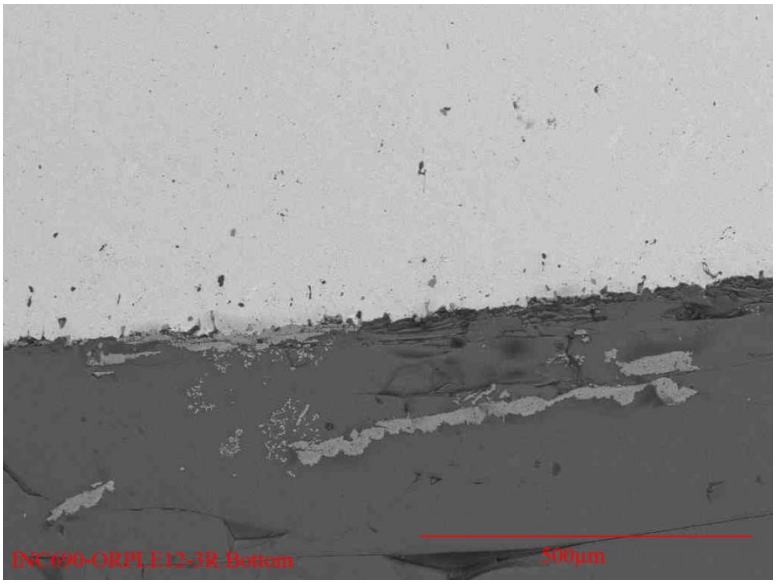

(6) Inconel 690 alloy (light grey) at Bottom region with detached scale on low half within glass

Figure 4.4.c. SEM images of Inconel 690 coupon after LE12-3 test (closed crucible corrosion) in ORPLE12 (continued).

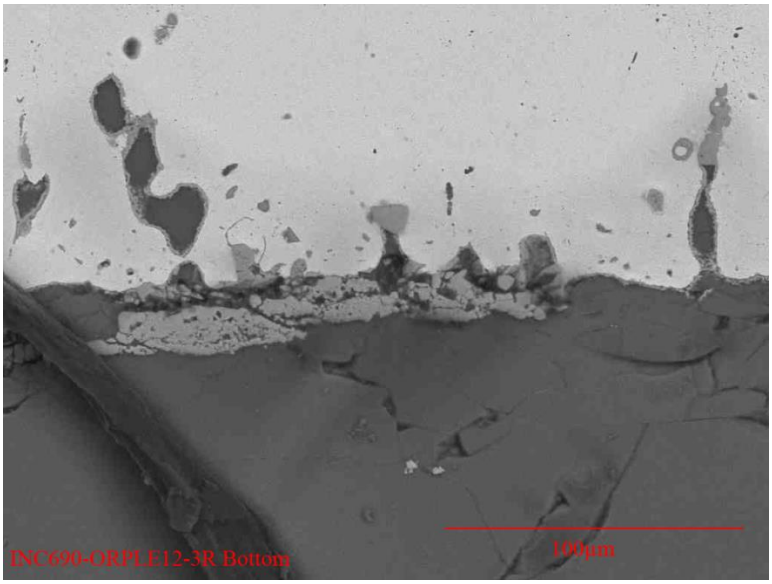

(7) Inconel 690 alloy (light grey) at Bottom region with grain boundary damage

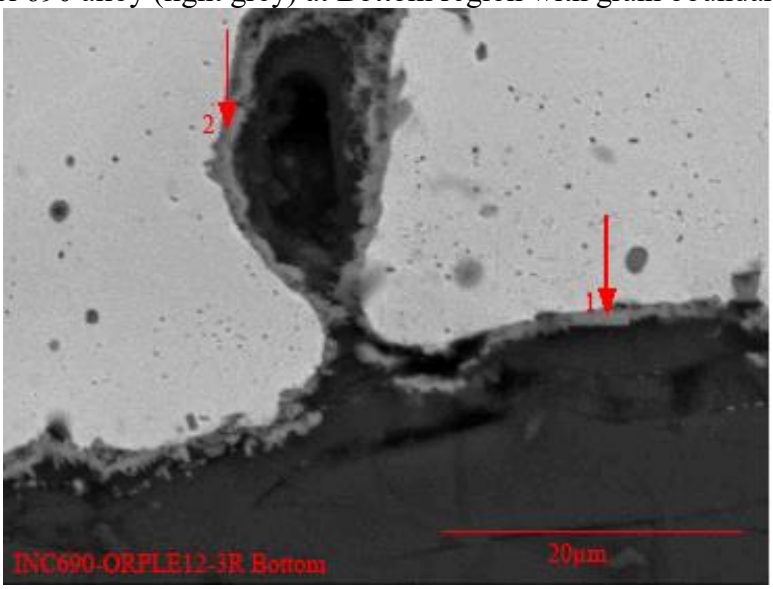

(8) Details of grain boundary damage at Bottom region with layer of Cr oxide, (#1, #2)

Figure 4.4.c. SEM images of Inconel 690 Coupon after LE12-3 test (closed crucible corrosion) in ORPLE12 (continued).

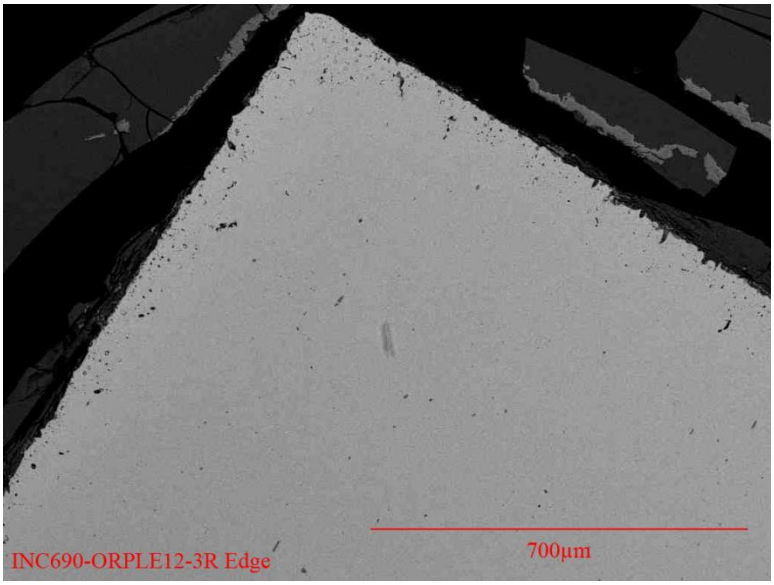

(9) Inconel 690 alloy (light grey) at edge

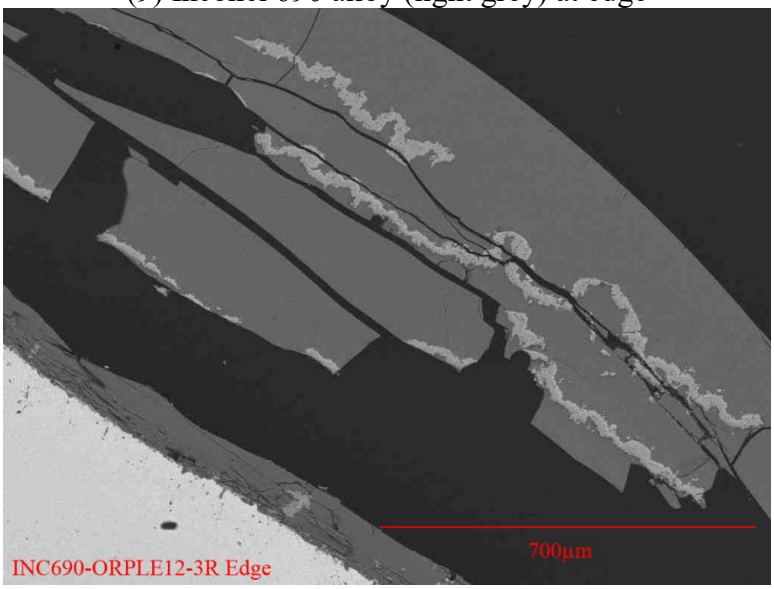

(10) Inconel 690 alloy (light grey, low left) at Edge with detached oxide scale in middle of the image

Figure 4.4.c. SEM images of Inconel 690 coupon after LE12-3 test (closed crucible corrosion) in ORPLE12 (continued).

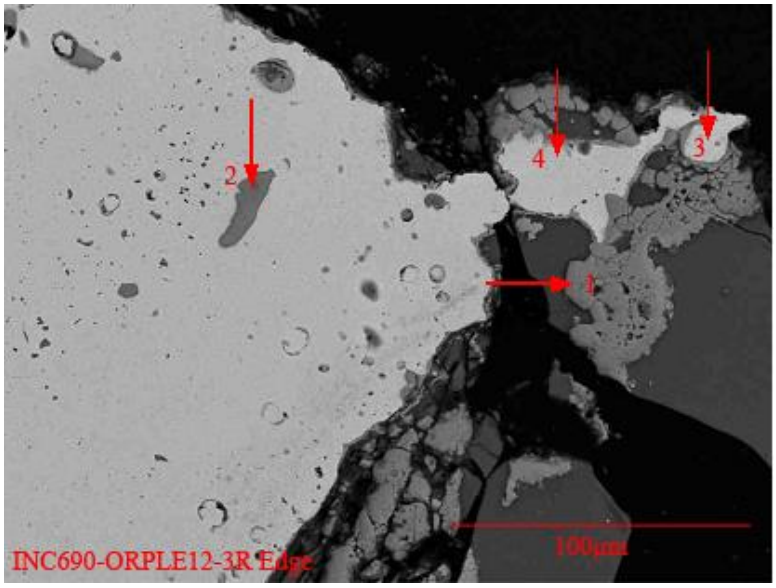

(11) Details of reformation of Inconel alloy at edge (#1, #2: Cr oxide; #3: 73 wt% Ni; #4: 77 wt% Ni)

Figure 4.4.c. SEM images of Inconel 690 coupon after LE12-3 test (closed crucible corrosion) in ORPLE12 (continued).

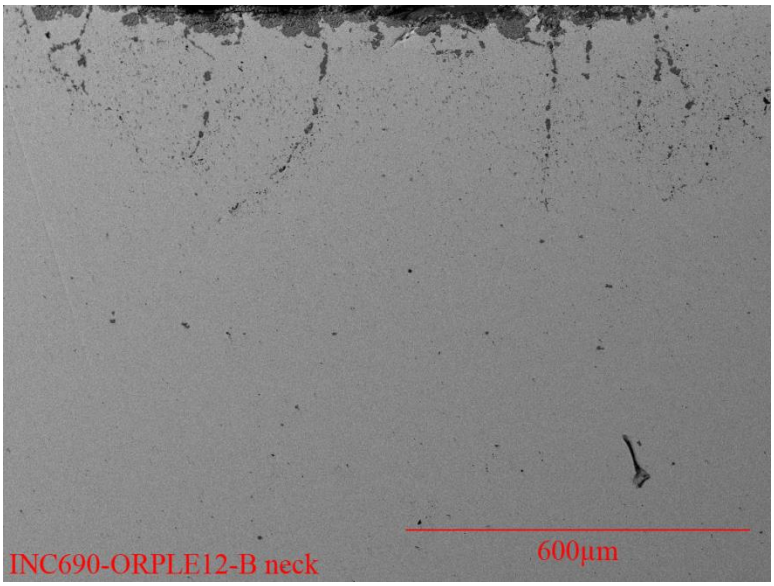

(1) Inconel 690 alloy (light grey) at Neck region

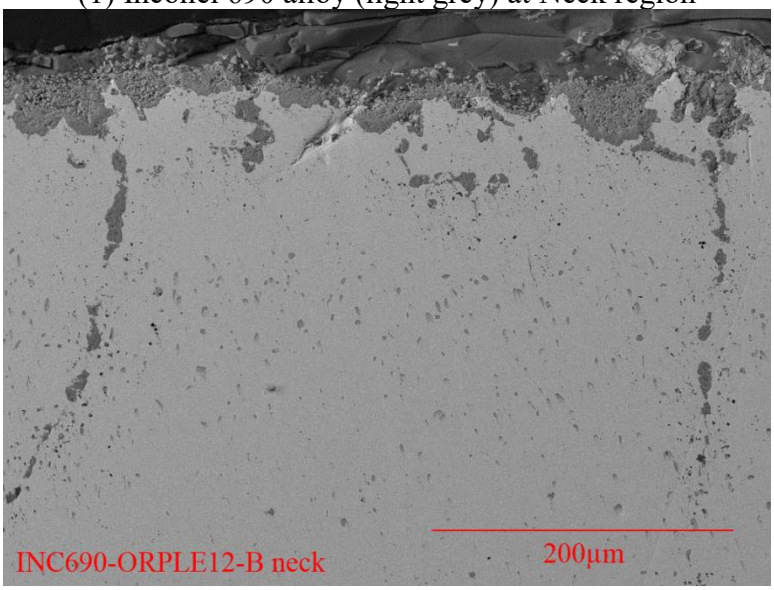

(2) Inconel 690 alloy (light grey) at Neck

Figure 4.4d. SEM images of Inconel 690 coupon after LE12-4 test (closed crucible corrosion) in ORPLE12.

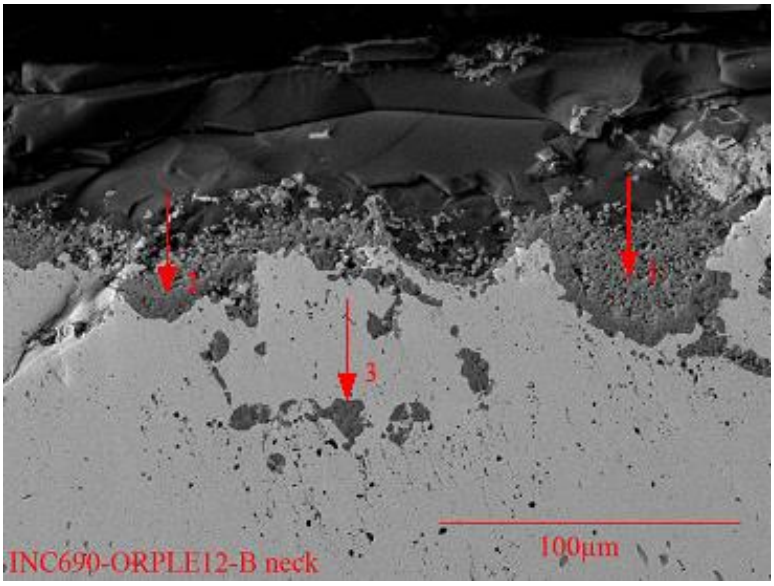

(3) Inconel 690 alloy (light grey) at Neck (#2, #3: Cr oxide; #1: Zn-Cr spinel)

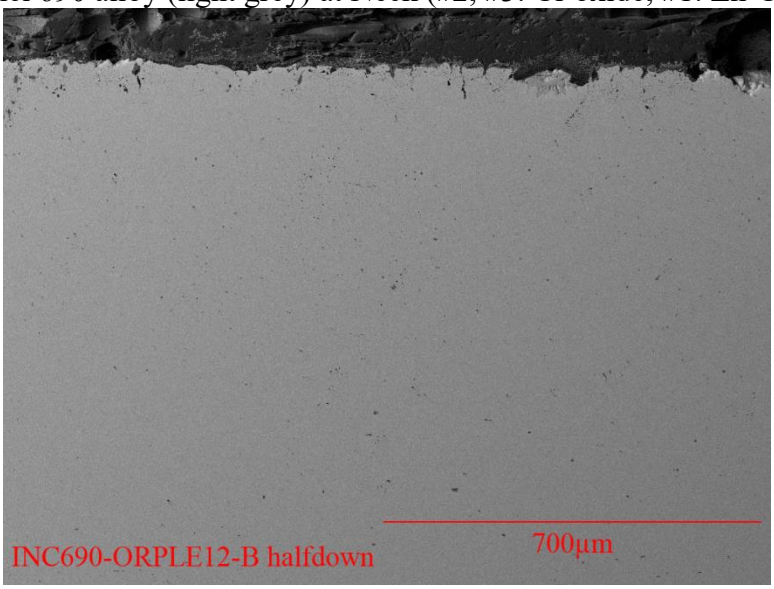

(4) Inconel 690 alloy (light grey) at Half-down region.

Figure 4.4d. SEM images of Inconel 690 coupon after LE12-4 (closed crucible corrosion) in ORPLE12 (continued).

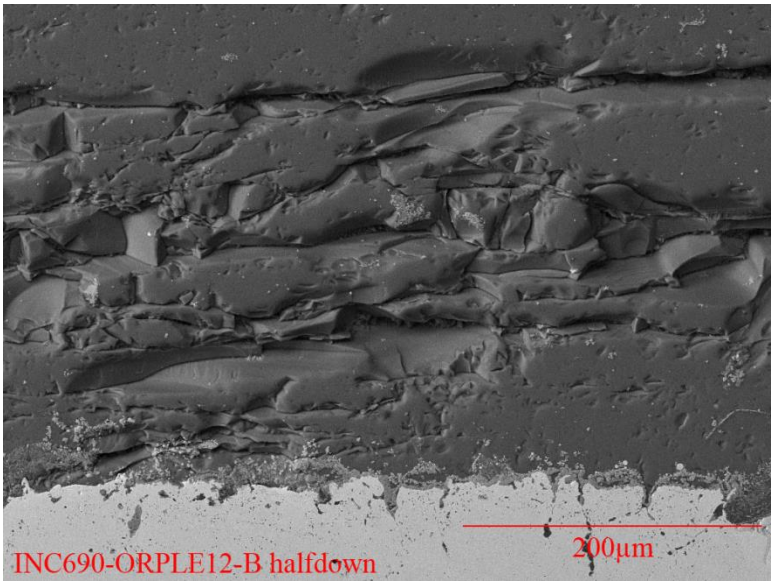

(5) Inconel 690 alloy (light grey) at Half-down region

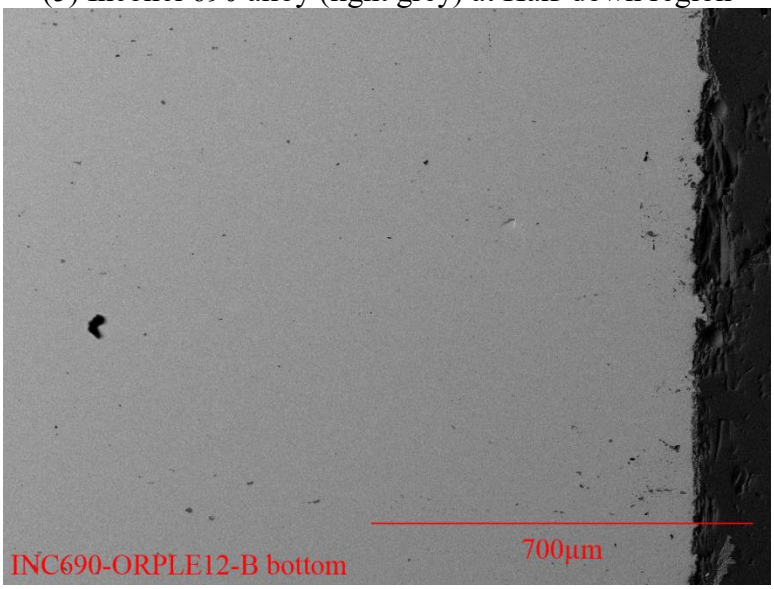

(6) Inconel 690 alloy (light grey) at Bottom region

Figure 4.4d. SEM images of Inconel 690 coupon after LE12-4 (closed crucible corrosion) in ORPLE12 (continued).

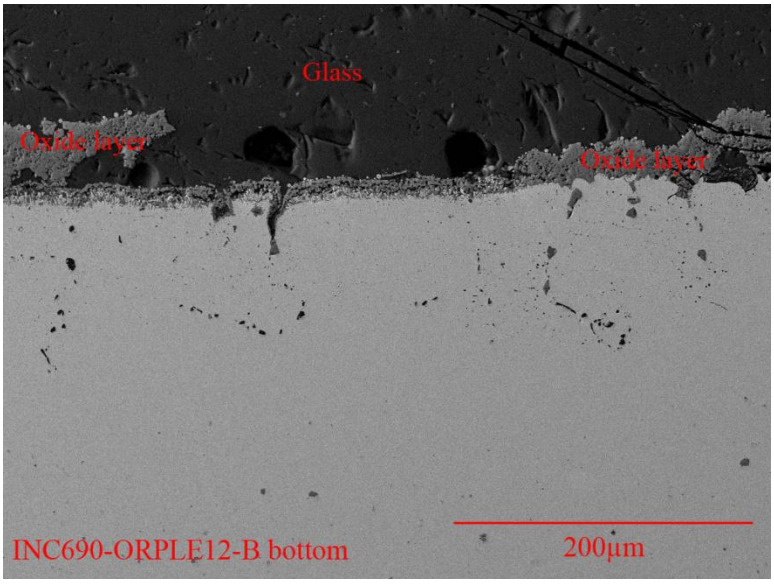

(7) Inconel 690 alloy (light grey) at Bottom region

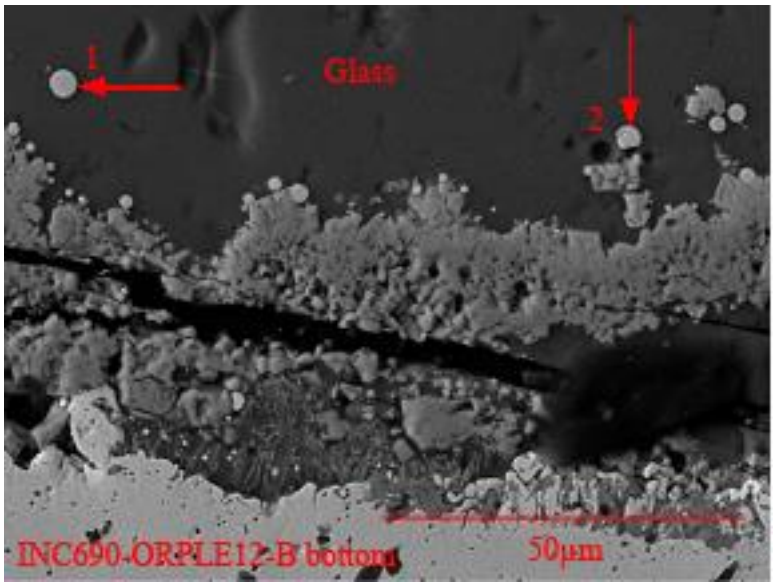

(8) Ni sulfide drops near oxide scale at Bottom region (#1, #2)

Figure 4.4d. SEM images of Inconel 690 coupon after LE12-4 (closed crucible corrosion) in ORPLE12 (continued).

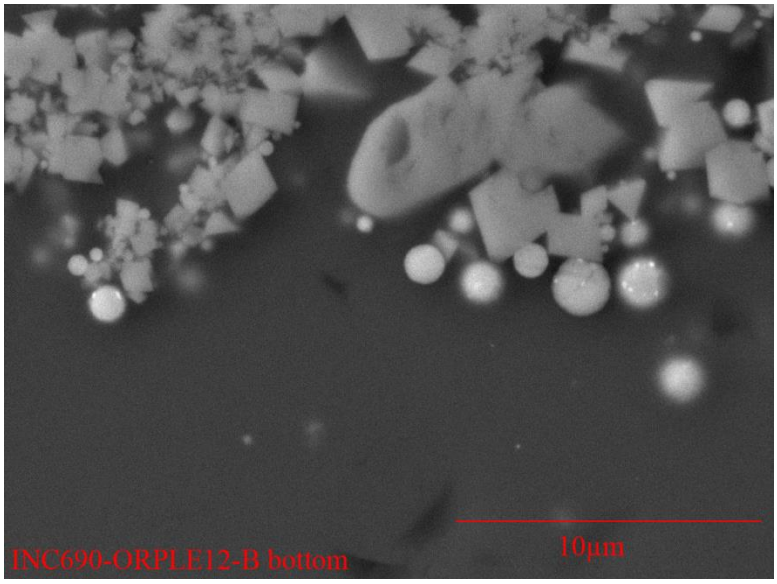

(9) Ni sulfide drops next to Zn-Cr spinel near Bottom region of alloy (not included)

Figure 4.4d. SEM images of Inconel 690 coupon after LE12-4 (closed crucible corrosion) in ORPLE12 (continued).

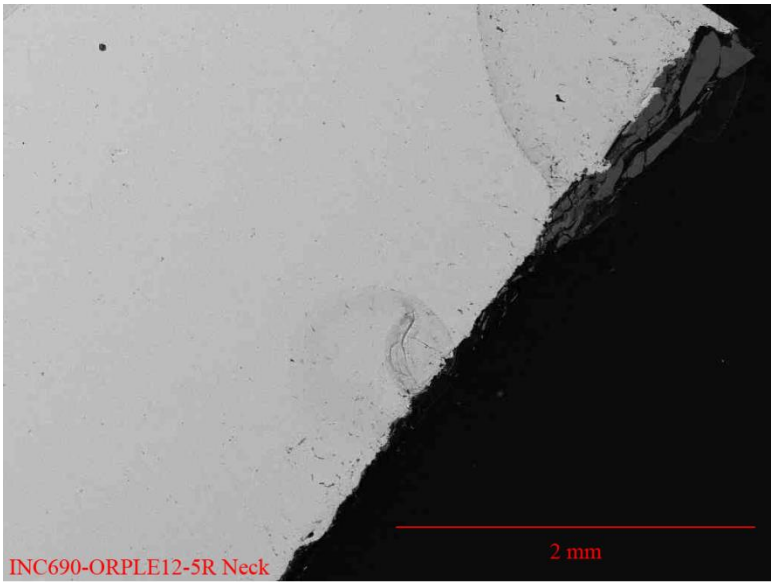

(1) Inconel 690 alloy (light grey) at Neck region

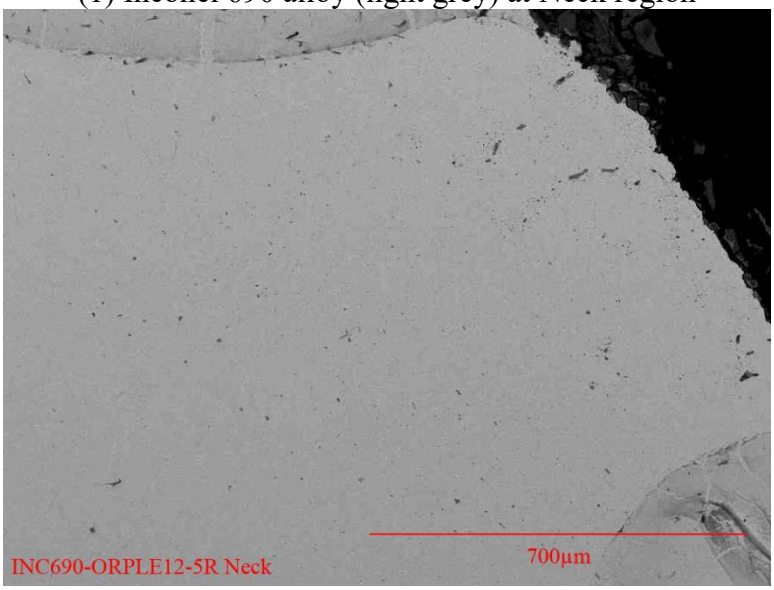

(2) Inconel 690 alloy (light grey) at Neck region

Figure 4.4e. SEM images of Inconel 690 coupon after LE12-5 test (closed crucible corrosion) in ORPLE12.

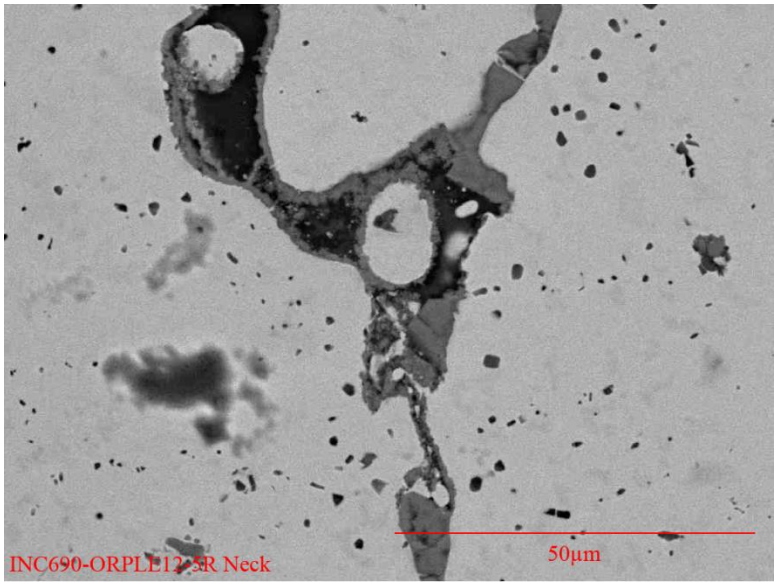

(3) Details of grain boundary damage at Neck region

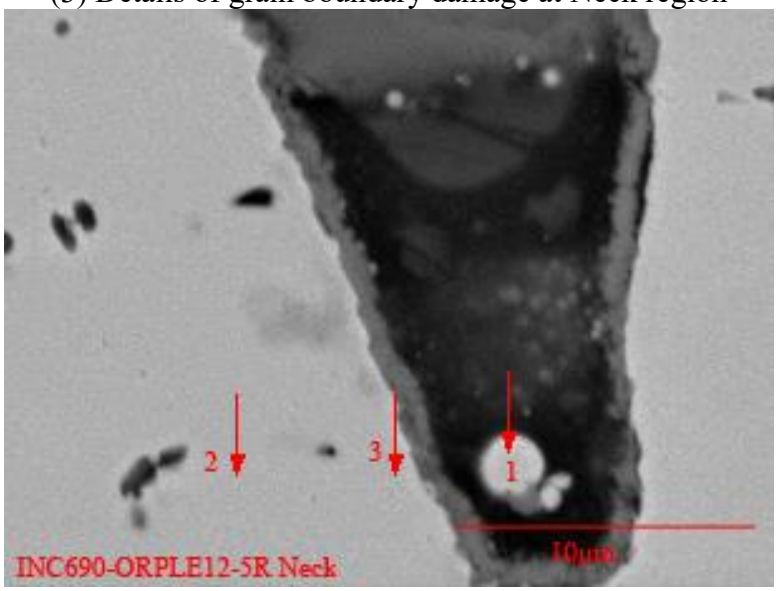

(4) Details of grain boundary damage at Neck region (formation of Ni-enriched nodule within grain boundary. #1-#3: all ~70 wt% Ni with Cr and Fe)

Figure 4.4e. SEM images of Inconel 690 coupon after LE12-5 test (closed crucible corrosion) in ORPLE12 (continued).

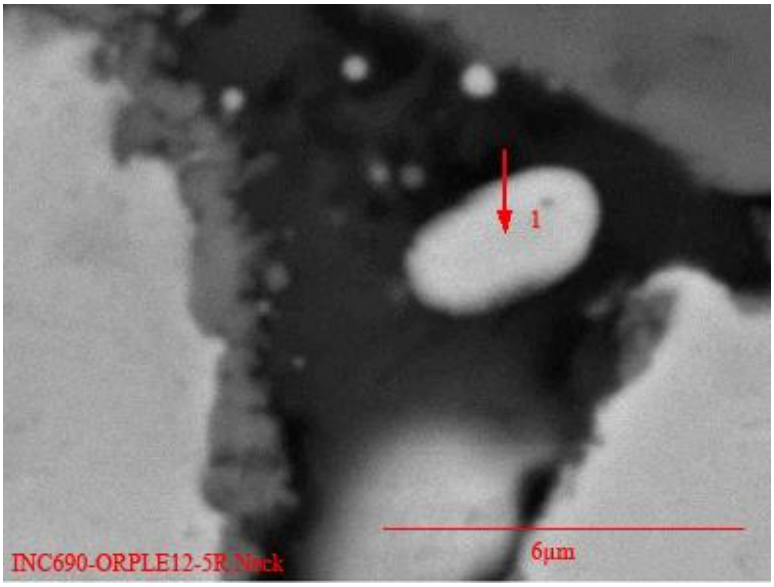

(5) Details of grain boundary damage at Neck region (formation of Ni-enriched nodule within grain boundary)

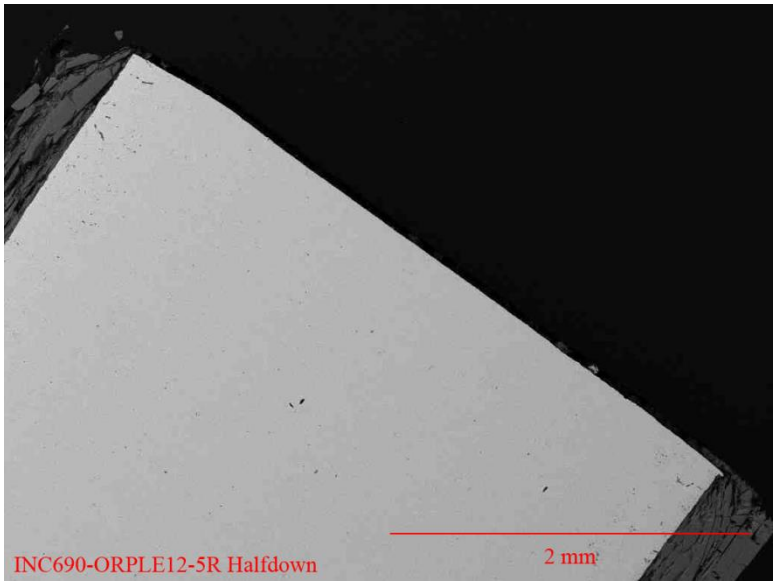

(6) Inconel 690 alloy (light grey) at Half-down region

Figure 4.4e. SEM images of Inconel 690 coupon after LE12-5 test (closed crucible corrosion) in ORPLE12 (continued).

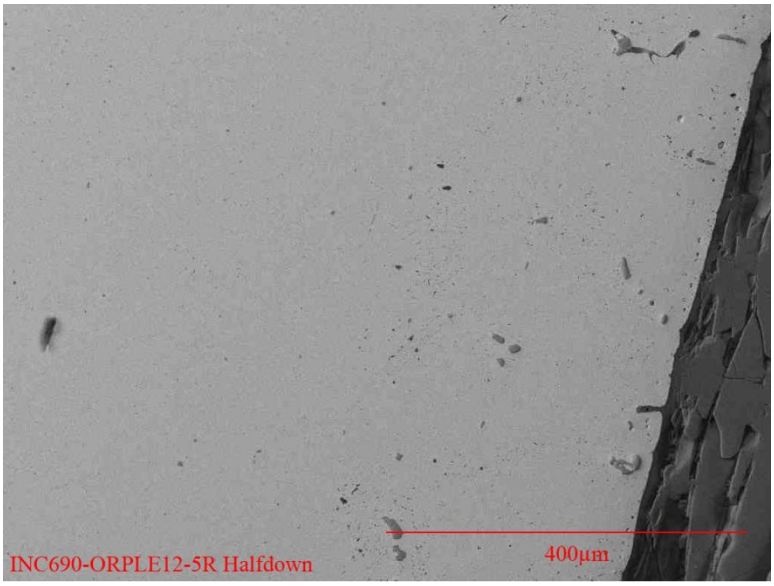

(7) Inconel 690 alloy (light grey) at Half-down region

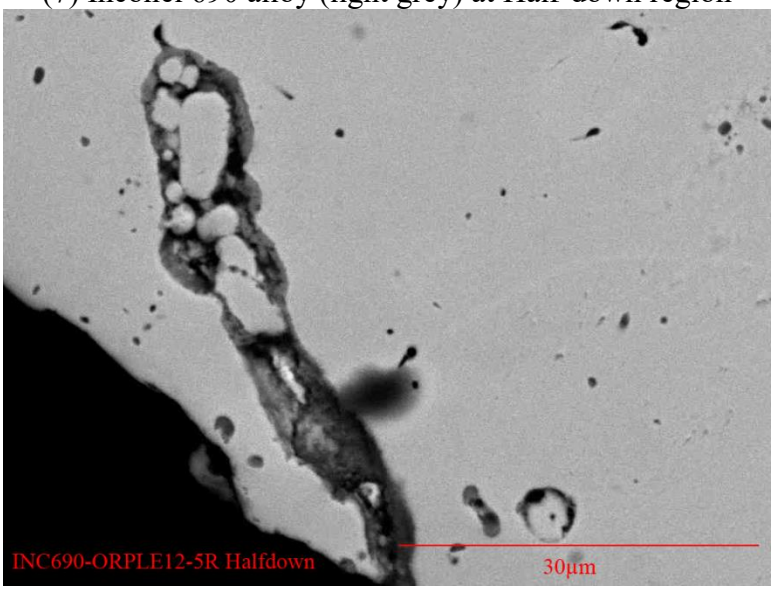

(8) Details of grain boundary damage at Half-down region

Figure 4.4e. SEM images of Inconel 690 Coupon after LE12-5 test (closed crucible corrosion) in ORPLE12 (continued).

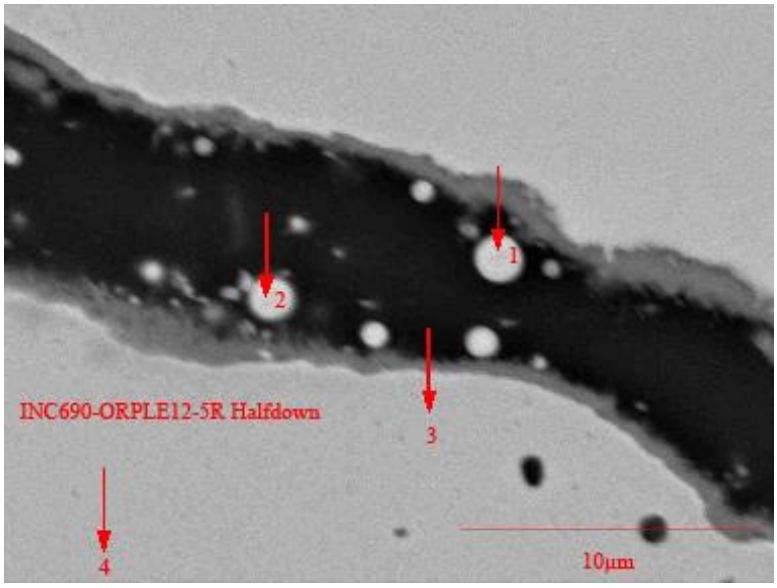

(10) Details of grain boundary damage at Half-down region. (Nodule #1, #2: 7-8 wt% Cr, #3:18 wt% Cr and #4: 21 wt% Cr)

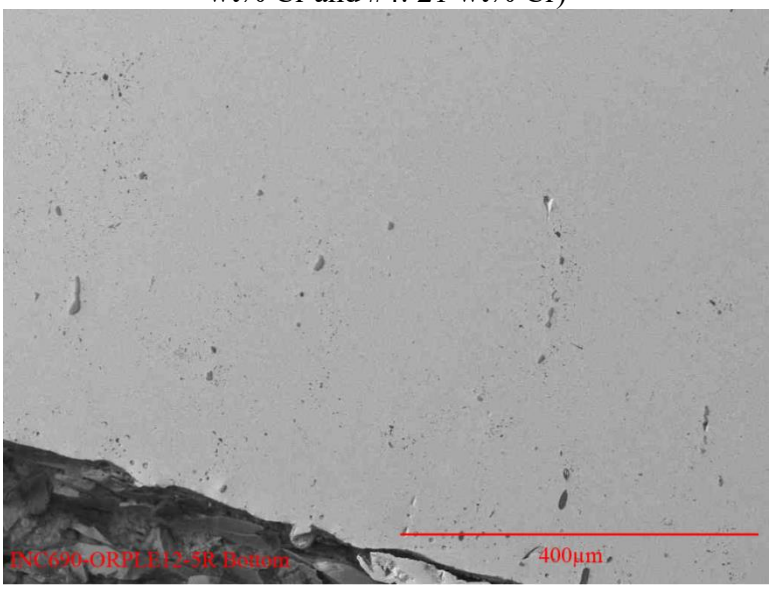

(11) Inconel 690 alloy (light grey) at Bottom (metal strip on lower right side has peeled over during cutting)

Figure 4.4e. SEM images of Inconel 690 coupon after LE12-5 test (closed crucible corrosion) in ORPLE12 (continued).

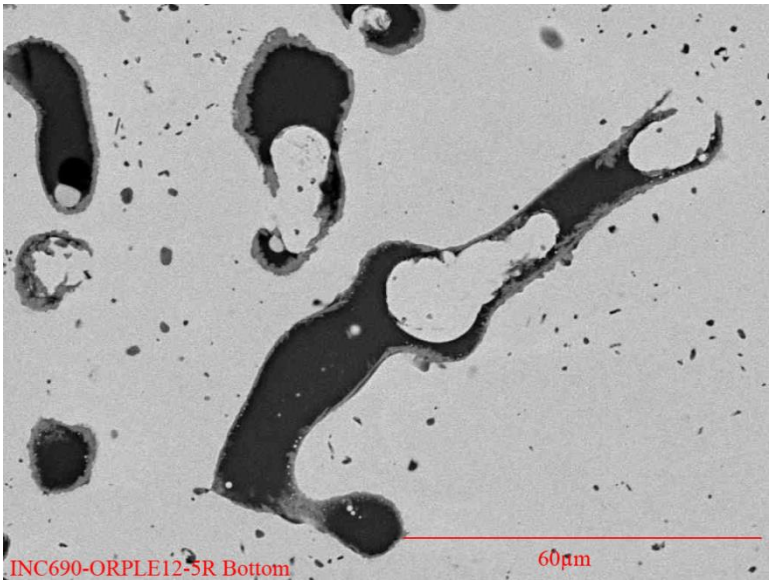

(12) Details of grain boundary damage at Bottom region

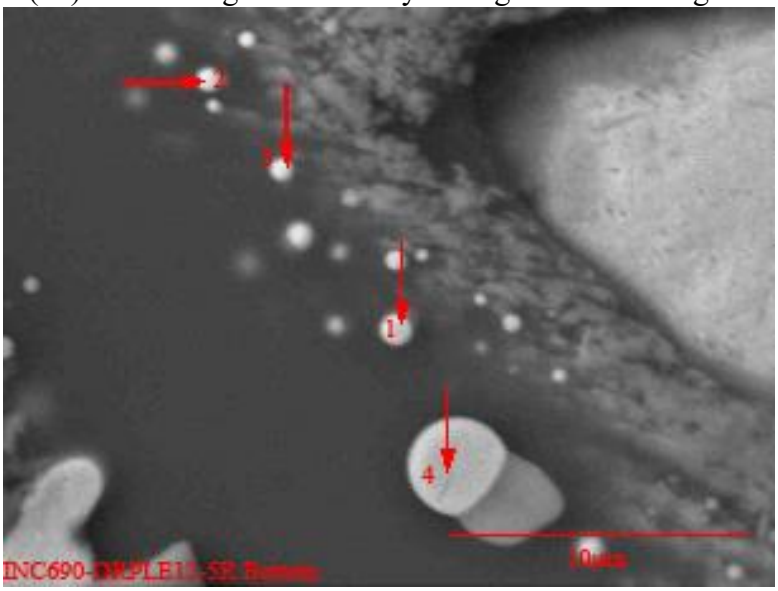

(13) Details of grain boundary damage at Bottom region (#1-#4: Cr-depleted Inconel nodule, Cr from 13 -18 wt%)

Figure 4.4e. SEM images of Inconel 690 coupon after LE12-5 test (closed crucible corrosion) in ORPLE12 (continued).

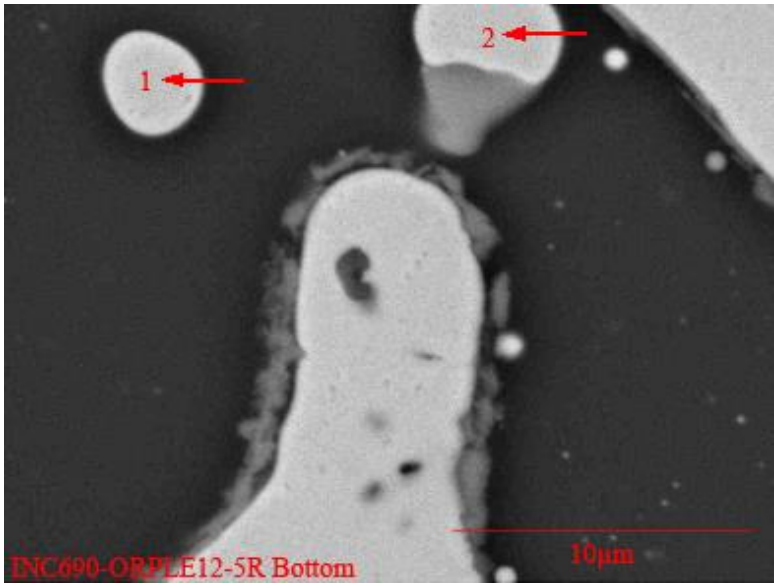

(14) Details of grain boundary damage at Bottom (#1, #2: Cr-depleted Inconel nodule, Cr from 16 -17 wt%)

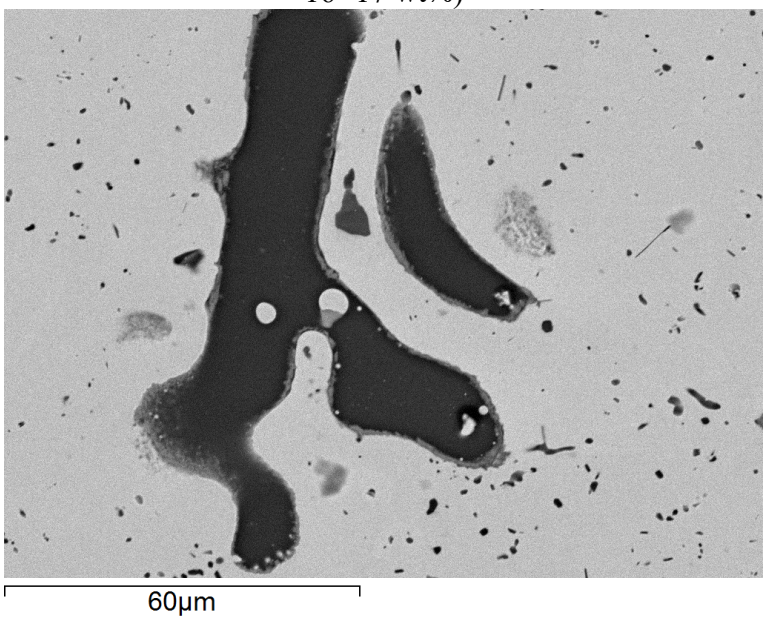

(15) Details of grain boundary damage

Figure 4.4e. SEM images of Inconel 690 coupon after LE12-5 test (closed crucible corrosion) in ORPLE12 (continued).

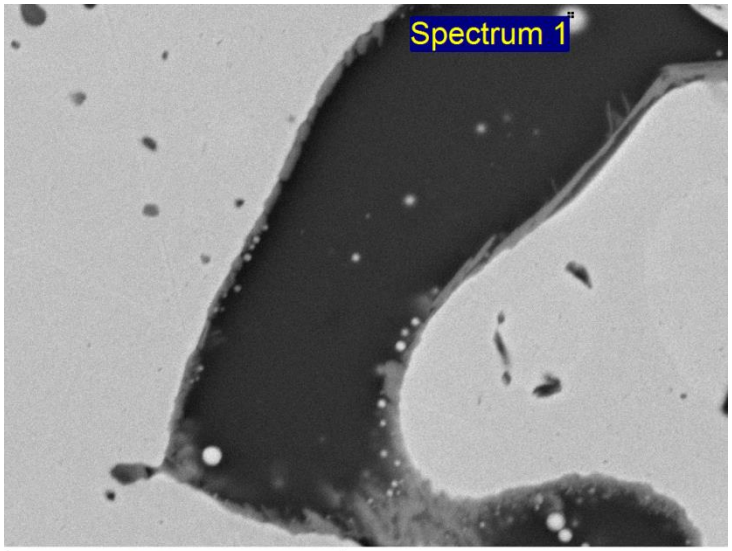

(16) Details of grain boundary damage

Figure 4.4e. SEM images of Inconel 690 coupon after LE12-5 test (closed crucible corrosion) in ORPLE12 (continued).

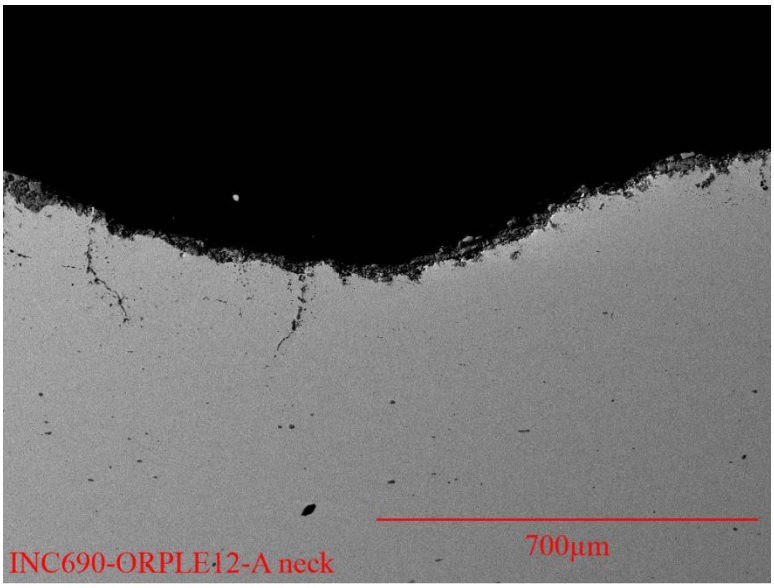

(1) Inconel 690 (light grey) at Neck region.

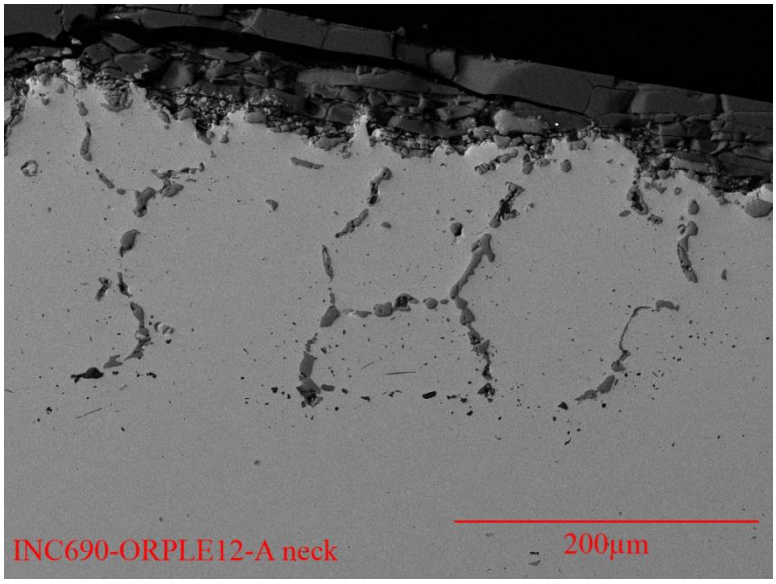

(2) Inconel 690 (light grey) at Neck region with intensive internal oxidization along grain boundary

Figure 4.4f. SEM images of Inconel 690 coupon after LE12-A corrosion test (open to air) in ORPLE12.

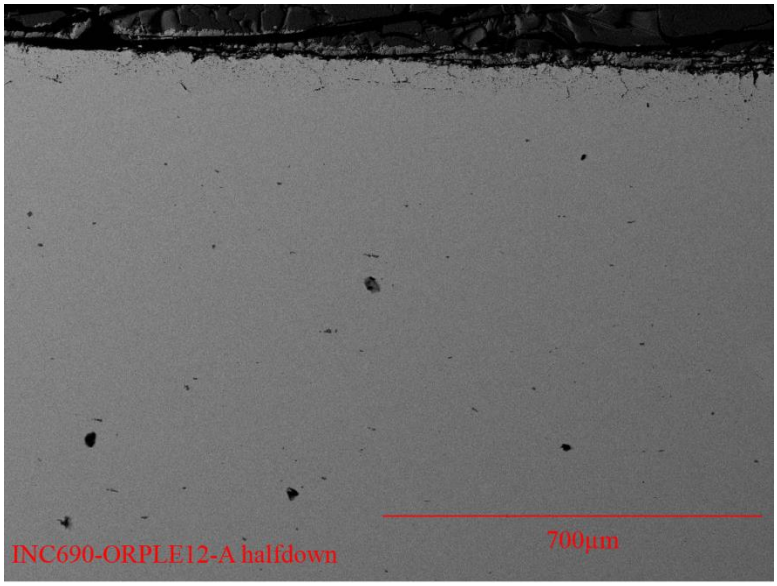

(3) Inconel 690 (light grey) at Half-down region

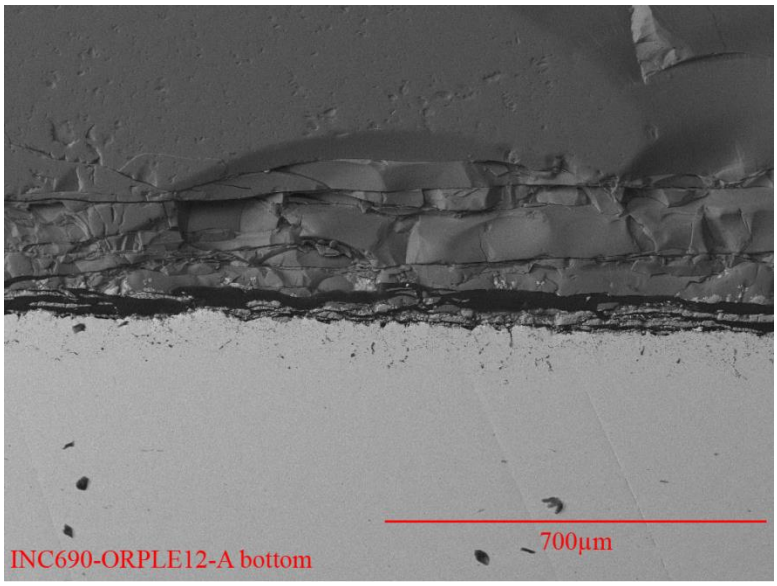

(4) Inconel 690 (light grey) at Bottom region

Figure 4.4f. SEM images of Inconel 690 coupon after LE12-A corrosion test (open to air) in ORPLE12 (continued).

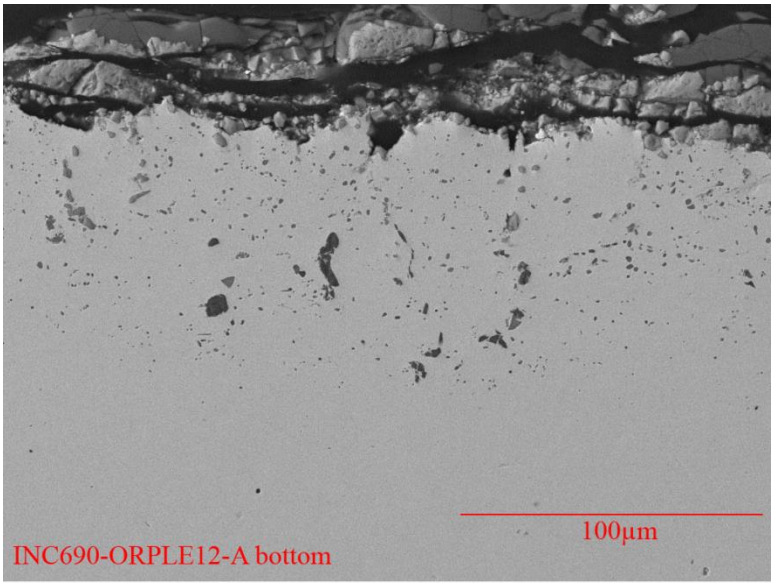

(5) Inconel 690 (light grey) at Bottom region

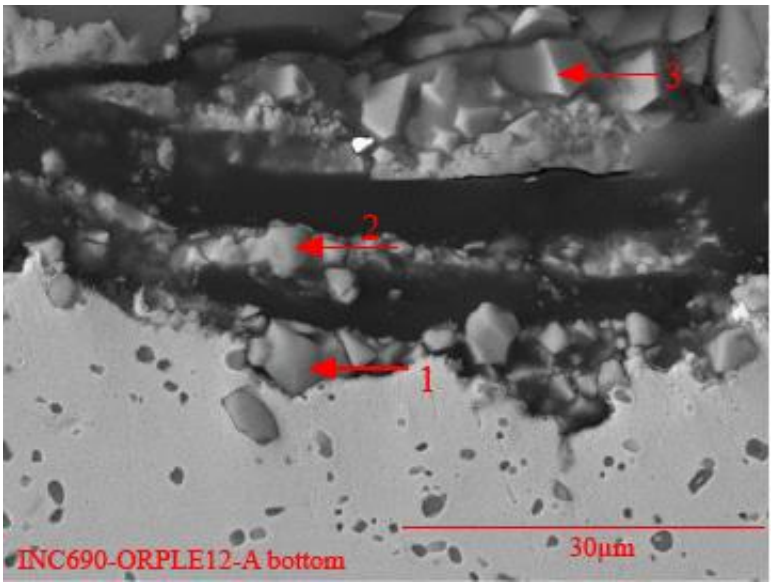

(6) Inconel 690 (light grey) at Bottom (#1, #2: Cr oxide; #3: Zn-Cr spinel)

Figure 4.4f. SEM images of Inconel 690 coupon after LE12-A corrosion test (open to air) in ORPLE12 (continued).

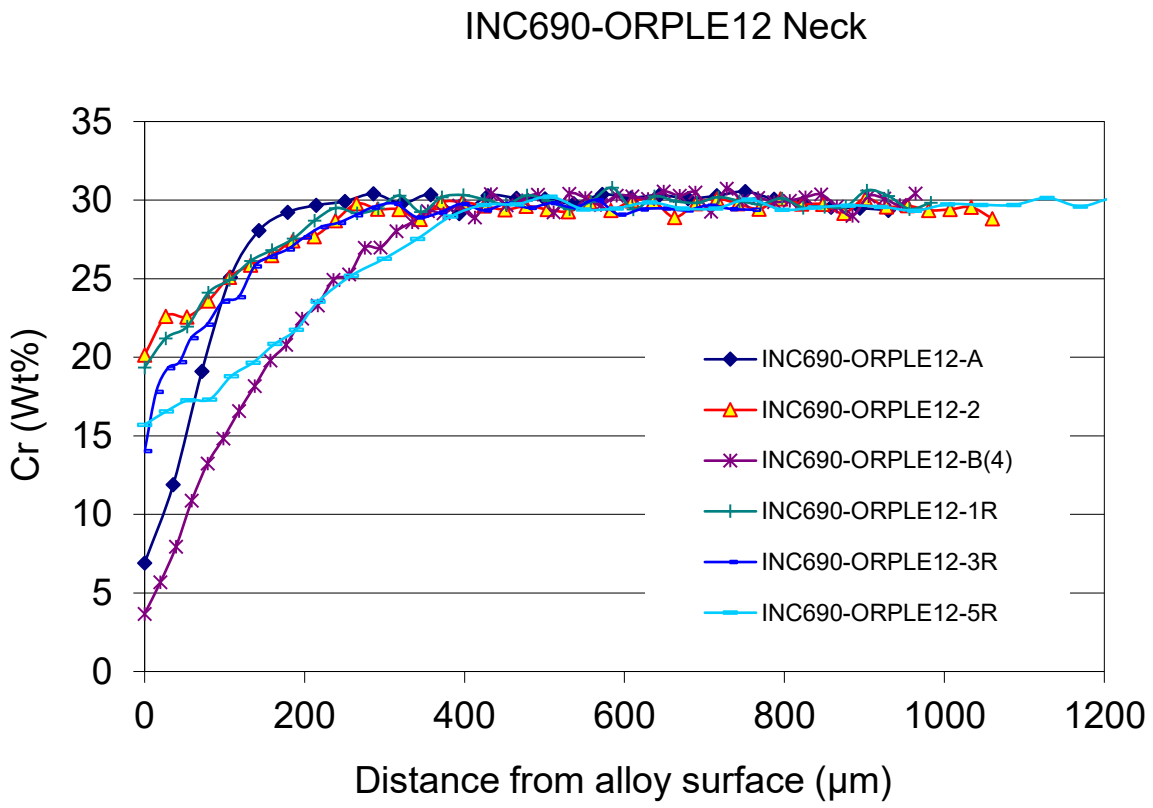

Figure 4.5a. Chromium concentration (Cr wt% in alloy) vs. distance from alloy surface at neck location for ORPLE12 glasses for tests LE12-1 (INC690-ORPLE12-1R), LE12-2 (INC690-ORPLE12-2), LE12-3 (INC690-ORPLE12-3R), LE12-4 (INC690-ORPLE12-B(4)), LE12-5 (INC690-ORPLE12-5R), and LE12-A (INC690-ORPLE12-A).

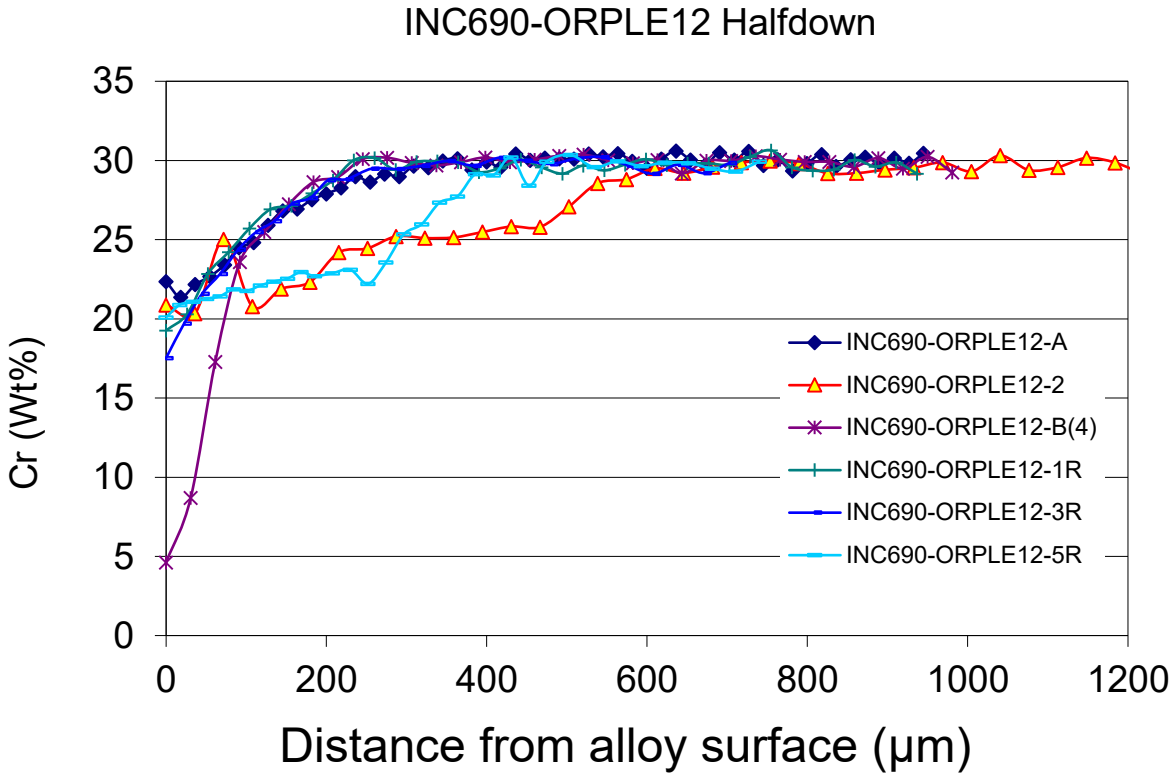

Figure 4.5b. Chromium concentration (Cr wt% in alloy) vs. distance from alloy surface at half-down location for ORPLE12 glasses for tests LE12-1 (INC690-ORPLE12-1R), LE12-2 (INC690-ORPLE12-2), LE12-3 (INC690-ORPLE12-3R), LE12-4 (INC690-ORPLE12-B(4)), LE12-5 (INC690-ORPLE12-5R), and LE12-A (INC690-ORPLE12-A).

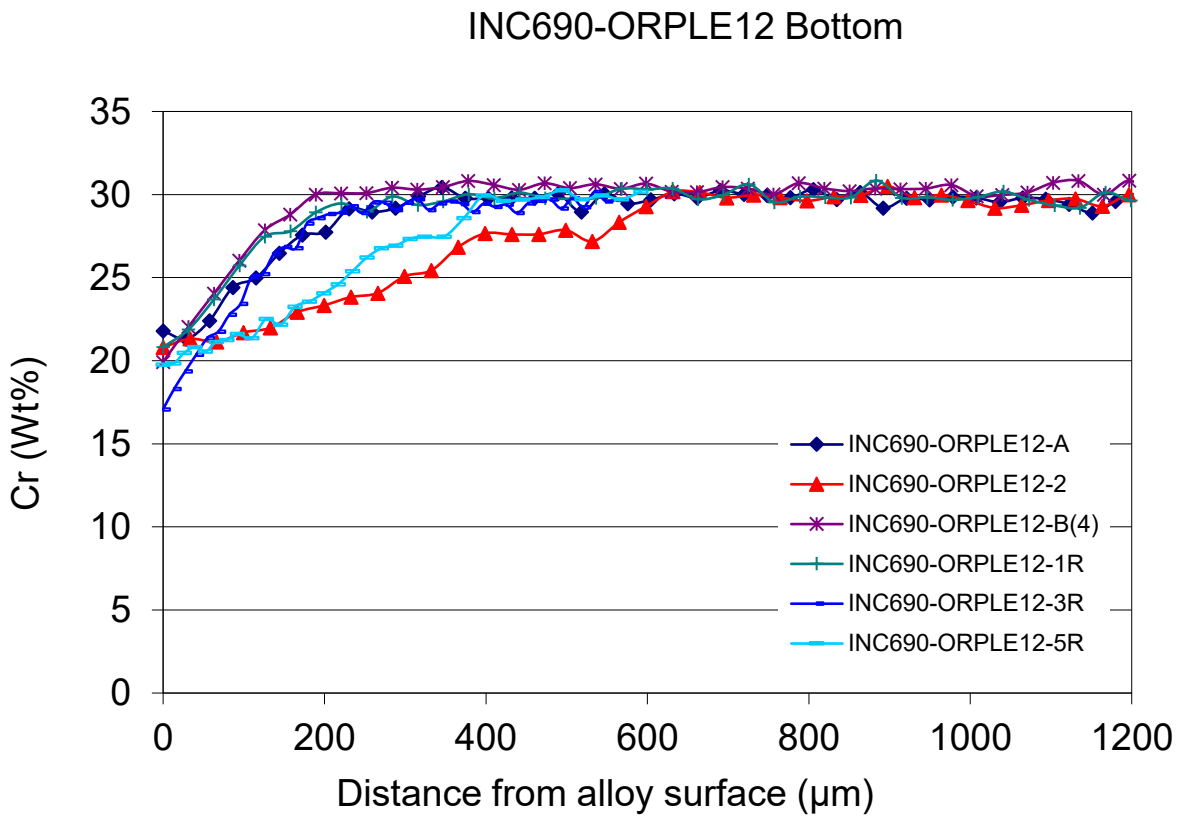

Figure 4.5c. Chromium concentration (Cr wt% in alloy) vs. distance from alloy surface at bottom location for ORPLE12 glasses for tests LE12-1 (INC690-ORPLE12-1R), LE12-2 (INC690-ORPLE12-2), LE12-3 (INC690-ORPLE12-3R), LE12-4 (INC690-ORPLE12-B(4)), LE12-5 (INC690-ORPLE12-5R), and LE12-A (INC690-ORPLE12-A).